The University Of Sheffield.

Access to Electronic Thesis

Author:	Janine Bijsterbosch
Thesis title:	Behavioural and neural correlates of sensorimotor timing and error correction
Qualification:	PhD

This thesis was embargoed until December 2013.

If this electronic thesis has been edited by the author it will be indicated as such on the title page and in the text.

Behavioural and neural correlates of sensorimotor timing and error correction

A thesis submitted to the Medical School, University of Sheffield, for the degree of Doctor of Philosophy

by

Janine Bijsterbosch

June 2011

Department of Academic Clinical Psychiatry
Sheffield Cognition and Neuroimaging Laboratory (SCANLab)
The Longley Centre
Sheffield, United Kingdom

Acknowledgements

First and foremost I offer my sincerest gratitude to my supervisors, Dr Kwang-Hyuk Lee and Professor Peter Woodruff, for their support and guidance throughout my PhD. I am also very grateful to my collaborators for providing me with many opportunities to develop the work presented in this thesis and to expand my knowledge and skills. In particular, I would like to thank Professor Tony Barker, Dr Michael Hunter, Dr Simon Eickhoff, Dr Tom Farrow and Professor Iain Wilkinson for their continued contribution to this work and to my general academic and personal development.

In addition, I am grateful for all the help from the support staff in the Department of Academic Clinical Psychiatry. In particular, I would like to thank Helen Hickson, Beverly Nesbitt and Martin Brook, without whom this and many other people's work would not have been possible. I would also like to thank Glyn Hallam for keeping me company during my PhD. In addition, I remember fondly all the students who worked with me and contributed to this work through their efforts in data collection. I would like to especially thank William Dyson-Sutton for his enthusiasm and drive during his research project with me.

Finally, I would like to take this opportunity to thank my boyfriend, Maarten Vooijs, my parents and my lovely friends both in the Netherlands and in Sheffield for their encouragement, patients and support throughout my PhD.

Abstract

Timing is essential for human movement and cognition and is affected in many psychiatric and neurological disorders. The aim of this thesis was to determine the behavioural and neural correlates of sensorimotor timing and of temporal error correction. Motor timing can be studied using a sensorimotor synchronization (SMS) task. In SMS, timing accuracy is assessed during synchronized finger tapping with a regular pacing stimulus and error correction performance is measured based on responses following induced local timing shifts. Study one addressed the effects of task-related and subject-specific factors on SMS performance and showed that tapping variability was reduced during bimanual SMS, compared with unimanual SMS. Study two examined the role of the primary and pre-motor cortices in SMS using theta burst transcranial magnetic stimulation (TBS). The findings suggested that the left-lateralized pre-motor cortex may play a role in temporal error correction. This hypothesis was tested in study three which confirmed that suppression TBS over the left pre-motor significantly affected error correction responses following supraliminal timing shifts. Study four used functional magnetic resonance imaging (fMRI) to determine the neural correlates of timing and error correction. It was shown that connectivity emerges in a cortico-cerebellar network including the left-lateralized cerebellum and frontal regions during the correction of supraliminal timing shifts. Study five further examined the role of functional connectivity using fMRI and revealed that interhemispheric connectivity between the primary motor cortices was significantly greater during bimanual SMS, compared with unimanual SMS. Lastly, studies six and seven addressed the efficacy of TBS and showed that the local distribution of subarachnoid cerebrospinal fluid can significantly alter TBS-induced stimulation. In the general discussion it is suggested that sensorimotor timing and error correction may be achieved using internal feedforward models in the cerebellum that inform movement initiation controlled by the left pre-motor cortex.

Table of contents

List of abbreviations

ACN	Anti-correlated network
AC-PC	Anterior commissure – posterior commissure
BOLD	Blood oxygenation level dependent
CCA	Cross-correlation analysis
CSF	Cerebrospinal fluid
cTBS	Continuous theta burst stimulation
DLPFC	Dorsolateral prefrontal cortex
DMN	Default mode network
ECG	Electrocardiography
EEG	Electroencephalography
EHI	Edinburgh handedness inventory
FL	Florida
fMRI	Functional magnetic resonance imaging
FWHM	Full width half maximum
Hz	Hertz
IOI	Inter-onset interval
IRI	Inter-response interval
iTBS	Intermittent transcranial magnetic stimulation
LTD	Long-term depression
LTP	Long-term potentiation
MA	Massachusetts
MEG	Magnetoencephalography
MNI	Montreal neurological institute
MPRAGE	Magnetization prepared rapid acquisition gradient echo
MRI	Magnetic resonance imaging
MSE	Mean square error
PCC	Posterior cingulate cortex
PET	Positron emission tomography
PPI	Psychophysiological interaction
RMT	Resting motor threshold

ROI	Region of interest
rTMS	Repetitive transcranial magnetic stimulation
SD	Standard deviation
SET	Scalar expectancy theory
SMA	Supplementary motor area
SMS	Sensorimotor synchronization
T	Tesla
TBS	Theta burst stimulation
TE	Echo time
TMS	Transcranial magnetic stimulation
TR	Repetition time
UK	United Kingdom
USA	United States of America
WTC	Wavelet transform coherence

List of tables and figures

1 General Introduction

1.1 General overview

Temporal order forms an integral part of human physiology (for example in breathing, heart rate, muscle tone and motor coordination) and of human cognition (for example in causality, learning, memory, language and consciousness) (Dawson, 2004). Disruptions to temporal order can be caused by shift work, jet-lag, aging, altered states of consciousness induced by drugs and by mental disorders such as autism, schizophrenia, Alzheimer's disease and anxiety and affective disorders (Lee et al., 2009; Wimpory et al., 2002). Such temporal disorganization can lead to disturbed sleep-wake cycles, altered (and variable) subjective experiences of time, cognitive decline and psychosis (Dawson, 2004). Hence, an improved understanding of the psychological and neuronal mechanisms of timing is imperative in (clinical) neuroscience. Timing is manifested in our ability to interact physically with objects in the external world, which critically depends on temporal coupling between perception and movement (sensorimotor timing) and swift behavioural adjustment to changes in the environment (error correction). The central aim of this thesis is to determine the behavioural and neural correlates of sensorimotor timing and error correction.

The remainder of this Chapter provides a literature review of sensorimotor timing and error correction. Firstly, various theoretical models of interval timing that have been developed over the past decades are introduced. Subsequently, sensorimotor timing and error correction are discussed in detail, including experimental paradigms and associated performance measures that can be used to asses timing ability. Lastly, an overview of prior research on the neural correlates of interval timing is presented. Subsequently, Chapter two provides an introduction to three methodologies that are used in several studies in this thesis, namely the linear phase correction model that can be used to assess timing performance, functional magnetic resonance imaging (fMRI) and transcranial magnetic stimulation (TMS). Chapters three to nine present and discuss data from seven experimental studies

that were performed as part of this thesis. Each experimental study addresses one or more of the objectives for this thesis, which are presented in the next section. The general conclusion in Chapter ten begins with a brief summary of the main findings of each experimental study, which are then integrated in a proposed theoretical framework. Chapter ten ends with suggestions for future research.

1.2 Thesis objectives

The first objective of this thesis is to characterize sensorimotor timing performance and to explore factors that may influence performance. To this end, Chapter three assesses sensorimotor timing ability in a large cohort of healthy subjects. Specifically, Chapter three determines how sensorimotor timing performance is affected by subject-specific factors (such as musical training, gender and handedness) and by task-related aspects. The first task-related aspect studied in Chapter three compares performance with the dominant hand with performance with the non-dominant hand. The second task-related aspect explores the difference in motor timing ability between performance with one hand (unimanual) compared with performance with both hands in synchrony (bimanual). A critical examination of these potentially confounding factors forms an important initial step of this thesis because it informs the design and interpretation of later studies. In Chapter seven, the difference between unimanual and bimanual motor timing is revisited to explore the neural mechanism.

The second objective is to investigate the neural correlates of sensorimotor timing and error correction. From the literature review of previous research on the neural correlates of interval timing (presented in Chapter 1.6) it is clear that there is much controversy with regards to the neural basis of timing. This thesis addresses some controversial issues related to the contribution of several brain regions that are generally associated with motor control (namely, the primary and pre-motor cortices and the cerebellum), to the temporal control of movement. The role of the primary and pre-motor cortices in sensorimotor timing and error correction is examined in Chapters four and five with the use of transcranial magnetic

stimulation. In Chapter six, functional magnetic resonance imaging is used to describe the whole-brain network associated with sensorimotor timing and error correction, and the particular role of the cerebellum is tested with the use of transcranial magnetic stimulation.

The third objective of this work is to investigate functional connectivity in brain networks during sensorimotor timing and error correction. It follows from the results presented in Chapters four, five and six (objective 2) that a wide network of brain regions is involved during timing and error correction. In this network, some particular regions may play a specific role in a certain aspect of temporal processing, for example the pre-motor cortex and the cerebellum (as seen in Chapters five and six). However, it is of crucial importance to understand how the brain areas in these wider networks connect and communicate with each other in order to achieve accurate temporal coupling between sensory input and coordinated motor output. In Chapter six, the cortico-cerebellar network associated with the correction of timing errors is described. Chapter seven investigates changes in inter-hemispheric connectivity between the left and right primary motor cortices during unimanual and bimanual performance in a motor timing task.

The fourth objective of this thesis is to investigate the efficacy of transcranial magnetic stimulation (TMS). TMS is the neural interference technique that is used in Chapters four, five and six to determine the specific causal role of the primary and pre-motor cortices and of the cerebellum in interval timing and error correction (objective 2). However, the physiological effect of TMS on the complex neural micro-circuitry of the human brain (which is reviewed in Chapter two) is not fully understood. In addition, it is possible that local TMS stimulation travels via functional connections between brain regions and may therefore affect a more extensive functional brain network such as those described in Chapters six and seven (objective three). Hence, the focal precision and extent of magnetic stimulation achieved with TMS is currently unknown. To address this issue, Chapter eight uses computational modelling to estimate the distribution of TMS-induced stimulation for thirteen different coil positions including those used in

previous Chapters. The findings presented in Chapter eight highlight the importance of the thin, highly conductive, layer of cerebrospinal fluid that lies between the skull and the grey matter surface of the brain on the distribution of TMS-induced stimulation. In Chapter nine, structural magnetic resonance imaging is used to assess changes in the local thickness of this layer of cerebrospinal fluid when the head is positioned in different orientations with respect to gravity.

1.3 Theoretical models of interval timing

Over the past decades, a number of theoretical models have been developed that attempt to describe the mechanism used to achieve interval timing. These theoretical accounts of interval timing can be categorized into dedicated and intrinsic models of temporal processing. Dedicated models assume that timing is achieved using a neural system that is specialized for temporal control. Intrinsic models are based on the hypothesis that temporal information is an intrinsic property of neural fyring that emerges inherently from modality-specific brain processing without the need for a dedicated mechanism.

Evidence for the existence of a dedicated neural mechanism for temporal processing is based on the fact that humans can easily compare and reproduce temporal intervals in different sensory modalities (Grondin & Rousseau, 1991; Ulrich et al., 2006). Additional evidence for a dedicated timing mechanism is based on behavioural observations of the scalar property. The scalar property is a manifestation of Weber's law and describes the characteristic linear relationship between performance variability and the target duration of the task interval (Gibbon et al., 1997). It has been shown that that the standard deviation of the performance measure increases proportionally with increased intervals, independent of the type of task (Matell & Meck, 2000). Dedicated models can be further subdivided into localized accounts that assume a 'centralized clock mechanism' and distributed accounts of timing that involve multiple brain regions.

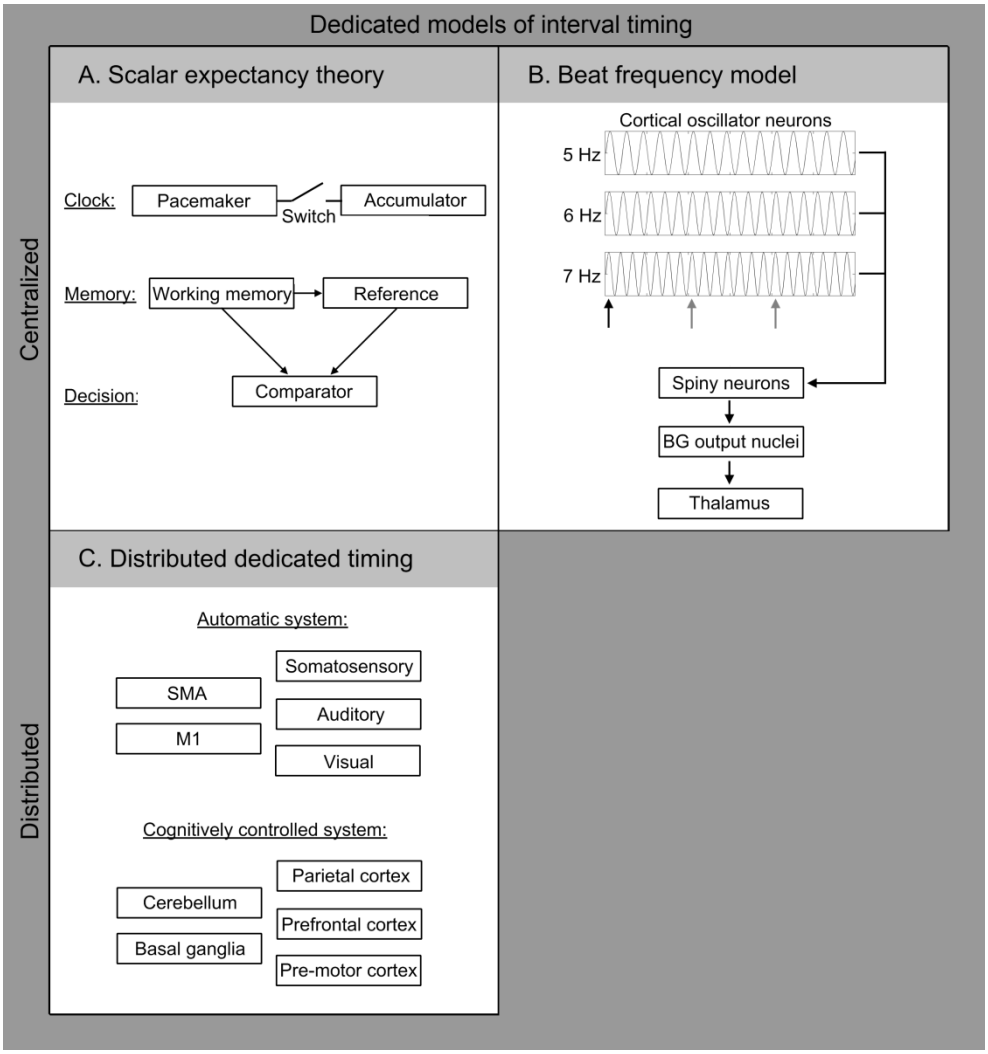

Figure 1.1: Dedicated models of interval timing. Dedicated models of interval timing hypothesize that temporal information is processed in a specialized neural system. Two models (the scalar expectancy theory in figure A and the beat frequency model in figure B) assign temporal processing to a centralized 'clock' mechanism. The third model (the distributed dedicated timing model in figure C) states that timing may be achieved in dedicated networks that are distributed throughout the brain.

One localized, dedicated model of interval timing, the scalar expectancy theory (SET), was primarily designed to describe manifestations of the scalar property in animal research. In SET, the internal clock consists of two main components; a

pacemaker produces pulses at a continuous rate and interval, while the accumulator counts the pulses (Gibbon et al., 1997). The accumulation of pacemaker pulses is controlled by a switch which is triggered by stimulus onset (Lejeune, 1998). The measured duration is then stored in the short-term memory and may be reproduced or compared with previously learned intervals. Although the SET model successfully explains a wide range of psychophysical timing data, the implementation of the theory in a neural circuitry is problematic. In particular, a large set of pacemakers is required to allow the encoding of a wide range of intervals and the detection of minor differences between these intervals. Physiologically, it appears inefficient and therefore unlikely that multiple pacemakers exist. Furthermore, the physiological implementation of the accumulator process is problematic due to lack of clarity on how the process could be accurately bounded and appropriately reset in varying task settings (Matell & Meck, 2000).

An alternative dedicated timing model is based on the properties of neural firing and describes the internal clock in terms of oscillating neurons and coincidence detection. In the beat frequency model, cortical neurons function as oscillators which are synchronized at the start of a trial and oscillate at different, individually fixed frequencies throughout the interval to be timed (Buhusi & Meck, 2005). A group of oscillator neurons firing at different frequencies produce a Fourier waveform of the beat frequency (based on the stimulus). This beat frequency represents the period at which all oscillators spike simultaneously and can be much lower than the frequency of individual neurons (Miall, 1989). A duration is encoded into memory through coincidence detection of the beat frequency in striatal neurons using experience-based long-term depression and potentiation (LTD and LTP) processes. Although less successful at reproducing behavioural features of timing, this model is biologically more feasible and has previously been mapped onto the basal ganglia (Matell & Meck, 2000).

A further dedicated timing model suggests that a specialized system for temporal processing exists and may operate within a larger functional network. In this

distributed theory of timing, different functional networks may exist to control varying timing tasks. There may, for example, be dissociable networks for automatic and cognitively controlled timing (Lewis & Miall, 2003). Hence, demanding timing tasks may recruit a more extensive network of brain areas including cortical regions that control related cognitive processes such as attention, working memory and long-term or reference memory (Ivry & Schlerf, 2008). The main feature of the distributed account of dedicated timing is that, within a certain network, a specialized neural mechanism operates to encode and control timing.

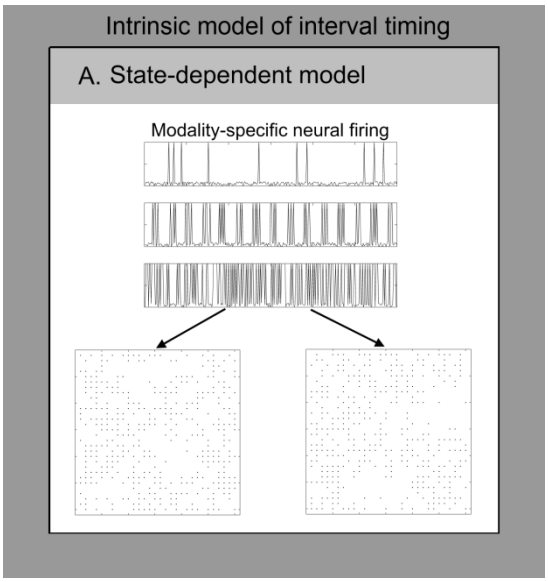

Figure 1.2: Intrinsic model of interval timing. The state depend theory of interval timing hypothesizes that temporal information is intrinsic to all neural processing. Modality-specific neurons create a unique spatial pattern (as visualized at the bottom of the figure) without the need for a dedicated mechanism to process temporal information.

In contrast to dedicated timing models, intrinsic models hypothesize that temporal information is inherent to neural processing without the need for a dedicated mechanism. In the state-dependent network theory, temporal information is inherent in the neural firing pattern of modality-specific neurons, without the need for an explicit linear metric of time (Ivry & Schlerf, 2008; Karmarkar & Buonomano, 2007; Mauk & Buonomano, 2004). According to this theory, the

spatial pattern of evolving neural activity following a stimulus provides a unique snapshot at each consecutive time point, much like the ripples on a water surface following disruption (Karmarkar & Buonomano, 2007). These uniquely evolving spatial patterns allow temporal differentiation without explicit time encoding. Intrinsic timing models predict that temporal processing is modality specific and context-dependent because temporal encoding is intrinsic in the neural processing of the specific task at hand (and the modality and context in which this task is performed). As such, evidence for intrinsic models is derived from physiological studies that reveal that performance on temporal tasks can be predicted by neural firing in modality specific neurons (Bueti et al., 2008; Cohen & Newsome, 2004; Liu & Newsome, 2005). Additionally, it has been shown that performance on timing tasks is context-dependent because temporally irregular distracters interfered with temporal processing (Karmarkar & Buonomano, 2007). However, evidence for cross-modal transfer of performance improvements after training on a temporal task in a single modality is not easily accounted for in intrinsic models of timing (Meegan et al., 2000; Roberts, 1982; Warm et al., 1975).

It is conceivable that two models of dedicated and intrinsic timing are not mutually exclusive and may describe different ranges of temporal abilities. For example, state-dependent intrinsic timing is well suited to explain timing in the range of milliseconds, whereas distributed dedicated timing networks may be required for timing in the range of several seconds to minutes. Longer intervals are not easily mapped onto rapid neural firing patterns and may require additional cognitive processes such as attention and (working-) memory, which supports their representation in extensive dedicated neural networks. Although this thesis does not directly test dedicated and intrinsic timing models, the results are interpreted within this theoretical framework and the findings of this thesis may be used to inform more specific hypotheses regarding timing models. The rest of the literature review will focus on sensorimotor timing and error correction, which form the main subjects of this work.

1.4 Sensorimotor timing

Motor timing requires rhythmic coordination of perception and movement and can be studied in a laboratory environment with a variety of behavioural paradigms. These paradigms can be categorized into judgement-based tasks which require little movement, and movement-based tasks that involve timed repetitive motor responses (Meck, 2003). A judgement-based task may require the subject to reproduce a previously learned duration, bisect a tone into two equal halves or compare two interval-durations. A well-known example of a movement-based timing task is sensorimotor synchronization (SMS). In SMS, participants produce repetitive movements (such as finger tapping) synchronized to a pacing stimulus such as an isochronous auditory or visual sequence. There are many experimental parameters that can be adjusted to produce a variety of different SMS paradigms. For example, SMS tasks can vary in their response requirements (one or both hands, in phase or anti-phase), stimulus modality (auditory or visual pacing) or interval-duration (sub- or supra-second, isochronous or rhythmic) (Repp, 2005). Other possible modulations include occasional perturbations in the pacing stimulus (requiring explicit error correction) or feedback control (eliminating regular sensory feedback or providing additional performance feedback). This variability in experimental designs complicates comparisons between studies and diminishes exact replication of findings. Although both movement and judgement-based task categories are of interest for interval timing, this literature review will focus mainly on sensorimotor synchronization because it is used as the paradigm to study motor timing performance in this thesis.

It requires relatively little effort to tap in synchrony with a regular pacing stimulus, when the inter-stimulus interval falls within the rate limits of approximately 200 to 2000 ms (Repp, 2005). Previous research has shown that subjects, on average, have a tendency to tap 20 to 80 milliseconds before the onset of the predicted stimulus, demonstrating an anticipatory negative mean asynchrony (Aschersleben, 2002). The negative mean asynchrony is a consistent feature of SMS performance, although there are large individual differences. There are several hypotheses that

attempt to explain the causes of the negative asynchrony. The most common explanation assumes that SMS is performed by synchronizing central representations of the taps and tones derived from sensory afferents. Here, the negative asynchrony results from differences in processing speed either at the level of sensory nerve-conduction or at the level of central processing (Aschersleben, 2002). Alternatively, tapping can be regarded as an internal motor oscillator that is only weakly coupled to an external pacing stimulus, which may cause the asynchrony (Pikovsky et al., 2001). Lastly, the negative asynchrony can be explained statistically because a slight negative asynchrony minimizes overall tapping variance (Vorberg & Wing, 1996). None of the explanatory hypotheses can account for all available data and, as such, the causes of the negative mean asynchrony are not fully understood. However, the tap-tone asynchrony is used as an indicator of performance in SMS as it provides an absolute measure of timing accuracy.

Another important measure of SMS performance is the temporal variability in the response sequence. The variability of finger tapping can be calculated as the standard deviation or as the autocovariance of the inter-response intervals (IRIs). The variability of IRIs decreases as the inter-onset interval of the pacing stimulus decreases, as predicted by the scalar property (Gibbon et al., 1997). According to the two-level Wing-Kristofferson model of timing, the total performance variability can be separated into variability that originates in the central internal time-keeper and variability that originates during peripheral motor implementation (Wing & Kirstofferson, 1973). According to this model, only the central time-keeper variability is dependent on the inter-onset interval and the central time-keeper also forms the main source of individual differences in performance variability (Repp, 2005). In order to avoid the accumulation of tap-tone discrepancies over time that are caused by peripheral variability (tapping movement) and, to a lesser extent, by central variability (tempo drift), ongoing error correction is essential in SMS. Sensorimotor error correction is discussed in greater detail in the next section.

1.5 Sensorimotor error correction

Due to inherent variability in the motor response, error correction is required during SMS to sustain a consistent tap-tone relationship even when the pacing stimulus is regular (Repp, 2005). Such error correction mechanisms can be explicitly studied using a pacing sequence that contains occasional local timing perturbations such as phase shifts (local changes in the otherwise regular inter-stimulus interval). Following these perturbations, subjects show a rapid behavioural adjustment and return to their baseline negative mean asynchrony levels within several taps (Repp, 2002b).

Two different error correction processes have been proposed. Phase correction appears to be a largely automatic response to minor local perturbations, whereas period correction involves resetting the period of the internal timekeeper mechanism and may be subject to conscious control (Repp, 2001b; Repp & Keller, 2004). The correction of phase shifts may rely mainly on automatic phase correction and may not be aided by conscious perception of the perturbation (Repp, 2005). This hypothesis is consistent with previous research that showed that the error correction response to subliminal phase shifts that fall below the perceptual threshold was equivalent in speed and accuracy to the response to supraliminal phase shifts (Repp, 2000). However, when subjects intend not to react to perturbations, phase correction can be partially suppressed (Repp, 2002a, 2002b). This may suggest that conscious perception of the phase shift allows modulation of the error correction response. This issue is addressed further in Chapter six, which studies the neural correlates of error correction following subliminal and supraliminal phase shifts.

Conceptually, ongoing error correction during SMS can be seen as an adjustment in the response timing based on the perceived tap-tone asynchrony (Semjen et al., 2000). This assumption that error correction relies on the perceived interval forms the basis for the first order linear error correction model that is discussed further in Chapter two. Alternatively, the timing of each response may be based on temporal

reference points such as the pacing tone and the preceding tap, instead of relying on a temporal interval. In the mixed phase resetting model, the timing of each finger tap is reset relative to the preceding tap and the pacing tone (Hary & Moore, 1985, 1987a, 1987b). Although this model is mathematically equivalent to the first order linear error correction model, it may provide a more attractive explanation of accurate responses to subliminal shifts because it assumes that behavioural correction is based on the absolute timing of reference points instead of the (imperceptible) tap-tone interval.

1.6 Neural correlates of interval timing

1.6.1 Basal Ganglia

Research on the involvement of the basal ganglia in timing mainly focuses on patients with dopaminergic dysfunction (for example Parkinson's disease and Huntington's disease), lesions studies and pharmacological interventions in animals. The most consistent finding that links the dopamine system of the basal ganglia to timing is a respective increase or decrease in clock-speed following dopamine agonist or antagonist medication (Buhusi & Meck, 2005). This effect of dopaminergic manipulation is evident in both judgement-based and movement-based timing tasks. In addition, patients suffering from Parkinson's disease are impaired in time perception and display increased variability during motor timing in some studies (Meck, 2003). However, the existence of timing impairment is largely dependent on medication and on the severity of the disorder (Ivry & Spencer, 2004). Recent brain imaging studies add to the controversy, as basal ganglia activation during timing is found in some studies (Rao et al., 1997), but not others (Jäncke et al., 2000). It has been suggested that involvement of the basal ganglia during timing is dependent on the complexity of the task, or may only occur during timing of longer intervals that last several seconds to minutes (Ivry & Spencer, 2004; Lewis & Miall, 2003; Lewis et al., 2004; Mayville et al., 2002). Some authors have argued that the dopaminergic system is a suitable candidate for coincidence detection (Matell & Meck, 2000, 2004). However, the evidence for a

critical role of the basal ganglia in timing remains inconclusive. Investigations into the role of the basal ganglia during timing are complicated by the involvement of this structure in many, potentially confounding cognitive functions such as decision making, reward processing, attention and motor gaiting.

1.6.2 Cerebellum

The cerebellum has received much attention in timing research because patients with cerebellar lesions or atrophy consistently show increased variability in motor timing tasks (Ivry & Spencer, 2004; Meck, 2003; Synofzik et al., 2008; Torriero et al., 2007). The increase in timing variability following cerebellar disruption has been replicated in studies that use transcranial magnetic stimulation (Theoret et al., 2001). Furthermore, imaging studies consistently indicate cerebellar activation during performance of timing tasks (Jäncke et al., 2000; Mayville et al., 2002; Ullen et al., 2003). This evidence of cerebellar involvement during interval timing has led some researchers to suggest that the cerebellum may function as an internal clock (Ivry & Spencer, 2004).

However, opposing findings challenge the view that the cerebellum may serve as internal clock for interval timing. For example, it was noted that the scalar property is unaffected in patients with cerebellar lesions (Buhusi & Meck, 2005). Furthermore, although temporal precision and consistency may be impaired, it is never fully disrupted following cerebellar damage. Research has also shown that temporal control of continuous movement (such as circle drawing) is unaffected in cerebellar patients (Schaal et al., 2004; Spencer et al., 2003). Lastly, only timing in the millisecond range, and not of supra-second intervals, is affected by cerebellar dysfunction (Lee et al., 2007; Lewis & Miall, 2003). Hence, although it is clear that the cerebellum is important during interval timing, the degree of retained temporal processing following damage suggests that a primary function as internal clock mechanism may be unlikely.

Instead of an internal clock function, it has been suggested that the role of the cerebellum during timing may involve feedforward control. Evidence of cerebellar involvement during predictive movement control (Bastian, 2006) and during procedural learning (Blakemore & Sirigu, 2003) supports this suggestion. Feedforward processing uses previous experience to predict appropriate output in order to allow fast, automated performance of pre-learned behaviour (Ohyama et al., 2003; Pollok et al., 2008a). Feedforward control is essential to synchronize movement to predictable sensory stimuli and may therefore explain the importance of the cerebellum during motor timing. However, timing impairment is also found in cerebellar patients after controlling for motor impairments (Bares et al., 2007; Fierro et al., 2007; Koch et al., 2007) and performance on judgement-based timing tasks is also associated with the cerebellum (Ivry & Spencer, 2004; Lee et al., 2007; Lewis & Miall, 2003). These findings of cerebellar involvement during non-motor timing may suggest a role beyond feedforward movement control.

An alternative view suggests that the function of the cerebellum in timing paradigms is associated with sensorimotor processing (Molinari et al., 2007). This hypothesis is primarily based on findings that reveal preserved temporal processing in cerebellar patients, suggesting that the cerebellum plays a generalized role that extends beyond temporal control. For example, patients with cerebellar damage show a negative tap-tone asynchrony similar to healthy subjects during SMS, which indicates that anticipatory control is unaffected (Harrington et al., 2004). A sensorimotor processing function of the cerebellum is further supported by its involvement during passive movement (Grube et al., 2010a; Grube et al., 2010b; Jueptner et al., 1997; Thickbroom et al., 2003) and during illusory ownership of a moving alien hand (Hagura et al., 2008). Hence, it was suggested that the cerebellar circuitry may function to fine-tune and adequately modulate sensory processing through neural synchronization (Molinari et al., 2007). Such an optimization function of the cerebellum may explain its role in a variety of perceptual, motor and cognitive functions including timing.

In summary, it is evident that the cerebellum is involved during interval timing. However, disagreement remains concerning the functional interpretation of cerebellar involvement. Retained timing abilities following damage may suggest that a general internal clock function is unlikely. Rather, the role of the cerebellum during timing may be explained in the framework of feedforward control. Alternatively, the cerebellar circuitry may function to optimize sensorimotor processing. Based on currently available data, these interpretations seem equally plausible. Indeed, the two theories are not mutually exclusive and it is not inconceivable that the cerebellum controls both feedforward and sensorimotor processes because accurate processing of sensorimotor feedback is essential to update future internal models in feedforward control. Accordingly, the functional significance of the cerebellum during timing may be a complex combination of feedforward and feedback processing, of which the balance is dictated by task requirements. In Chapter six of this thesis, the role of the cerebellum in sensorimotor timing and error correction is determined with the use of functional magnetic resonance imaging and transcranial magnetic stimulation.

1.6.3 The cognitive system

There is evidence that the inferior and posterior parietal cortices and the dorsolateral prefrontal cortices are involved in interval timing. Activations in parietal and frontal cortices are reported in several imaging studies that use motor timing paradigms (Jäncke et al., 2000; Pollok et al., 2008a). Furthermore, timing abnormalities have been reported in patients suffering from neglect syndrome (Danckert et al., 2007) and in a patient with a lesion in the parietal-occipital region (Gooddy, 1969). Transcranial magnetic stimulation (TMS) of the temporal-parietal junction was found to increase tap-tone asynchrony in an SMS task (Malcolm et al., 2008). TMS over the right dorsolateral prefrontal cortex led to an underestimation of long (1600 – 2400 ms) intervals compared with short (400 – 600 ms) intervals in a reproduction task (Jones et al., 2004). Involvement of a parietal-frontal system possibly depends on the attention or cognitive load required for the task. This suggestion is supported by previous research that showed

consistent frontal activations during unpaced continuation tapping following an SMS task (Rao et al., 1997) and when correcting for large phase perturbations (Stephan et al., 2002), which may both require additional attention and cognition.

Within the cognitive system, there is evidence for a right-lateralized specialization of temporal control. Findings from neuroimaging studies reveal that parietal-frontal activations are mostly found in the right hemisphere. Additionally, previous research revealed that a split-brain patient showed superior time perception performance when visual stimuli were presented in the left visual field compared with the right visual field (Funnell et al., 2003). Furthermore, patients with right hemispheric temporal lobe epilepsy showed impaired time perception performance, compared with patients with left hemispheric temporal lobe epilepsy or healthy controls (Vidalaki et al., 1999). Similarly, patients with right hemispheric cortical lesions exhibited impaired performance in a task that required temporal reproduction of intervals longer than three second compared with patients with left cortical lesions or controls (Kagerer et al., 2002). In contrast, a left-lateralization of cognitive regions is seen during temporal attention and during implicit timing in which temporal information or context can be used to improve performance (Coull & Nobre, 1998; Praamstra et al., 2006). It is possible that initial entrainment and resulting temporal expectancy may be achieved in a left-lateralized cortical network based on cerebellar feedforward models. Right-lateralized cortical regions, on the other hand, may be involved with higher cognitive expectations that develop and change as time passes by (Coull et al., 2011).

1.6.4 The motor system

It is perhaps not surprising that the cortical network responsible for motor control is involved during motor-timing tasks. In particular, regions in the primary motor cortex, pre-motor cortex and supplementary motor area (SMA) are activated during timing tasks. However, more recent investigations of these cortical motor regions may suggest that their role during temporal processing goes beyond simple movement control.

The primary motor cortex contralateral to the hand performing the task is consistently activated in motor timing. Magnetoencephalographic (MEG) recordings show that primary motor cortex activation occurs approximately 100 milliseconds prior to movement onset, which suggests that it may be related to the motor command (Pollok et al., 2006a). However, TMS over the primary motor cortex has been shown to result in a decrease in tap-tone asynchrony, effectively enhancing timing accuracy (Doumas et al., 2005). TMS over the primary motor cortex has also been related to the variability of the inter-tap interval (Verstynen et al., 2006). These TMS findings may suggest that the role of the primary motor cortex is more advanced than simple muscle innervation and may interact with temporal processing. However, since timing is manifested in many perceptual as well as motor tasks, a primary function of primary motor cortex in timing is unlikely.

In addition to the primary motor region, the pre-motor cortex has also been associated with timing. Growing evidence suggests that pre-motor control of timing may be distinctly lateralized (Pollok et al., 2008a; Pollok et al., 2006a). MEG recordings during an SMS task show that the left pre-motor cortex controls timing of both hands independent of the hand used (Pollok et al., 2006a). Coherence measures in this study suggest that the influence of the left pre-motor cortex occurs through connectivity with the bilateral primary motor cortices. It was subsequently shown that connectivity between the left pre-motor cortex and contralateral primary motor cortex may be indirect via additional synapses (Pollok et al., 2008b). Although the findings of left pre-motor cortex involvement in interval timing are mostly consistent, one study failed to find any timing disruption following TMS over the left pre-motor cortex (Doumas et al., 2005). This negative finding may be explained by insufficient statistical power to detect an effect due to the low TMS stimulation intensity, short task duration and limited number of subjects. One further study failed to find timing disruptions following TMS stimulation over the left pre-motor cortex (Malcolm et al., 2008). However, the

target stimulation area of this study was located in the ventral rather than the dorsal pre-motor cortex.

It is evident that a localized and lateralized region in the left dorsal pre-motor cortex is important during motor timing and that this influence occurs through direct or indirect connections with the primary motor cortices. However, much less is understood about the functional significance of the pre-motor region for motor timing. It has been suggested that the left pre-motor cortex may control preparation (and possibly inhibition) of individual movements based on temporal information derived from the cerebellum (Pollok et al., 2008b). It is therefore possible that the left pre-motor cortex implements feedforward control information (derived from the cerebellum) into accurately timed movements through its function in motor inhibition and preparation (Seidler et al., 2004). Although currently highly speculative, the hypothesis that the left premotor region is associated with movement preparation and inhibition is supported by evidence of connectivity between the cerebellum and pre-motor cortex (Del Olmo et al., 2007), and of the role of the left pre-motor region in motor preparation during non-timing tasks (Churchland & Shenoy, 2007).

The supplementary motor area (SMA) is activated in many neuroimaging studies of motor timing (Jäncke et al., 2000; Mayville et al., 2002; Pollok et al., 2006a; Ullen et al., 2003). Similarly to the other motor structures, it is difficult to dissociate between a timing function and simple motor control. However, SMA activation has also been found during non-motor judgement-based timing tasks (Macar et al., 2002). It has been suggested that involvement of the SMA is particularly related to temporal complexity, based on findings of increased SMA activation during rhythmic timing paradigms (Lewis et al., 2004; Teki et al., 2011). However, two imaging studies suggest that the SMA may play a more substantial role in temporal encoding. In one study, stronger SMA activation was found during the production of a particular duration compared with the production of force in a non-rhythmic task (Macar et al., 2004). The second study showed that SMA activation parametrically increased with attention to time, compared with colour,

during a perceptual timing task (Coull et al., 2004). Although these findings provide evidence for a role of the SMA in timing, this interpretation is complicated because of the importance of attention and memory in both paradigms. The possibility that SMA activation is related to these confounding cognitive functions is supported by its strong connectivity with the basal ganglia, which are known to be involved in both attention and memory processes (Macar et al., 2006; Teki et al., 2011). Hence, the SMA appears to play a role during timing beyond movement control, but the functional significance of this role is currently unclear. SMA involvement during interval timing may be related to rhythmic complexity, attention or memory.

In summary, there is evidence that the primary motor cortex, left dorsal pre-motor cortex and supplementary motor area are involved in timing-related processes beyond movement control. However, a possible functional interpretation of their role during timing is complicated by many confounding motor and cognitive processes. Fortunately, these motor regions are relatively straightforward targets for transcranial magnetic stimulation (TMS) as they lie superficially in the cortex and are comparatively easy to localize. Consequently, it is likely that the recent increase in TMS investigations will continue to provide more knowledge on the role of the motor areas during interval timing in the near future. In Chapters four and five of this thesis, TMS is used to determine the specific role of the primary and pre-motor cortices in sensorimotor timing and error correction.

2 General methods and techniques

This Chapter begins with a detailed explanation of the analysis of sensorimotor synchronization data according to the extended Wing-Kristofferson model ('linear phase correction model'), because this analytical model is applied in Chapters three and four. Thereafter, this Chapter describes two techniques that are used repeatedly in this thesis, namely functional magnetic resonance imaging (fMRI) and transcranial magnetic stimulation (TMS). The sections on fMRI and TMS are intended as a general introduction to these techniques and a more detailed description of the materials and methods will be provided for each study.

2.1 Linear phase correction model

Chapter one introduced the Wing-Kristofferson model, which proposes that the total tapping variability can be separated into variability in central (internal timekeeper) and peripheral (motor implementation) components (Wing & Kirstofferson, 1973). As illustrated in Figure 2.1A, the model assumes a two-level representation such that the observable inter-response intervals (IRI_n) are determined by a linear combination of the timekeeper command (T_n) and the motor implementation variability (M_n) as follows:

$$IRI_n = T_n + M_{n+1} - M_n$$

Following from this expression, the motor variability contributes to the variance of the inter-response intervals and introduces negative dependence between successive intervals. As a result, the model parameters for timekeeper and motor implementation variability can be estimated from the autocovariance function of the inter-response intervals. The autocovariance function describes the dependence structure within a particular sequence and can be calculated at different lags by comparing the data against a time-shifted (lagged) version of itself.

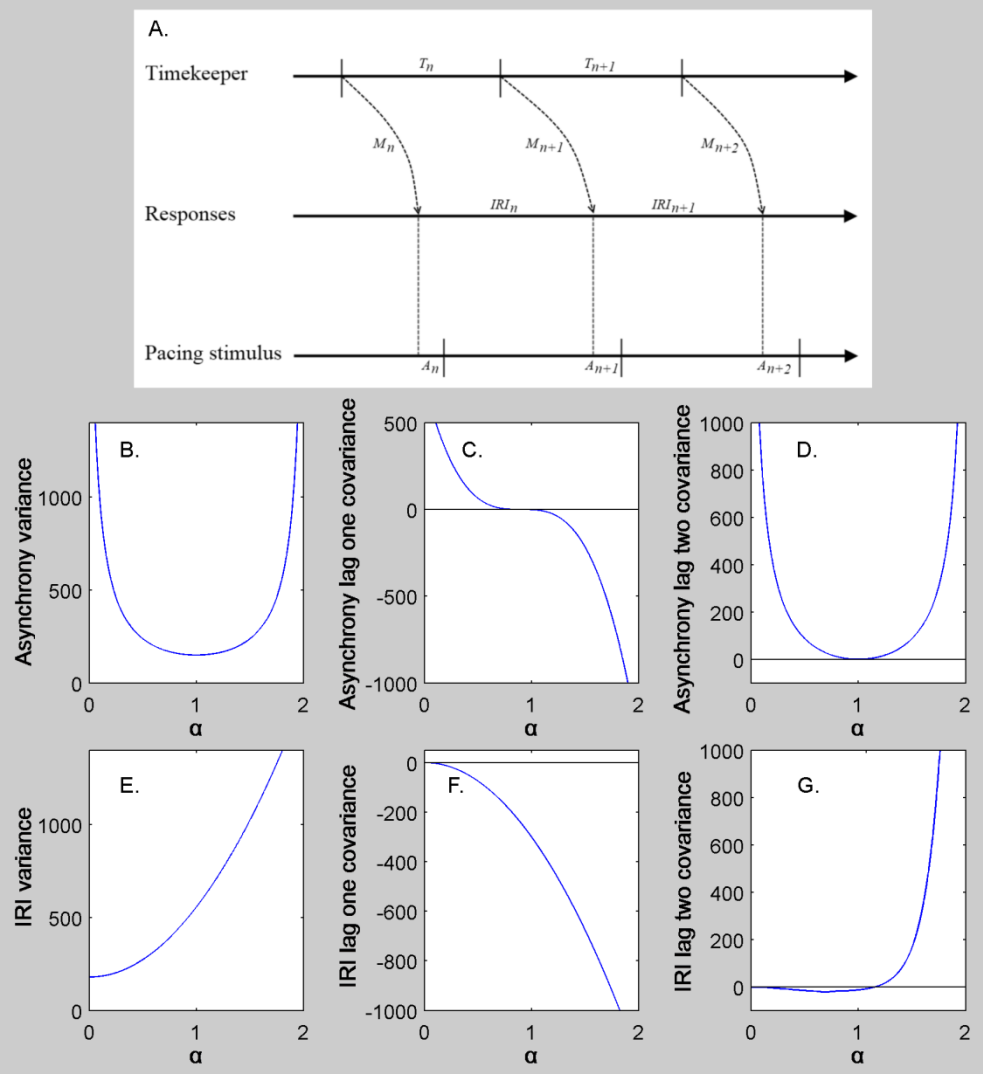

Figure 2.1: Schematic of the linear phase correction extension of the Wing-Kristofferson model (A) and associated model predictions for the autocovariance function (at lag 0 – 2) of tap-tone asynchrony (B-D) and of inter-response intervals (E-G). The inter-response intervals (IRI_n) are a linear combination of the timekeeper (T_n) and motor delay (M_n) components following from the two-level assumption of the linear phase correction model (Figure A; A_n = tap-tone asynchrony). Predicted asynchrony and IRI statistics are shown as a function of the error correction estimate (α). Predictions of the first order linear phase correction model for asynchrony and IRI variance (B&E), lag one covariance (C&F) and lag two covariance (D&G) are shown. Figures are based on Vorberg and Schulze (2002).

The original Wing-Kristofferson model applies to continuation tapping performance, which is measured during a period of un-paced finger tapping that immediately follows a 'synchronization' phase of paced finger tapping. The linear phase correction model forms an extension of the original Wing-Kristofferson model that was developed to account for ongoing error correction during paced synchronization tapping (Semjen et al., 2000). The linear phase correction extension is based on the assumption that participants use the perceived tap-tone asynchrony to adjust for ongoing variability in synchronization tapping. Specifically, it is assumed that subjects correct for a fixed proportion of the last tap-tone asynchrony in the timing of the subsequent response (a first-order linear feedback mechanism).

The linear phase correction model can be used to estimate parameters for central and peripheral variability components and for error correction from SMS data based on the autocovariance function of the tap-tone asynchrony (or of the inter-response interval which contains the same information according to the model assumptions). The linear phase correction model predicts that the lag zero and the lag two autocovariance function of both the asynchrony and of the IRI are positive, whereas the lag one autocovariance of the IRI is predicted to be negative and the lag one autocovariance of the asynchrony can take both negative and positive values for different error correction estimates (Figure 2.1).

The output parameters of the linear phase correction model can be estimated from the autocovariance function as follows:

$$\alpha = 1 - \frac{\gamma_2}{\gamma_1}$$

$$\sigma_M^2 = \gamma_0 \frac{\gamma_2}{\gamma_1} - \gamma_1$$

$$\sigma_T^2 = \left(1 - \frac{\gamma_2}{\gamma_1}\right)\left[\gamma_0\left(1 - \frac{\gamma_2}{\gamma_1}\right) + 2\gamma_1\right]$$

It is clear that the error correction estimate (α), the motor variability estimate (σ_M^2) and the central timekeeper variability estimate (σ_T^2) can all be identified from the lagged autocovariance function (γ_j, in which *j* indicates the lag). For the proofs of these derived equations please refer to the original work by Vorberg and colleagues (Vorberg & Schulze, 2002; Vorberg & Wing, 1996).

There are some methodological issues to consider in the implementation of the linear phase correction model to data obtained from a sensorimotor synchronization task. These methodological considerations refer to the estimation of the autocovariance function. In short data samples it is possible that (by chance) the estimated autocovariance value differs from the theoretical value predicted from the model (Vorberg & Wing, 1996). This discrepancy is referred to as the 'estimation bias' and the effect on the autocovariance estimate (and on parameters computed from this estimate) can be large in smaller sample sizes (approximately N=20). However, as the data sequences that are analyzed in Chapters three and four are relatively long (N=300), the estimation bias is reduced considerably. Secondly, it is possible that predictions that follow from the linear phase correction model may not fit each dataset due to the finite sampling problem. As a result, erroneous negative estimates for motor variability can arise by chance (Semjen et al., 2000). In Chapters three and four, the percentual occurrence of negative motor variance estimates is provided and these negative estimates are set to zero in line with previous work (Vorberg & Schulze, 2002).

2.2 Functional magnetic resonance imaging

Functional magnetic resonance imaging (fMRI) makes use of the different magnetic properties of oxygenated and deoxygenated haemoglobin to measure the blood oxygenation level dependent (BOLD) signal. Functional MRI can be used to localize brain areas associated with particular aspects of performance because activated brain regions receive a surplus of oxygenated blood. General limitations of fMRI are the indirect nature and delayed latency of the BOLD signal. BOLD is an indirect measure of brain activation that is intermediated by the slow

hemodynamic response which causes the increase in oxygenated blood-flow to the active region. The hemodynamic response begins approximately three seconds after the onset of neural activity, peaks around six seconds after the onset of activity and returns to baseline after 12 to 20 seconds. Nonetheless, the spatial resolution of fMRI is superior to any other imaging technique, and therefore fMRI is widely used in neuroscience research.

Functional MRI has been used for several decades to localize brain activity associated with particular behavioural tasks ('specialization'). Recently, there has been an increased interest in connections and communication between distributed brain regions ('integration'). In addition to specialization, integration between distributed brain areas (or 'connectivity') may be crucial for our understanding of brain function. Brain connectivity may not only be of relevance to perception and cognition in the normal brain, but could also play a role in many complex clinical disorders (Fox & Greicius, 2010). It has for example been shown that connectivity in cortico-cortical and cortico-cerebellar pathways is altered in schizophrenia (Harrison, 2005), suggesting that schizophrenia may be a 'disconnection syndrome' (Friston, 1998). Also, altered connectivity patterns in the limbic system may be associated with susceptibility to depression and responsiveness to treatment (Matthews et al., 2006). Hence, brain connectivity may be crucial to our understanding of normal brain function and might have a potential diagnostic value in complex psychiatric disorders. Accordingly, the third objective for this thesis is to investigate functional connectivity networks associated with timing and error correction. This objective is addressed in Chapters six and seven.

The study of brain connectivity can be approached from three fundamentally different perspectives termed anatomical, functional and effective connectivity (Li et al., 2009). Anatomical connectivity describes physical connections between neurons or groups of neurons through white-matter tracts. Functional and effective connectivity, on the other hand, both describe functional associations between brain areas. Functional connectivity is defined as 'temporal correlations between spatially remote neurophysiological events' and is therefore a descriptive measure

of brain interactions (Friston et al., 1993). Effective connectivity is defined as 'the influence one neuronal system exerts over another' and can be understood in terms of directional functional connectivity that has to be constrained by a predefined model (Friston, 1994). Functional and effective connectivity can be mathematically defined as the correlation or covariance between two BOLD time series derived from different parts of the brain. Although theoretically simple, the analysis of covariance in functional imaging data is complicated by the large number of time series obtained. A typical fMRI dataset contains approximately 300,000 voxels (three dimensional pixels) and therefore many potential functional connections.

One of the most adopted functional connectivity methods is cross-correlation analysis (CCA), which calculates the correlation between a selected seed region of interest (ROI) and all other voxels in the brain. In CCA, a seed ROI is chosen based on anatomical or functional prior knowledge. The ROI may consist of a single voxel or the eigenvariate of a number of voxels in a particular location. The eigenvariate is best understood as a weighted mean of the selected voxels and is therefore less sensitive to heterogeneity within the selected region. CCA analysis is performed by calculating the correlation coefficients between the selected ROI and all other voxels in the brain (Cordes et al., 2000; Li et al., 2009). The resulting correlation coefficients are converted to standardized z-scores to allow a second-level group analysis. The output of a CCA analysis is a brain map that highlights those regions whose BOLD time series significantly correlate with the selected ROI time course, which indicates functional connectivity. Although CCA is the earliest and mathematically the simplest analysis of functional connectivity, it was recently shown that it is one of the most sensitive approaches to accurately determine functional connectivity (Smith et al., 2011).

Effective connectivity differs from functional connectivity in that it describes the directional influence (mediated by direct or indirect neuronal connections) of one region over another, whereas functional connectivity describes only co-variations between two regions (Friston et al., 1993). One commonly adopted method to investigate effective connectivity is a psychophysiological interaction analysis

(PPI). A PPI analysis investigates how activation in one brain region modulates activation in a second brain region in the context of the experimental design. Mathematically, PPI analysis is a special type of whole brain cross correlation analysis for which the BOLD time series from a region of interest is convolved with a time series that describes the experimental design (Friston et al., 1997). The resulting interaction term is used for the whole brain correlation analysis. Hence, PPI analysis identifies brain regions that exhibit enhanced functional connectivity with the seed ROI during one experimental condition compared with another experimental condition.

The main methodological issue associated with functional and effective connectivity analyses is the presence of confounding factors such as scanner and physiological noise (Horwitz, 2003). In order to reduce spurious correlations due to hardware and physiological noise, the data are pre-processed prior to connectivity analyses. In addition to standard fMRI pre-processing stages, temporal filtering may be applied (low-pass filter of 0.1 Hz) to isolate the signal in the frequency-range of interest (Van Dijk et al., 2010). If cardiac and respiratory data are concurrently acquired during scanning, a regression analysis can be used to reduce confounding physiological effects (Birn et al., 2006; Glover et al., 2000; Shmueli et al., 2007). Additional regressors that can be incorporated include BOLD time series derived from ventricles and white matter and movement parameters (Chang & Glover, 2009; Kay et al., 2008). Finally, global signal correction is often applied prior to connectivity analyses, although the effects of this pre-processing stage are not entirely clear (Fox et al., 2009; Murphy et al., 2009). Global signal correction is achieved by removing the averaged BOLD signal across the entire brain from the signal at each individual voxel. In summary, pre-processing approaches have been developed that attempt to address the influences of hardware and physiological noise in functional and effective connectivity analyses.

2.3 Transcranial magnetic stimulation

Since the first demonstration of Transcranial Magnetic Stimulation (TMS) in 1985 (Barker et al., 1985), the technique has been widely adopted to transiently alter neural excitability in the human brain. In TMS, a brief, but intense electric current flows through a coil positioned over the head. The resultant time-varying magnetic field induces an electric field in the underlying tissue by Faraday's law of electromagnetic induction. This electric field can directly depolarize neurons leading to an action potential or can result in transient changes in the threshold for future action potentials (Thickbroom, 2007). In practice, magnetic stimulation is experienced by the subject as a slight tap to the head at the stimulation site accompanied by a ticking sound. As such, TMS causes minimal discomfort and is considered safe when the recommended safety guidelines are adhered to (Wassermann, 1998). Hence, TMS can be used, for example, in research to investigate the causal relationship between activation in a target cortical region and its function as measured in behavioural tests (Hallett, 2007; O'Shea & Walsh, 2007; Walsh & Cowey, 2000). Clinical applications of TMS have also been explored, but evidence for effective clinical usage is limited, with the exception of antidepressant effects of left prefrontal TMS (George et al., 2009).

The neuro-physiological effects of TMS are influenced by many parameters. For example the shape and size of the coil interact with the geometry of the skull to affect the extent, intensity and depth of stimulation (Sack & Linden, 2003). In research, a figure-of-eight shaped coil made up of two overlapping circular coils is often used, because it provides a strong and focal stimulation. Furthermore, stimulation parameters such as the number of pulses and their intensity, frequency, duration and wave form may result in different neural effects (Barker et al., 1991; Jalinous, 1991; Salinas et al., 2009; Stokes et al., 2007; Toschi et al., 2008). Single pulses of TMS result in neural innervation at the target location which only lasts for the duration of the pulse. Single pulse TMS can, for example, induce a muscular response when applied over the primary motor cortex or a visual experience (phosphene) when applied over the primary visual cortex (Huerta &

Volpe, 2009). Alternatively, multiple pulses can be applied to induce an effect that outlasts the stimulation period. Repetitive TMS (rTMS) typically requires 10 to 20 minutes of stimulation and may alter neural activity in the target brain region for a limited time following this period. Repetitive TMS at a low frequency (1 Hz) is thought to decrease neural excitability, whereas high frequency rTMS (5 Hz or more) may increase neural activity (Chen et al., 1997; Pascual-Leone et al., 1994). The suppression or facilitation of neural activity immediately following rTMS can lead to measurable effects on performance in cognitive tasks.

Various patterns of repetitive stimulation have been developed which aim to enhance the strength or duration of the TMS effect. A complete overview of these patterns in beyond the scope of this work, but can be found elsewhere (Huang et al., 2009). One repetitive TMS pattern will be discussed in more detail since it is used in Chapters four, five and six. In Theta Burst transcranial magnetic Stimulation (TBS) a burst of three pulses at 50 Hz is applied every 200 milliseconds (5 Hz). The TBS pattern of triple-pulse bursts of gamma frequency stimulation nested in a theta cycle mimics *in vivo* neural activity. For example, gamma waves nested within a theta rhythm form the characteristic oscillation pattern recorded in the rodent hippocampus (Buzsáki et al., 2003). TBS can be applied continuously (cTBS) to achieve a reduction in neural excitability, whereas intermittent TBS (iTBS) may increase neural excitability in the target region (Huang et al., 2005). Research has shown that theta burst stimulation of the human primary motor cortex results in lasting changes in excitability, causing measurable effects sometimes lasting over 1 hour (Huang et al., 2005). Although there is no difference in the effect size between conventional rTMS and TBS (Zafar et al., 2008), TBS does provide several practical advantages over conventional rTMS. These advantages include a shorter stimulation time, lower stimulation intensity and longer-lasting neural effects. Therefore TBS was used as the preferred method throughout this thesis and was applied in accordance with safety guidelines (Oberman et al., 2011).

The physiological mechanism of the longer-lasting effect of rTMS and TBS is thought to operate at the synaptic level by mirroring the processes of long term depression (LTD) or long term potentiation (LTP). Animal studies have used electric stimulation of rodent hippocampal slices to show that both high frequency rTMS and intermittent TBS produce long-term potentiation (Tominaga et al., 2002). Here, theta burst electric stimulation resulted in a wider-spread and longer-lasting effect compared with standard high frequency repetitive stimulation. However, the human cortex is more complex than the rodent hippocampus and electric stimulation used in animal research is applied more focally and at a higher intensity and frequency than TMS applied to humans (Hoogendam et al., 2010). There is evidence to suggest that the effects of rTMS and TBS in the human brain are also mediated by LTP and LTD. It has, for example, been shown that effects of TBS stimulation over the human motor cortex on the motor evoked potential (measurable muscular innervations) can be blocked using pharmacological agents which affect receptors involved in LTP and LTD (Huang et al., 2007; Huang et al., 2011).

Although there is convincing evidence to suggest that effects of rTMS and TBS are mediated by LTP and LTD processes, this does not provide a full understanding of the effects of stimulation. The target region stimulated by TMS applied with a figure-of-eight coil extents approximately 1 square centimetre and can reach a depth of up to 2 centimetres (Fitzpatrick & Rothman, 2000). As a result, a great variety of neural tissue is targeted by the current flow (Hoogendam et al., 2010; Huerta & Volpe, 2009). Various types of neural tissue in the heterogeneous target region may respond differently to stimulation. Furthermore, the effect of TMS may travel through synaptic connections and produce effects in remote brain regions. It has for example been shown that TBS affects cortical inter- and intra-hemispheric synchronization in EEG recordings in humans (Bestmann et al., 2003; Schindler et al., 2008). Hence, future work is needed to elucidate the effects of rTMS and TBS in heterogeneous tissue and on (functionally) connected brain regions further. In Chapters eight and nine of this thesis, data from two studies that aim to determine the efficacy of transcranial magnetic stimulation are presented.

3 Study 1: Effects of task-related and subject-specific factors on sensorimotor timing performance

3.1 Aims and rationale

Chapter one introduced the anticipatory negative mean asynchrony (accuracy) and the variability of inter-response intervals (variability) as the two main performance measures in a sensorimotor synchronization task. The first study in this thesis describes sensorimotor timing performance and explores factors that may influence performance (objective 1). The aim of this study was to explore how SMS performance is affected by task-related aspects and by subject-specific factors. In particular, this study investigates task-related aspects of the hand used to perform the task (dominant or non-dominant hand) and of unimanual versus bimanual performance. The subject-specific factors that are explored in this study are the effects of amateur musical training, gender and strength of right-handedness.

It has previously been shown that tapping variability is significantly reduced when the task is performed bimanually with both hands in synchrony compared with unimanual performance (Helmuth & Ivry, 1996; Pollok et al., 2007). However, it is currently unclear whether this task-related bimanual variability advantage is due to decreased variability in the central level at the internal timekeeper or in the peripheral motor implementation component of the Wing-Kristofferson model that was discussed in Chapters one and two. Furthermore, previous research on the maximum speed of finger tapping has shown an advantage of the dominant hand over the non-dominant hand (Peters, 1980), which may suggest that similar differences in SMS performance may occur. However, the effect of the task-related aspect of the hand used (dominant or non-dominant) on SMS performance has not previously been studied.

Sensorimotor timing performance can vary considerable between different subjects. One of the main subject-specific factors known to affect sensorimotor

timing performance is musical training. Musically trained individuals show a smaller negative mean asynchrony compared with subjects with no musical training, tapping on average 10 ms closer to the pacing tones (Aschersleben, 2002). Professional musicians often show an even smaller negative mean asynchrony and may achieve perfect synchrony (Repp, 1999). It has been shown that musical training also leads to a reduction in the variability of the inter-tap interval during SMS (Repp, 2005). Whilst previous research has consistently suggested that musical training leads to improved performance on an SMS task, most studies were performed in small, specialized groups of professional musicians. Therefore, an investigation of the effects of amateur musical training in a larger sample is of interest. Other potential subject-specific factors that may influence performance, such as gender and strength of handedness have, to my knowledge, not yet been explored. Gender and handedness may affect motor timing because they are associated with structural changes in motor areas that are similar to the effects of musical training in the brain (Aramaki et al., 2006; Gaser & Schlaug, 2003). Such structural changes in brain areas that are involved during motor timing may affect SMS performance.

Based on previous work it was hypothesized that 1) tapping accuracy would be greater for the dominant hand compared with the non-dominant hand, 2) tapping variability would be lower during bimanual tapping compared with unimanual performance, 2) musical training would reduce the negative mean asynchrony and the inter-tap interval variability, 3) variability would be lower in males than in females and 4) a stronger degree of right-handedness would reduce tapping variability.

3.2 Materials and methods

3.2.1 Subjects

Eighty-five subjects participated in this study. All subjects were right-handed as measured on the Edinburgh Handedness Inventory (EHI). One subject with an EHI

score below +30 was classified as ambidextrous and was excluded from further analysis. Four further subjects were excluded based on their poor performance (see section 3.2.4). As such, data from eighty subjects (38 male, mean age 22.8±5.7, mean EHI score of 67.8±18.5, Table 3.1) are reported in the results section of this study. All subjects were naive to the experimental task and none of them reported a history of psychiatric or neurological disorders. None of the subjects was a professional musician. All gave written informed consent prior to participating and this study was approved by the local Research Ethics Committee.

			N	Age	Handedness
Gender	**Musically trained?**	**Level of right handedness**	**Total**	**Mean ± SD**	**Mean ± SD**
Males	Yes	Strong	6	23.5 ± 4.1	86.7 ± 8.8
		Mild	12	22.1 ± 3.4	55.4 ± 12.3
	No	Strong	6	23.5 ± 5.7	94.2 ± 9.2
		Mild	14	24.6 ± 7.3	55.0 ± 11.4
Females	Yes	Strong	5	22.2 ± 2.2	82.0 ± 4.5
		Mild	16	21.3 ± 2.9	61.6 ± 10.6
	No	Strong	9	25.4 ± 11.8	93.3 ± 8.3
		Mild	12	21.1 ± 1.6	55.8 ± 8.2
Total			**80**	**22.8 ± 5.7**	**67.8 ± 18.5**

Table 3.1: Demographic data. Participants were divided according to gender, musical training and handedness. Classification of musical training was based on self report of previous training in the musical training questionnaire. Handedness groups were defined according to their scores of the Edinburgh Handedness Inventory (EHI) scale. Strongly right-handed indicates an EHI of 80 or above and handedness in the mildly right-handed group ranged from 30-80.

3.2.2 Questionnaires

Prior to the experiment, subjects completed a short questionnaire concerning musical training and the Edinburgh Handedness Inventory (Oldfield, 1971). The EHI provides a scale ranging from -100 (completely left handed) to +100 (completely right handed) based on 10 questions regarding preferred handedness in

everyday tasks. In order to explore the relationship between handedness and SMS performance, all subjects were divided into a strongly right-handed group with handedness scores of 80 or above (n=24, 30%) and a mildly right-handed group with scores below 80. The musical training questionnaire included questions concerning rhythmic and musical abilities of the subjects. In particular, subjects were asked whether they 1) enjoyed listening to music and 2) had had any musical training (if the answer was yes, the subject was asked to write details of the training). For the question on previous musical training, any form of training was regarded, including self-taught instrument play, music GSCE's and singing. Based on the musical training questionnaire, the group was subdivided into those who reported to have received musical training (n=39, 49%) and those who did not. The level of musical training ranged from self-taught play to the highest level (grade 8) as defined by the Associated Board of the Royal Schools of Music, UK. The type of training included a variety of musical instruments as well as singing lessons. None of the subjects was a professional musician. Demographic details of all groups are summarized in Table 3.1

3.2.3 Stimuli and task conditions

All subjects performed an identical auditory paced SMS task. The task consisted of three conditions, in which subjects were asked to tap either (1) with their right index finger (dominant), (2) left index finger (non-dominant), or (3) with both index fingers at the same time (bimanual). The pacing stimulus was a simple isochronous auditory sequence consisting of metronome tones at a frequency of 500 Hz and duration of 50 ms, presented at an inter-onset interval (IOI) of 600 ms. Subjects were asked to press a keyboard button (m for right finger, z for left finger) in synchrony with the auditory stimulus, aiming for their button presses to coincide with each tone. Following a 30 second practice block, each condition was repeated twice in a total of 6 blocks of 3 minutes (300 stimuli) each, with periods of rest in between. The order of the conditions was pseudo-randomized and subjects were encouraged to take sufficient rest between the blocks. At the start of each block instructions appeared on the screen indicating the condition and reminding the

subject of the response buttons. During the blocks subjects viewed a fixation cross in the centre of the screen. Control of stimuli and recording of behavioural responses was performed using Presentation® software (version 12.8, www.neurobs.com).

3.2.4 Analysis

The behavioural data were analyzed using MATLAB (Mathworks, Natick, MA, USA). From each of the six experimental blocks, the first ten taps were discarded to allow the subject to establish tapping synchrony, which left 290 pacing stimuli per block and a total of 580 stimuli in each condition. Prior to analysis, subjects who responded to less than 480 stimuli in any experimental condition were removed from further analysis (n = 2).

Tap-tone asynchronies were defined as the delay between the button press and the onset of the corresponding pacing stimulus. A negative value indicated that the response preceded the pacing tone. For each subject, the tap-tone asynchronies were averaged over two blocks for the three different conditions after the removal of outliers (values greater or less than two standard deviations away from the subject mean). Outliers are defined as observations that deviate markedly from the rest of the sample in which they occur and various approaches to outlier removal are available (Grubbs, 1969). In the case of normally distributed data, adopting a cut-off of two standard deviations away from the mean results in the removal of 4.6% of the tail, and a cut-off of three standard deviations removes 0.3%. Alternative, principled model-based methods for outlier removal such as Grubbs' method for extreme studentized deviates and Chauvenet's criterion are also available (Hodge & Austin, 2004). The cut-off of two standard deviations adopted in this Chapter and throughout this thesis results in the removal of 4.6% of data points per normally distributed sample. As this method effectively reduces the width of the tails in the sample distribution, it results in a decrease in the variability of the data. Hence, inclusion of outliers would affect the variability results

presented below. However, some form of outlier removal is essential in the analysis of sensorimotor synchronization data (Repp, 2010).

The first-order linear phase correction model described in Chapter two was used to obtain parameter estimates for error correction, motor variability and central variability from the empirical inter-response interval (IRI) data (Vorberg & Schulze, 2002). To this end, autocovariance estimates of the IRI time series were computed for lag 0 to lag 2 with the use of the 'autocov' script available from the Matlab file exchange (Feldman, 2006). The IRI time series were linearly detrended prior to autocovariance estimation with the use of the standard 'detrend' script in Matlab to ensure stationarity. The average lag 0 autocovariance estimate was 2963 (SD 3371) for tap-tone asynchrony and 4436 (SD 4898) for the IRI. At lag 1 the average was 1935 (SD 2258) for asynchrony and -442 (SD 987) for IRI and at lag 2 the average was 1462 (SD 1727) for asynchrony and -146 (SD 510) for IRI. These figures suggest that the data generally match the predictions from the linear phase correction model (see Figure 2.1 for model predictions). Although IRI dependencies, that are not predicted beyond lag 1 by the linear phase correction model, occur at greater lags in the experimental data. Any resulting negative estimates of motor variance were set to zero (1.1%). Two further subjects were removed prior to statistical analysis due to extreme outlier values for error correction ($\alpha > 9$) or for the motor variability estimate ($\sigma_M^2 > 3000$).

*3.3 **Results***

Subjects tapped, on average, 56 ms (SD 49 ms) before the onset of the pacing stimulus, demonstrating an anticipatory negative mean asynchrony. The average motor variability was 221 ms^2 (SD 243 ms^2) and the average central variability was 1116 ms^2 (SD 1590 ms^2). The average estimated error correction parameter (α) was 0.29 (SD 0.16).

A multivariate, repeated measures, analysis of variance (MANOVA) was performed on the measures for mean tap-tone asynchrony, IRI standard deviation,

alpha and motor- and central- variance components. Two within-subject factors described the hand used in the task (left or right) and the condition (unimanual or bimanual) and between-subject factors described previous musical training, gender and strength of right-handedness (>80 EHI compared with <80 EHI).

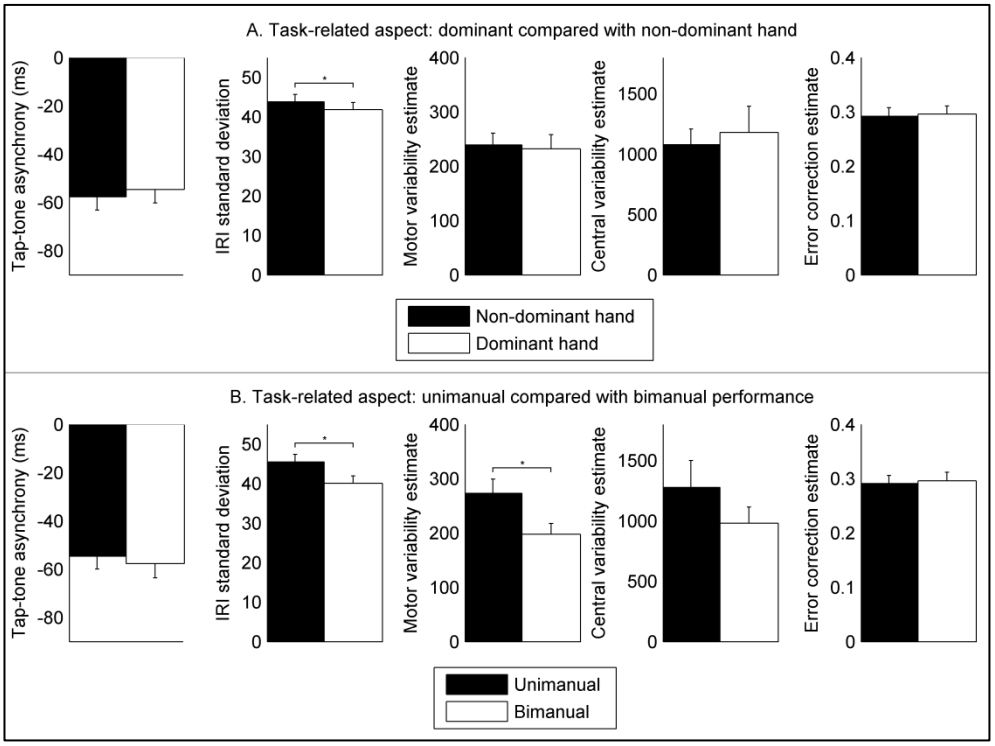

*Figure 3.1: Effects of task-related aspects. The influences of the hand used (dominant or non-dominant, A) and of the condition (unimanual or bimanual, B) are shown for tap-tone asynchrony, inter-response interval (IRI) standard deviation, motor variability estimates, central variability estimates and error correction estimates. The data shown are group averages and the error bars represent one standard error. Significant main effects in the MANOVA are indicated by * (p<.05). Variability was significantly greater in the non-dominant hand compared with the dominant and also during unimanual SMS compared with bimanual SMS.*

3.3.1 Task-related aspects

The within-subject factor of the hand used (dominant or non-dominant) had a significant main effect on IRI variability [$F(8,72)$ = 9.4, MSE = 264.6, p = .003] such that variability was lower during performance with the dominant right hand compared with left-handed performance (Figure 3.1 A). The advantage of the dominant hand was evident in both unimanual and bimanual performance. There was no significant difference between performance with the dominant and non-dominant hand on measures of asynchrony, motor or central variability components or on error correction ($p > .1$).

The within-subject factor of condition (unimanual or bimanual) had a significant main effect on IRI variability [$F(8,72)$ = 28.7, MSE = 1957.1, $p < .001$] and on motor variability [$F(8,72)$ = 11.9, MSE = 383717.9, p = .001] and a trend-level effect on central variability [$F(8,72)$ = 3.95, MSE = 5960000, p = .051]. Here, variability was lower in bimanual tapping than during unimanual performance (Figure 3.1 B). There was no significant difference between uni- and bi-manual performance on measures of asynchrony or error correction ($p > .2$).

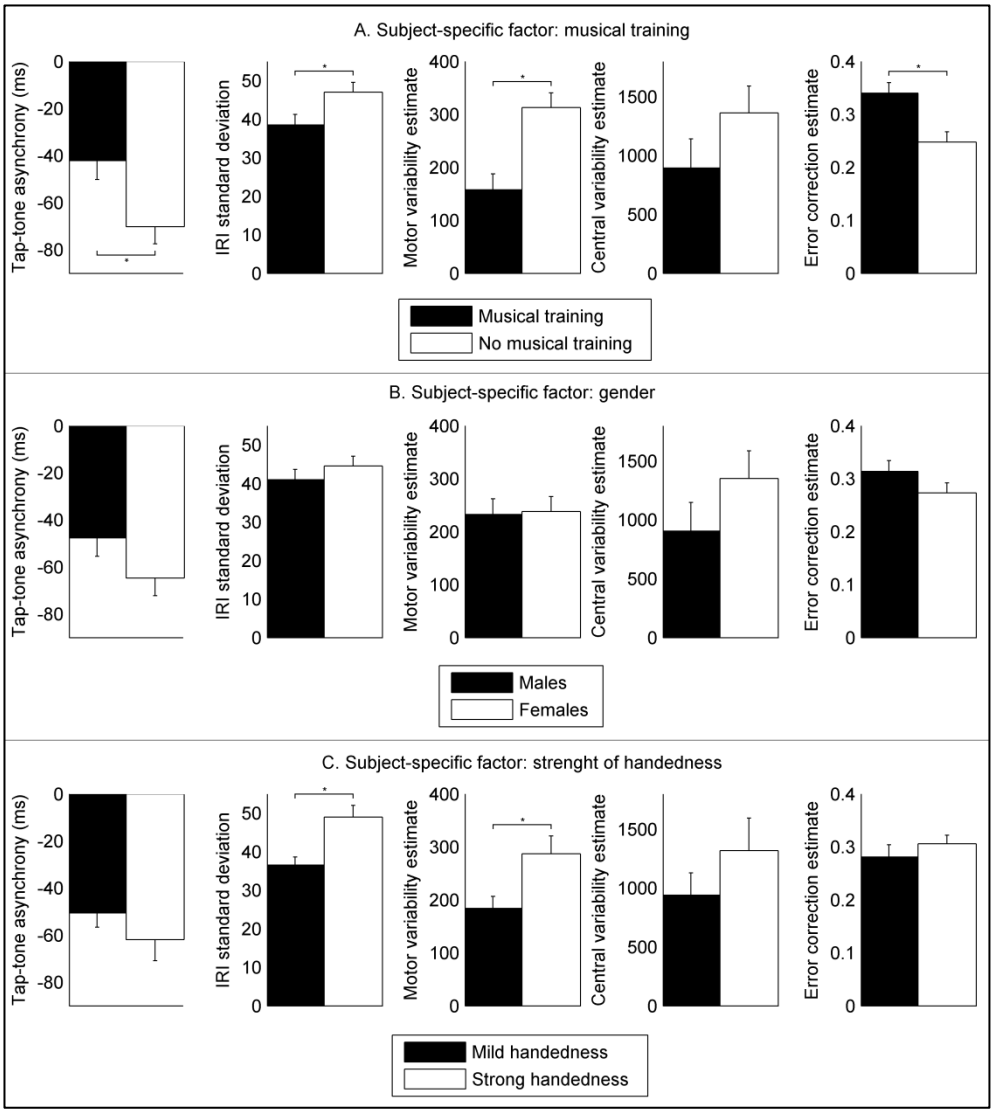

*Figure 3.2: Effects of subject-specific factors. The influences of the musical training (A), gender (B) and the level of right-handedness (C) are shown for tap-tone asynchrony, inter-response interval (IRI) standard deviation, motor variability estimates, central variability estimates and error correction estimates. The data shown are group averages and the error bars represent one standard error. Significant main effects in the MANOVA are indicated by * ($p<.05$). Musical training influenced all measures of SMS performance apart from the central variability estimate. The results also showed that variability was lower in mildly right-handed subjects (Edinburgh Handedness Inventory score < 80) compared with strongly right-handed subjects.*

3.3.2 Subject-specific factors

Between subject results show a significant main effect of musical training on asynchrony [$F(8,72)$ = 6.7, MSE = 53238.1, p = .012], IRI variability [$F(8,72)$ = 5.1, MSE = 4930.7, p = .023], motor variability [$F(8,72)$ = 14.5, MSE = 1633000, p < .001] and error correction [$F(8,72)$ = 10.9, MSE = 0.57, p = .001]. These findings indicate that musically trained individuals had a lower tap-tone asynchrony, lower IRI variability, lower motor component variability and increased error correction (as shown by a higher alpha) compared with untrained subjects (Figure 3.2 A).

There was no significant main effect of gender on any of the performance measures (p > .1) However, the gender by task interaction effect was significant for error correction [$F(8,72)$ = 7.1, MSE = .11, p = .009]. Post hoc investigation of this interaction effect showed that there was a significant gender difference in bimanual error correction (p = .015), such that females exhibited lower error correction estimates than males during bimanual SMS (Figure 3.3 A). During unimanual SMS there was no gender difference in error correction performance (p > .9). Furthermore, the gender by musical training interaction effect was also significant for error correction [$F(8,72)$ = 6.4, MSE = .34, p = .014]. Post hoc comparisons showed that musical training led to a significant increase in error correction in males (p < .001), but not in females (p > .5) (Figure 3.3 B).

The between-subject factor for strength of right-handedness had a significant main effect on IRI variability [$F(8,72)$ = 11.5, MSE = 10501.3, p = .001] and on the motor variability component[$F(8,72)$ = 6.4, MSE = 719027.9, p = .014]. Here, both IRI and motor variability were lower in mildly right-handed subjects (EHI<80) compared with strongly right-handed subjects (EHI>80) (Figure 3.2 C). There was no significant effect of the strength of right-handedness on measures of asynchrony, central variability or error correction (p > .2).

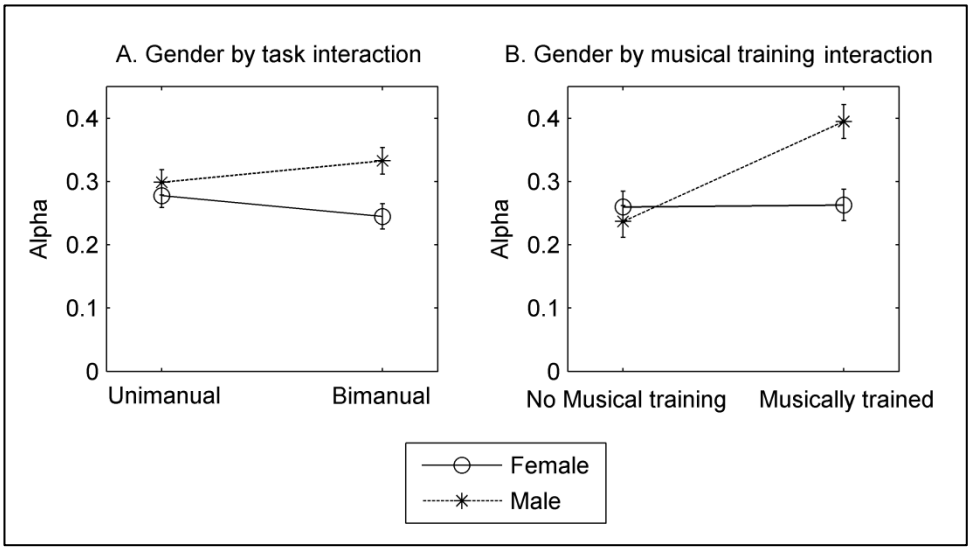

Figure 3.3: Interaction effects on the error correction estimate (alpha) between gender and task and between gender and musical training. Error bars represent one standard error. Males performed significantly more error correction than did females during bimanual SMS, but the difference was not significant during unimanual performance (A). There was a significant effect of musical training (such that musical training led to an increased error correction estimate) in males, but not in females (B).

3.4 Discussion

The aim of this study was to investigate the effects of task-related aspects and of subject-specific factors on SMS performance in a large cohort of healthy subjects (n=80). The results showed that task-related aspects such as the hand used (dominant or non-dominant) and the condition (uni- or bi-manual) significantly affected tapping variability. Furthermore, subject-specific factors of amateur musical training, gender and the level of right-handedness also affect motor timing ability and should be carefully considered when SMS performance is compared between groups. In the remainder of the discussion potential neural mechanisms that may underlie these effects are proposed.

3.4.1 Task-related aspects

The results of this study revealed that tapping variability was lower during performance with the dominant (right) hand compared with the non-dominant hand (Figure 3.1), consistent with previous research (Hammond, 2002). There is evidence for an anatomical asymmetry in the primary motor cortex associated with hand preference. For example, the central sulcus of the dominant primary motor cortex was larger compared with the non-dominant motor cortex, particularly in men (Amunts et al., 1996). There is also evidence for a functional asymmetry, because the extent of contralateral primary motor cortex activity was greater during performance with the dominant hand compared with the non-dominant hand during a sequential movement task (Dassonville et al., 1997). Hence, the relative stability of SMS performance with the dominant right hand may be associated with the size and activity of the dominant primary motor cortex.

The results showed that tapping variability was lower during bimanual SMS than in unimanual SMS (Figure 3.1), consistent with earlier findings (Drewing & Aschersleben, 2003; Helmuth & Ivry, 1996; Pollok et al., 2007). However, to my knowledge, this study is the first to suggest that the bimanual advantage for SMS may be reflected in both the central- and the motor- variability components. This finding was unexpected given that previous research has shown that the bimanual advantage in continuation tapping was due to a decrease in the central variability component alone (Helmuth & Ivry, 1996). It has been suggested that bimanual continuation tapping may be more stable because it combines two separate central timing mechanisms that are each independently used to control one of the hands during unimanual performance (Helmuth & Ivry, 1996). Alternatively, the decrease in bimanual variability may be related to an increase in sensory feedback from both hands (Drewing & Aschersleben, 2003). Both hypotheses can account for increased accuracy of the central timing component. However, they do not explain the decrease in motor variability during bimanual tapping because neither of the hypotheses addresses the issue of response implementation variability.

It is possible that the reduction in bimanual motor variance indicates that motor implementation is not a fully independent, effector-specific process, but rather, benefits from the synchronized use of both hands. This interpretation is consistent with previous work that showed that reaction time variability was lower in bimanual than in unimanual responses (Eliassen et al., 2000). One may suspect that the reduction in motor variability may reflect problems surrounding parameter estimation (Semjen et al., 2000). However, this is unlikely because there was still a significant reduction in motor variance when subjects with one or more negative motor variance estimates (for whom estimation problems may be suspected) were excluded from the analysis. Alternatively, a change in perceptual delay could produce the reduction in motor variance, because perceptual delay variance is indistinguishable from motor variance in the linear phase correction model (Semjen et al., 2000; Vorberg & Schulze, 2002). Hence, it is possible that the perceptual delay becomes more stable when somatosensory information is received from both hands, which may be reflected as a decrease in the motor variability estimate.

Neurophysiologically, the bimanual advantage in tapping variability may be related to differential patterns of inter-hemispheric connectivity between the motor regions. Electroencephalography (EEG) coherence studies have shown 1) that inter-hemispheric connectivity between the primary motor cortices is reduced in bimanual SMS compared with unimanual performance (Serrien, 2008) and 2) that bimanual connectivity is driven from the dominant to the non-dominant motor cortex (Serrien et al., 2003). During unimanual performance, interhemispheric connectivity between the primary motor cortices is inhibitory and is directed from the active hemisphere contralateral to the moving limb to the ipsilateral primary motor cortex (Serrien et al., 2003). Suppression of the ipsilateral motor cortex may be required in order to avoid undesirable mirror movements (Duque et al., 2005; Perez & Cohen, 2009). During bimanual tapping, mirror movements are no longer suppressed which may allow increased emphasis on timing and may thereby partly explain the reduction in bimanual tapping variability. The neural basis of unimanual and bimanual SMS is investigated further in Chapter seven.

3.4.2 Subject-specific factors

The findings presented in this study indicated that musical training significantly affected tap-tone asynchrony, IRI variability, motor variability and error correction (Figure 3.2). Musical training led to an average reduction in tap-tone asynchrony of 28 ms, which is consistent with previous studies (Aschersleben, 2002). These findings show that musical training at an amateur level significantly improved both temporal accuracy and stability of motor responses. Previous research has shown that musical training caused structural changes in the brain even at an amateur level. In particular, grey matter volume was increased in musically trained individuals in motor and pre-motor cortex, auditory and parietal cortex and in the cerebellum (Gaser & Schlaug, 2003). These structures are consistently involved during sensorimotor synchronization (Pollok et al, 2006). Increased grey matter volume in structures involved during SMS may explain the improvements in motor timing performance in musically trained individuals. Additionally, the observation that the size of the anterior corpus callosum was increased as a result of musical training may suggest that interhemispheric functional connectivity was altered (Lee et al., 2003). As such, musical training may modify grey matter size and interhemispheric connectivity of the motor cortices in such a way as to enhance the efficiency of motor timing performance.

The findings of this study revealed a significant gender by musical training interaction effect on the estimate for ongoing error correction. In particular, there was a significant difference in error correction between subjects with musical training compared with subjects with no musical training in males, but not in females (Figure 3.3). A similar gender by musical training interaction was previously reported in a morphometric magnetic resonance imaging study of corpus callosum size (Lee et al., 2003). In this study, a significant increase in the size of the anterior corpus callosum was associated with professional musical training in males, but not in females. The authors proposed that this gender difference might be related to the earlier finding that motor control in the untrained female brain was more symmetric compared with the strong hemispheric

dominance normally found in males (Amunts et al., 2000). Musical training would therefore lead to a greater shift towards symmetry in males than in females. Accordingly, the gender-specific increase in error correction found in this study may be associated with an increase in interhemispheric connectivity in males. This explanation is consistent with the finding of a significant gender by task interaction effect, which showed that males perform more error correction than females during bimanual SMS, but not during unimanual SMS.

Contrary to the hypothesis, the results of this study revealed that SMS variability was lower in mildly right handed subjects compared with strongly right-handed subjects (Figure 3.2). This surprising finding may be explained by the degree of anatomical and functional asymmetry in the primary motor cortices. For example, previous research has shown that the asymmetry in the size of the primary motor cortices was more prominent in strongly right-handed males compared with more mixed-handed subjects (Amunts et al., 2000). Additionally, stronger hand preference was associated with a greater extent of activation in the contralateral primary motor cortex and less in the ipsilateral primary motor cortex during a sequential movement task (Dassonville et al., 1997). Hence, it is possible that the decreased variability in mildly right-handed subjects may reflect a more symmetric organization of motor regions in the brain. This symmetry may be linked to an improvement in performance in line with the advantage of musically trained subjects, which may be also associated with anatomical and functional symmetry.

In conclusion, the results presented in Chapter three showed that task-related aspects such as the hand used and the condition (unimanual or bimanual) and subject-specific factors such as musical training, gender and handedness significantly affected SMS performance. In Chapter four, the role of the left and right primary motor cortices in the control of unimanual and bimanual sensorimotor timing is assessed further.

4 Study 2: The role of the primary and pre-motor cortices in sensorimotor timing

4.1 Aims and rationale

The results of Chapter three revealed that tapping variability decreased during bimanual in-phase SMS compared with unimanual SMS, consistent with previous research (Helmuth & Ivry, 1996; Pollok et al., 2007). It was suggested that suppression of mirror movements is not required during bimanual tapping, which may explain the bimanual advantage in tapping variability. Aramaki and colleagues showed that the non-dominant primary motor cortex was significantly less active during bimanual SMS compared with unimanual performance with the non-dominant hand (Aramaki et al., 2006). There was no difference in the amount of activity in the dominant primary motor cortex between uni- and bi-manual SMS. Electroencephalographic (EEG) coherence studies have revealed that inter-hemispheric connectivity was driven by the dominant primary motor cortex during bimanual SMS (Serrien et al., 2003). Hence, these findings may suggest that bimanual SMS is asymmetrically controlled by the dominant primary motor cortex.

As discussed in Chapter one, the previous literature provides consistent evidence for a specialized modulatory role of the left pre-motor cortex in unimanual motor timing. However, much less is understood about the functional significance of the left pre-motor cortex for motor timing. In addition, there is some evidence that the right pre-motor cortex may become increasingly important during bimanual SMS. An MEG coherence study has suggested that interhemispheric connectivity between the bilateral pre-motor cortices was directed from the right to the left hemisphere during bimanual in-phase SMS (Pollok et al., 2005). This may indicate that the right pre-motor cortex drives activity in the left pre-motor cortex, or it may suggest that information is integrated in the left pre-motor region. There is evidence for right pre-motor cortex involvement in tasks of increased complexity such as anti-phase bimanual SMS (Aramaki et al., 2010; Meyer-Lindenberg et al., 2002; Sadato et al., 1997; van den Berg et al., 2010). However, during unimanual

SMS, the right pre-motor cortex was exclusively involved when the task was performed with the non-dominant left hand (Aramaki et al., 2010).

To elucidate the lateralized function of the primary and pre-motor cortices during uni- and bi-manual sensorimotor timing further, this study aimed to investigate the effect of suppression and facilitation TBS applied over the left and right primary and pre-motor cortices on SMS performed uni- and bi-manually. The linear phase correction model for SMS (Chapter two) was adopted in addition to conventional measures such as the tap-tone asynchrony and the variability of the inter-response intervals in order to capture the complex dynamics of SMS performance. It was hypothesized that 1) suppression TBS over the dominant left primary motor cortex would affect bimanual and right-handed unimanual SMS and 2) suppression of the left pre-motor cortex would affect unimanual SMS performance in both hands, whereas suppression of the right pre-motor cortex would affect bimanual SMS and left-handed unimanual SMS.

4.2 Materials and methods

4.2.1 Subjects

Ninety-seven subjects participated in this study. All subjects were right-handed as measured on the Edinburgh Handedness Inventory (EHI). Nine subjects were excluded based on their poor performance (see section 4.2.4). As such, data from 88 subjects (43 male, mean age 22.4 ± 5.4, mean EHI score of 66.4 ± 18.8, Table 4.1) are reported in the results section of this study. They were naive to the experimental task and did not report any history of psychiatric or neurological disorders. None of them was a professional musician. All subjects gave written informed consent prior to participating. This study was approved by the local Research Ethics Committee.

4.2.2 Stimuli and task conditions

All subjects performed an identical auditory paced SMS task before and after Theta burst Transcranial Magnetic Stimulation. The task consisted of three conditions, in which subjects were asked to tap either with their (1) right index finger, (2) left index finger, or (3) with both index fingers at the same time (bimanual). The pacing stimulus was a simple isochronous auditory sequence consisting of metronome tones at a frequency of 500 Hz and duration of 50 ms, presented at an inter-onset interval (IOI) of 600 ms. Subjects were asked to press a keyboard button (m for right finger, z for left finger) in synchrony with the auditory stimulus, aiming for their button presses to coincide with each tone. Following a 30 second practice, each condition was repeated twice in a total of 6 runs of 3 minutes each, with periods of rest in between. The order of the conditions was pseudo-randomized. At the start of each run instructions appeared on the screen indicating the condition and reminding the subject of the response buttons. During the blocks subjects viewed a fixation cross in the centre of the screen. Control of stimuli and recording of behavioural responses was performed using Presentation® software (version 12.8, www.neurobs.com).

		N	**Age**	**Handedness**
		Total (males)	**Mean ± SD**	**Mean ± SD**
Right primary	Suppression	10 (5)	21.4 ± 1.8	67.5 ± 18.1
motor cortex	Facilitation	10 (5)	24.6 ± 5.3	63.0 ± 18.0
Left primary	Suppression	12 (6)	21.7 ± 3.7	59.2 ± 22.7
motor cortex	Facilitation	9 (4)	24.9 ± 11.8	72.8 ± 29.5
Right pre-motor	Suppression	10 (5)	23.8 ± 8.1	64.0 ± 20.0
cortex	Facilitation	9 (4)	22.7 ± 2.9	65.6 ± 13.3
Left pre-motor	Suppression	9 (5)	21.6 ± 2.1	66.7 ± 10.3
cortex	Facilitation	10 (5)	20.8 ± 3.0	72.5 ± 18.3
Sham TBS		9 (4)	20.8 ± 1.4	68.9 ± 14.7
Total		**88 (43)**	**22.4 ± 5.4**	**66.4 ± 18.8**

Table 4.1: Demographic data. Participants were assigned to one of nine TBS groups. The TBS groups reflect the coil position (right primary motor cortex, left primary motor cortex, right pre-motor cortex, left pre-motor cortex or sham) and

the TBS protocol (suppression cTBS, and facilitation iTBS). Sham TBS was performed by placing the coil perpendicular to the head over the vertex.

4.2.3 TBS protocol

All subjects were randomly assigned into nine different TBS groups as described in Table 4.1 and received either suppression or facilitation TBS. The suppression protocol consisted of 40 seconds of continuous TBS and facilitation involved 190 seconds of intermittent TBS (Huang et al., 2005). In both suppression and facilitation TBS protocols, a total of 600 TBS pulses were applied at 80% of the resting motor threshold using a 70mm figure-of-eight coil and a Magstim Super Rapid stimulator (Magstim Company, Whitland, UK). The resting motor threshold of each subject was determined using the thumb movement visualization method (Pridmore et al., 1998). The target location for primary motor cortex TBS was experimentally defined as the coil position that induced the maximum thumb movement ('motor hotspot'). The target location for pre-motor cortex TBS was identified by moving the coil 2 cm anterior to, and 1 cm medial from, the left or right motor hotspot (Bestmann et al., 2005). Sham TBS was performed by placing the coil perpendicular to the head over the vertex. Immediately after stimulation, all subjects performed the identical SMS task. During and following TBS, none of the subjects reported any adverse effects.

4.2.4 Analysis

The behavioural data were analyzed using MATLAB (Mathworks, Natick, MA, USA). From each of the six experimental runs the first ten taps were discarded to allow the subject to establish tapping synchrony, which leaves 290 pacing stimuli per run and a total of 580 stimuli in each condition. Prior to analysis, subjects who responded to less than 400 stimuli in any experimental condition were removed from further analysis (n = 4).

Tap-tone asynchronies were defined as the delay between the button press and the corresponding pacing stimulus, where a negative value indicates that the response

preceded the pacing tone. The tap-tone asynchronies were averaged for each condition over two runs after the removal of outliers (values greater or less than two standard deviations away from the subject mean asynchrony). Inter-response intervals (IRIs) were defined as the time in milliseconds between two subsequent responses. The total variance of the IRIs was calculated for each condition after the removal of IRIs that deviate more than 40% from the target interval (<360 or >840 ms). Subsequently, error correction and motor- and central- variance components were estimated based on the Wing-Kristofferson model as described in Chapter two. Autocovariance estimates were computed for lag 0 to lag 2 with the use of the 'autocov.m' script available from the Matlab file exchange (Feldman, 2006). Linear drift was removed from the IRI data prior to variance estimations with the use of the standard Matlab detrending procedure. The average lag 0 autocovariance estimate averaged between pre and post TMS sessions was 3197 (SD 4441) for tap-tone asynchrony and 4644 (SD 5213) for the IRI. At lag 1 the average was 2069 (SD 3036) for asynchrony and -437 (SD 888) for IRI and at lag 2 the average was 1568 (SD 2423) for asynchrony and -164 (SD 533) for IRI. These figures suggest that the data generally match the predictions from the linear phase correction model (see Figure 2.1 for model predictions). Although IRI dependencies, that are not predicted beyond lag 1 by the linear phase correction model, occur at greater lags in the experimental data. There were no systematic differences in the autocovariance estimates between the data acquired before and after TMS. Negative estimates of motor variance were set to zero (10.7%). Five further subjects were removed prior to statistical analysis due to extreme outlier values for error correction ($\alpha > 9$) or for the motor variability estimate ($\sigma_M^2 > 3000$).

4.3 Results

To explore whether there were any between-group differences in performance prior to TBS, a two-way ANOVA was performed with within-subject factors for the hand used (left or right) and for the condition (unimanual or bimanual) and a between-subject factor for TBS group. Results indicate that there were no differences in pre-TBS performance on any of the performance measures ($p > .1$).

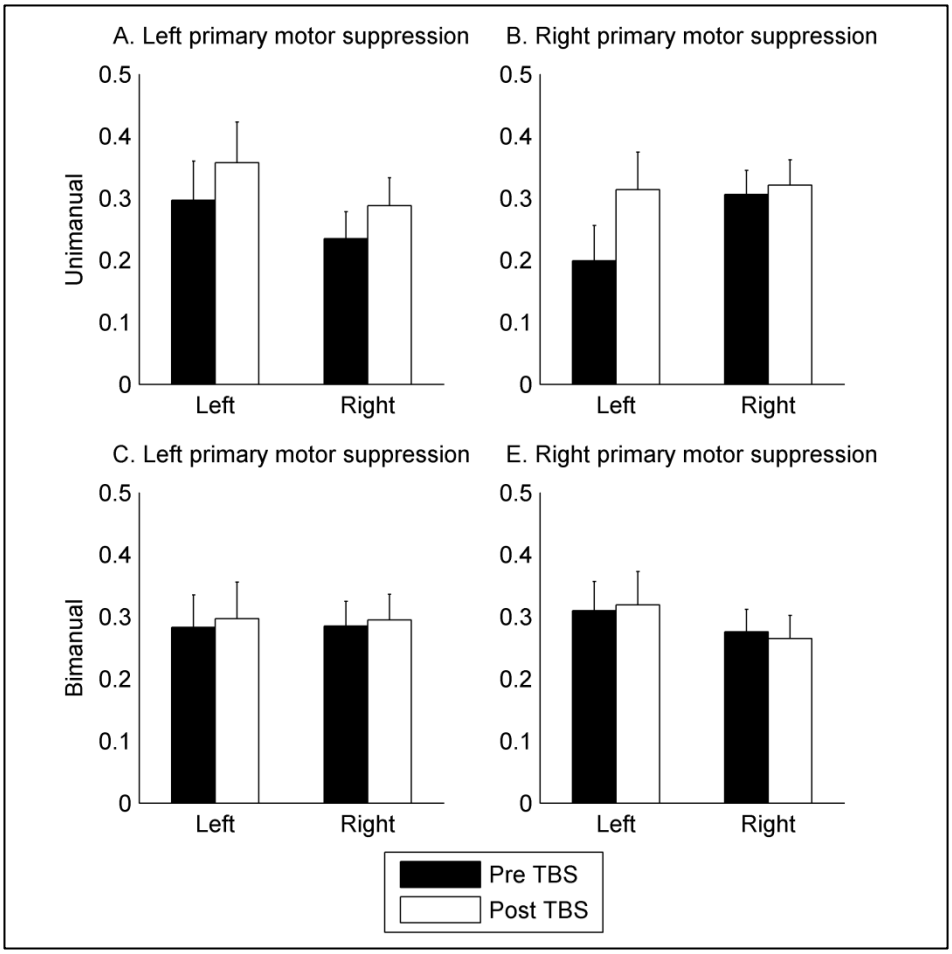

Figure 4.1: Effects of suppression TBS over the primary motor cortex on the error correction estimate during uni- and bi-manual SMS. Performance before TBS is shown in black bars and performance after TBS is shown in white bars. During unimanual SMS, suppression TBS over the right primary motor cortex led to a significant increase in the error correction estimate in the left hand (B). However, this effect may be due to a spuriously low baseline error correction estimate before TBS. The error bars represent one standard error.

The effects of TBS were assessed separately for primary motor cortex suppression, primary motor cortex facilitation, pre-motor cortex suppression, pre-motor cortex facilitation and for sham TBS. To investigate the effects of TBS (suppression or facilitation) over the left and right target (primary or pre-motor cortex) on unimanual SMS performance, a three-way ANOVA was performed with within-

subject factors for the hand used (left or right) and TBS (pre or post stimulation) and a between-subject factor for the TBS side (left or right primary motor cortex). Bimanual SMS performance was assessed in a separate three-way ANOVA. In each analysis, the performance measures of interest included tap-tone asynchrony, standard deviation of the IRI and estimates for motor and central variability and for error correction derived from the linear phase correction model. The results of each analysis are described below.

4.3.1 Primary motor cortex

In the analysis of unimanual data, results indicated that there was a significant main effect of suppression TBS over the primary motor cortex on the error correction estimate [$F(2,20) = 8.7$, $MSE = 0.038$, $p = .008$], such that the estimated proportion of the previous tap-tone asynchrony that is corrected increased after TBS. On further inspection, this increase in ongoing error correction was driven by the effect of suppression TBS over the right primary motor cortex on performance with the left hand which may be caused by a spuriously low baseline error correction estimate before TBS (Figure 4.1). The three-way TBS by hand by TBS side interaction effect was significant for the standard deviation of the IRI [$F(2,20) = 10.2$, $MSE = 899.4$, $p = .005$]. Post-hoc investigation showed that suppression TBS over the primary motor cortex decreased variability in the contralateral hand, but increased variability in the ipsilateral hand, although pairwise comparisons were not significant ($p > .05$). In the analysis of the bimanual data, there were no significant effects of suppression TBS over the primary motor cortices on any of the performance measures ($p > .05$).

During unimanual performance, facilitation TBS over the primary motor cortex resulted in a significant TBS by hand interaction effect on the motor variability estimate [$F(2,17) = 4.8$, $MSE = 87058.3$, $p = .042$]. However, post-hoc investigation showed that facilitation TBS did not significantly affect motor variability in the left or the right hand ($p > .09$). There were no further significant main effects or interaction effects following facilitation TBS. During bimanual

performance, facilitation TBS over the primary motor cortex did not significantly affect any of the performance measures ($p > .05$).

4.3.2 Pre-motor cortex

In the analysis of the unimanual data, there was a significant main effect of suppression TBS over the pre-motor cortices [$F(2,19) = 7.1$, $MSE = 0.091$, $p = .014$] and a significant hand by TBS interaction effect [$F(2,19) = 5.1$, $MSE = 0.029$, $p = .037$] on the error correction estimate. Here, there was a significant increase in the estimated error correction after TBS, and the effect was most pronounced in performance with the non-dominant left hand. On further inspection, suppression of the right pre-motor cortex only affected error correction performance in the contralateral left hand, whereas suppression of the left pre-motor cortex led to an increase in the error correction estimate for both hands (Figure 4.2). The three-way TBS by hand by TBS side interaction effect was significant for the motor variability component [$F(2,19) = 5.6$, $MSE = 602768.4$, $p = .03$]. However, post-hoc pairwise comparisons did not reveal a significant effect of suppression TBS over the pre-motor cortex on motor variability. In the analysis of the bimanual data, there was a significant main effect of TBS on the error correction estimate [$F(2,19) = 5.1$, $MSE = 0.076$, $p = .038$], such that the estimated error correction parameter increased following suppression TBS over the pre-motor cortices. Further investigation showed that suppression of both the left and the right pre-motor cortex equally affected the error correction estimate (Figure 4.2). There were no further significant main effects or interaction effects on bimanual performance following suppression TBS over the pre-motor cortices.

There were no significant main effects or interaction effects after facilitation TBS over the pre-motor cortices in the analysis of unimanual or bimanual performance ($p > .07$).

4.3.3 Sham TBS

There were no significant effects of sham TBS on any of the performance measures in unimanual or bimanual SMS performance ($p > .05$).

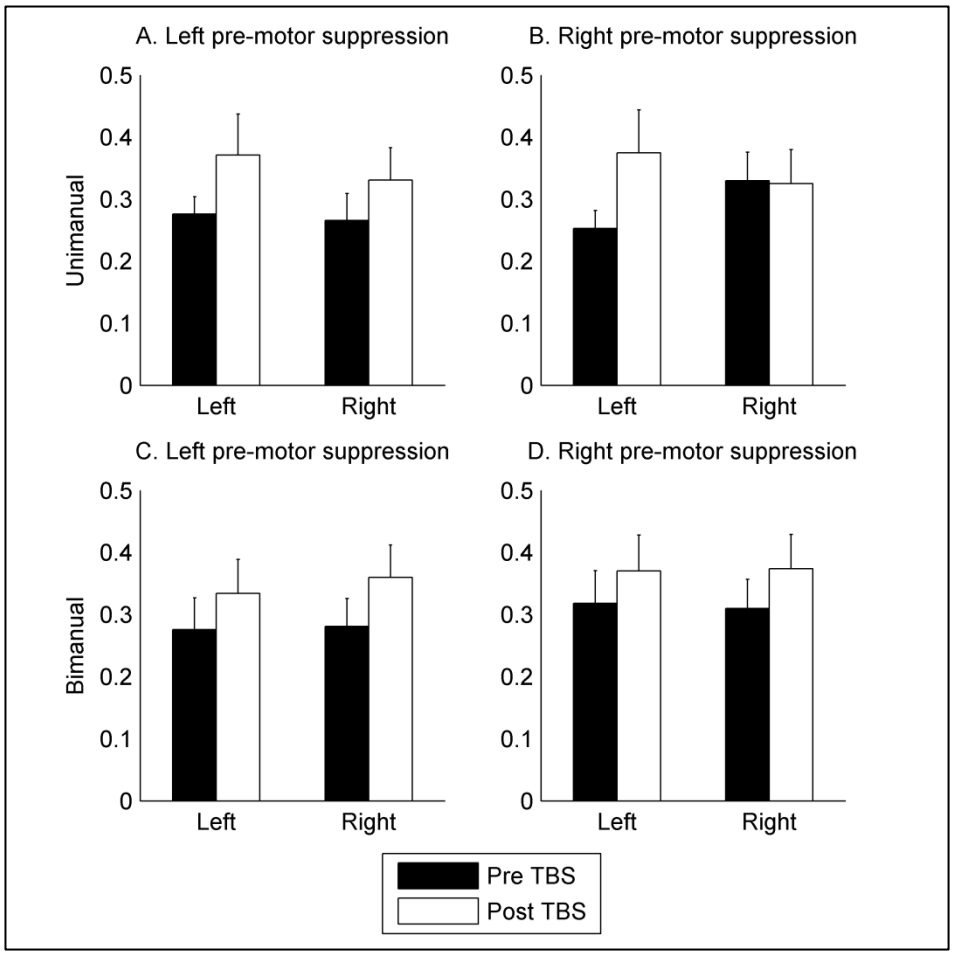

Figure 4.2: Effects of suppression TBS over the pre-motor cortex on the error correction estimate during uni- and bi-manual SMS. Performance before TBS is shown in black bars and performance after TBS is shown in white bars. During unimanual SMS, suppression TBS over the left pre-motor cortex led to a significant increase in the error correction estimate in both hands (A), whereas suppression over the right pre-motor cortex only affected error correction in the contra-lateral left hand (B). During bimanual SMS, suppression TBS over either the left or right

pre-motor cortex resulted in a significant increase in the error correction estimate in both hands (C & D). The error bars represent one standard error.

4.4 Discussion

This study used the linear phase correction model in order to investigate the role of the left and right primary and pre-motor cortices in uni- and bi-manual SMS. The main finding of this study was that unimanual and bimanual performance were differentially affected by lateralized TBS over the left or right pre-motor cortices. The results showed that suppression TBS over the left pre-motor cortex led to an increase in continuous error correction in both hands during unimanual SMS. In contrast, suppression TBS over the right pre-motor cortex only affected left-handed unimanual performance. Furthermore, the findings showed that bimanual error correction in both hands was affected following suppression of either the left or right pre-motor cortex. An increased error correction estimate suggests that subjects corrected for a greater proportion of the perceived tap-tone asynchrony after TBS suppression over the pre-motor cortex as estimated by the linear phase correction model. These findings suggest that the left-lateralized control of the pre-motor region during unimanual SMS is not maintained in bimanual performance.

During unimanual SMS, TBS suppression over the left pre-motor cortex led to an increase in the error correction estimate for both hands, whereas suppression of the right pre-motor cortex only affected left-handed SMS (Figure 4.2). This finding is consistent with previous research, which suggested that the left pre-motor cortex plays a role in the control of motor timing in both hands (Pollok et al., 2008b). The results presented here also support previous imaging studies that have shown that the right pre-motor cortex was exclusively activated during unimanual SMS performed with the contralateral left hand (Aramaki et al., 2006; Aramaki et al., 2010). When the task was performed bimanually, suppression TBS over either the left or the right pre-motor cortex led to a significant increase in the error correction estimate in both hands (Figure 4.2). This finding suggests that the left hemispheric dominance in the pre-motor cortex for motor control was only evident during

unimanual SMS, whereas the temporal control of both hands appeared to be linked in bimanual SMS. The data presented in this study did not support any lateralized pre-motor dominance during bimanual SMS, because the increase in error correction was equally evident following suppression of both the left and right pre-motor regions. However, these findings are consistent with the hypothesis that bimanual motor timing requires interhemispheric connectivity and coherent activity in both pre-motor cortices (Pollok et al., 2005).

The findings of this study suggested that the role of the pre-motor cortex in the temporal control of movement may be associated with sensorimotor error correction. This hypothesis is tested in Chapter five using an error correction paradigm in which the SMS pacing stimulus contains occasional local timing shifts. The error correction response following these induced timing shifts provides a direct measure of error correction performance that is not mediated by a theoretical model and therefore not susceptible to biases that may be problematic for the linear phase correction model (as discussed in Chapter two).

5 Study 3: The role of the left pre-motor cortex in sensorimotor error correction

5.1 Rationale

The findings presented in Chapter four suggested that the functional role of the pre-motor cortices during sensorimotor timing may be associated with ongoing error correction. Specifically, the results presented in Chapter four indicated that suppression TBS over the pre-motor cortices led to an increase in the estimate for ongoing error correction, which implied that subjects corrected for a greater proportion of the previous tap-tone asynchrony in their subsequent response. There is further evidence to suggest that the pre-motor cortices play a role in the correction of phase shifts. A previous positron emission tomography (PET) study showed that the bilateral pre-motor cortices were activated during the correction of timing shifts (Stephan et al., 2002). The findings suggested that pre-motor activity was specifically associated with shifts that were consciously perceived. In contrast, suppression rTMS over the left pre-motor cortex did not significantly change error correction in a study by Doumas and colleagues (Doumas et al., 2005).

This study aimed to test the hypothesis that the pre-motor cortices are essential for error correction during sensorimotor synchronization. To this end, both continuous and intermittent TBS protocols were applied over the left pre-motor cortex. The effects of TBS on sensorimotor timing and supraliminal error correction were measured during unimanual performance with either the left or the right hand. The focus of this study is on the left pre-motor cortex and on unimanual task performance because the results of Chapter four showed the strongest TBS effects in these conditions.

5.2 Experiment 1

5.2.1 Aims and hypotheses

The aim of Experiment 1 was to examine the effects of continuous and intermittent TBS over the left pre-motor cortex on motor timing during regular SMS and on error correction following supraliminal phase shifts. Based on previous research (Pollok et al., 2008b), it was hypothesized that cTBS over the left pre-motor cortex would lead to an increase in tap-tone asynchrony and variability during regular SMS. It was furthermore hypothesized that cTBS over the left pre-motor cortex would impair error correction performance. Lastly, it was hypothesized that facilitatory iTBS over the left pre-motor cortex may improve timing and error correction performance.

5.2.2 Materials and methods

Subjects

A total of 16 subjects (8 males, mean age 23.3 ± 3.9) took part, all of whom were students at the University of Sheffield. All subjects were right handed (mean Edinburgh Handedness Inventory score of 73.1 ± 19.1). Twelve subjects responded positively when asked whether they had had any previous musical training. The level of musical training ranged from self-taught play to the highest level (grade 8) as defined by the Associated Board of the Royal Schools of Music, UK. None of them was a professional musician. They were naive to the experimental task and did not report any history of psychiatric or neurological disorders. All subjects gave written informed consent prior to participating. This study was approved by the local Research Ethics Committee.

Stimuli and task conditions

All subjects performed an identical auditory paced SMS task before and after TBS on two separate days. The task consisted of four runs that each lasted approximately four minutes. For two of the runs, the pacing stimulus was regular in order to measure SMS performance (one run performed with the left, and one with

the right, index finger). The other two runs were designed to measure error correction performance (one performed with the left, and one with the right, index finger). In the two regular runs used to measure SMS performance, the pacing stimulus was a simple isochronous auditory sequence consisting of metronome tones at a frequency of 500 Hz and duration of 50 ms, presented at an inter-onset interval (IOI) of 600 ms (400 stimuli per run). In the two runs that were designed to measure error correction, occasional supraliminal phase shifts were introduced such that the tone occurred either 90 ms earlier than expected (negative shift), or later than expected (positive shift). Following 10 initial regular tones to allow the subjects to synchronize their tapping to the pacing tone, a total of 20 negative and 20 positive shifts were introduced in semi-random order in each run. At least seven regular stimuli occurred between two subsequent perturbations to allow subjects to re-establish synchronization before each shift. To achieve the sequences, a fixed epoch (T-3 to T+3 in which the shift occurs at time T) was repeated 40 times during which the occurrence of positive and negative shifts was randomized. Between two fixed epochs 1, 2, 3 or 4 stimuli at the standard IOI were added to achieve a semi-random and unpredictable pacing stimulus.

Subjects were instructed to press a keyboard button (‘m’ for right index finger, ‘z’ for left index finger) in synchrony with the auditory stimulus, aiming for their button presses to coincide with each tone. Following a 30 second practice, all four conditions (left hand SMS and error correction and right hand SMS and error correction) were presented in pseudo-randomized order, with periods of rest in between. At the start of each run instructions appeared on the screen indicating the hand that should be used and reminding the subject of the correct response button. During the runs subjects viewed a fixation cross in the centre of the screen. Control of stimuli and recording of behavioural responses was performed using Presentation® software (version 12.8, www.neurobs.com). To assess the perception and randomization of the shifts, all subjects were asked two questions after each run: 1) whether they noticed any irregularities and 2) if so, whether they thought they could predict the irregularities.

TBS protocol

A cross-over design was adopted in order to avoid between-group differences in pre-TBS performance. All subjects returned on two separate days (at least 48 hours apart). On each day the subjects received either continuous or intermittent TBS over the left pre-motor cortex. The order of the two protocols was randomized across the subjects such that half received cTBS on day 1 and half received iTBS on day 1. All subjects were naive to TBS and no information was provided regarding potential differences in the effects between the continuous and intermittent protocols.

Subjects received 40 seconds of continuous TBS (cTBS) or 190 seconds of intermittent TBS (iTBS) between two sessions on each day (Huang et al., 2005). In both the cTBS and iTBS protocols 600 TBS pulses were applied at 90% of the resting motor threshold using a 70mm figure-of-eight coil and a Magstim Super Rapid stimulator (Magstim Company, Whitland, UK). The resting motor threshold of each subject was determined on both days using the thumb movement visualization method over the left primary motor cortex (Pridmore et al., 1998). The target TBS coil position was located by moving 2 cm anterior to, and 1 cm medial from, the left 'motor hotspot' (Bestmann et al., 2005). During and following TBS, none of the subjects reported any adverse effects.

Analysis

The behavioural data were analyzed using MATLAB (Mathworks, Natick, MA, USA). From the two regular runs the first ten taps were discarded to allow the subject to establish tapping synchrony. Performance measures of regular SMS included tap-tone asynchrony, inter-response interval (IRI) and the standard deviation of the IRI. Tap-tone asynchronies were defined as the delay between the button press and the corresponding pacing stimulus, where a negative value indicated that the response preceded the pacing tone. The tap-tone asynchronies were averaged over each run after the removal of outliers (values greater or less than two standard deviations away from the subject mean asynchrony). Inter-response intervals were defined as the time in milliseconds between two

subsequent responses and were averaged over each run. The standard deviation of the ongoing IRI was calculated over each run to provide a measure of sensorimotor timing variability.

Explicit error correction data from the two error correction runs were analyzed in an event-related approach including four taps before and four taps after (T-4 to T+4) each shifted stimulus (T). Within each subject, outlier responses (tap-tone asynchronies more than 2 standard deviations away from the average asynchrony) were identified separately for each position (T-4 to T+4) and were removed prior to averaging. In order to allow a direct comparison of the error correction response in all conditions, the asynchrony during T to T+4 was normalized to range from baseline asynchrony (set to zero) to the maximum initial shift at time T (set to one) and the sign was removed. Baseline performance was defined as the average tap-tone asynchrony over trials T-4 to T-1 (Praamstra et al., 2003; Repp, 2000). The resulting normalized error correction data were averaged over all trials.

5.2.3 Results

Prior to group data analysis, one subject was excluded due to extreme values (more than three standard deviations away from the group mean) for normalized error correction at more than one position during T+1 to T+4. One further subject was removed because of a high number of missed responses in two runs (more than 10% of the total number of pacing stimuli in each run). Data from 14 subjects (6 males, mean age 23.1 ± 3.9, mean EHI 73.2 ± 20.3, 10 with previous musical training) are presented below. Due to the removal of two subjects, 8 subjects received suppression TBS on day one and 6 subjects received facilitation TBS on day one.

The average time between the start of the experiment on day 1 and day 2 was 59 hours (SD 22 hours). Feedback reports acquired following each individual run revealed that all fourteen subjects detected the occurrence of irregularities in the

error correction runs, but were unable to predict the exact temporal occurrence and the direction of the shifts.

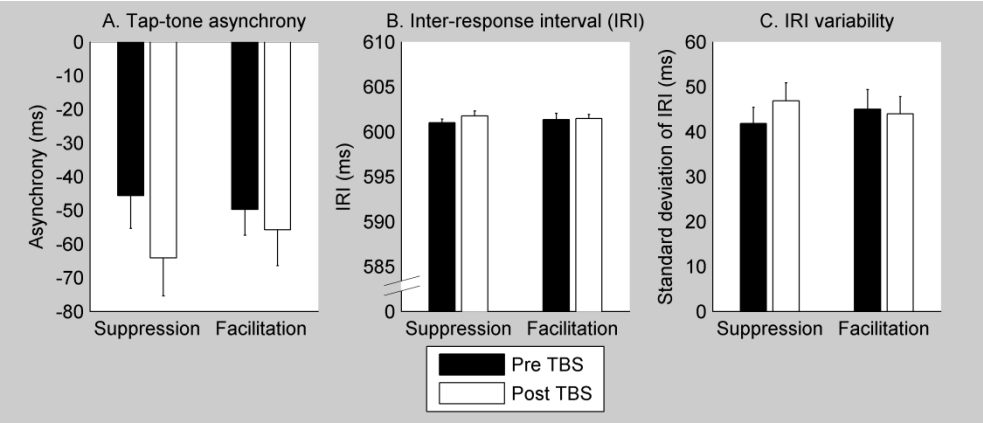

Figure 5.1: Effect of suppression and facilitation TBS over the left pre-motor cortex on timing performance during sensorimotor synchronization. Performance before TBS is shown in black bars and performance after TBS is shown in white bars. There was a significant increase in the tap-tone asynchrony (A), inter-response interval (B) and in the standard deviation of the inter-response interval (C) following suppression TBS over the left pre-motor cortex. Facilitation TBS did not affect performance. Error bars represent one standard error.

Regular SMS results

Firstly, baseline SMS performance data from day 1 and day 2 obtained before TBS were compared. A two-way ANOVA using within-subject factors for the day (day 1 or 2) and for the hand used (left or right hand) showed that there was no significant difference in any of the SMS measures between pre-TBS performance on day 1 and day 2.

A three-way ANOVA with within subject factors for the hand used (left or right), TBS (pre or post) and TBS type (iTBS or cTBS) and a between subject factor for the order of the days (cTBS or iTBS on the first day) was performed on measures of tap-tone asynchrony, standard deviation of the tap-tone asynchrony, IRI and IRI variability. Results indicated a significant interaction effect between TBS type and

TBS on tap-tone asynchrony [*F(1,13)* = 5.64, *MSE* = 1197.4, *p* = .035] and a significant main effect of TBS on tap-tone asynchrony [*F(1,13)* = 4.93, *MSE* = 4106.8, *p* = .046]. Additionally, there was a significant main effect of the hand used on IRI [*F(1,13)* = 4.93, *MSE* = 18.89, *p* = .046] and on IRI variability [*F(1,13)* = 4.92, *MSE* = 844.67, *p* = .047]. Both the IRI and IRI variability were higher in the left hand (601.9 and 47.5 respectively) compared with the right hand (601.0 and 41.9 respectively).

Subsequently, the effects of continuous and intermittent TBS over the left PMC on regular SMS performance were assessed separately using a two-way ANOVA including within subject factors for the hand used and TBS (pre or post) and a between-subject factor for the order of the days. Results indicated that iTBS did not affect any of the performance measures ($p > 0.3$). In the analysis of iTBS effects, there was a significant main effect of the hand used on both IRI and the variability of the IRI ($p < .03$), which reflected the right-hand advantage discussed in the previous paragraph. In the analysis of cTBS data there was a significant main effect of cTBS on tap-tone asynchrony [*F(1,13)* = 8.42, *MSE* = 4869.7, *p* = .013], inter-response intervals [*F(1,13)* = 7.16, *MSE* = 7.156, *p* = .02] and IRI variability: [*F(1,13)* = 7.60, *MSE* = 321.1, *p* = .017]. Following cTBS, the tap-tone asynchrony increased from -46.4 (standard error 10.1) to -65.2 (standard error 11.6) ms, IRI increased from 601.1 (standard error 0.39) to 601.8 (standard error 0.57) ms and the standard deviation of the IRI increased from 42.1 (standard error 3.7) to 46.9 (standard error 4.2) ms (Figure 5.1). After cTBS there was also an increase in the standard deviation of the tap-tone asynchrony from 35.3 to 38.2, but this did not reach significance ($p = 0.122$). There was no difference in the effects of cTBS on regular timing performance between the left hand and the right hand and there was no significant main effect of the hand used.

Error correction results

The average number of outliers removed from the error correction trials (T-4 to T+4) was less than one (out of 180 responses, range 0-2) per subject for each

condition (left and right hand, negative and positive shifts). The number of outliers did not differ between the different TBS conditions.

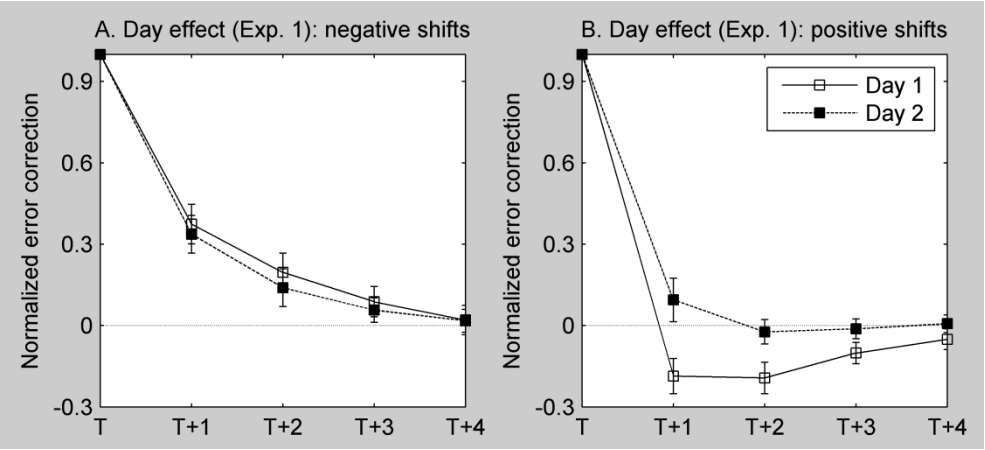

Figure 5.2: Difference in baseline error correction performance during the sessions before TBS on day 1 and day 2. Error correction of positive shifts (delays, B) approached baseline asynchrony (zero, dotted line) more rapidly on day 2 (filled squares) compared with day 1 (open squares). Error correction performance (y-axis) has been normalized to range from baseline performance (zero), to the maximum shift at time T (one). Baseline performance is defined as the average tap-tone asynchrony over T-4 to T-1. Error bars represent one standard error.

Firstly, the effects of TBS on regular SMS measures of tap-tone asynchrony, standard deviation of the tap-tone asynchrony, IRI and IRI variability were analyzed during baseline performance (T-4 to T-1). There was a significant main effect of cTBS on the tap-tone asynchrony [$F(1,13)$ = 12.86, MSE = 6318.6, p = .004], which increased from -50.8 ms to -72.2 ms after cTBS. There was also an increase in the standard deviation of the tap-tone asynchrony from 38.0 to 40.3, but this did not reach significance (p = 0.2). In the analysis of the iTBS data, there was a significant main effect of TBS on the standard deviation of the tap-tone asynchrony [$F(1,13)$ = 5.48, MSE = 190.1, p = .037]. After iTBS the standard deviation of the tap-tone asynchrony decreased from 43.7 to 40.0. The tap-tone

asynchrony increased after iTBS from -60.0 ms to -62.3 ms, but this difference was not significant (p = 0.6).

For the error correction runs, data of the sessions before TBS were compared between day 1 and day 2 to examine potential differences in baseline performance. A four-way ANOVA was performed using within-subject factors for day (day 1 or 2), hand used (left or right), direction of the shift (positive or negative) and time (T+1 or T+2). The results showed a significant day by direction interaction [$F(1,13)$ = 11.86, MSE = 1.039, p = .004] and a significant main effect of day [$F(1,13)$ = 6.08, MSE = 0.446, p = .028]. Post hoc investigations suggested that there was a significant effect of day on the pre-TBS correction of positive shifts (p = .001), but not of negative shifts (p > .3, Figure 5.2A). Figure 5.2B shows that subjects no longer over-correct for positive shifts on day 2.

Due to the significant difference in pre-TBS performance between day 1 and 2, a between-subject factor that coded for the order of the days (cTBS or iTBS on the first day) was added in the analysis of the effects of TBS on error correction. In the analysis of cTBS data there was a significant three-way interaction between TBS, direction and order of the days [$F(1,13)$ = 9.42, MSE = 0.675, p = .01]. Post hoc comparisons showed that cTBS over the left PMC affected the correction of positive and negative shifts in those who received cTBS on day 1 (p < .01; Figure 5.3A and 5.3B), but not in those who received cTBS on day 2 (p > .3; Figure 5.3C and 5.3D). As can be seen in 5.3A, the normalized error correction of negative shifts was closer to baseline performance after cTBS. Overcorrection of positive shifts (i.e. a normalized error correction below zero) did not occur after cTBS over the left PMC (Figure 5.3B). There was no difference in the effects of cTBS on error correction performance between the left hand and the right hand. Results also indicated a significant TBS by order of the days interaction [$F(1,13)$ = 5.91, MSE = 0.085, p = .032] and a significant TBS by direction interaction [$F(1,13)$ = 6.07, MSE = 0.435, p = .03]. There was no effect of iTBS on error correction performance (p > .1; Figure 5.4). A direct statistical comparison was carried out to compare the effect of cTBS and iTBS on error correction performance in those

subjects who received the stimulation on day one. An ANOVA was performed with within-subject factors for hand used (left or right), direction of the shift (positive or negative) and time (T+1 or T+2) and a between-subject factor for group (cTBS or iTBS on day one) on the difference in normalized error correction values (post TBS – pre TBS performance). There was a significant group by direction interaction [$F(1,13) = 4.97$, $MSE = 1.11$, $p = .046$], which confirmed that suppression cTBS had a significantly greater effect on error correction performance compared with facilitation iTBS.

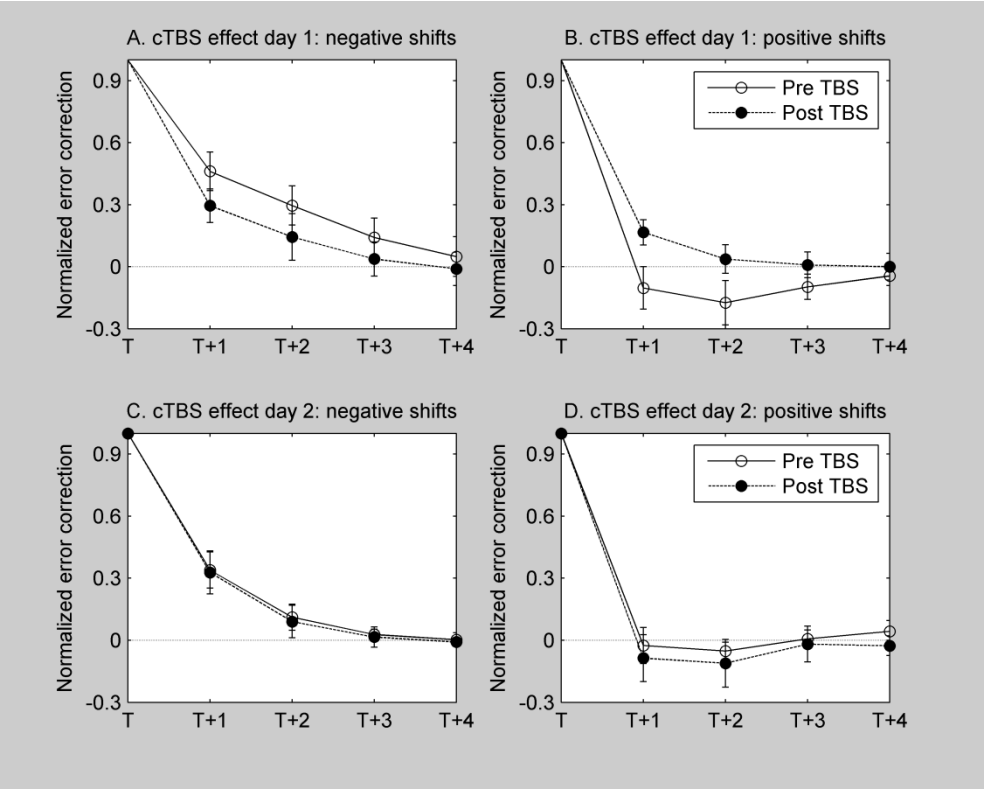

Figure 5.3: Effects of continuous theta burst stimulation (cTBS) over the left pre-motor cortex on error correction performance. In those subjects who received suppression cTBS on day 1 (n = 8), cTBS affected the correction of both negative (A) and positive (B) shifts such that baseline performance was approached faster after suppression cTBS (filled circles) compared with before cTBS (open circles). There was no effect of suppression cTBS on those subjects who received this type of TBS on day 2 (n = 6, figures C and D).

In addition, there were significant main effects of direction and of time in all the statistical comparisons that were performed ($p < .004$). The direction effect represents the tendency to react more strongly to positive than to negative shifts, especially on day 1 (Figure 5.2). The main effect of time is caused by the fact that error correction is not complete at T+1, such that further error correction occurs at T+2 (especially on day 2, where there was undercorrection overall). The responses at times T+3 and T+4 have not been included in the statistical comparisons because previous research has shown that error correction is largely achieved during the first two taps following an induced phase shift (Bijsterbosch et al., 2011; Repp, 2001a).

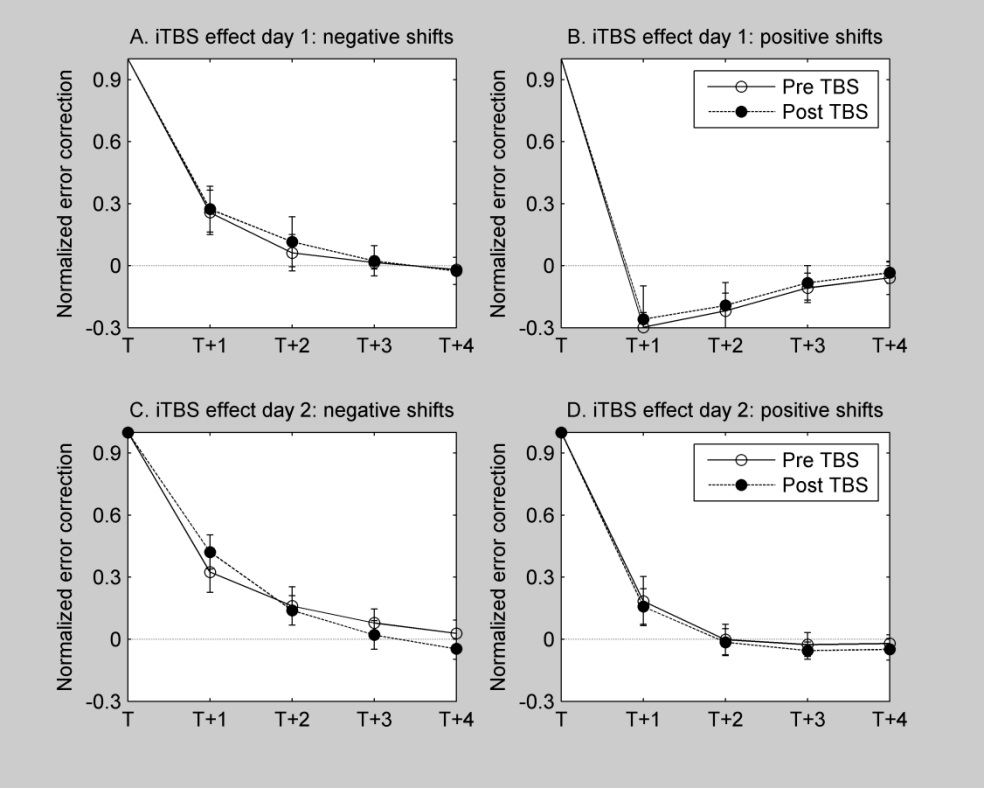

Figure 5.4: Effects of intermittent theta burst stimulation (iTBS) over the left pre-motor cortex on error correction performance. Facilitation iTBS did not affect error correction performance in those subjects who received iTBS on day 1 (n = 6,

figures A and B) or in those subjects who received iTBS on day 2 (n = 8, figures C and D).

In summary, the results of Experiment 1 showed that suppression TBS over the left pre-motor cortex significantly increased the tap-tone asynchrony, inter-response intervals (IRIs) and the variability of IRIs as measured during regular SMS, consistent with previous research (Pollok et al., 2008b). In contrast, suppression TBS over the left pre-motor cortex led to an improvement in explicit error correction such that subjects returned closer to baseline performance after suppression TBS compared with pre-TBS performance. The latter effect of suppression TBS over the left pre-motor cortex only occurred in those subjects who received TBS on day 1. The lack of TBS effect on day 2 may be explained by a practice effect that was found when pre-TBS performance on day 1 was compared with pre-TBS performance on day 2. Lastly, the results showed that there was a significant difference between the correction of positive and negative shifts such that overcorrection only occurred following positive (delayed) shifts.

5.3 Experiment 2

5.3.1 Aims and hypotheses

The findings of Experiment 1 showed that suppression TBS over the left pre-motor cortex resulted in a faster return to baseline tap-tone asynchrony following supraliminal phase shifts. Experiment 1 also suggested that there was a practice effect on error correction performance. The aim of Experiment 2 was to replicate the practice effect from day 1 to day 2 seen in Experiment 1 without TBS intervention. Furthermore, Experiment 2 aimed to confirm that the TBS effect found in Experiment 1 was related to suppression TBS over the left pre-motor cortex and not to a practice effect between two sessions on the same day. Therefore, Experiment 2 used the identical experimental set-up to Experiment 1, but instead of TBS between two sessions on each day, subjects took a 10 minute break. Hence, Experiment 2 essentially acts as a control condition for Experiment

1. It was hypothesized that A) an improvement in error correction performance would be evident when performance on day 1 was compared with performance on day 2 and B) error correction performance would not differ between the two sessions on the first day.

5.3.2 Materials and methods

A new group of 16 subjects (8 males, mean age 22.3 ± 2.5) took part, all of whom were students from the University of Sheffield. All subjects were right handed (mean Edinburgh Handedness Inventory score of 74.4 ± 16.4). Twelve subjects responded positively when asked whether they had had any previous musical training. The level of musical training ranged from several years of childhood lessons to the highest level (grade 8) as defined by the Associated Board of the Royal Schools of Music, UK. None of them was a professional musician. They were naive to the experimental task and did not report any history of psychiatric or neurological disorders.

The experimental set-up was identical to Experiment 1 such that each subject performed the identical task a total of four times on two separate days (at least 48 hours apart). However, instead of receiving theta burst stimulation between the two sessions on day 1 and 2, all subjects took a ten minute break between the two sessions on each day. Data analysis was identical to that of Experiment 1.

5.3.3 Results

Prior to statistical data analysis, two subjects were excluded due to extreme values (more than 3 standard deviations away from the group mean) for the normalized error correction at more than 1 position during T+1 to T+4. Data from 14 subjects (7 males, mean age 22.1 ± 2.5, mean EHI 72.9 ± 16.6, 11 with previous musical training) are presented below.

The average time between participation on day 1 and day 2 was 53 hours (SD 14 hours). Similarly to the results of Experiment 1, feedback reports showed that all

fourteen subjects detected the occurrence of irregularities in the error correction runs, but were unable to predict the exact temporal occurrence and the direction of the shifts.

Regular SMS results

A three-way ANOVA with within subject factors for the hand used (left or right), day (day one or day two) and session (session 1 or session 2) was performed on measures of tap-tone asynchrony, standard deviation of the tap-tone asynchrony, IRI and IRI variability. There were no significant main effects of day, session or of the hand used and there were no significant interaction effects. The tap-tone asynchrony was -54.2 ms and -56.4 ms in sessions 1 and 2 on day 1 and -47.2 ms and -46.5 ms in sessions 1 and 2 on day 2. The standard deviation of the tap-tone asynchrony was 34.8 and 33.6 in sessions 1 and 2 on day 1 and 31.7 and 31.1 in sessions 1 and 2 on day 2. The IRI was between 600.5 and 600.7 ms in all sessions and the standard deviation of the IRI was 36.4 and 40.3 in sessions 1 and 2 on day 1 and 38.4 and 39.1 in sessions 1 and 2 on day 2.

Error correction results

The average number of outliers removed from the error correction trials (T-4 to T+4) was less than one (out of 180 responses, range 0-2) per subject for each condition (left and right hand, negative and positive shifts). The number of outliers did not differ between the sessions or between day one and day two.

Firstly, the effects of practice on regular SMS measures of tap-tone asynchrony, standard deviation of the tap-tone asynchrony, IRI and IRI variability was analyzed during baseline performance (T-4 to T-1). There was a significant main effect of day on the tap-tone asynchrony [$F(1,13)$ = 4.90, MSE = 4261.2, p = .047], which revealed that the tap-tone asynchrony was lower on day 2 (-51.6 ms) compared with day 1 (-64.4 ms). There was a day by session interaction effect [$F(1,13)$ = 8.06, MSE = 492.2, p = .015] and a main effect of session [$F(1,13)$ = 5.63, MSE = 298.1, p = .035] on IRI variability. IRI variability reduced from 61.8 to 54.1 from

session 1 to session 2 on day 1, but did not change significantly from session 1 to session 2 on day 2 (52.2 and 53.2 respectively).

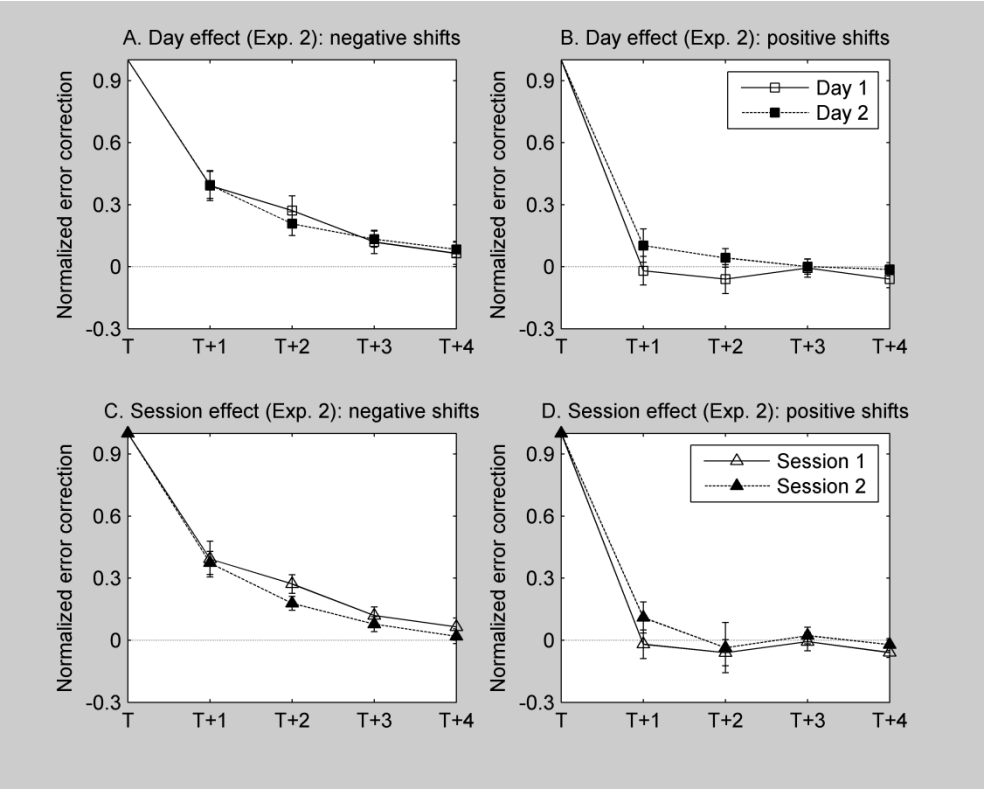

Figure 5.5: Error correction results of Experiment 2 comparing performance in session 1 on day 1 to session 1 on day 2 (A & B) and comparing session 1 to session 2 on day 1 (C & D). Results of Experiment 2 confirm that the correction of positive shifts (Figure B) is significantly different between day 1 (open squares) and day 2 (filled squares). Figures C and D show that there was no significant difference in error correction performance between session 1 on day 1 (open triangles) and session 2 on day 1 (filled triangles).

To assess whether there was an practice effect from day 1 to day 2 in Experiment 2 (hypothesis A), a four-way repeated measures ANOVA using within-subject factors for day (1 or 2), hand used (left or right), direction of the shift (positive or negative) and time (T+1 or T+2) was performed to compare normalized error correction values from session 1 on day 1 to session 1 on day 2. The results showed

a trend-level day by direction interaction [$F(1,13)$ = 3.46, MSE = 0.285, p = .086]. Post hoc comparisons revealed that there was a significant change in the normalized error correction of positive shifts (p = .038) but not in the correction of negative shifts (p > .5). Figures 5.5 A and B show that the difference in performance from day 1 to day 2 is comparable to the day effect shown in Experiment 1 (Figure 5.2). There was no significant effect of the day on any of the measures for regular SMS (asynchrony, IRI or IRI variability).

To investigate whether a practice effect occurred from session 1 to session 2 on the first day (hypothesis B), a four-way ANOVA was performed with a factor indicating session instead of day, which showed a trend-level session by direction effect [$F(1,13)$ = 3.38, MSE = 0.246, p = .089] and a trend-level session by hand effect [$F(1,13)$ = 3.63, MSE = 0.296, p = .079]. However, post hoc investigation of pair-wise comparisons revealed no significant difference in error correction performance between session 1 and 2 on day 1 (p > .09, Figure 5.4 C and D). Furthermore, as in Experiment 1, there were significant main effects of direction and of time in all statistical comparisons that were performed (p < .02).

A direct statistical comparison was performed to compare the day effect and the session effect (on day one) using an ANOVA with within-subject factors for hand used (left or right), direction of the shift (positive or negative), time (T+1 or T+2) and comparison (day effect or session effect) on the difference in normalized error correction values (day 2 – day 1 or session 2 – session 1). There was a significant three-way interaction effect between comparison, direction of the shift and hand used [$F(1,13)$ = 6.996, MSE = 0.23, p = .02]. However, post-hoc comparisons did not reveal a significant difference between the day effect and the session effect on error correction performance (p > .099).

A second direct statistical comparison was performed to compare the session effect shown in Experiment 2 (on day one) with the effect of suppression cTBS (on day one) shown in Experiment 1. An ANOVA was performed with within-subject factors for hand used (left or right), direction of the shift (positive or negative) and

time (T+1 or T+2) and a between-subject factor for group (session effect Experiment 2 or cTBS effect Experiment 1) on the difference in normalized error correction values (session 2 – session 1 or post cTBS – pre cTBS performance). There was a significant group by direction interaction [$F(1,21) = 5.21$, $MSE = 0.73$, $p = .034$], which confirmed that suppression cTBS (Experiment 1) had a significantly greater effect on error correction performance than the difference between session 2 and session 1 without TBS intervention (Experiment 2).

In summary, results of Experiment 2 reproduced a trend-level practice effect on the correction of positive phase shifts between day 1 and day 2 without TBS. Results from both Experiment 1 and 2 showed that the overcorrection of positive shifts seen on day 1 was no longer evident on day 2. Additionally, a direct comparison between the session effect on day 1 in Experiment 2 and the cTBS effect on day 1 in Experiment 1 revealed a significantly greater effect of cTBS. Hence, the change in performance seen after continuous TBS over the left pre-motor cortex in Experiment 1 was a result of TBS rather than an improvement in performance due to practice on the second session.

5.4 Discussion

This study aimed to test the hypothesis that the pre-motor cortex is essential for sensorimotor error correction. The results showed that error correction of induced supraliminal phase shifts improved after suppression TBS over the left pre-motor cortex (because baseline performance was approached more rapidly after TBS). These findings are consistent with the results presented in Chapter four, which suggested that suppression TBS over the pre-motor cortices increased the estimate for ongoing error correction during SMS. To my knowledge, these studies are the first to show that the left pre-motor cortex plays an important role in temporal error correction.

Suppression TBS over the left pre-motor cortex produced differential effects on sensorimotor timing and supraliminal error correction because sensorimotor timing

was affected negatively, whereas error correction performance improved. At present, it is not entirely clear why suppression TBS over the left pre-motor cortex affects timing accuracy and error correction performance differently. It is possible that the improvement in error correction following suppression TBS over the left pre-motor cortex may result from more accurate automated responses enabled by the reduction of conscious control. In line with this hypothesis, it has been suggested that both automatic and voluntarily controlled processes contribute to supraliminal phase correction, whereas subliminal phase correction is thought to be fully automatic (Repp, 2002a). This suggestion was based on the findings that subjects could not influence their phase correction responses to subliminal shifts. On the other hand, subjects were able to reduce, but not to fully eliminate, their correction responses to supraliminal phase shifts when they were asked to do so (Repp, 2002b). Hence, it is possible that the role of the left pre-motor cortex in supraliminal error correction may be associated with the expression of partial voluntary control over the phase correction response to large, perceivable shifts. This suggestion is consistent with neuroimaging evidence that showed that activity in the pre-motor cortex was specifically associated with error correction responses to consciously perceived phase shifts (Stephan et al., 2002). One may argue that the left pre-motor cortex might not be crucial for supraliminal error correction because there were no effects of cTBS after practice on day two. However, it is possible that the relative contribution of the voluntary phase correction process is reduced with practice because previous research has shown that phase correction of larger, supraliminal shifts was less effective than responses to smaller shifts, which may be due to the effect of voluntary control (Repp, 2002b). Hence, the voluntary control hypothesis for the left pre-motor cortex can explain the finding that suppression cTBS over the left pre-motor cortex significantly affected error correction performance on day one, but not on day two. That is, disruption of the left pre-motor cortex may affect performance on day one when voluntary control is engaged, but not on day two when voluntary control is reduced in favour of more automatic responses. Further research will be needed to test the hypothesis that the left pre-motor cortex may play a particular role in voluntarily controlled phase correction responses to supraliminal phase shifts. For example, a paradigm that

varies the intention to respond to phase shifts (Repp, 2002b) may be useful in elucidating this particular proposal using either TMS or fMRI.

There is evidence to suggest that accurate timing and error correction performance rely on the same cortico-cerebellar network. A previous MEG study showed directional coupling from the cerebellum, via the thalamus, to the pre-motor cortex during SMS (Pollok et al., 2006b). The existence of a strong functional connection between the left pre-motor cortex and the cerebellum was confirmed by functional imaging research that showed cerebellar activation following repetitive TMS over the left pre-motor cortex (Bestmann et al., 2005). Cerebellar disruption can also lead to timing impairments that are similar to the effects of TBS over the pre-motor cortex presented in this study. For example, previous research has shown that variability during SMS increased following repetitive TMS over the cerebellum and in cerebellar lesion patients (Spencer et al., 2003; Theoret et al., 2001). Although, at present, the information flow within this network is not completely understood, one possible explanation is that the left pre-motor cortex receives input regarding sensorimotor mismatch from the cerebellum. In this model, suppression TBS over the cerebellum would interfere with the transfer of information to the left pre-motor cortex and therefore lead to comparable changes in timing and error correction behaviour. Functional connectivity within this cortico-cerebellar network during sensorimotor timing and error correction is further studied in Chapter six.

The results of both experiments presented in this study revealed a practice effect on the correction of supraliminal positive shifts (which occur unexpectedly late). Overcorrection of positive shifts occurred during initial performance on day one, but was no longer evident on day two in both experiments (Figures 5.2 and 5.4). Relative overcorrection is evident when the normalized error correction curve dips below the zero (baseline) line. There was no evidence for a practice effect on the correction of negative phase shifts. It is possible that positive and negative error correction may be controlled differently. Positive error correction may rely on a temporal expectancy mechanism because the tone occurs later than expected,

whereas the response to negative shifts (which occur unexpectedly early) may be reactive. Hence, there may be scope for a practice effect in the temporal expectancy mechanism, whereas reaction time remains stable regardless of practice. The improvement of positive error correction performance could, for example, be mediated by enhanced attention to the occurrence of phase shifts as a result of familiarity with the task. Alternatively, the practice effect on positive error correction may be associated with an enhanced understanding of the structure of the pacing stimulus following a phase shift (subsequent inter-onset intervals are unchanged by the local shift). One may ask why the practice effect was only evident during performance on the second day and not during performance in the second session on the first day. Previous research has suggested that consolidation of motor skills occurs over a period of four to six hours after initial performance (Fischer et al., 2005; Kantak et al., 2010). It is therefore possible that a practice effect was not seen in session two on day one, because the second session was performed approximately 10 minutes after the first session, which does not allow sufficient time for motor consolidation.

The practice effect may explain why suppression TBS over the left pre-motor cortex only affected error correction performance in those subjects who received TBS on day one (Figure 5.3). The findings showed that familiarity with the task on day two affected pre-TBS performance in the same direction as the effect of suppression TBS, at least for positive error correction. Therefore, baseline performance was already shifted in the subjects who received suppression TBS on day two and there was no additional significant effect of TBS on error correction performance. In line with these findings, practice effects may explain why Doumas and colleagues did not find an effect of suppression rTMS over the left pre-motor cortex on error correction performance, because the subjects had previously participated in an element of the study that investigated the primary motor cortex and were therefore familiar with the task (Doumas et al., 2005). The practice effect may also explain why a significant difference between the correction of positive and negative phase shifts is reported in some previous studies (Praamstra et al., 2003), but not in other similar work (Repp, 2000, 2001a, 2002a; Repp & Keller,

2004). The findings presented in this study showed that only positive error correction was affected by a practice effect, thereby reducing the difference between the response to positive and negative shifts (Figure 5.2). Previous studies that do not show a significant effect of direction on error correction have used participants that are familiar with the task. The results of this study suggest that practice effects will have diminished the difference between positive and negative error correction in these well-practiced subjects. In contrast, studies that do report a significant direction effect in error correction performance have used novices.

There are some issues to consider in interpreting the results presented in this study. Firstly, the findings did not reveal an effect of facilitation TBS on any of the performance measures for sensorimotor timing or error correction. This negative finding may suggest that a network of brain regions is responsible for accurate performance. In a network, a significant reduction in the contribution from one area does significantly affect the performance of the whole network (a 'virtual lesion' effect), whereas an increase in activity may not have a measurable effect on the behavioural performance of the network as a whole. Furthermore, no stereotaxic coregistration technique was used to determine the site of TBS stimulation. However, the target location was determined experimentally in each subject and on each day by moving the coil 2 cm anterior to, and 1 cm medial from, the left 'motor hotspot'. Previous work has used functional imaging to show significant activation in the left pre-motor cortex following rTMS over this 'presumed' target location (Bestmann et al., 2005).

In conclusion, this study provides evidence that the left pre-motor cortex is not only important for timing accuracy, but also for temporal error correction in both hands. Connectivity between the left pre-motor cortex and the cerebellum may be crucial to achieve accurate timing and error correction (Pollok et al., 2006b). The importance of a cortico-cerebellar network for sensorimotor synchronization and error correction performance is determined in Chapter six.

6 Study 4: Neural correlates of sensorimotor timing and sub- and supra-liminal error correction

6.1 Rationale

The findings presented in Chapters four and five showed that the left pre-motor cortex plays an essential role in sensorimotor timing and in the correction of supraliminal timing errors. It was suggested that functional connectivity between the left pre-motor cortex and the cerebellum may be crucial to achieve accurate timing and error correction. As discussed in Chapter one, previous research has consistently shown the importance of the cerebellum for sensorimotor timing. Co-activation of the left pre-motor cortex and the right cerebellum was reported during regular right-handed synchronization tapping in various neuroimaging studies (Jäncke et al., 2000; Lutz et al., 2000; Rao et al., 1997). Furthermore, Lutz and colleagues found activations in the sensory-motor cortex including the pre-motor region, and in the right cerebellum when comparing visually paced irregular to regular SMS performed with the right hand (Lutz et al., 2000). Another study used Positron Emission Tomography (PET) to demonstrate activations in frontal, parietal, basal ganglia and cerebellar regions during the correction of predictable supraliminal shifts in a unimanual right-handed SMS task (Stephan et al., 2002). Hence, there is evidence for the importance of both the left pre-motor cortex and the cerebellum in timing and error correction. This study aimed to further investigate the cortico-cerebellar network associated with timing and error correction.

This study adopted two complementary techniques to investigate the neural correlates of timing and of error correction responses to subliminal and supraliminal perturbations. In Experiment 1, functional magnetic resonance imaging was used to investigate the neural correlates of regular SMS and error correction of sub- and supra-liminal phase shifts. The aim of Experiment 1 was to describe the whole brain networks associated with sensorimotor timing and error

correction and to determine effective connectivity within these cortico-cerebellar networks. In Experiment 2, the causal role of the cerebellum during sub- and supra-liminal error correction was examined using theta burst transcranial magnetic stimulation (Huang et al., 2005).

6.2 Experiment 1

6.2.1 Aims and hypotheses

The aim of Experiment 1 was to examine the neural correlates of timing measured during SMS, and of the correction of unexpected subliminal and supraliminal phase shifts, using fMRI. To investigate connectivity patterns within cortico-cerebellar pathways further, a psychophysiological interaction analysis was used in order to determine changes in effective connectivity during regular timing and during error correction. It was hypothesized that a) the left pre-motor cortex and the cerebellum would be active during regular timing and during error correction, and b) the left pre-motor cortex and parietal and frontal cortices would be involved in the correction of supraliminal errors.

6.2.2 Materials and methods

Subjects

Sixteen healthy subjects (8 males, mean age 25 ± 5 years) took part in the study. All subjects were right handed (mean Edinburgh Handedness Inventory score of 59, range 30-90). The subjects were naive to the experimental task and none of them was a professional musician. The subjects had no history of psychiatric or neurological disorders.

Stimuli and task conditions

Subjects performed an auditory paced sensorimotor synchronization task inside the fMRI scanner. The pacing stimulus was a simple auditory sequence consisting of metronome tones at a frequency of 500 Hz and duration of 50 ms presented through MRI-compatible headphones. Subjects were asked to press a button using

their right index finger in synchrony with the auditory stimulus, aiming for their button presses to coincide with each tone. The task consisted of three conditions; a regular condition, and two irregular conditions containing perturbations of three (subliminal) and fifteen (supraliminal) percent of the sequence inter-onset interval (IOI). In the regular condition the pacing stimulus was isochronous with an IOI of 600 ms. In the two irregular conditions, perturbation events were introduced that shifted a single stimulus interval by three or fifteen percent (18 or 90 ms respectively) in either direction with respect to the expected time of occurrence, constituting negative and positive phase shifts. In a box-car design a resting block (15 seconds) and a tapping block (45 seconds) were alternated nine times and a further 15-second resting block was added at the end of the final tapping block, resulting in 9 minutes and 15 seconds total scanning time. Each tapping condition (regular, subliminal and supraliminal) lasted for 45 seconds (75 stimuli) and was repeated three times. In each of the irregular blocks a total number of eight perturbations (4 negative and 4 positive) of equal magnitude were introduced. Because each condition was repeated three times (in separate blocks), this resulted in twelve events for all four possible perturbations (positive and negative for subliminal and supraliminal shifts). At least seven regular stimuli occurred between two subsequent perturbations to allow subjects to re-establish synchronization before each shift. To achieve the sequences, a fixed epoch (T-3 to T+3 in which the shift occurs at time T) was repeated eight times and either 0, 1 or 2 tones at the standard IOI were introduced between two subsequent epochs. The order of positive and negative shifts was randomized. As such, the position of the perturbations in the sequence was semi-random and subjects were not able to anticipate the occurrence of the next shift. In order to allow the subjects to focus on the synchronization task, they were not asked to report whether or not they were aware of perturbations. However, a previous study showed that detection of perturbations of 4% of the IOI (of 500 ms) was approximately equal to chance, whereas 90 ms shifts (18% of IOI) were detected more than 90% of the time (Repp, 2002a). Stimuli were controlled using Presentation® software (version 12.8, www.neurobs.com) and behavioural responses were measured with a MRI compatible button box.

Functional Magnetic Resonance Imaging

Functional imaging datasets were acquired using a 3T scanner (Achieva 3.0T, Philips Medical Systems, Best, The Netherlands) at the University of Sheffield. A single-shot, gradient recalled, echo-planar technique was used to acquire 23 x 6mm contiguous transverse slices at 370 time points (TR = 1500 ms, TE = 35 ms, in-plane resolution 1.8x1.8 mm, Sense factor = 1.5). A standard receive-only six-channel headcoil was used and subject-specific, localized shimming was performed. Subjects viewed a projected black screen with a white fixation cross in the centre through a mirror in the head coil throughout the experiment. Subjects were told that the sounds would start and asked to start tapping in synchrony with the tones as soon as it started.

Behavioural data analysis

From each of the nine experimental blocks the first ten taps were discarded to allow the subject to establish tapping synchrony. In the regular SMS condition, measures of timing performance include the mean and standard deviation of tap-tone asynchrony and of inter-response-interval. These were calculated over the three regular blocks and represent the timing performance for all subjects. Subsequently, error correction data from the irregular blocks were analyzed in an event-related approach including four taps before and four taps after (T-4 to T+4) each shifted stimulus (T). Within each subject, outlier responses (tap-tone asynchronies more than 2 standard deviations away from the average asynchrony) were identified separately for each position (T-4 to T+4) and were removed prior to averaging. In order to allow a direct comparison of the error correction response in all conditions, the asynchrony during T to T+4 was normalized to range from baseline asynchrony to the maximum initial shift at time T and the sign was removed (Figure 6.1). Baseline performance was defined as the average tap-tone asynchrony over trials T-4 to T-1 (Praamstra et al., 2003; Repp, 2000). The resulting normalized error correction data were averaged over all trials. If the averaged normalized error correction scores represented extreme values (more than three times the interquartile range away from the group median) at three or four positions (in T+1 to T+4) for a single subject, these data were replaced by the

group average of the value. This led to the replacement of data from two subjects in the negative subliminal condition and data from one subject from the positive subliminal condition.

In order to investigate the natural occurrence of error correction (following spontaneous motor variability in the absence of perturbations in the sequence), a data-driven analysis was performed using only data from regular blocks. For each subject the data were searched for instances (minimally 5 taps apart) where the asynchrony deviated from the subject's mean asynchrony by more than 50 ms. All subjects showed such spontaneous deviations; on average 13 shifts (SD 5, range 7-21) occurred during the three regular blocks (5 in the positive direction and 8 negative). These data were analyzed in the same way as for externally induced error correction events (see above) to show the correction response to spontaneous errors (Figure 6.1 C).

Imaging data: cognitive subtraction

The imaging data were analyzed using SPM5 (http://www.fil.ion.ucl.ac.uk/spm). Motion correction was performed by realigning the images to the central image with a 6-parameter (rigid body) spatial transformation. Further pre-processing stages involved normalization into standard space and smoothing using Gaussian Kernels of 5 mm full width half maximum. On an individual level, statistical analysis was based on the General Linear Model using the boxcar design convolved with a canonical hemodynamic response function; creating contrast images for all conditions. Thereafter a one-sample t-test was performed to obtain second-level group results (Figure 6.2 A & B). Subsequently, parameter estimates were derived from single-voxel locations in order to allow closer investigation of activation patterns in several regions of interest. These locations were experimentally informed MNI coordinates resulting from local maxima in second level functional contrasts (regular – rest for right cerebellar ROI and supraliminal – regular for left cerebellar ROI). Figure 6.2 C & D show parameter estimates for the contrasts between all active conditions (regular, subliminal and supraliminal) and rest.

In order to further investigate the lateralization of cerebellar activation, a laterality analysis was performed. Parameter estimates were extracted for a 5 mm sphere centered on the left cerebellar ROI [-20 -80 -44] and on the mirrored right cerebellar region [20 -80 -44]. A paired t-test was performed to analyze whether there was a statistically significant difference between the parameter estimates indicating a lateralization of activation.

Imaging data: normalization to cerebellar template

Individual subject contrast images resulting from first level General Linear Model analysis were normalized to a spatially unbiased template of the human cerebellum with the use of the SUIT toolbox in SPM5 (Diedrichsen, 2006). In each subject the cerebellum and brainstem were isolated based on a segmentation algorithm and functional images were normalized to the SUIT template using non-linear deformation. The subsequent cerebellar contrast images were smoothed and entered into a second level one-sample t-test producing group results to create Figures 6.2 E and F.

Imaging data: psychophysiological interaction analysis

In order to further investigate the role of the cerebellum during supraliminal error correction, a psychophysiological interaction (PPI) analysis was performed (Friston et al., 1997) using SPM5. For each subject, a left cerebellar seed ROI was identified by locating the supra-threshold voxel nearest to the group ROI (left cerebellar local maxima in supraliminal – regular contrast [-20 -80 -44]). A suitable ROI in the left posterior cerebellar cortex was located from the first-level contrast (supraliminal – regular) for all subjects. The zero-mean corrected first principle component was extracted from all voxels in a radius (5 mm) centered on the subject-specific ROI to form the physiological time course. The psycho-physiological interaction term was produced by convolving the physiological time series with a psychological vector that described the paradigm (1 for the supraliminal condition, -1 for regular tapping). The interaction term was entered at the first level as the effect of interest, and the psychological and physiological time series were entered as effects of no interest. Subject-specific interaction contrasts were entered into a second-level one-sample t-test to achieve group results (Figure

6.3). The identical PPI analysis was also performed with a seed ROI in the right cerebellum. Here, subject-specific physiological time series were extracted from a radius centered on the nearest supra-threshold voxel to the group ROI [4 -68 -16] in the regular – rest contrast.

6.2.3 Results

During regular blocks, taps preceded the tones by an average of 53 milliseconds demonstrating an anticipatory negative mean asynchrony. The standard deviation was 45 milliseconds as calculated by averaging the within-block SD over three regular blocks and over all subjects. The average inter-response-interval (IRI) was 600 ms (group averaged within-block SD 45 ms). In the subliminal condition the average tap-tone asynchrony was 65 ms (group averaged within-block SD 43 ms) and the IRI was 600 ms (group averaged within-block SD 37 ms). During supraliminal blocks the average tap-tone asynchrony was 53 ms (group averaged within-block SD 56 ms) and the average IRI was 599 ms (group averaged within-block SD 50 ms).

Event-related error correction analysis revealed a behavioural error correction response in all four possible phase shifts (Figure 6.1). The average number of outlier responses removed was 3.4 (SD 2) out of 108 responses. There was no difference in the number of outlier responses removed from the analysis between the conditions ($p>.2$). A 3-way repeated measures ANOVA on the normalized relative asynchrony with factors direction (positive or negative), size (subliminal or supraliminal) and position (T+1 to T+4) indicated a significant main effect of direction [$F(1,15) = 5.59$, $p = .032$], such that the correction of negative shifts was less efficient than of positive shifts. Furthermore, there was a main effect of size [$F(1,15) = 8.20$, $p = .012$] in which baseline performance was achieved faster after the correction of supraliminal errors compared with subliminal error correction. The main effect of position did not reach significance ($p>.5$) and none of the interactions were significant ($p>.1$).

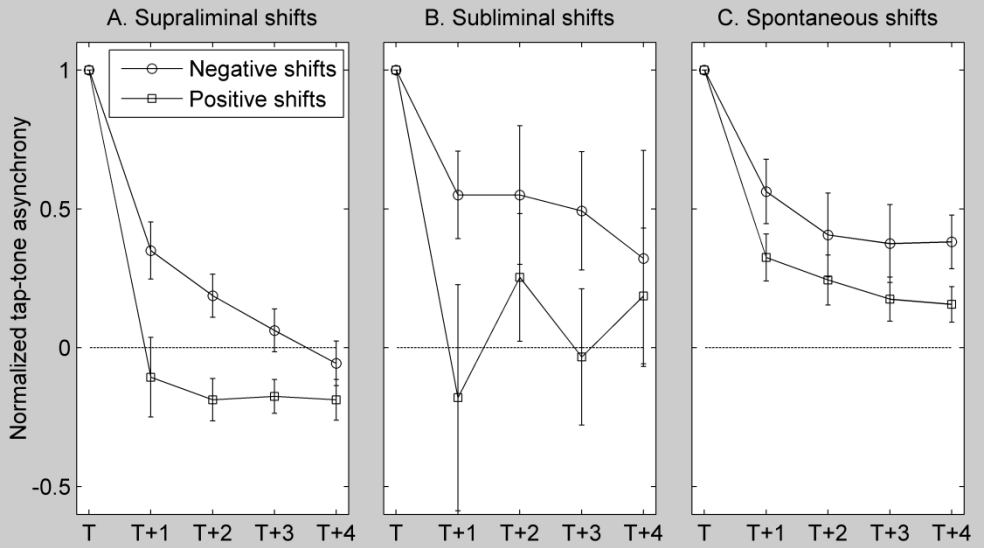

Figure 6.1: Normalized error correction response as a function of stimulus position following induced subliminal (A) and supraliminal (B) perturbations and spontaneous motor variability (C) in Experiment 1. Error correction of positive shifts is faster compared with negative error correction. Error correction following spontaneous large deviation from the average tap-tone asynchrony does occur, but baseline asynchrony is not achieved within 4 taps. Tap-tone asynchronies are shown for the time of the perturbation (T) and four subsequent taps (T+1 – T+4). The data are normalized to range from baseline asynchrony (0, dashed line) to the magnitude of the initial shift at time (T) and the sign is removed. Baseline performance is defined as the subject mean tap-tone asynchrony during T-4 to T-1. Spontaneous shifts are defined as deviations from the subject mean asynchrony greater than 50 ms during the standard blocks. In negative shifts (circles) the tone occurs earlier than expected and in positive shifts (squares) the tone occurs later than expected. Error bars express a standard error.

Subliminal phase shifts (18 ms) fall within the range of tapping variability (SD of 46 ms) as opposed to supraliminal shifts (90 ms). In view of this, the behavioural response following extreme cases of motor variability (deviations from the mean asynchrony greater than 50 ms) were analyzed and compared with the error correction response to phase shifts introduced in the pacing stimulus (Figure 6.1 C). Error correction following spontaneous motor variability was apparent, but

baseline asynchrony was not achieved within the four taps following the deviation. Hence, it may well be that this form of 'error correction' following spontaneous motor variability is better interpreted as a general regression to the mean asynchrony.

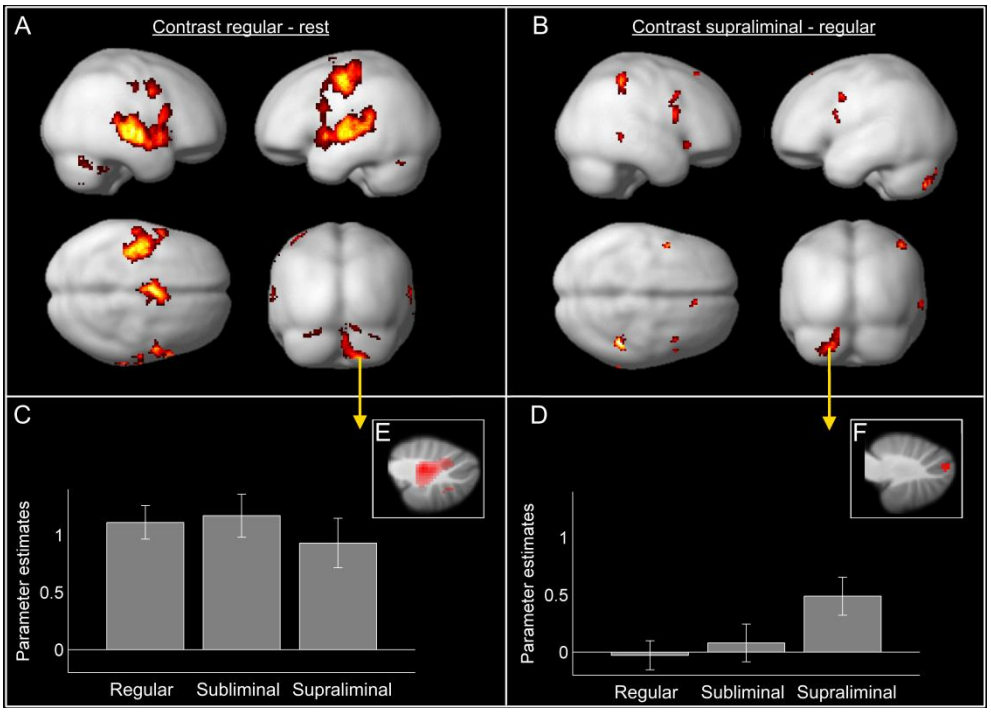

Figure 6.2: Functional imaging contrasts between regular tapping and rest (A) and between the supraliminal and regular conditions (B) and associated parameter estimates (C&D) in peak cerebellar foci (E&F). fMRI activations are rendered on a normalized smooth brain surface showing (clockwise starting at the upper left corner): a sagittal view from the right and left, axial view from the top and coronal view from the back. Findings are significant at p<0.001 uncorrected and exceed a cluster-extent threshold of 20 voxels. Plots C and D show parameter estimates for the three active conditions compared with rest in two regions of peak activation in the right dentate nucleus [20 -52 -28] and left posterior cerebellar cortex [-20 -80 -44]. Error bars indicate the 90% confidence interval. In-plot figures E and F show the same fMRI activations on a sagittal slice through the cerebellum to illustrate the differential position of activation foci in the deep nuclei (right dentate

nucleus) and in the cortex (left posterior cerebellar cortex). Figures E and F were created with the SUIT toolbox in SPM5 (Diedrichsen, 2006).

Functional imaging data from all three experimental conditions were contrasted with baseline rest and the subliminal and supraliminal error correction conditions were contrasted with regular SMS. Compared with baseline rest, the regular condition showed activations in the right pre-motor cortex, left primary motor cortex, bilateral primary auditory cortices and right cerebellum extending to vermis (Figure 6.2 A, Table 6.1). The subliminal condition compared with regular SMS did not produce any significant activations. The contrast between the supraliminal and regular conditions revealed that bilateral frontal cortices, right inferior parietal cortex and the left cerebellum were significantly activated during the supraliminal condition (Figure 6.2 B, Table 6.1). To investigate whether subliminal error correction may lead to less activity in the same circuitry, the significance threshold of the comparison between subliminal correction and regular tapping was lowered ($p<0.01$ uncorrected). Lowering the threshold resulted in scattered activity which was not consistent with the contrast between supraliminal and regular tapping. In summary, the right cerebellum was active in all three conditions compared with rest, whereas the left cerebellum was only engaged in the condition including perceivable shifts.

	Regular – rest (Figure 2A)		**Subliminal – rest**		**Supraliminal – rest**		**Supraliminal – regular (Figure 2B)**	
	Left	Right	Left	Right	Left	Right	Left	Right
Cerebellum	-24 -66 -26 (5.23; 292)	4 -68 -16* (6.07; 2157)	-24 -62 -26 (4.23; 61)	4 -66 -22 (4.86; 1424) 36 -58 -36 (4.58; 25) 12 -66 -50 (4.10; 118)	-18 -72 -32 (5.29; 798)	12 -52 -22 (5.42; 1946) 0 -56 -2 (4.16; 21)	-20 -80 -44* (4.46; 161)	
Temporal cortex	-54 -20 0 (5.63; 4871)	60 -18 -2 (5.94; 2381)	-48 -22 2 (5.55; 1576) -34 -64 8 (3.69; 22) -58 8 4 (3.51; 25)	62 -18 -4 (5.65; 522) 46 0 -4 (3.95; 59) 42 -16 -20 (4.30; 29)	-52 -20 0 (5.58; 6229)	64 -16 -2 (6.03; 3440)		34 18 -10 (4.21; 25) 66 -42 0 (3.53; 23)
Motor cortex	-48 -8 54 (5.14; [1])		-44 -14 52 (5.04; 1057)		-42 -6 54 (4.71; [1])			
Parietal cortex					-44 -40 46 (4.80; 392)	42 -38 38 (4.60; 282)		50 -40 54 (4.34; 247)
Frontal cortex				54 4 44 (4.17; 121)		34 20 -6 (5.29; 1766)	-48 4 40 (4.54; 34) -48 10 22 (3.43; 26)	42 8 34 (4.23; 45) 6 30 58 (3.86; 22) 52 10 16 (3.63; 68)
Pre-motor cortex/ SMA (BA 6)	-4 -4 54 (5.16; 837)	54 0 40 (4.32; 169) 62 -14 44 (4.58; 35)	-4 -6 56 (4.01; 90)			12 4 64 (4.39; 798)		
Thalamus	-16 -22 -2 (4.23; 104)	22 8 -16 (4.35; 390)	-14 -24 -2 (4.12; 43)					
Basal ganglia		32 18 6 (3.57; 42)	-26 2 -8 (5.09; 385)	20 4 8 (3.89; 121)				

*Table 6.1: Statistical contrasts between regular, subliminal and supraliminal conditions and rest and between the supraliminal and regular conditions. MNI coordinates of local maxima are provided (x y z in mm) for all clusters that were significant at p<0.001 uncorrected and exceed a cluster-extent threshold of 20 voxels. Values in brackets provide corresponding Z scores and cluster sizes (voxels). Voxel locations marked with * are used as seed regions of interest in the psychophysiological interaction analysis. Notes: 1) Motor cortex local maxima included in left temporal cortex clusters. BA: Brodmann's Area.*

A laterality analysis was performed to compare activation in the left cerebellar local maximum with the mirrored right cerebellar region in the contrast between the supraliminal and regular conditions. Results of the laterality analysis confirmed that the cerebellar activation during the supraliminal conditions was significantly left-lateralized [$t(1,15) = 4.47$, $p < .001$]. The lateralization of cerebellar activation was also confirmed by the parameter estimates for the two local maxima in the left and right cerebellar hemispheres (Figure 6.2 C & D). Furthermore, when the subtraction results were normalized to a template confined to the cerebellum, a dissociation in activation foci was highlighted: activation in the right cerebellum was mainly located in the dentate nucleus, whereas activity on the left-hand side was confined to the cortex (Crus I, Figure 6.2 E & F).

PPI left cerebellum [-20 -80 -44]

	Left	Right
Cerebellum		24 -70 -50 (3.76; 21)
Temporal cortex (BA 21, 22)	-50 -46 8 (3.75; 60) -52 4 10 (3.65; 39)	
Somatosensory cortex (BA 1,2,3)	-54 -16 28 (3.99; 40)	
Inferior frontal cortex (BA 45)		46 20 20 (4.34; 26)

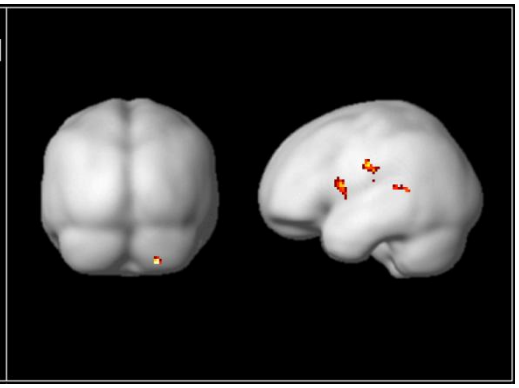

Figure 6.3: Psychophysiological interaction analysis results with a seed region of interest (ROI) in the left cerebellum [-20 -80 -44]. In the table, MNI coordinates of local maxima are provided (x y z in mm) and values in brackets provide corresponding Z scores and cluster sizes (voxels). Areas that display enhanced effective connectivity with the left cerebellum during the supraliminal condition compared with regular SMS are shown on a normalized smooth brain surface showing a coronal view from the back (left) and a sagittal view from the left (right). Findings are significant at p<0.001 uncorrected and exceed a cluster-extent threshold of 20 voxels.

Functional imaging data were further analyzed in a psychophysiological interaction (PPI) analysis using a seed ROI in the left cerebellum. Group results are

summarized in Figure 6.3. The PPI analysis identified brain areas that exhibit enhanced connectivity with the left cerebellum during the condition that included supraliminal perturbations compared with regular tapping. Significantly enhanced connectivity with the left cerebellum was observed in the frontal, auditory and sensory cortices and in the right cerebellum. The same PPI analysis was also performed using a seed ROI in the right cerebellum. Results showed no change in effective connectivity of the right cerebellum during supraliminal tapping compared with regular SMS.

In summary, the cerebellar vermis and right cerebellar dentate were activated in all active conditions compared with rest, whereas the left lateral cerebellar cortex was activated only during the condition that required supraliminal error correction. Furthermore, the left cerebellum exhibited enhanced functional connectivity with a cerebello-cortical network during supraliminal error correction compared with regular timing. These findings suggest that the left cerebellum may play an essential role during supraliminal error correction.

6.3 Experiment 2

6.3.1 Aims and hypotheses

Results from Experiment 1 indicated that the left cerebellum is involved only during the correction of supraliminal phase shifts. Experiment 2 investigated the effect of theta burst transcranial magnetic stimulation (TBS) over the medial, left lateral and right lateral cerebellum on error correction performance. Based on Experiment 1, it was hypothesized that suppression TBS over the left cerebellum would impair supraliminal error correction, whereas suppression of the medial or right cerebellum would not affect error correction performance.

6.3.2 Materials and methods

Subjects

Forty right-handed healthy subjects (mean age 23 ± 5 years) took part in the study. They were students from the University of Sheffield. All were randomly assigned to one of four experimental groups: 1) medial cerebellar TBS, 2) left cerebellar TBS, 3) right cerebellar TBS and 4) sham TBS. The groups were matched for age (mean age group 1: 22±6, group 2: 22±2, group 3: 24±6, group 4: 24±6) and gender (6 males and 4 females in each group).

Stimuli and task conditions

All subjects performed an identical auditory paced SMS task before and after TBS. As in Experiment 1, four different perturbations (subliminal: 3%, 18 ms and supraliminal: 15%, 90 ms in both the positive and negative direction) were introduced into an otherwise regular auditory pacing sequence consisting of metronome tones presented at an inter-onset interval (IOI) of 600 ms (frequency of 500 Hz and duration of 50 ms). The occurrence of sub- and supra-liminal perturbations was inter-mixed within blocks to further avoid anticipation effects. Following an initial 30-second practice block, subjects performed a total of three 5-minute SMS blocks with period of rest in between. At the beginning of each 5-minute block, 10 regular tones were presented to allow subjects to synchronize their tapping to the regular pacing stimulus and these data are excluded from all further analysis. Following the initial 10 tones, a fixed epoch (T-4 to T+4 in which the shift occurs at time T) was repeated 8 times for each of 4 different shifts in pseudo-randomized order. Between two subsequent epochs, 2 to 6 stimuli at the standard IOI were introduced to avoid predictability of the next perturbation. Hence, over the three 5-minute blocks a total of 24 event-related error correction responses were obtained for each of the 4 shift conditions. Data analysis was identical to that of Experiment 1, and was based on an event-related approach including four taps before and four taps after (T-4 to T+4) each shifted stimulus (T). As with Experiment 1, if average normalized error correction scores represented extreme values (more than three times the interquartile range away

from the group median) at three or four positions (in T+1 to T+4) for a single subject, these data were replaced by the group average of the value calculated within the relevant cerebellar TBS group. This led to the replacement of data from two subjects in the pre-TBS positive subliminal condition.

TBS protocol

Following completion of the full SMS task, the TBS procedure was explained to the subjects in detail and any questions were answered. Subsequently, the resting motor threshold (RMT) of each subject was determined using the thumb movement visualization method (Pridmore et al., 1998). Each subject then received 40 seconds of continuous theta burst stimulation (TBS) (Huang et al., 2005). A total of 600 pulses were applied at 80% of the resting motor threshold using a 70mm figure-of-eight coil and a Magstim Super Rapid stimulator (Magstim Company, Whitland, UK). The target TBS locations were 1) the medial cerebellum (1 cm below inion), 2) left lateral cerebellum (1 cm below inion and 3 cm left of midline), 3) right lateral cerebellum (1 cm below inion and 3 cm right of midline), or 4) sham TBS (1 cm below inion) (Lee et al., 2007; Theoret et al., 2001). The coil was positioned vertically with the handle pointing upwards (Lee et al., 2007). For sham TBS, the coil was held at 90˚ angle to the scalp over the medial cerebellum. During and following TBS, none of the subjects reported any adverse effects.

6.3.3 Results

To assess whether there were any differences in error correction performance between the four different TBS groups before stimulation, a multivariate general linear model with a fixed factor for the TBS group and within-subject factors for direction (positive and negative), size (subliminal and supraliminal) and position (T+1 to T+4) was performed. The results indicate a trend-level effect of TBS group on pre-TBS performance ($p=.073$, Figure 6.4). Closer investigation of individual subject performance showed that the difference in pre-TBS performance was explained by two outlier subjects (one subject from the left and one from the medial cerebellar TBS groups). There was no significant difference in pre-TBS performance when data from these two subjects were removed ($p>.1$). Because the

removal of these subjects did not affect the significance of the TBS findings, data from all subjects were included in the results presented below.

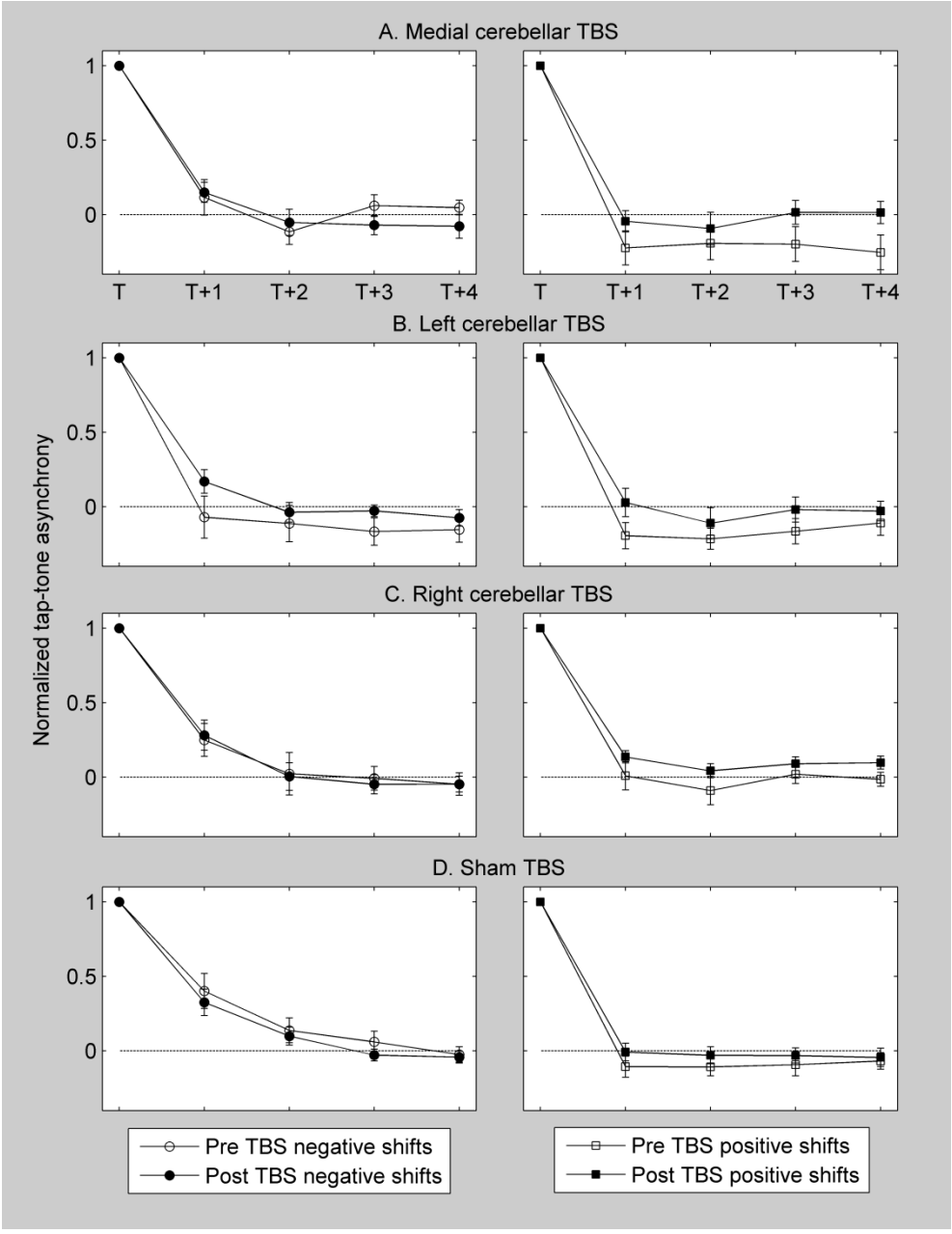

Figure 6.4: Normalized error correction response as a function of stimulus position before and after suppression of the medial (A), left (B) and right (C) cerebellum with theta burst transcranial magnetic stimulation (TBS) and after sham TBS (D). Suppression of the left cerebellum (A) produced a slowing of

supraliminal error correction of positive and negative shifts. Suppression of the medial cerebellum (B) only affected the correction of positive (right) supraliminal phase shifts. TBS over the right lateral cerebellum (C) had no effect on error correction performance. Tap-tone asynchronies are shown for the time of the perturbation (T) and four subsequent taps (T+1 – T+4). The data are normalized to range from baseline asynchrony (0, dashed line) to the magnitude of the initial shift at time (T) and the sign is removed. Baseline performance is defined as the subject mean tap-tone asynchrony during T-4 to T-1. Performance before TBS (open circles and squares) is compared with post-TBS performance (filled circles and squares). In negative shifts (left side, circles) the tone occurs earlier than expected and in positive shifts (right side, squares) the tone occurs later than expected. Error bars express a standard error. Data were provided by Dr Kwang-Hyuk Lee, Academic Clinical Psychiatry, University of Sheffield.

In order to compare error correction performance before and after transcranial magnetic stimulation of the cerebellum, a repeated measures ANOVA with within subject factors for TBS (before and after stimulation), direction (positive and negative) and position (T+1 tot T+4) was performed separately for the subliminal and supraliminal conditions on normalized error correction values for each group. In the left cerebellar TBS group results indicate a trend-level main effect of TBS [$F(1,9) = 4.84$, $p = .055$] and a significant TBS by position interaction [$F(3,27) = 3.31$, $p = .035$]. Post hoc analysis indicated that there was a significant effect of left cerebellar TBS at T+1 ($p=.013$), but not at T+2 to T+4 ($p>.09$). At T+1 the average normalized error correction value increased from -0.13 to 0.09 (Figure 6.4 B). Left cerebellar TBS did not affect subliminal error correction performance ($p>.2$). By contrast, suppression of the right cerebellum did not change error correction of sub- or supra-liminal phase shifts (Figure 6.4 C). In the medial cerebellar TBS group there was a trend-level TBS by direction interaction [$F(1,9) = 3.75$, $p = .085$]. Post hoc analysis shows a trend-level difference between performance before and after TBS during positive supraliminal error correction ($p=.09$), but not during negative supraliminal error correction ($p>.3$, Figure 6.4 A). Further investigation showed a significant effect of medial cerebellar TBS at time T+1 on positive supraliminal

error correction (p=.045), but not at the other time points (p>.1) and no effect on negative supraliminal error correction at any time point (p>.1). Medial cerebellar TBS did not affect subliminal error correction. There were no significant changes in error correction performance following sham TBS (Figure 6.4 D). In the dataset, the number of outlier error correction responses removed from the analysis was not statistically different between the conditions (p>.4) and was not affected by TBS (p>.7). The average number of outlier error correction responses removed across subjects was 10.4 (SD 2.4) out of 216 total responses.

In summary, suppression TBS over the left cerebellum significantly affected supraliminal error correction at the tap immediately following the phase shift. Suppression TBS over the right cerebellum did not affect error correction performance. As such, the findings of Experiment 2 support results of Experiment 1 and provide further evidence that the left cerebellar cortex is necessary for the correction of supraliminal phase shifts during sensorimotor synchronization.

6.4 Discussion

This study aimed to determine the neural correlates of sensorimotor timing and of the correction of sub- and supra-liminal phase shifts. The main results provide evidence for a functionally lateralized response in the cerebellum, such that the right cerebellar dentate and vermis were activated in all SMS conditions compared with rest, whereas the left posterior cerebellar cortex was only engaged during the correction of large, supraliminal phase shifts. Furthermore, the left cerebellum exhibited enhanced connectivity with a cerebello-cortical network including the right lateral frontal cortex and the right cerebellum during the condition that included supraliminal error correction compared with regular SMS. In Experiment 2, theta burst magnetic stimulation (TBS) applied to the left cerebellum significantly affected the correction of positive and negative supraliminal errors, which confirms the causal contribution of the left cerebellum to the supraliminal error correction process.

The imaging results of Experiment 1 showed that the right cerebellum was activated in all experimental conditions compared with rest (Figure 6.2 C). The activation was mainly localized in the right dentate nucleus extending to the vermis (Figure 6.2 E). The finding of persistent right cerebellar dentate activation closely replicates an earlier fMRI study investigating right-handed sensorimotor synchronization and continuation (Rao et al., 1997). It is possible that cerebellar activation ipsilateral to the moving limb is related to movement control, in line with a traditional view of the cerebellum (Ramnani, 2006). However, activation of the right cerebellum during sensorimotor synchronization may play a critical role in the timing of movement. There is neuroimaging evidence to suggest that the right cerebellum is essential for perceptual timing even when little or no movement is required (Lewis & Miall, 2003). Furthermore, it was shown in two independent rTMS studies that suppression of the right, but not the left, cerebellum affects perceptual timing abilities (Fierro et al., 2007; Lee et al., 2007). Nonetheless, future research will be needed to differentiate conclusively between the control of timing and movement within the cerebellum. For example, the present study may be replicated using the left hand to examine whether the right cerebellum is consistently activated during movement timing.

The left cerebellum was only involved during the condition that included error correction of perceivable changes in the pacing stimulus (Figure 6.2 D). In contrast to the right dentate activation, activity in the left cerebellar hemisphere was located exclusively in the cortex (Figure 6.2 F). The finding of involvement of the left lateral cerebellum during the correction of supraliminal errors closely replicates earlier findings (Stephan et al., 2002). Furthermore, the PPI results showed that during supraliminal error correction the left cerebellum displayed enhanced effective connectivity with a cerebello-cortical network that included frontal and sensory cortices and the right cerebellum (Figure 6.3). The pattern of task-dependent effective connectivity between the left cerebellum and auditory, sensory and frontal cortices has, to my knowledge, not been shown in previous studies. Although the functional significance of this cerebello-cortical network is currently unclear, it may be that sensory input from the auditory and somatosensory domains

are rapidly integrated in the frontal region and passed to the left cerebellum in order to facilitate prompt behavioural error correction. Further research will be needed to fully understand the function of the emerging cerebello-cortical network during supraliminal error correction. Lastly, the findings of Experiment 2 showed that suppression of the left lateral cerebellum significantly affected the correction of supraliminal errors at the tap immediately following the perturbation (Figure 6.4), whereas suppression of the right cerebellum did not affect error correction performance. Hence, Experiment 2 provided evidence that the left cerebellum causally contributes to supraliminal error correction.

The results of the PPI analysis did not reveal any enhanced functional connectivity between the left cerebellum and the left pre-motor cortex during supraliminal error correction. This negative finding is unexpected because it was shown in Chapter Five that the left pre-motor cortex plays an essential role in the correction of supraliminal timing errors. It is possible that connectivity between the left cerebellum and the left pre-motor cortex emerges indirectly, for example via the thalamus. Cerelbello-premotor connectivity may be investigated further using additional PPI analyses that adopt a seed region of interest in the left pre-motor cortex or in the thalamus in order to further disentangle functional connectivity patterns during sensorimotor error correction.

In both Experiments, behavioural error correction occurred following subliminal perturbations. Yet no left cerebellar activation was found during subliminal error correction compared with regular SMS in Experiment 1. Furthermore, in Experiment 2, the correction of subliminal phase shifts was not affected by any of the TBS protocols. These findings suggest that the mechanism of subliminal error correction differs from that of supraliminal error correction. It was suggested in Chapter one that ongoing error correction during SMS may be achieved through a continuous phase resetting mechanism (Repp, 2005). In the phase resetting hypothesis, the timing of each response is calculated based on the temporal reference point provided by the previous pacing tone rather than the tap-tone asynchrony. Phase resetting following a perturbation that falls below the perceptual

threshold is not different from phase resetting after a tone at the regular interval. Hence, the use of the same neural mechanism to achieve both regular SMS and subliminal error correction may explain why there was no additional brain activation during subliminal error correction in Experiment 1 and why cerebellar TBS did not affect subliminal error correction in Experiment 2. The phase resetting hypothesis is also consistent with the finding that spontaneous error correction was less efficient than induced error correction (since baseline asynchrony was not achieved within four taps (Figure 6.1 C)). This less efficient response to spontaneous shifts is expected if response timing is relative to the previous pacing tone rather than to the tap-tone asynchrony. Overall, these findings provide evidence that the correction of subliminal shifts may be achieved by a continuous phase resetting process that also controls accurate timing during regular SMS.

In addition to involvement of the left cerebellum, inferior parietal and frontal areas were activated during the condition that involved perceivable phase perturbations in Experiment 1. These results replicate findings by Stephan and colleagues (Stephan et al., 2002). However, the PPI analysis did not show increased connectivity between the left cerebellum and the parietal-frontal network. The lack of effective connectivity between the left cerebellum and parietal-frontal cortices may suggest that the parietal-frontal network is engaged in more cognitive processes associated with the perception of errors rather than behavioural error correction. Consistent with this interpretation, a number of studies have indicated the role of the parietal-frontal network in error perception. One study investigated the perception of supraliminal irregularities in pitch and duration of an auditory sequence (Molholm et al., 2005) and another study looked at awareness of behavioural errors in a go/no-go task (Hester et al., 2005). Both studies showed activation in a parietal-frontal network similar to the findings presented here, but without involvement of the cerebellum. Activation of a parietal-frontal network during the perception of irregularities and during awareness of behavioural errors may suggest that these regions are involved in conscious error detection. The right-hemispheric lateralization of parietal-frontal activation in Experiment 1 of this study provides further evidence that these areas are associated with conscious error

detection. The right parietal and frontal areas are thought to play a role in directing attention (Posner & Raichle, 1994) and processing sensory feedback (Coull & Nobre, 2008), whereas the left cerebral hemisphere may be specialized in movement control (Serrien et al., 2006) and temporal attention (Coull & Nobre, 1998). In summary, activation of a parietal-frontal network during the condition that included supraliminal phase shifts may be related to conscious detection of supraliminal irregularities and of behavioural errors. Furthermore, the lack of cerebellar activation (despite cerebellar coverage) during the detection of irregularities and of behavioural errors (Hester et al., 2005; Molholm et al., 2005) supports the hypothesis that the left posterior cerebellum plays a crucial role in error correction rather than in the detection of perceptual mismatch or of sensorimotor error.

Behavioural data from both experiments showed that the correction of positive shifts was faster than that of negative shifts (Figure 6.1), which is consistent with the results presented in Chapter five and with previous research (Praamstra et al., 2003). It was suggested in Chapter five that the behavioural response to positive and negative shifts may be achieved by different mechanisms. A temporal expectancy mechanism may be used to prepare the correction response to positive phase shifts. In response to negative shifts, the expectancy mechanism may not be utilized as the errors should be corrected reactively (similar to a simple reaction time task). Although the experimental paradigm used in Experiment 1 did not allow a direct comparison between positive and negative shifts, the findings of Experiment 2 provide evidence that different neural mechanisms are involved in the correction of supraliminal positive and negative phase shifts. Experiment 2 showed that suppression of the medial cerebellum affected the correction of only positive phase perturbations, whereas left cerebellar suppression affected both positive and negative error correction. Hence, the results of Experiment 2 suggest that the medial cerebellum may play a role in the expectancy mechanism, although future studies are needed to specifically test this hypothesis.

In summary, the results of Experiments 1 and 2 provided evidence for a lateralized role of the cerebellum in sensorimotor timing and error correction. The medial and right cerebellum were engaged in all active conditions in Experiment 1 suggesting that these areas play a general role in the temporal control of movement. The left cerebellum was only activated during the correction of supraliminal error correction in Experiment 1 and the results of Experiment 2 provided further evidence for a crucial role of the left cerebellum in supraliminal error correction.

7 Study 5: Inter-hemispheric functional connectivity during uni- and bi-manual sensorimotor timing

7.1 Rationale

In Chapter six, the importance of functional connectivity in dynamic whole brain networks during sensorimotor timing and error correction was shown. Furthermore, the results presented in Chapter three revealed a significant difference in tapping variability between sensorimotor synchronization performed unimanally or bimanually with both index fingers in synchrony. Specifically, tapping variability was significantly lower during bimanual performance compared with unimanual SMS. It was suggested that the reduction in bimanual tapping variability may be associated with changes in functional connectivity between the left and right primary motor cortices (Serrien, 2008; Serrien et al., 2003).

This study aimed to investigate changes in interhemispheric functional connectivity between the left and right primary motor cortices during bimanual compared with unimanual SMS. In this chapter, a novel mathematical approach to functional connectivity was adopted in order to capture dynamic changes in interhemispheric connectivity over time and in different frequency ranges. Wavelet coherence analysis can be used to transform data into time-frequency space and thereby measure cross-correlation between two time series localized in time and frequency (Torrence & Compo, 1998). Time-frequency decomposition approaches have been used to analyze EEG and MEG data (Klein et al., 2006; Li et al., 2007; Zhan et al., 2006). Wavelet coherence analysis has previously been used to explore non-stationary signal relationships in fMRI data obtained during a visual task and during rest (Chang & Glover, 2010; Müller et al., 2004). The results of these studies revealed that dynamic relationships between functionally connected brain regions were characterized by non-stationary fluctuations in coherence and phase. The wavelet coherence approach is particularly suited to analyze fMRI data obtained during awake rest (resting state) because previous research has shown that resting state functional connectivity occurred primarily in the low frequency range

(Cordes et al., 2001; Cordes et al., 2000). As such, the wavelet coherence analysis is applied to fMRI data obtained during awake rest in Experiment 2 of this Chapter.

7.2 Experiment 1

7.2.1 Aims and hypotheses

The aim of Experiment 1 was to use wavelet coherence analysis in order to investigate changes in interhemispheric connectivity between the left and right primary motor cortices during bimanual, compared with unimanual, sensorimotor synchronization. It was hypothesized that there would be greater interhemispheric functional connectivity during bimanual than during unimanual SMS because both hemispheres are engaged in the same task.

7.2.2 Materials and methods

Subjects

A total of three healthy, right-handed male subjects (mean age 25 ± 4 years) took part in this study. The subjects did not report any history of psychiatric or neurological disorders. All subjects gave written informed consent prior to participating.

Paradigm

Subjects performed an auditory paced sensorimotor synchronization task inside the fMRI scanner. In two separate functional runs, subjects performed the task either unimanually with the right index finger or bimanually with both index fingers in synchrony. The pacing stimulus was a simple isochronous auditory sequence consisting of metronome tones (frequency of 500 Hz and duration of 50 ms) presented through MRI-compatible headphones. Subjects were asked to tap in synchrony with the auditory stimulus, aiming for their button presses to coincide with each tone. Each functional run was set up as a box-car design with 20 second blocks alternating between resting and tapping. Each run started with a resting block and contained a total of 24 tapping blocks, resulting in 16 minutes duration

per functional run. The pacing stimulus was presented at three different speeds in semi-random order such that the pacing speed in two successive blocks was never the same. The three tapping speeds (1 Hz, 2 Hz or 4 Hz for a total of 8 blocks each) fall within rate limits that have been determined by previous research, which showed that the fastest tapping speed is determined by the maximum frequency of finger movements (5-7 Hz). The lower rate limit is less well defined, but previous research has suggested that successful synchronization is possible up to about 0.5 Hz (Repp, 2005). Stimuli were controlled using E-Prime® software (run on Eloquence, InVivo Corp, Orlando, FL, USA) and behavioural responses were measured with a MRI compatible button box.

Functional magnetic resonance imaging

Functional imaging datasets were acquired using a 3T scanner (Achieva 3.0T, Philips Medical Systems, Best, The Netherlands) at the University of Sheffield. A single-shot, gradient recalled, echo-planar technique was used to acquire 30 x 5mm contiguous transverse slices covering the entire brain at 480 time points in each of the two functional runs (TR = 2000 ms, TE = 35 ms, in-plane resolution 1.8x1.8 mm, Sense factor = 1.5). A standard receive-only six-channel headcoil was used and subject-specific, localized shimming was performed. Concurrent cardiac and respiratory data were acquired with the scanner's built-in system using ECG leads on the subject's back and a pneumatic belt strapped around the ribcage.

Pre-processing

The imaging data were analyzed using SPM5 (http://www.fil.ion.ucl.ac.uk/spm). Motion correction was performed first by realigning the images to the central image with a 6-parameter (rigid body) spatial transformation (Jones et al., 2008). Additional physiological noise correction was achieved by removing polynomials (zero to fourth degree), lagged respiratory volume (-10 sec to +15 sec in steps of 1 TR) and lagged cardiac rate (0 to +24 sec in steps of 1 TR) (Birn et al., 2006; Kay et al., 2008; Shmueli et al., 2007). Further pre-processing stages involved slice timing correction, normalization into standard space and smoothing using Gaussian Kernels of 5 mm full width half maximum.

Defining regions of interest

Statistical analysis at the individual subject level was based on the General Linear Model using the boxcar design convolved with a canonical hemodynamic response function. The resulting contrast images were entered into a one-sample t-test to obtain second-level group results. Seed ROI locations in the left and right primary motor cortices were determined based on the group analysis of the contrast between bimanual tapping and rest. Unfiltered time series were extracted for each subject from the left (MNI [-36 -18 54]) and right (MNI [32 -22 64]) primary motor cortex during the unimanual and the bimanual functional runs (3 mm sphere).

Wavelet coherence analysis

Wavelet transform coherence (WTC) is a method that can be used to measure the cross-correlation between two time series localized in time and frequency (Torrence & Compo, 1998). Wavelets are zero-mean functions that are localized in both time and frequency and can be convolved with a uniform time series to obtain the continuous wavelet transform:

$$W_n^X(s) = \sqrt{\frac{\delta t}{s}} \sum_{n'=1}^{N} X_{n'} \psi_0 \left[(n' - n) \frac{\delta t}{s} \right]$$

where n denotes time and s denotes wavelet scale. Here, the Morlet wavelet function was chosen because it provides a good trade-off between time and frequency localization (Grinsted et al., 2004). The Morlet wavelet is defined as:

$$\psi_{0(\eta)} = \pi^{-1/4} e^{i\omega_0 \eta} e^{-1/2\eta^2}$$

where η is dimensionless time and ω_0 is frequency (here ω_0 = 6). From the continuous wavelet transforms of two time series, it is possible to calculate the cross-wavelet spectrum as follows:

$$W_n^{XY}(s) = W_n^X(s) W_n^{Y*}(s)$$

Wavelet coherence can be calculated from the continuous wavelet transforms and the cross-wavelet transform of two time series and is defined as:

$$R_n^2(s) = \frac{\left|S\left(s^{-1}W_n^{XY}(s)\right)\right|^2}{S(s^{-1}|W_n^X(s)|^2) \cdot S(s^{-1}|W_n^Y(s)|^2)}$$

This definition results in a complex quantity where the real part (R^2) describes coherence between the two time series in time-frequency space (ranging from 0 to 1). The complex argument describes the local phase difference between the two time series. Implementation of the wavelet transform coherence was based on available mathematical processing scripts (http://www.pol.ac.uk/home/research/waveletcoherence/, Grinsted et al., 2004, applied in Matlab R2008b, The Mathworks Inc., Natick, MA, USA, 2008).

Statistical comparison of wavelet coherence

Wavelet transform coherence analysis was applied as described above to produce time-frequency coherence spectra for inter-hemispheric functional connectivity between the left and right primary motor cortices during uni- and bi-manual tapping in each subject. Subsequently, a paired one-tailed t-test was performed to determine the points in time-frequency space at which there was greater inter-hemispheric coherence during bimanual tapping compared with unimanual performance.

Analysis of phase variance

The variance of the inter-hemispheric phase relationship between the primary motor cortices over time was determined by applying circular statistics to the complex argument of the wavelet transform coherence with the use of a Matlab toolbox (CircStat, Berens, 2009). This branch of statistics accounts for the circularity (0 – 360 degrees) and non-linearity (0 = 360 degrees) of directional data. Firstly, the average phase difference (over time) was calculated at each frequency. Secondly, to assess the temporal variance of the phase relationship, the circular standard deviation over time was calculated at each frequency point. A paired t-test

was performed at each frequency point to determine whether there was a significant difference between the temporal variability between the interhemispheric primary motor cortices during unimanual and bimanual finger tapping.

7.2.3 Results

From each tapping block, all responses during the first five seconds were discarded to allow the subject to establish tapping synchrony. Measures of timing performance include the mean and standard deviation of tap-tone asynchrony and of the inter-response-interval (IRI). Table 7.1 shows the behavioural results of finger tapping performance for all conditions. Taps preceded the tones by an average of 47 milliseconds (calculated over all tapping speeds), demonstrating an anticipatory negative mean asynchrony. The average IRI was 1035 ms when the speed of the pacing stimulus was 1 Hz, 524 ms when the pacing speed was 2 Hz and 244 ms when the pacing speed was 4 Hz.

		Asynchrony (ms)	**Asynchrony SD (ms)**	**IRI (ms)**	**IRI SD (ms)**
1 Hz	Unimanual (right)	-55.2 (34.9)	37.0 (8.3)	994.5 (3.9)	48.8 (10.0)
	Bimanual (right)	-75.6 (44.0)	39.4 (12.3)	1115.8 (122.7)	313.1 (141.0)
	Bimanual (left)	-77.9 (42.6)	36.3 (10.2)	993.3 (4.1)	71.1 (18.3)
2 Hz	Unimanual (right)	-30.4 (27.3)	26.7 (4.6)	498.8 (2.2)	28.2 (2.0)
	Bimanual (right)	-64.7 (27.6)	34.9 (14.6)	573.4 (15.6)	184.7 (8.9)
	Bimanual (left)	-67.6 (28.0)	29.5 (9.4)	498.8 (1.0)	38.4 (2.0)
4 Hz	Unimanual (right)	-20.8 (10.5)	33.0 (14.2)	245.5 (6.8)	17.3 (3.5)
	Bimanual (right)	-12.4 (9.2)	48.7 (26.0)	252.2 (6.0)	67.9 (15.5)
	Bimanual (left)	-19.7 (11.8)	42.1 (19.4)	235.7 (12.2)	26.7 (5.2)

Table 7.1: Behavioural finger tapping results. The tap-tone asynchrony and the inter-response-interval (IRI) are provided for each tapping speed and for each condition (uni- and bi-manual tapping). Standard deviations (within subjects) of

the tap-tone asynchrony and of the IRI are also provided (SD). All results are averaged over three subjects and the between-subject standard deviations are provided in parenthesis. All results are given in milliseconds.

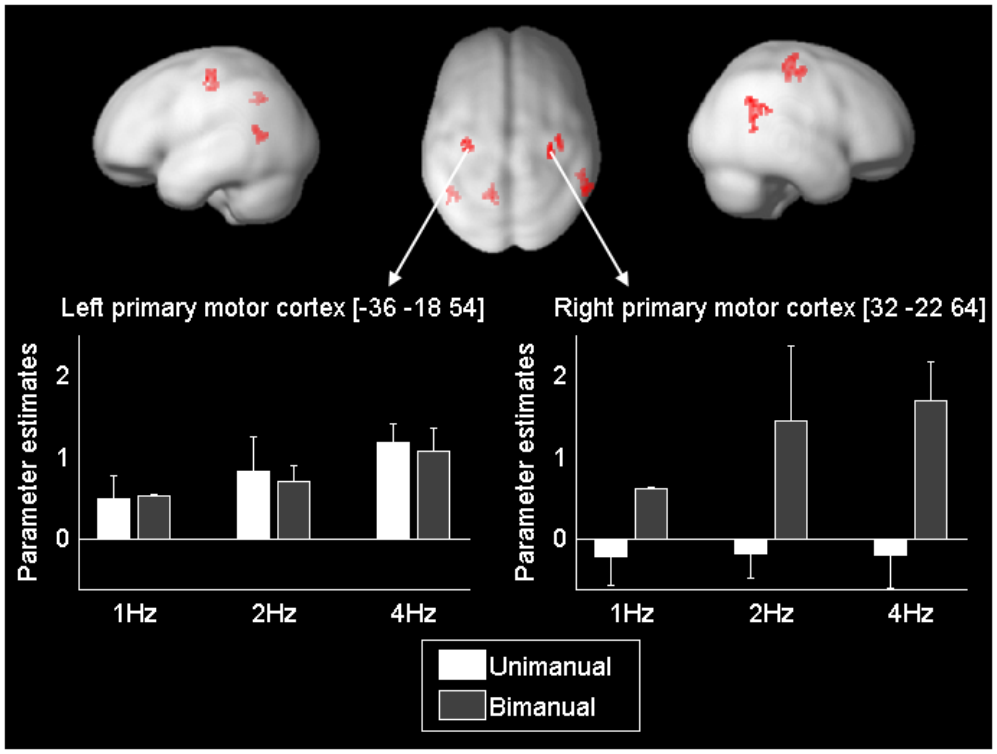

Figure 7.1: Functional imaging contrasts between regular tapping and rest. Functional MRI activations are rendered on a normalized smooth brain surface showing (from left to right): a sagittal view from the left, axial view from the top and sagittal view from the right. Findings are significant at p<.01 uncorrected and exceed a cluster-extent threshold of 25 voxels. The bottom two graphs show average parameter estimates for the active conditions (uni- and bi-manual tapping with a pacing speed of 1, 2 or 4 Hz) compared with rest in the left primary motor cortex [-36 -18 54] and in the right primary motor cortex [32 -22 64]. Error bars indicate the standard deviation calculated over three subjects.

The location of the seed regions of interest (ROIs) for the left and right primary motor cortex were based on the contrast between bimanual finger tapping at a speed of 1 Hz and rest (p<0.01 uncorrected, cluster extent threshold 25 voxels).

Compared with rest, bimanual finger tapping (at a speed of 1Hz) resulted in activations in the bilateral primary motor cortices, bilateral primary auditory cortices and in the somatosensory association cortex (Brodmann Area 7) (Figure 7.1). Parameter estimates were extracted from the resulting ROIs in the left and right primary motor cortices for each contrast between all active conditions and rest (Figure 7.1). These parameter estimates show that the ROIs accurately localize the primary motor cortices because they are significantly activated in all tapping conditions despite the fact that the ROIs were selected based on the contrast between 1Hz bimanual tapping and rest.

Pearson's cross-correlation coefficients show that, on average, the left and right primary motor cortex are positively correlated during bimanual tapping (mean 0.67, SD 0.05). On the contrary, during unimanual tapping the inter-hemispheric correlation coefficient was close to zero (mean -0.04, SD 0.36).

Figure 7.2 (A) shows the points in time-frequency space where there was significantly greater inter-hemispheric coherence between the left and right primary motor cortices during bi-manual finger tapping compared with unimanual tapping. The time-frequency spectrum in Figure 7.2 (A) is further summarized to show the relative contributions of different frequencies (Figure 7.2 B) and the relative coherence over time (Figure 7.2 C). The results show that the increase in inter-hemispheric coherence during bimanual tapping is relatively stable over time and peaks around 0.02 Hz. The opposite contrast was also performed (greater coherence during unimanual tapping compared with bimanual tapping) and yielded no significant results.

The mean and temporal variance of the phase relationship between the left and right primary motor cortex during uni- and bi-manual finger tapping are shown in Figure 7.3. The primary motor cortices were in phase during bimanual tapping, compared with the fluctuating phase relationship during unimanual tapping (Figure 7.3 A). Figure 7.3 B shows that the temporal variability of the inter-hemispheric phase relationship was generally lower during bimanual tapping than during

unimanual tapping. Results of a paired t-test performed separately at each frequency indicated the frequencies at which there was a significant difference in temporal variability between the uni- and bi-manual tapping ($p < .05$; marked * in Figure 7.3 B).

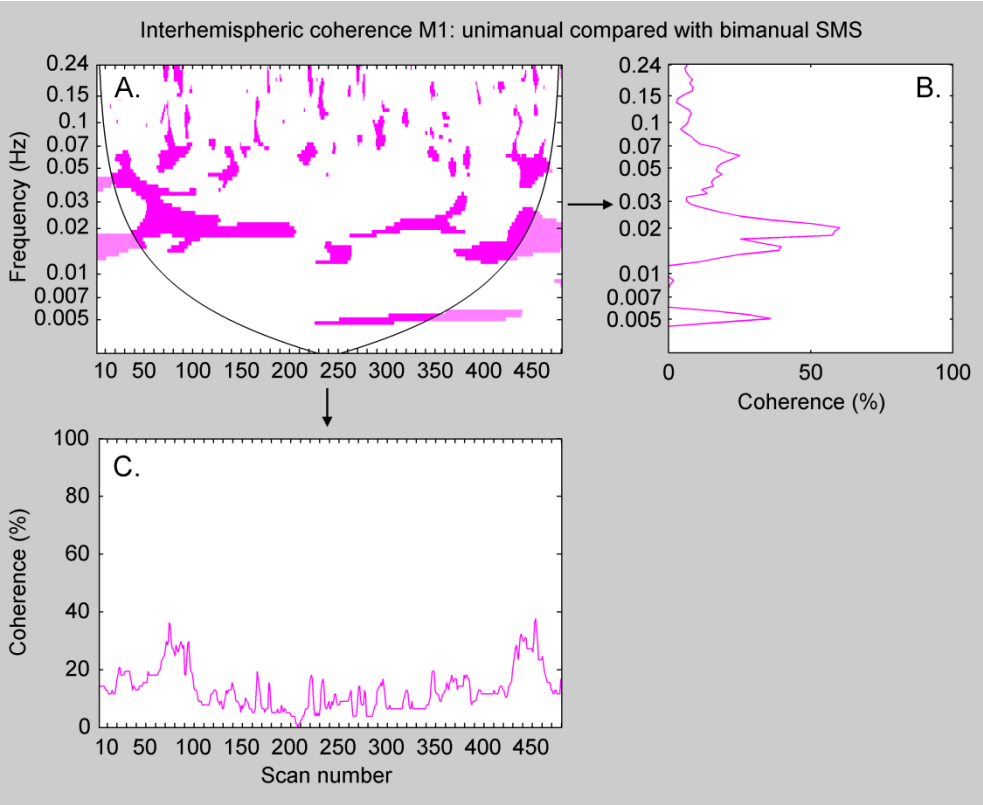

Figure 7.2: Inter-hemispheric coherence between the primary motor cortices. The binary image in figure A shows the points in time-frequency space where there was significantly greater inter-hemispheric coherence between the left and right primary motor cortices during bimanual synchronized finger tapping compared with unimanual finger tapping ($p < .05$). The graph in figure B summarizes the relative contributions of different frequencies by expressing the number of time points with significant coherence as a percentage of the total number of time points for each frequency. The graph in figure C summarizes the relative coherence over time by expressing the number of frequencies with significant coherence as a percentage of all frequencies for each time point. A peak in bimanual coherence can be seen around 0.02 Hz, with additional peaks around 0.005 and 0.07 Hz.

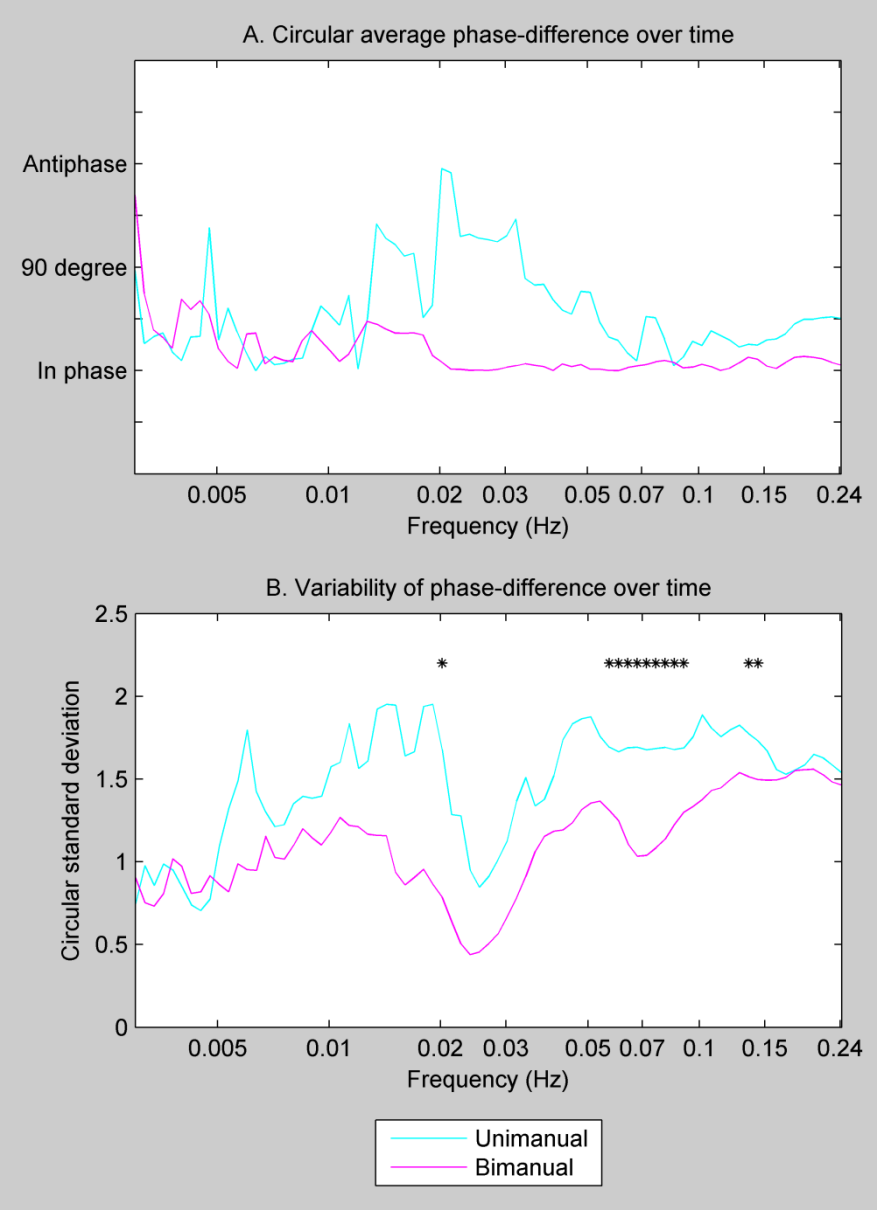

Figure 7.3: Averages and temporal standard deviations of the inter-hemispheric phase relationship between the primary motor cortices. The graph in figure A shows the average inter-hemispheric phase relationship between the left and right primary motor cortices during unimanual (cyan) and during bimanual (magenta) finger tapping. It is evident that the inter-hemispheric primary motor cortices are mostly in phase during bimanual tapping compared with unimanual performance. The graph in figure B shows the average standard deviation of the phase relationships calculated over time at each frequency. A paired t-test was performed

to compare the standard deviations during uni- and bi-manual finger tapping at each frequency. The frequencies at which the standard deviation of the phase relationship was significantly lower during bimanual tapping than during unimanual tapping are marked (*). The results indicate that the inter-hemispheric phase relationship is more stable during bimanual finger tapping compared with unimanual performance.

In summary, the results of Experiment 1 showed that there was greater interhemispheric functional connectivity between the bilateral primary motor cortex during bimanual SMS compared with unimanual SMS. In particular, wavelet coherence between the primary motor cortices was highest at a frequency of 0.02 Hz. In addition, the left and right primary motor cortices were primarily in phase during bimanual SMS, and the variability of the phase relationship over time was lower during bimanual SMS compared with unimanual SMS. In Experiment 2, the wavelet coherence analysis is applied to fMRI data obtained during awake rest in order to investigate the time-frequency markers of different resting state networks.

7.3 Experiment 2

7.3.1 Aims and hypotheses

Functional connectivity measured during awake rest has revealed that the brain is intrinsically organized into distinct networks (Fox et al., 2005). Since the first demonstration of resting state connectivity by Biswall and colleagues (1995), several resting state networks have been identified with considerable consistency and reliability over subjects, scanner protocols and statistical approaches (Damoiseaux et al., 2006; Shehzad et al., 2009). The default mode network (DMN) comprises several midline regions including the posterior cingulate cortex, lateral parietal cortex and medial pre-frontal cortex, that exhibit a relative decrease in activity during task performance compared with intrinsic activity during awake rest (Greicius et al., 2003; Raichle et al., 2001). A second resting state network, termed

the task-positive or anti-correlated network (ACN), includes brain areas associated with goal-directed attention such as the inferior parietal lobule and the dorsolateral pre-frontal cortex (Fox et al., 2005; Fransson, 2005). Regions in the ACN are negatively correlated with the DMN and show increased activity during task performance relative to rest.

The application of a frequency domain analysis such as wavelet coherence to resting state data is of interest because previous work has suggested that intrinsic functional connectivity occurred primarily in the low frequency range (Cordes et al., 2001; Cordes et al., 2000). Wavelets are well-suited for the analysis of fMRI data because of their adaptivity to non-stationary, localized signal fluctuations (Bullmore et al., 2004). Previous applications of wavelet analysis to fMRI data have attempted to address problems of time series modelling, multiple hypothesis testing and of resampling fMRI time series in both space and time (Brammer, 1998; Bullmore et al., 2004; Bullmore et al., 2001; Fadili & Bullmore, 2002, 2004). Additionally, wavelet coherence analysis has previously been used to explore non-stationary signal relationships in fMRI data obtained during rest (Chang & Glover, 2010; Müller et al., 2004). Chang and Glover (2010) showed significant variability in coherence between the DMN and the ACN over time, which may explain why negative between-network correlations are often of a lower magnitude than positive correlations within the DMN (Shehzad et al., 2009). These results suggest that functional connectivity between brain regions fluctuates over time which may result in temporal variability of the phase relationship. The use of wavelet coherence analysis invites numerous unanswered questions with regards to the dynamic features of functional connectivity within and between resting state brain networks. For instance, does resting state functional connectivity occur uniformly at low frequencies or are different networks characterized by distinct frequency footprints?

In Experiment 2, time-frequency dynamics of functional connectivity that occurs within and between resting state networks was investigated with the use of wavelet coherence analysis. The first aim of Experiment 2 was to examine coherence

within nodes of the DMN and the ACN (intra-network) and between nodes of these two resting state networks (inter-network). Network coherence was assessed at a group-level by contrasting time-frequency coherence between the nodes of interest against time-frequency coherence between nodes of a reference network. The reference network was made up of regions that typically show zero correlation and comprised the primary motor, auditory and visual cortices (Van Dijk et al., 2010). It was hypothesized that there would be increased coherence within and between the resting state networks compared with the reference network. Secondly, Experiment 2 aimed to determine the temporal variance of the phase relationship within and between the DMN and ACN. Based on previous research (Chang & Glover, 2010), it was hypothesized that the temporal variance of the inter-network phase relationship would be greater than the temporal variance of the intra-network phase relationship between nodes of the DMN.

7.3.2 Materials and methods

Subjects

A total of twelve healthy, right-handed male subjects (mean age 23.8 ± 2.2 years) took part in the study. The subjects did not report any history of psychiatric or neurological disorders. All subjects gave written informed consent prior to participating.

Functional Magnetic Resonance Imaging

Functional imaging datasets were acquired using a 3T scanner (Achieva 3.0T, Philips Medical Systems, Best, The Netherlands) at the University of Sheffield. A single-shot, gradient recalled, echo-planar technique was used to acquire 16 x 8mm contiguous transverse slices covering the entire brain at 400 time points (TR = 1050 ms, TE = 35 ms, in-plane resolution 1.8x1.8 mm, Sense factor = 1.5). A standard receive-only six-channel headcoil was used and subject-specific, localized shimming was performed. The subjects were deprived of sensory input with the use of earplugs covered with head phones and blindfolds. Scanning data were acquired during awake resting state for seven minutes. Subjects were instructed to remain awake and avoid structured thinking (such as counting). Concurrent cardiac and

respiratory data were acquired with the scanner's built-in system using ECG leads on the subject's back and a pneumatic belt strapped around the ribcage. Data from two subjects had to be excluded from further analysis due to a failure of the physiological data acquisition.

The pre-processing stages were identical to the pre-processing of the SMS data and included motion correction, physiological noise regression, slice timing correction, normalization and smoothing (5mm FWHM). One subject was removed from further analysis due to excessive movement during the resting state scan (> 4 mm translation and > 3 degrees rotation).

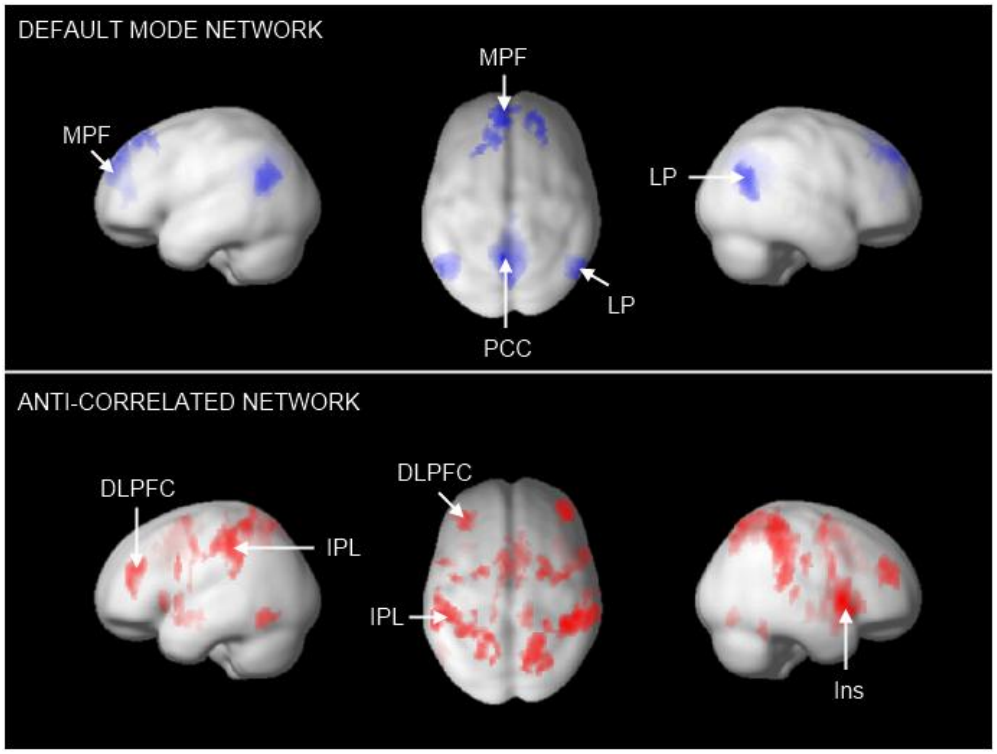

Figure 7.4: Resting state network regions of interest. Figure 7.4 shows the results of a second-level group analysis of whole-brain correlation coefficients with a seed region of interest (ROI) in the posterior cingulate cortex (PCC: 3mm radius sphere centred at [-6 -58 28]). Positive correlations with the PCC are shown at the top in blue and represent the default mode network (DMN) and negative correlations are shown at the bottom in red and represent the anti-correlated network (ACN).

Results are rendered on a normalized smooth brain surface showing (from left to right): a sagittal view from the left, axial view from the top and sagittal view from the right. Findings are significant at p < .001 uncorrected and exceed a cluster-extent threshold of 50 voxels. For both the DMN and the ACN the three regions with the highest t scores are labelled. These regions were used as ROIs for further analysis and cluster locations and corresponding t scores are summarized in Table 7.2.

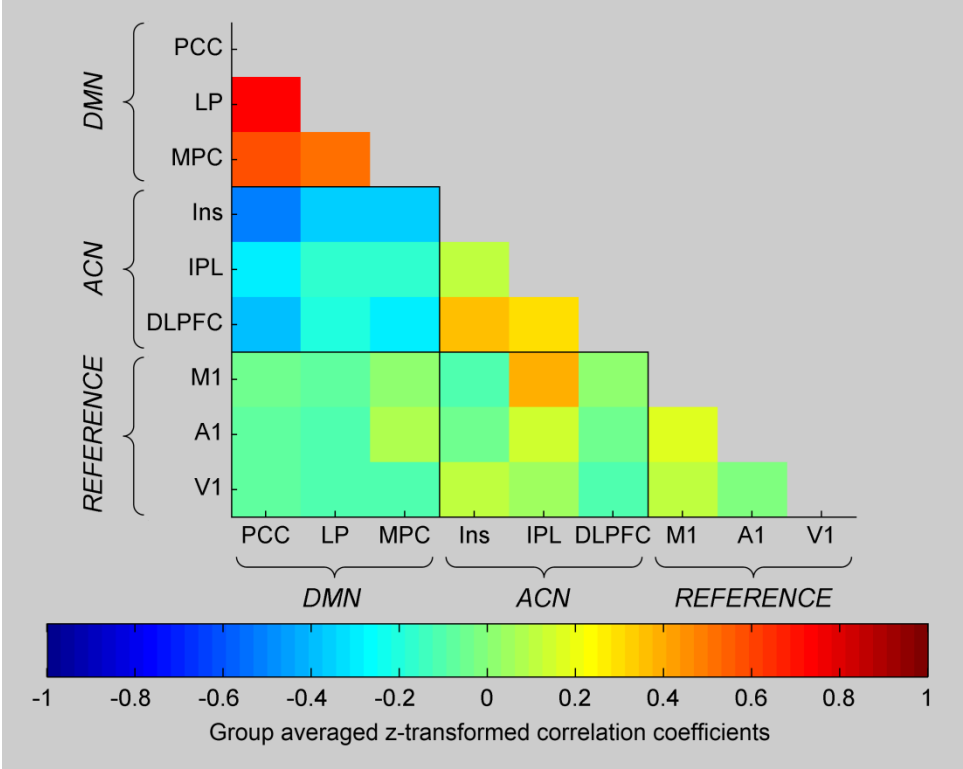

Figure 7.5: Cross-correlation coefficients between resting state network regions. Group averaged z-transformed correlation coefficients between the nine selected regions of interest after temporal filtering (cut-of .08 Hz). The results show positive correlation coefficients between regions of the DMN and between regions of the ACN and negative inter-network correlation coefficients between the DMN and ACN. Furthermore, the correlation coefficients within the reference network are close to zero. Abbreviations are explained in Table 7.2.

Defining the region of interest

An *a priori* region of interest (ROI) in the posterior cingulate cortex (PCC) was selected based on previous studies (Chang & Glover, 2010; Shehzad et al., 2009; Toro et al., 2008). Pearson's correlation coefficients were calculated between the time series extracted from this PCC ROI (3mm radius sphere centred at [-6 -58 28]) and all other voxels in the brain for each subject after low-pass filtering (cut-off 0.08Hz) (Biswal et al., 1995). The z-transformed whole-brain Pearson's correlation coefficients were entered into a second level one-sample t-test. Three ROIs were selected for the default mode network as identified by the highest t-scores in the second level group results with a positive contrast weight (threshold: $p < 0.001$ uncorrected, $t > 4.5$, Figures 7.4 & 7.5). Three ROIs were also selected for the anti-correlated network as identified by the highest t-scores in the second level group results with a negative contrast weight (threshold: $p < 0.001$ uncorrected, $t > 4.5$, Figures 7.4 & 7.5). Unfiltered data at each DMN and ACN ROI (as summarized in Table 7.2) were extracted from a 3mm radius sphere.

Network	Region of interest	Abbreviation	MNI coordinates			T-score
			x	y	z	
Default mode	Posterior cingulate cortex	PCC	-6	-58	28	905.4
network	Lateral parietal cortex	LP	56	-66	20	11.8
	Medial pre-frontal cortex	MPF	-6	58	26	11.0
Anti-correlated	Insula	Ins	58	10	0	26.3
network	Inferior parietal lobule	IPL	-44	-34	48	24.5
	Dorsolateral pre-frontal cortex	DLPFC	-38	36	26	16.2
Reference	Primary motor cortex	M1	36	-25	57	
network	Primary auditory cortex	A1	43	-26	12	
	Primary visual cortex	V1	30	-88	0	

Table 7.2: Resting state network regions of interest. Cluster locations and corresponding t scores of selected regions of interest (ROIs) used for further

investigation with wavelet transform coherence analysis. MNI coordinates of local maxima are provided (x y z in mm) for the top three clusters that were significant (p < .001 uncorrected, cluster-extent threshold of 50 voxels). Note that the t score for the PCC is artificially high because this region was chosen as the seed ROI for the correlation coefficient analysis. The location of the reference network ROIs is based on previous research and is therefore not accompanied by a corresponding t score (Van Dijk et al., 2010).

Three additional ROIs were selected from brain regions of which fluctuations over time were not expected to be correlated. The location of these reference ROIs was identified based on previous research (Van Dijk et al., 2010). Unfiltered data at each reference ROI (as summarized in Table 7.2) were extracted from a 3mm radius sphere.

Statistical comparison of wavelet coherence

The first aim of Experiment 2 was to achieve a group-level statistical analysis of intra-network wavelet coherence and inter-network wavelet coherence in the time-frequency domain. In total there are 9 ROIs (3 each for DMN, ACN and the reference network). The objective was to summarize intra-network coherence for the DMN (Figure 7.6 A: constituted by 3 ROI combinations) and for the ACN (Figure 7.6 B: constituted by 3 ROI combinations), and to summarize inter-network coherence between the DMN and the ACN (Figure 7.6 C: constituted by 3x3=9 ROI combinations). To achieve these objectives, wavelet coherence spectra of all ROI combinations that make up the total intra- and inter-network coherence were averaged for each subject as visualized in Figure 7.6. Subsequently, a paired one-tailed t-test was performed at each point in time-frequency space to compare the averaged coherence of the network of interest (intra-network DMN or ACN or inter-network) against the same point in time-frequency space in the averaged intra-network reference coherence (Figure 7.6 D). Hence, this statistical approach identifies points in time-frequency space where the averaged coherence between the nodes of the network of interest is greater than the average coherence between the nodes of the reference network.

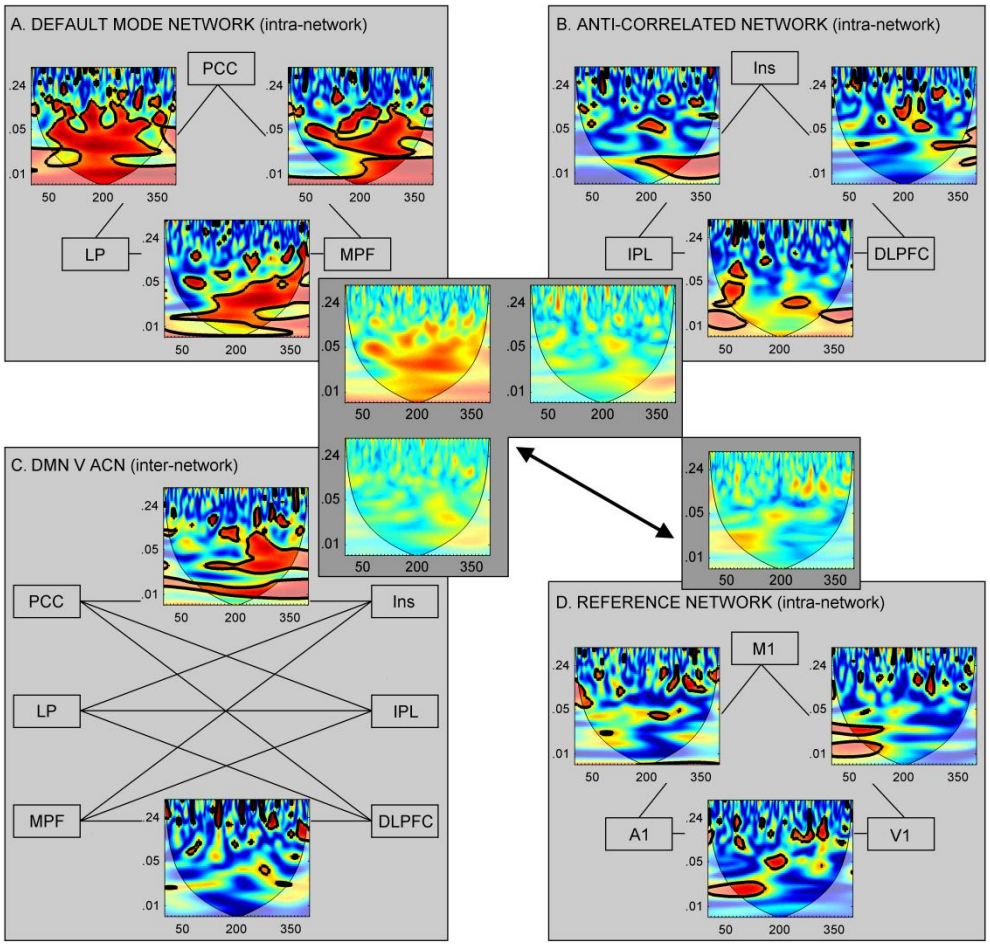

Figure 7.6: Summary that explains the averaging over wavelet transform coherence spectra. Intra-network DMN connectivity is made up by three ROI combinations between the PCC, LP and MPF (A), intra-network ACN is also made up by three ROI combinations (B), as is the intra-network reference coherence (D). Inter-network coherence between the DMN and the ACN is made up of connections between the three DMN ROIs and the three ACN ROIs, thereby creating nine ROI combinations (C). For each subject, the coherence spectra are averaged over these ROI combinations to achieve a single coherence spectrum for intra-network DMN, ACN and reference coherence and for inter-network coherence. A paired one-tailed t-test is then performed at each point in time-frequency space to investigate whether coherence in the network of interest (intra-network DMN, ACN or inter-network) is greater than intra-network reference coherence (D). Representative examples of first-level and averaged wavelet coherence spectra for one subject are shown here to illustrate the averaging process.

Analysis of phase variance

The second aim of Experiment 2 was to determine the variance of intra- and inter-network phase relationships over time. To achieve this, circular statistics were applied to the complex argument of the wavelet transform coherence. Firstly, the average phase difference (over time) was calculated at each frequency for each ROI combination. These frequency-specific phase differences were then averaged over all ROI combinations that constitute the networks of interest. The average phase differences of each network were then averaged over nine subjects to provide an indication of the intra- and inter-network phase relationships. Secondly, to assess the temporal variance of the phase relationship, the circular standard deviation over time was calculated at each frequency point for each ROI combination. These circular standard deviations were averaged within subjects over all ROI combinations that constitute the networks of interest. A one-way ANOVA was performed at each frequency point to determine whether there was a significant difference between the temporal variability of the intra-network DMN phase relationship, the intra-network ACN phase relationship and the inter-network phase relationship.

7.3.3 Results

Due to the removal of three subjects (2 with no physiological data and 1 with excessive movement), data from nine subjects (mean age 24.2 ± 2.2 years) are reported below. All subjects remained awake for the duration of the functional scan.

ROI selection

Figure 7.4 shows the results of a second-level group analysis of whole-brain correlation coefficients with a seed ROI in the posterior cingulate cortex. The six selected ROIs for further analysis are labelled in Figure 7.4 and cluster locations and corresponding t scores are provided in Table 7.2.

Group averaged z-transformed Pearson's correlation coefficients between the selected ROIs are summarized in Figure 7.5. Results confirm that the nodes of the

DMN exhibited positive intra-network correlation coefficients (mean 0.52, SD 0.19). The negative correlation coefficients between the DMN and the ACN nodes (inter-network) were lower in magnitude compared with the intra-network DMN (mean -0.29, SD 0.18). Similarly, the positive correlation coefficients between nodes of the intra-network ACN were lower in magnitude compared with the intra-network DMN (mean 0.24, SD 0.25). Results also confirmed that the nodes of the reference network exhibited correlation coefficients that were close to zero (mean 0.09, SD 0.202).

Resting state network wavelet coherence

Representative examples of wavelet coherence spectra of individual ROI combinations for one subject are shown in Figure 7.6. For each subject, these wavelet coherence spectra were averaged to achieve a single wavelet coherence spectrum for intra-network DMN, ACN and reference network coherence and for inter-network coherence (as summarized in Figure 7.6). Subsequently, a paired one-tailed t-test was performed across all subjects to compare each of the three networks of interest against the 'background' coherence within the reference network. Figure 7.7A shows the points in time-frequency space where there was significantly greater intra-network coherence in the DMN compared with the reference network ($p < .05$). The time-frequency spectrum in Figure 7.7A is further summarized to show the relative contributions of different frequencies (Figure 7.7B) and the relative coherence over time (Figure 7.7C). The results in Figure 7.7 reveal that coherence within the DMN was maintained for the duration of the scan and peaked around 0.007 Hz. Figure 7.8 shows the points in time-frequency space at which there was significantly greater intra-network coherence in the ACN compared with the reference network ($p < .05$). As can be seen in Figure 7.8B, coherence within the ACN peaked around 0.02 Hz and mainly occurred during the middle part of the resting state scan (Figure 7.8C). Lastly, Figure 7.9 shows the points in time-frequency space where the inter-network coherence between the DMN and the ACN was greater than coherence within the reference network ($p < .05$). Figure 7.9B reveals that inter-network coherence between the DMN and the ACN peaked around 0.07 Hz.

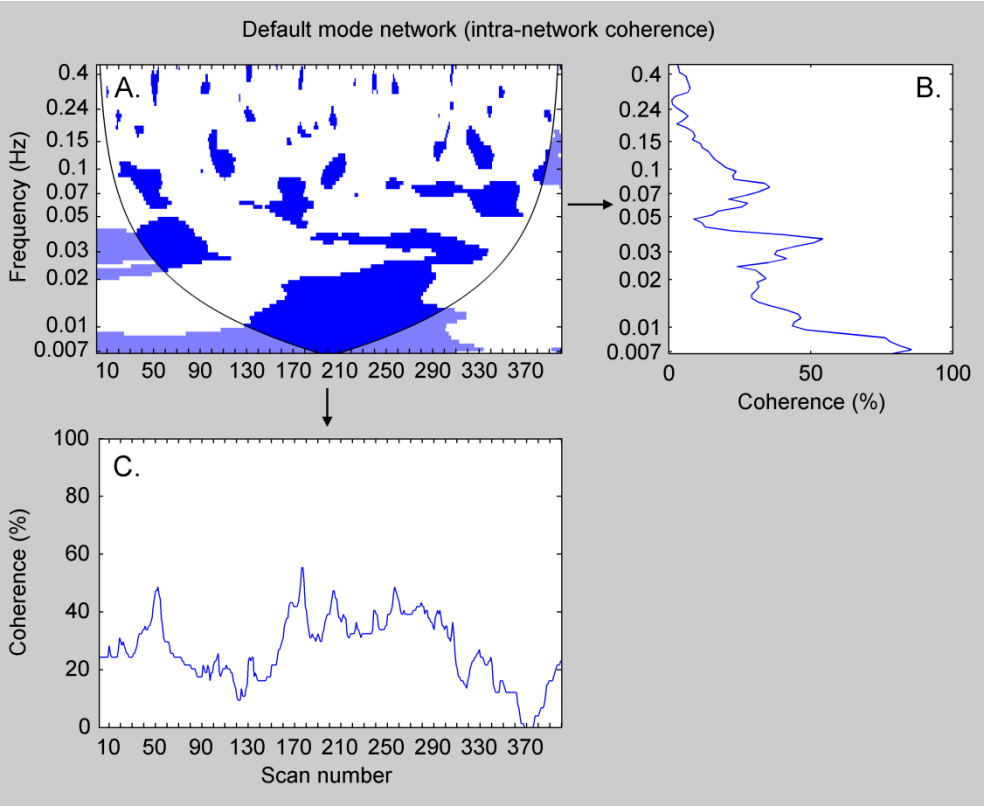

Figure 7.7: Default mode network coherence. The binary image in figure A shows the points in time-frequency space where there was significantly greater intra-network coherence in the default mode network (DMN) compared with the reference network ($p < .05$). The graph in figure B summarizes the relative contributions of different frequencies by expressing the number of time points with significant coherence as a percentage of the total number of time points for each frequency. The graph in figure C summarizes the relative coherence over time by expressing the number of frequencies with significant coherence as a percentage of all frequencies for each time point. A peak in DMN coherence can be seen around 0.007 Hz, with additional peaks around 0.03 and 0.07 Hz.

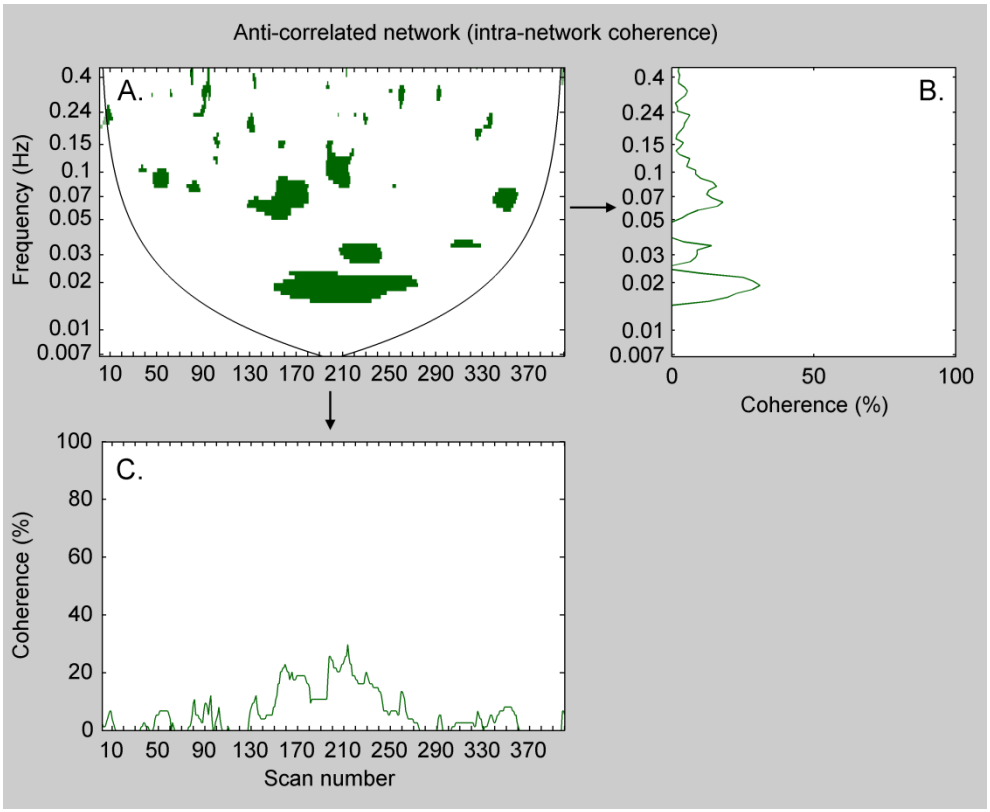

Figure 7.8: Anti-correlated network coherence. The binary image in figure A shows the points in time-frequency space where there was significantly greater intra-network coherence in the anti-correlated network (ACN) compared with the reference network ($p < .05$). The graph in figure B summarizes the relative contributions of different frequencies by expressing the number of time points with significant coherence as a percentage of the total number of time points for each frequency. The graph in figure C summarizes the relative coherence over time by expressing the number of frequencies with significant coherence as a percentage of all frequencies for each time point. A peak in ACN coherence can be seen around 0.02 Hz, with additional peaks around 0.03 and 0.07 Hz.

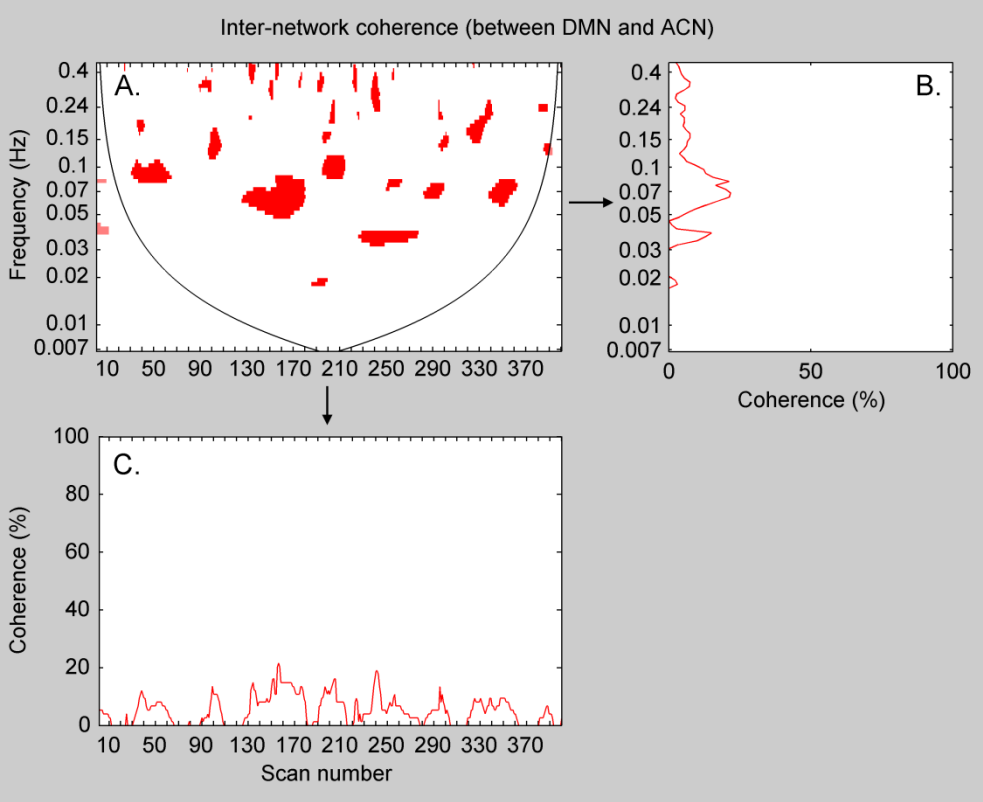

Figure 7.9: Inter-network coherence between the default mode and anti-correlated networks. The binary image in figure A shows the points in time-frequency space where there was significantly greater inter-network coherence between the default mode network and the anti-correlated network compared with intra-network coherence within the reference network ($p < .05$). The graph in figure B summarizes the relative contributions of different frequencies by expressing the number of time points with significant coherence as a percentage of the total number of time points for each frequency. The graph in figure C summarizes the relative coherence over time by expressing the number of frequencies with significant coherence as a percentage of all frequencies for each time point. Peaks in inter-network coherence can be seen around 0.03 and 0.07 Hz.

Temporal variance of phase relationships

Intra-network DMN and ACN and inter-network phase relationships were investigated by calculating the mean and standard deviation from the imaginary argument with the use of circular statistics. Figure 7.10A shows that, on average,

intra-network nodes of both the DMN and the ACN were in phase with each other, as expected based on the positive correlation coefficients between these ROIs. The inter-network relationship between nodes of the DMN and ACN were on average in anti-phase, in line with the negative correlation coefficients between these ROIs. However, as can be seen in Figure 7.10A, the phase relationships in all networks diverged from these expected values at higher frequencies (above approximately 0.2 Hz).

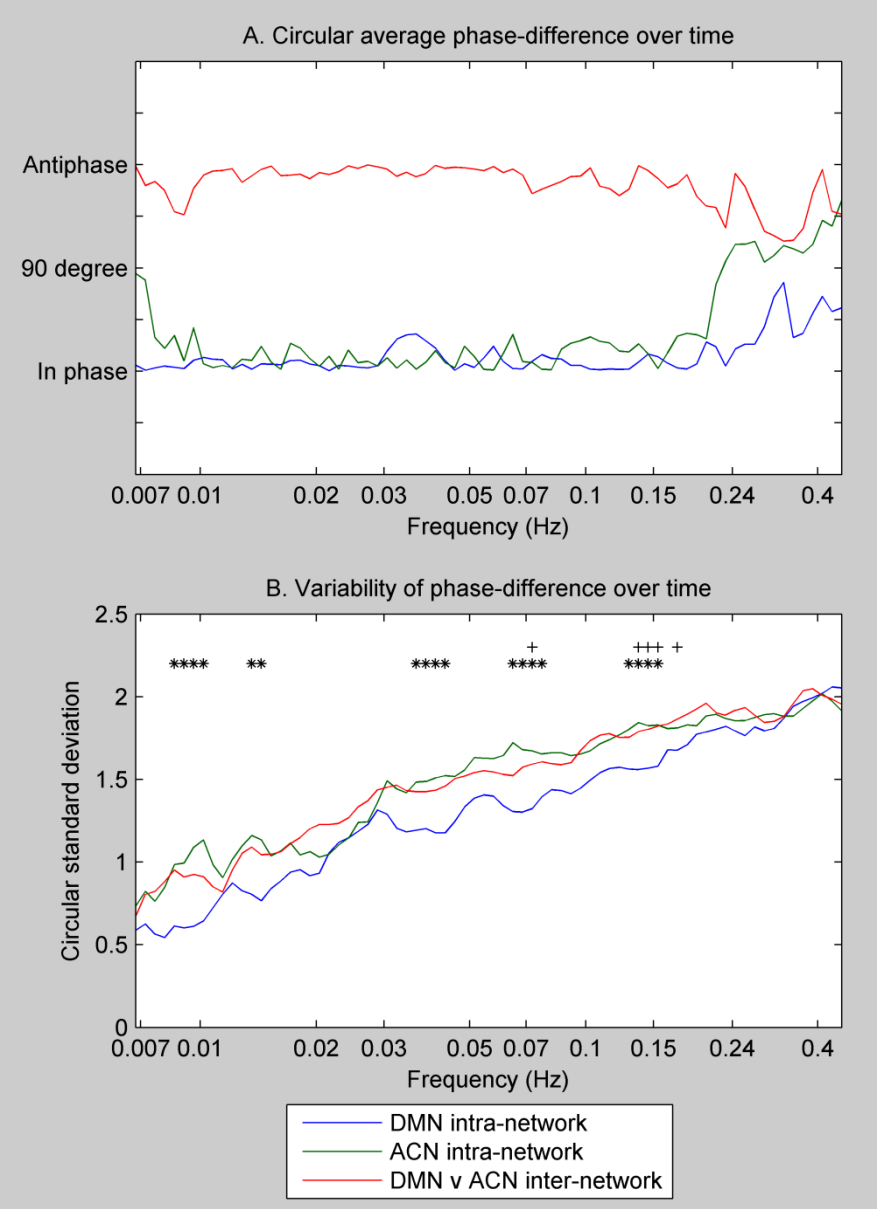

Figure 7.10: Averages and temporal standard deviations of the phase relationships for all resting state networks. The graph in figure A shows the average phase relationship between nodes of the DMN (blue, intra-network) and ACN (green, intra-network) and the average inter-network phase relationships between nodes of the DMN and ACN (red). It is evident that phase relationships are consistent in the mid-frequency range (i.e. intra-network nodes are in phase and inter-network nodes are in anti-phase), whereas phase relationships vary at higher frequencies (above ±0.2 Hz). The graph in figure B shows the average standard deviation of the phase relationships calculated over time at each frequency. Results reveal a positive linear relationship between frequency and standard deviation such that phase relationships become increasingly unstable at higher frequencies. A one-way ANOVA was performed to compare the standard deviations of the three networks (intra-network DMN and ACN and inter-network) at each frequency. The frequencies at which the standard deviation of the phase relationship within the DMN was significantly lower than the inter-network standard deviation are marked (+) and the frequencies at which the standard deviation was significantly lower within the DMN compared with the ACN are marked (*). The results indicate that the phase relationships within nodes of the DMN are more stable than the ACN or inter-network phase relationships.

Figure 7.10B shows the temporal variability of the phase relationship averaged over all subjects. The results revealed that there was a linear increase in the temporal variability of the phase relationship with frequency such that the variability was lowest at low frequencies and highest at high frequencies. The results of a Pearson's correlation coefficient analysis indicated a significant positive correlation between frequency and the temporal variability of the phase relationship in all subjects for intra-network DMN (mean correlation coefficient 0.76, SD 0.11) and ACN (mean correlation coefficient 0.67, SD 0.11) and for inter-network nodes (mean correlation coefficient 0.75, SD 0.07). Furthermore, it is evident that the temporal variability within the DMN was consistently lower than the temporal variability within the ACN and the inter-network temporal variability. Results of a one-way ANOVA performed separately at each frequency confirmed

that the intra-network variability was significantly lower within the DMN compared with the ACN at several frequencies ($p < .05$; marked * in Figure 7.10B).

In summary, the results of Experiment 2 revealed that wavelet coherence was greater within and between resting state networks compared with a reference network made up of uncorrelated brain regions. The results suggested that different resting state networks may be characterized by different frequency footprints because intra-network coherence in the DMN peaked around 0.007 Hz, intra-network coherence in the ACN peaked around 0.02 Hz and inter-network coherence peaked around 0.07 Hz. Secondly, the results of Experiment 2 revealed that the temporal variability of the phase relationship between nodes of the DMN (intra-network) was significantly lower than the temporal variability of phase relationships with in the ACN and between the two resting state networks (inter-network).

7.4 Discussion

The aim of this study was to investigate changes in interhemispheric functional connectivity between the bilateral primary motor cortices during uni- and bi-manual SMS. This aim was addressed in Experiment 1 using wavelet coherence analysis. The results revealed that there was greater interhemispheric functional connectivity during bimanual SMS compared with unimanual SMS. Previous studies have provided evidence for inhibitory interactions during unimanual SMS that are directed from the active primary motor cortex to the ipsilateral primary motor cortex (Aramaki et al., 2006; Aramaki et al., 2010; Pollok et al., 2005; Serrien, 2008; Serrien & Brown, 2002; Serrien et al., 2003). However, the correlation and coherence results presented here did not reveal this inhibitory functional connectivity during unimanual SMS. This negative finding may be explained by the relative insensitivity of the BOLD signal to inhibitory neural interactions (Tagamets & Horwitz, 2001). The relative increase in interhemispheric connectivity observed during bimanual SMS is consistent with previous findings

and most likely reflects an excitatory coupling that is driven by the dominant (left) primary motor cortex (Serrien et al., 2003). The results of Experiment 1 provide evidence for a dynamic shift in functional connectivity within a simple motor network that may be associated with a significant improvement in behavioural performance, as shown in Chapter three (Serrien, 2008; Walsh et al., 2008).

In Experiment 2, the wavelet coherence approach was used to analyze fMRI data obtained during awake rest because previous research has shown that resting state functional connectivity occurred specifically at low frequencies (Biswal et al., 2010). The findings of Experiment 2 provided proof-of-concept evidence for the applicability of wavelet coherence analysis to resting state fMRI data. The first main finding of Experiment 2 was that characteristic time-frequency patterns occurred in intra- and inter-network resting state functional connectivity. Some frequency peaks in the wavelet transform coherence were commonly seen in all resting state networks. For example, significant coherence occurred in all networks around 0.03 Hz and around 0.07 Hz (Figures 7.7, 7.8, 7.9). On the other hand, dissociable peaks in the resting state wavelet transform coherence may be used to differentiate between networks. For example, a peak in intra-network coherence in the DMN was found around 0.007 Hz, whilst there was no peak in coherence in this frequency-range for intra-network ACN or for inter-network functional connectivity. Moreover, intra-network ACN relationships were differentiated from the other resting state networks by a peak in coherence around 0.02 Hz. These findings suggest that network-specific frequency patterns emerge within what is jointly termed the 'low frequency range' (< 0.1 Hz; Biswal et al., 2010). Although replication of these findings is required to confirm that these differential frequency peaks are a consistent feature of resting state networks, a closer investigation of these frequency footprints may lead to a greater understanding of the cognitive processes that occur at rest. A comparison between wavelet transform coherence analysis of resting state data and of task-induced data may provide insights into the functions of these relatively unconstrained resting state networks. For example, the results of Experiment 1 and 2 revealed that the peak frequency of coherence found during bimanual finger tapping is the same as the peak frequency of intra-network

coherence within the ACN in the resting state data (0.02 Hz; Figure 7.2, 8.9). This may suggest that there is some overlap in the processes that occur in the ACN at rest and during bimanual tapping. Although these findings are preliminary, one might speculate, for example, that the coherence peak at the frequency of 0.02 Hz may reflect goal-directed attention to the external world.

The second main result of Experiment 2 indicated that the temporal variability of phase relationships was significantly lower between ROIs of the intra-network DMN compared with intra-network ACN and inter-network ROIs (Figure 7.10 B). Hence, dynamic changes in the direction of the correlation (as indicated by the phase) occurred over time in the ACN and between the DMN and the ACN, whereas the relationship between nodes of the DMN was relatively stable. A previous study by Chang and Glover (2010) showed scale-dependent fluctuations in the magnitude of coherence between ROIs of the DMN and the ACN (inter-network). The authors concluded that 'negative correlation coefficients may be weakened by inter-trial variability and may oversimplify dynamic relationships between time series' (Chang & Glover, 2010). The findings of Experiment 2 are consistent with the results presented by Chang and Glover and explain the reduced strength of inter-network correlation coefficients and coherence found in this study and in much of the previous literature. A speculative hypothesis may be that the cognitive processes associated with the DMN (such as rumination) are performed with relative consistency over time. On the contrary, the cognitive processes achieved by the ACN (such as the presence or absence of attention to the external world) may be more variable over time during a resting state fMRI scan. Alternatively, it may be that differences in temporal phase variability are associated with regional differences in noise components.

7.4.1 Limitations and areas for future work

This study demonstrated the use of wavelet coherence analysis to investigate dynamic coherence and phase relationships in functional connectivity networks during task performance and during awake rest. Future studies will be required to

further develop the wavelet coherence analysis presented here in order to address some methodological limitations. One remaining challenge is to develop principled approaches to correct for multiple comparisons in time-frequency datasets in the same way that corrections are applied to conventional fMRI analyses. Additionally, within-subject averaging was used in Experiment 2 to obtain summary wavelet transform coherence and phase plots for all resting state networks in each subject. Future work is needed to advance the combination of data at the single subject level, for example with the use of principle component analysis. Further research is also needed to investigate the consistency and reliability of the wavelet transform coherence findings on a larger scale over subjects and scanner protocols. Lastly, the group-level statistical analysis of coherence in resting state networks is predicated on the assumption that there is minimal (background) coherence between nodes of the reference network (between primary motor, auditory and visual cortices). The results showed that correlation coefficients between nodes of the reference network were on average close to zero, which suggests that this assumption is valid. However, inter-individual differences in reference network coherence may affect group-level results of significant resting state network coherence.

In conclusion, the findings of Experiment two reveal that resting state networks are typified by frequency-specific dynamic fluctuations in coherence and phase that are overlooked by conventional functional connectivity approaches. Although future research is required to optimize the wavelet transform coherence methodology, I suggest that this method provides a valuable tool that can complement existing functional connectivity analyses such as SCA and ICA in order to characterize functional connectivity networks in time-frequency space and perhaps begin to understand the processes that take place in the brain during awake rest.

8 Study 6: Where does transcranial magnetic stimulation (TMS) stimulate?

8.1 Aims and rationale

Theta burst transcranial magnetic stimulation (TBS) was applied in Chapters four, five and six to temporarily suppress or facilitate activity in a target brain region in order to determine its contribution to sensorimotor timing or error correction. Specifically, it was shown with the use of TBS that the left pre-motor cortex and the left cerebellum are essential for the correction of supraliminal timing errors. However, as discussed in Chapter two, the effects of transcranial magnetic stimulation (TMS), including TBS, on the heterogeneous and functionally connected human brain are, at present, not entirely understood.

Previous human physiological studies have shown that neural stimulation mainly occurs in areas where the amplitude of the induced electric field is high (Amassian et al., 1994; Maccabee et al., 1993; Wassermann et al., 1996). In air, or in electrically homogeneous material, the maximum electric field induced by the commonly used figure-of-eight coil geometry occurs directly under the centre of the coil, at the point where the two circular parts overlap (Cohen et al., 1990; Ueno et al., 1988). In practice, the real location and extent of the induced fields are affected by many parameters such as skull thickness and geometry and the electrical properties of different tissue types. In addition, TMS parameters such as the electric current in the coil (both waveform and duration), and the coil shape and winding geometry all affect the resultant induced fields and their biological potency (Barker et al., 1991; Jalinous, 1991; Salinas et al., 2009; Stokes et al., 2007; Toschi et al., 2008).

Several approaches have been used in an attempt to measure the induced electric field or neural responses resulting from TMS. Motor evoked potentials induced by TMS over the primary motor cortex have been used to investigate the effect of various TMS parameters and to assess intra-subject reliability (Dubach et al., 2004;

Kammer et al., 2001; Wolf et al., 2004). Intra-cranial recordings using implanted electrodes in monkeys and humans have been used to show the differences in response due to cortical depth and coil angle and orientation (Lisanby et al., 2001; Wagner et al., 2004a). Lastly, electroencephalography (EEG) and neuroimaging methods such as positron emission tomography (PET) and functional magnetic resonance imaging (fMRI) have been used to measure neural activity associated with TMS (Bestmann et al., 2004; Bohning et al., 1998; Paus et al., 1997; Paus et al., 2001). Although findings from these studies are very helpful to the understanding of the effect of TMS on neural tissue, they are predicated on having a readily observable metric directly related to the neuronal stimulus. Therefore, a full characterization of TMS-induced electric fields for a range of different cortical stimulation targets is currently beyond the scope of these approaches. Computational models of induced electric field, whilst having their own limitations, are able to provide an alternative insight into the stimulus delivered by TMS. In early computational models of TMS-induced electric field, the brain was commonly represented as an infinite half-plane or perfect sphere (Cohen & Cuffin, 1991; Ravazzani et al., 1996; Roth et al., 1991a; Roth et al., 1991b; Tofts, 1990). Recent models, that take account of detailed head geometry, tissue electrical conductivity and electrical anisotropy, approach a more realistic (*in vivo*) representation of the human brain. For example, Wagner et al used a five-layered model to show that boundaries between tissues of different conductivities can strongly affect the distribution of the induced field (Wagner et al., 2004b). In contrast, it has been shown that white matter fibre anisotropy has only minimal effects on the intensity and distribution of the electric fields induced in grey matter (De Lucia et al., 2007; Miranda et al., 2003).

The aim of this study was to determine the accuracy of TMS stimulation using an anatomically detailed computational model of the human head. To this end, the TMS coil was positioned over several target regions, including the primary motor and pre-motor cortices and the medial and lateral cerebellum. The Talairach coordinate system was used to describe the location and extent of the induced electric field for each target (Talairach & Tournoux, 1988).

8.2 Materials and methods

8.2.1 Model

The numerical evaluation of the induced electric field was performed using the finite element method as implemented in the low frequency solver of the simulation software package SEMCAD (version 13.2, SPEAG, Switzerland). All models were performed on a high-resolution model of the human head (male, age 34) from the SEMCAD 'Virtual Family' (Christ et al., 2010). To produce this model, a healthy volunteer (whose height and body mass index match worldwide averages) underwent a T1-weighted MPRAGE head scan (voxel size 0.5 x 0.5 x 1.0 mm^3) whilst lying horizontally facing upwards, and the data were manually segmented into different tissue types. Electrical conductivities were assigned to these tissue types from the inbuilt SEMCAD parametric database (Gabriel et al., 1996) at a frequency of 4 kHz which approximates to the fundamental frequency of a typical TMS current waveform. The values for the key tissue types are: skull (0.020 S/m), cerebrospinal fluid (CSF, 2.00 S/m), cerebral grey matter (0.108 S/m), white matter (0.066 S/m) and cerebellar grey matter (0.128 S/m). The high-resolution head model is normalized to Talairach space using nine anatomical reference points within the SEMCAD 'Talairach tool'. A rectilinear non-uniform computational grid optimized for cerebral grey matter was fitted to the human head model. The average voxel dimensions were 0.44 (range: 0.14 – 0.55) x 0.35 (range: 0.12 – 0.40) x 0.47 (range: 0.11 – 0.54) mm in cerebral grey matter and 0.46 (range: 0.14 – 0.54) x 0.36 (range: 0.14 – 0.40) x 0.49 (range: 0.11 – 1.45) mm in cerebellar grey matter. The results presented below represent the electric field solutions in cerebral and cerebellar grey matter.

8.2.2 Simulation methodology

The TMS coil geometry was based on the Magstim Company Ltd 'double 70' coil. This coil has a figure-of-eight geometry with each winding consisting of nine turns with a mean diameter of 70 mm. In the computer model each turn of wire was represented by a thin circular loop having a radius equal to that of the centre of the

real turn. Each turn was excited by a sinusoidal current of 5 kA peak at 4 kHz, these figures being an approximation to the values from a stimulator at full output. The choice of these parameters does not affect the resultant spatial distribution of induced field although its absolute amplitude will scale linearly with both frequency and current. The centre of the coil was located tangentially to the surface of the scalp at each target position.

Thirteen target TMS positions were chosen based on commonly used locations in neuroscientific research (Table 8.1). For six of the targets (left and right primary motor cortex, DLPFC and superior parietal cortex), the coil was located using previously reported Talairach coordinates of the International 10-20 system (Okamoto et al., 2004). In the left and right pre-motor cortices, the target position was identified by moving the coil 2 cm anterior and 1 cm medial from the primary motor cortex position (Bestmann et al., 2005). The left and right temporo-parietal targets were chosen as the midpoint between T3 and P3 and between T4 and P4 respectively (Hoffman et al., 2003; Okamoto et al., 2004). Cerebellar target positions were located by placing the coil 1 cm below the inion (medial cerebellum) and 3 cm to the left or right of this position (lateral cerebellum) (Lee et al., 2007; Theoret et al., 2001). The exact location of the coil was adjusted to the local geometry of the human head model such that the coil housing was on, and tangential to, the scalp surface. For each coil position a grey matter intersection point was determined by projecting a line along the coil central axis (orthogonal to the plane of the coil windings) from the midpoint between the coils toward the brain and determining the nearest grey matter surface location. Talairach coordinates of the coil locations and grey matter intersection points (Table 8.1) and of all results were obtained using the SEMCAD 'Talairach Tool'. For primary and pre-motor targets, the coil was orientated such that a line joining the centres of the two coils that comprised the figure-of-eight configuration was approximately perpendicular to the AC-PC line (the line through the anterior and posterior commissure). For all other cortical targets this line was positioned at an approximately 45˚ angle to the AC-PC line. In cerebellar targets, the line joining the centres of the two coils was positioned parallel to the coronal plane.

Target	Side	Coil centre position coordinate (mm)			10-20 position [1]	Grey matter intersection coordinate			Cortical depth (mm)
Primary motor	Left	-59	-9	61	C3	-50	-11	53	12.1
cortex	Right	59	-13	61	C4	51	-15	53	11.5
Pre-motor cortex	Left	-51	12	64	2cm anterior, 1cm medial of C3[2]	-43	8	55	13.1
	Right	52	7	64	2cm anterior, 1cm medial of C4[2]	43	4	54	12.4
Dorsolateral	Left	-43	61	35	F3	-33	54	30	12.6
prefrontal cortex	Right	48	58	34	F4	39	51	29	12.1
Temporo-parietal	Left	-77	-53	25	TP3 (halfway between T3- P3)[3]	-62	-50	21	16.1
cortex	Right	76	-51	31	TP4 (halfway between T4- P4)[3]	59	-48	26	17.5
Posterior parietal	Left	-46	-83	58	P3	-36	-73	47	18.4
cortex	Right	44	-82	59	P4	32	-71	48	19.1
Cerebellum	Medial	1	-115	-25	1cm below inion[4]	1	-93	-22	22.8
	Left	-29	-110	-25	3cm left of medial cerebellum[4]	-21	-92	-22	19.7

Table 8.1: TMS coil positions. The location of the coil centre was based on the head surface Talairach stereotactic coordinates of the International 10-20 system for electrode placement in Electroencephalography (1. Okamoto et al., 2004). Talairach coordinates are provided for the coil centre position after adjustments for head geometry to ensure that the coil-housing was placed tangentially, directly adjacent to the skull surface. Cortical depth is measured at each coil position as the distance (mm) from the scalp surface along the coil central axis to its intersection with the grey matter surface in Talairach space and the Talairach coordinates of this grey matter intersection point are provided. References: (2. Bestmann et al., 2005; 3. Hoffman et al., 2003; 4. Lee et al., 2007; 4. Theoret et al., 2001).

In addition to the 13 atlas target positions described above, two further computation models were run to assess the effects of: 1) coil orientation and 2) individual differences in cortical folding patterns. To address the effect of coil orientation, the left primary motor cortex target was repeated with the coil rotated such that the line joining the centres of the two coils was aligned parallel to the AC-PC line (90˚ rotation to the original orientation). The centre of the coil housing was kept tangential to the scalp surface in both coil orientations. Secondly, the original left primary motor cortex target (line joining the centre of the two coils perpendicular to AC-PC line) was repeated on a different high-resolution computer model of the human head (female, age 26) (Christ et al., 2010). The Talairach coordinates of the coil centres were adjusted minimally in order to achieve tangential coil orientation and did not differ more than 3 mm (Table 8.1).

8.2.3 Data analysis

For each coil position, the electric field intensities in cerebral and cerebellar grey matter calculated in SEMCAD were exported and post-processed in Matlab. The following three sequential processing steps were then carried out.

Outlier removal

To minimize the effect of artefacts caused by 'staircasing' at voxel edges, and possible mis-segmentation of single voxels at tissue boundaries, the data were processed as follows: Voxels for which the electric field intensity was greater than the local mean plus two standard deviations (calculated in a 5x5x5 voxel cube centred on the voxel of interest) were classified as outliers. All outliers were replaced by the maximum field intensity in the 5x5x5 voxel cube that falls below the mean plus two standard deviations. Multiple iterations of the outlier removal analysis were preformed until no further outliers were detected, the number of performed iterations ranged from 1 to 8 (mean 2.2).

Thresholding and clustering analysis

Prior to clustering analysis, a threshold was applied to the processed data such that all voxels with an electric field intensity greater than 50% of the overall maximum

electric field were identified as potential sites of significant TMS-induced stimulation and were included in the results (Ruohonen & Ilmoniemi, 1998). This threshold is an arbitrary definition of the extent of TMS-induced neural stimulation, but one which has been used previously in other modelling studies (De Lucia et al., 2007; Lontis et al., 2006; Thielscher et al., 2011). However, the data shown in panels A and B in the figures have been displayed in such a way as to enable the extent and location of the stimulus sites to be estimated for different (higher) threshold values. Similarly, the clustering data in Tables 8.3, 8.4, and 8.5 include relative amplitude to allow the effect of other thresholding values to be estimated. All voxels above the 50% threshold are subsequently referred to as 'supra-threshold'.

Lastly, all supra-threshold voxels were divided into separate three dimensional clusters. Supra-threshold voxels that were positioned within 5 voxels (Euclidean distance) of another supra-threshold voxel were grouped together. The distance criterion of 5 voxels was chosen to approximate the spatial grouping performed by the eye when visually examining the images. Clustering was also investigated using distance criterion thresholds of 8 and 10 voxels which led to comparable results, indicating that the choice of this parameter is not critical. For each target coil position, all supra-threshold clusters greater than 3 mm^3 are reported in the Results section below.

Target	Side	Peak location (Talairach)			Lateral displacement (mm)	Absolute intensity (V/m)	Relative intensity (% of left M1)
		x	y	z			
Primary motor	Left	-53	-6	49	7.3	1289	100
cortex	Right	59	-22	42	15.5	1485	115
Pre-motor cortex	Left	-42	16	52	8.3	1192	93
	Right	59	-22	42	33.0	1058	82
Dorsolateral	Left	-36	54	26	4.9	704	55
prefrontal cortex	Right	45	52	9	20.2	804	62
Temporo-parietal	Left	-60	-48	29	8.5	787	61
cortex	Right	59	-46	32	6.0	978	76
Posterior parietal	Left	-22	-69	58	18.4	596	46
cortex	Right	59	-22	42	56.6	698	54
Cerebellum	Medial	-4	-76	-18	4.4[a]	498	39

Table 8.2: Maximum electric fields. The Talairach coordinates and the intensity of the maximum electric field for each coil are shown. The relative intensity is expressed as a percentage of the maximum electric field in the left primary motor cortex model and thereby provides a comparative measure of stimulus strength, for the same stimulator output, when the coil is in different positions. The lateral displacement is measured as the distance (mm) from the coil central axis intersection point on the cortical grey matter surface (or with the cerebellar grey matter surface for those marked a) to the peak electric field location in Talairach

space. These results were obtained in collaboration with Professor Anthony Barker (Department of Medical Physics and Clinical Engineering, University of Sheffield).

8.3 Results

8.3.1 Maximum induced electric field

The TMS-induced electric field distribution in the primary and pre-motor cortices and in the cerebellum are shown in Figures 8.1 to 8.7. Table 8.2 summarises the results of the maximum induced electric fields for each of the thirteen TMS targets. The average distance between the centre of the coil on the scalp surface measured along the coil central axis to its intersection with the grey matter surface was 16.3 mm (range: 11 – 23 mm), this is a measure of cortical depth at each coil position (Table 8.1). The lateral distance from this grey-matter intersection point underneath the coil to the location of the peak electric field in grey matter was on average 16.5 mm (range 4 – 57 mm) and provides a measure of lateral displacement over the grey matter surface. The average intensity of the peak electric field for the coil drive current and frequency used in the model was 809 V/m (range: 427 – 1485 V/m), but all the intensity results can be scaled linearly for any chosen drive current amplitude. For frequencies that differ greatly from the representative value of 4 kHz chosen here, the models should be resolved using the appropriate values of tissue conductivity for the new frequency. The relative intensity (normalised to the maximum in the left primary motor cortex coil position) is also provided, as a comparative measure of relative field strength for different coil positions.

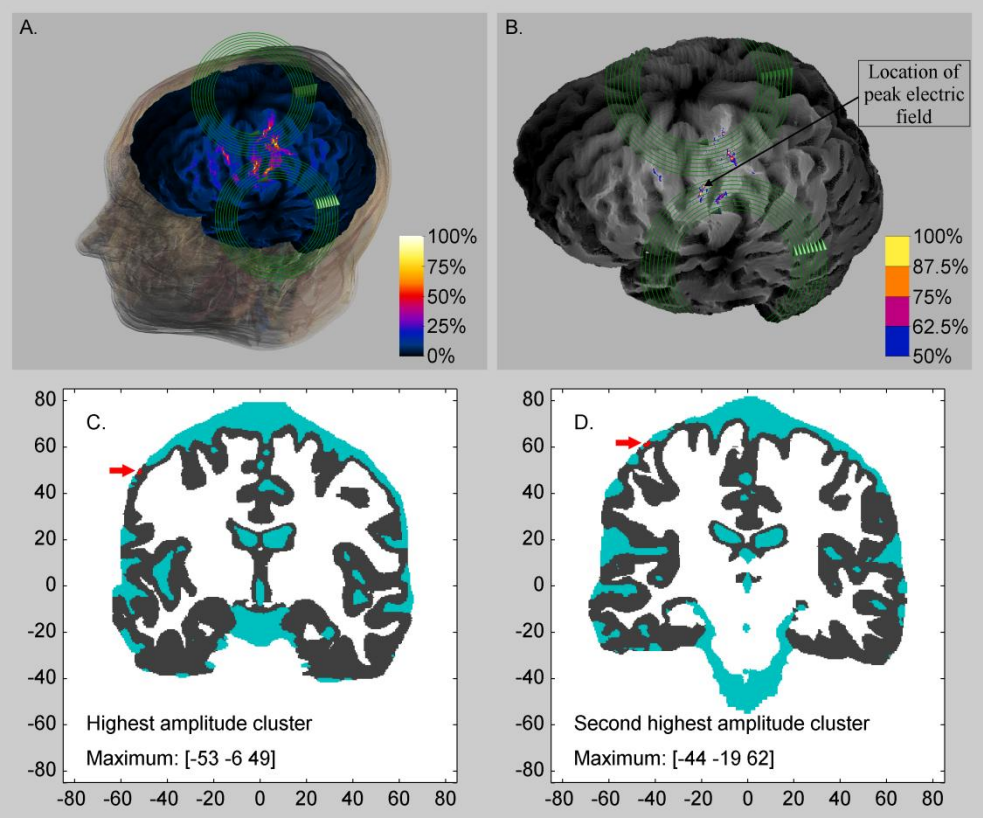

Figure 8.1: TMS-induced electric fields in the left primary motor cortex. The induced electric field strength is shown on a rendered view of the grey matter surface in the full range (Figure A: 0-100% of 1289 V/m) and in the threshold range (Figure B: 50-100% of 1289 V/m). The view is presented looking down the central axis of the coil. The windings of the coil are shown in green. Note that some darkening of the cortical structure occurs at the centre of each coil wing in figures A and B. This darkening is caused by local minima in the electric field results, which have been used to illuminate and thus reveal the cortical structure. Figures C and D show voxels with supra-threshold electric field intensity induced in grey matter (in red) on coronal slices through the peak electric field (C) and through the local maximum of the cluster with the next highest electric field strength (D). Grey matter is shown in grey and CSF is shown in cyan. The coordinates shown are those of the peak electric field voxels in the relevant cluster. These results were obtained in collaboration with Professor Anthony Barker (Department of Medical Physics and Clinical Engineering, University of Sheffield).

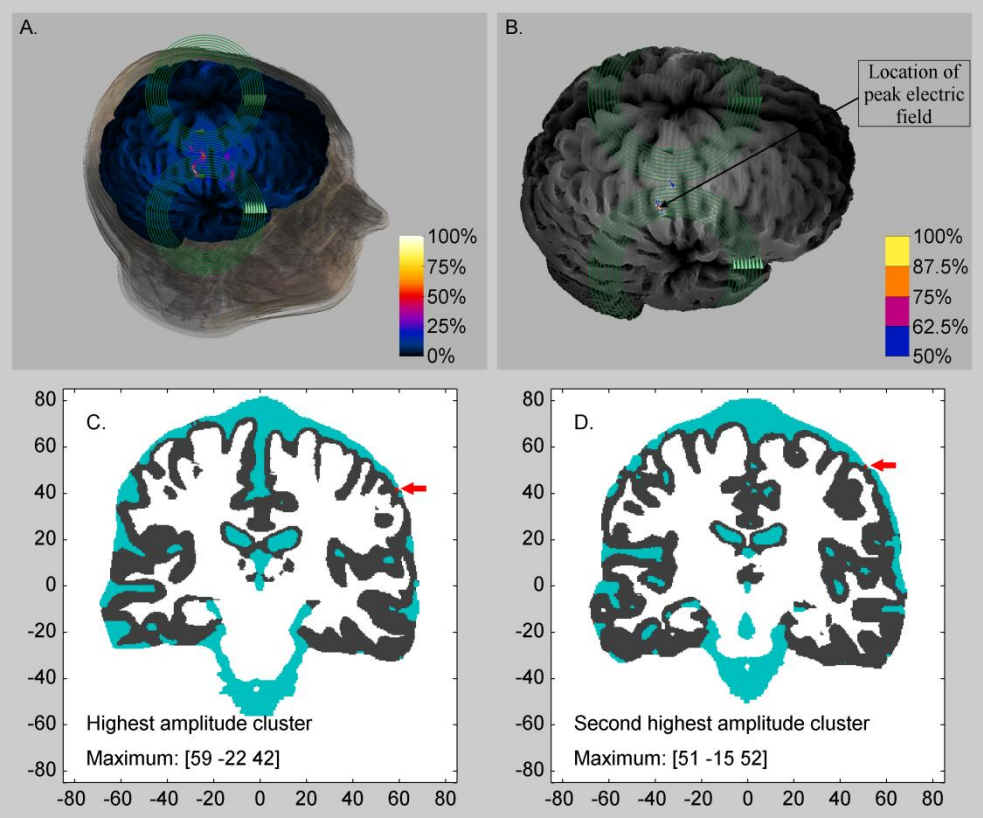

Figure 8.2: TMS-induced electric fields in the right primary motor cortex. The induced electric field strength is shown on a rendered view of the grey matter surface in the full range (Figure A: 0-100% of 1485 V/m) and in the threshold range (Figure B: 50-100% of 1485 V/m). Please see the legend to Figure 8.1 for further information.

There was a significant inverse correlation between the peak electric field intensity and cortical depth (defined as the distance from the scalp surface along the coil central axis to its intersection with the grey matter surface: R=-0.65, p=.004). In contrast, there was no correlation between the peak intensity and lateral displacement (defined as the distance from the grey matter intersection point to the peak electric field location: R=-.02, p=.9). Hence, the electric field intensity was primarily determined by cortical depth and not by lateral displacement in the grey matter plane.

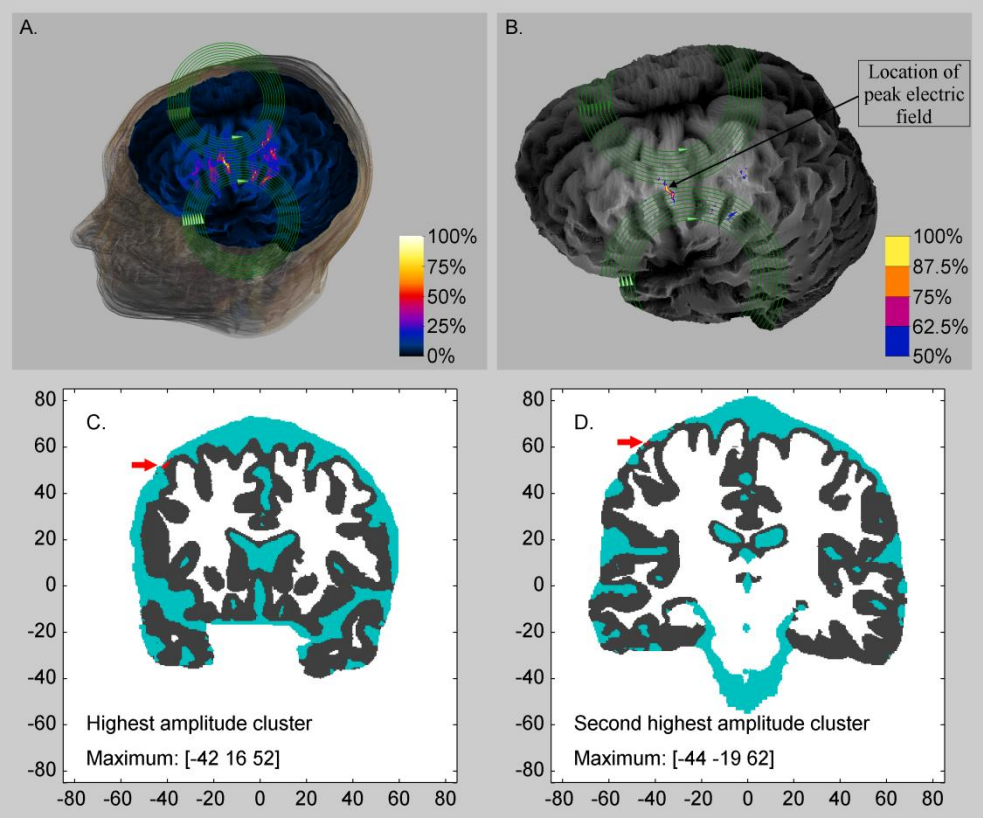

Figure 8.3: TMS-induced electric fields in the left pre-motor cortex. The induced electric field strength is shown on a rendered view of the grey matter surface in the full range (Figure A: 0-100% of 1192 V/m) and in the threshold range (Figure B: 50-100% of 1192 V/m). Please see the legend to Figure 8.1 for further information.

8.3.2 Supra-threshold electric field clusters

The summed volume of the supra-threshold voxels in grey matter was on average 92.7 mm^3 (range 11 – 180 mm^3). These supra-threshold voxels were clustered, as described above, based on Euclidian distance in order to explore the spatial distribution of the induced electric field. Tables 8.3 and 8.4 (presented at the end of this Chapter) summarize the local maximum and the size of all supra-threshold clusters for cortical and cerebellar targets.

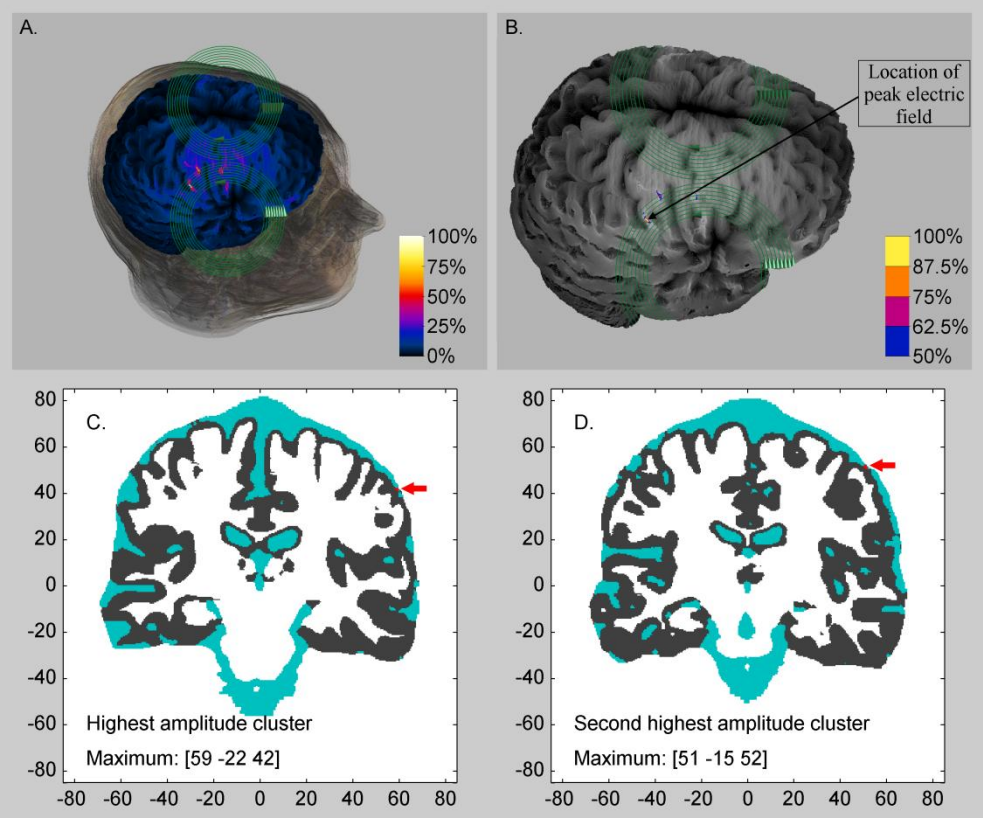

Figure 8.4: TMS-induced electric fields in the right pre-motor cortex. The induced electric field strength is shown on a rendered view of the grey matter surface in the full range (Figure A: 0-100% of 1058 V/m) and in the threshold range (Figure B: 50-100% of 1058 V/m). Please see the legend to Figure 8.1 for further information.

8.3.3 Effects of coil orientation

To assess the effect of the orientation of the coil relative to the head, the coil was positioned over one site, the left primary motor cortex, in two different orientations: 1) the line joining the centres of the two coils that comprised the figure-of-eight configuration approximately perpendicular to the AC-PC line (Figure 8.1), and 2) this line parallel with the AC-PC line (Figure 8.8) (90˚ difference between 1 and 2). In the latter position, the maximum electric field intensity was lower (1069 V/m versus 1289 V/m) and the summed total size of supra-threshold voxels was larger (89.3 mm^3 versus 69.6 mm^3) compared with the other coil orientation. Additionally, the distance between the location of the peak

electric field when the coil was aligned to the AC-PC line and the peak electric field when the coil was perpendicular to the AC-PC line was 8.6 mm. These variations are likely to be caused by the change in induced current direction with coil orientation. Table 8.5 (presented at the end of this Chapter) compares the spatial distribution of the supra-threshold electric fields in both models.

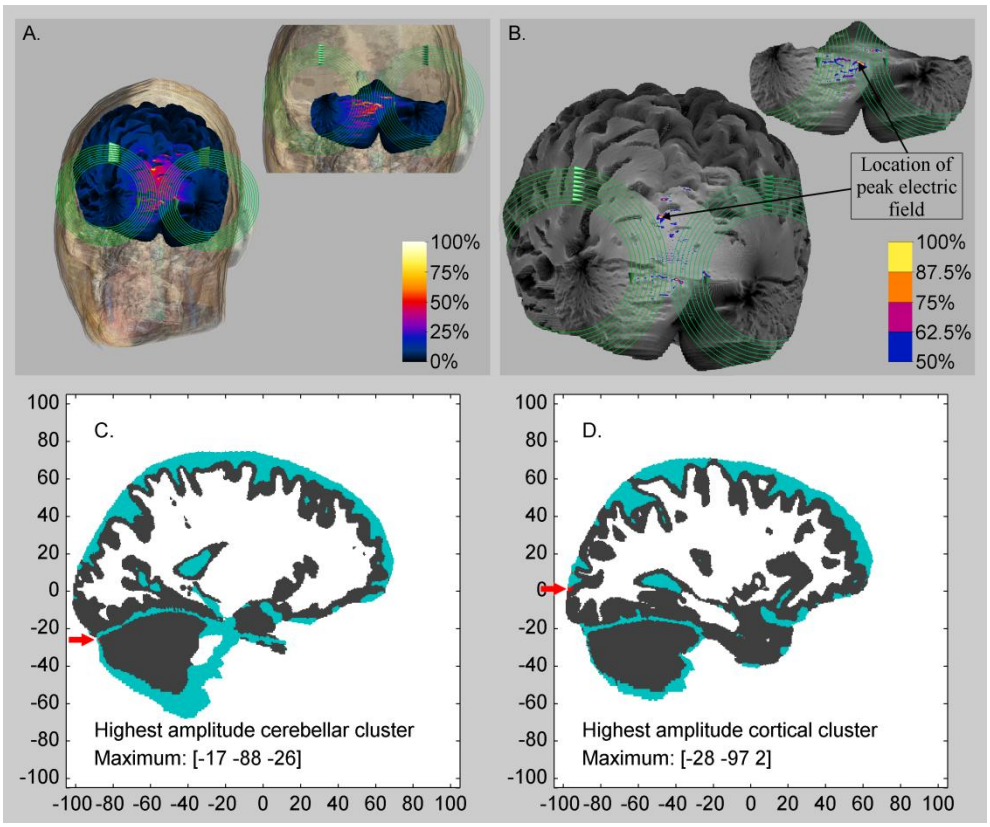

Figure 8.5: TMS-induced electric fields in the left cerebellum. The induced electric field strength is shown on a rendered view of the grey matter surface in the full range (Figure A: 0-100% of 638 V/m or of 525 V/m for the cerebellar insert) and in the threshold range (Figure B: 50-100% of 638 V/m or of 525 V/m for the cerebellar insert). Please see the legend to Figure 8.1 for further information.

8.3.4 Effects of individual differences in cortical folding

To investigate the generalisability of the induced electric field to other individuals, the left primary motor cortex coil position (coil oriented perpendicular to the AC-

PC line, Figure 8.1) was also performed on a model of the female brain provided by the Virtual Family tool (Figure 8.9) (Christ et al., 2010). Results indicated that the intensity of the peak electric field was lower (765 V/m versus 1289 V/m) and the summed total size of supra-threshold voxels was lower (51.7 mm^3 versus 69.6 mm^3) in the female head model compared with the male head model. The reduction in electric field intensity may, in part, be due to cortical depth, which was greater in the female head model (16.3 mm compared with 12.1 mm in the male head model). The location of the peak electric field in the female model was 10.3 mm removed from the peak electric field in the male model, reflecting differences in gyral structure. Table 8.5 (presented at the end of this Chapter) compares the distribution of the supra-threshold electric field into clusters.

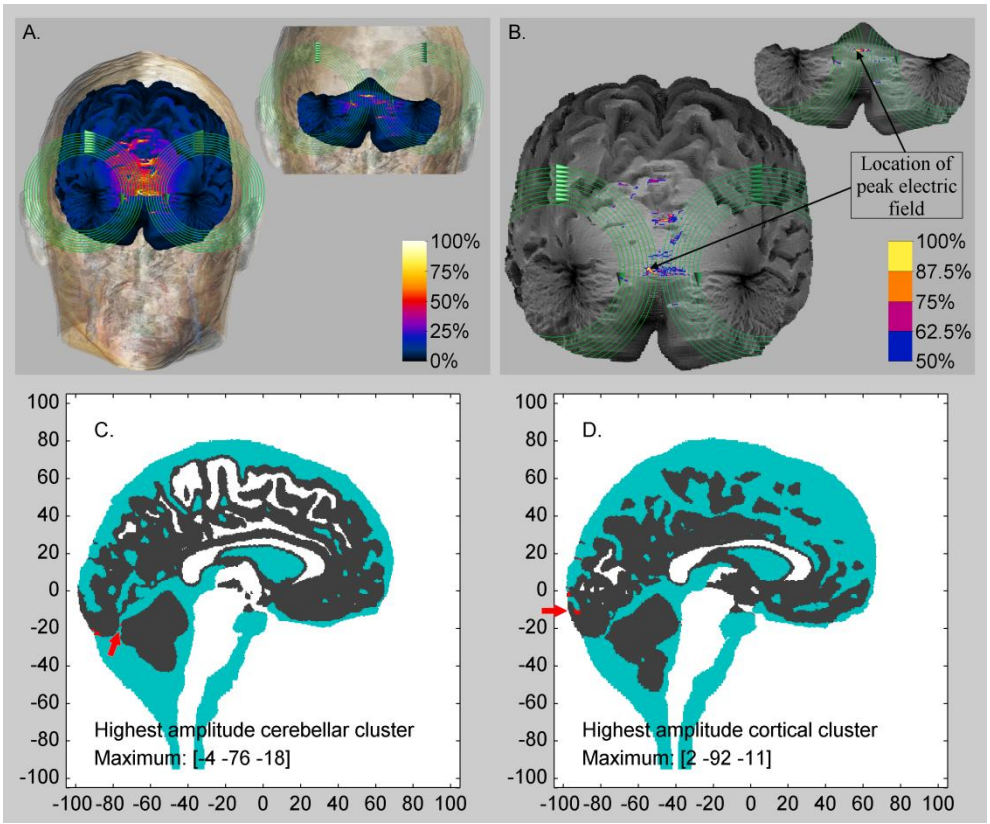

Figure 8.6: TMS-induced electric fields in the medial cerebellum. The induced electric field strength is shown on a rendered view of the grey matter surface in the full range (Figure A: 0-100% of 521 V/m or of 498 V/m for the cerebellar insert)

and in the threshold range (Figure B: 50-100% of 521 V/m or of 498 V/m for the cerebellar insert). Please see the legend to Figure 8.1 for further information.

8.4 Discussion

The aim of this study was to determine the accuracy of transcranial magnetic stimulation. Taken together, the findings indicated that for most coil positions (including the targets adopted in Chapters four, five and six) the supra-threshold electric field included, but was not restricted to, the target cortical region. In the remainder of the Discussion the most important factors that contributed to the electric field distribution and the generalisability of these results to individual subjects are discussed.

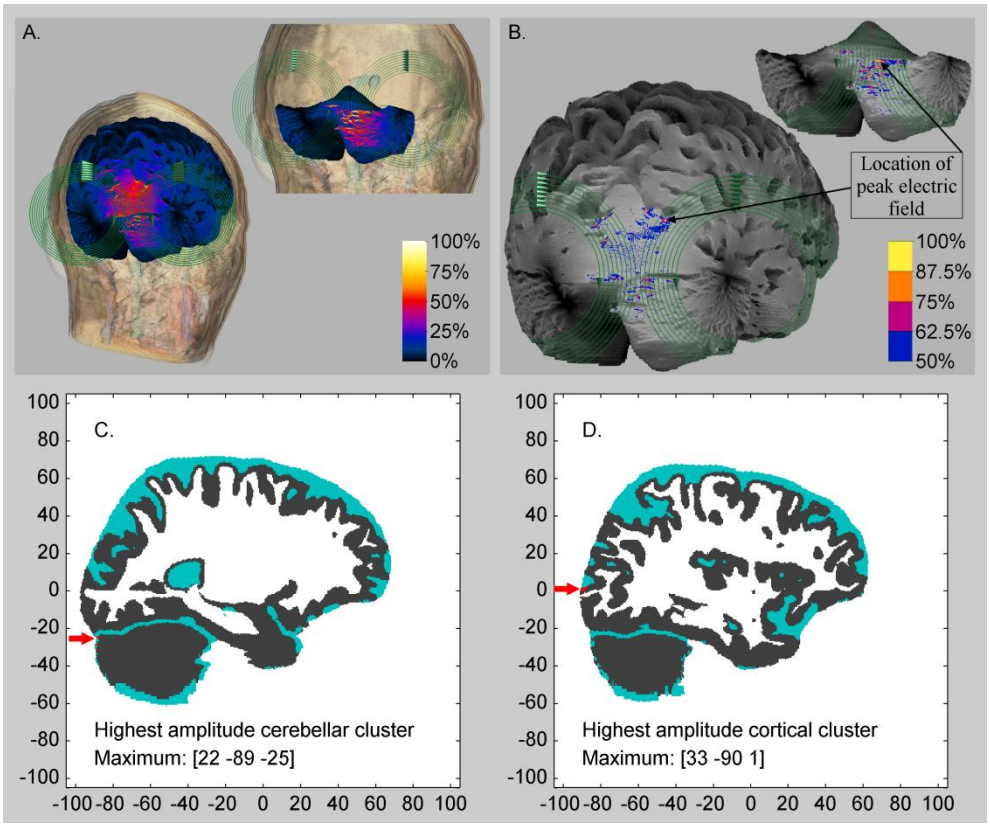

Figure 8.7: TMS-induced electric fields in the right cerebellum. The induced electric field strength is shown on a rendered view of the grey matter surface in the full range (Figure A: 0-100% of 530 V/m or of 427 V/m for the cerebellar insert)

and in the threshold range (Figure B: 50-100% of 530 V/m or of 427 V/m for the cerebellar insert). Please see the legend to Figure 8.1 for further information.

8.4.1 Cortical distance

The distance between the coil centre on the scalp surface and the peak induced electric field in grey matter is a combination of cortical depth (distance from the scalp surface along the coil central axis to its intersection with the grey matter surface) and lateral displacement over the grey matter surface (distance from this grey matter intersection point to the peak electric field location). The results revealed a significant inverse relationship between cortical depth and the intensity of the induced electric field, but no correlation between grey matter displacement and intensity. Hence, the magnitude of stimulation decreased linearly with increased cortical depth, but did not depend on the spread of stimulation over the grey matter surface. These findings are consistent with previous work that has shown that the resting motor threshold increased linearly with increased cortical depth (Stokes et al., 2007; Stokes et al., 2005). Future studies may wish to adjust the TMS stimulator output, relative to motor threshold, to achieve an appropriate stimulation intensity in the target cortical area. This could be achieved by using structural MRI to determine subject-specific cortical depth over the motor cortex and other target areas. Alternatively, relative electric field intensities provided in Table 8.2 could be used as a non-subject-specific approximation.

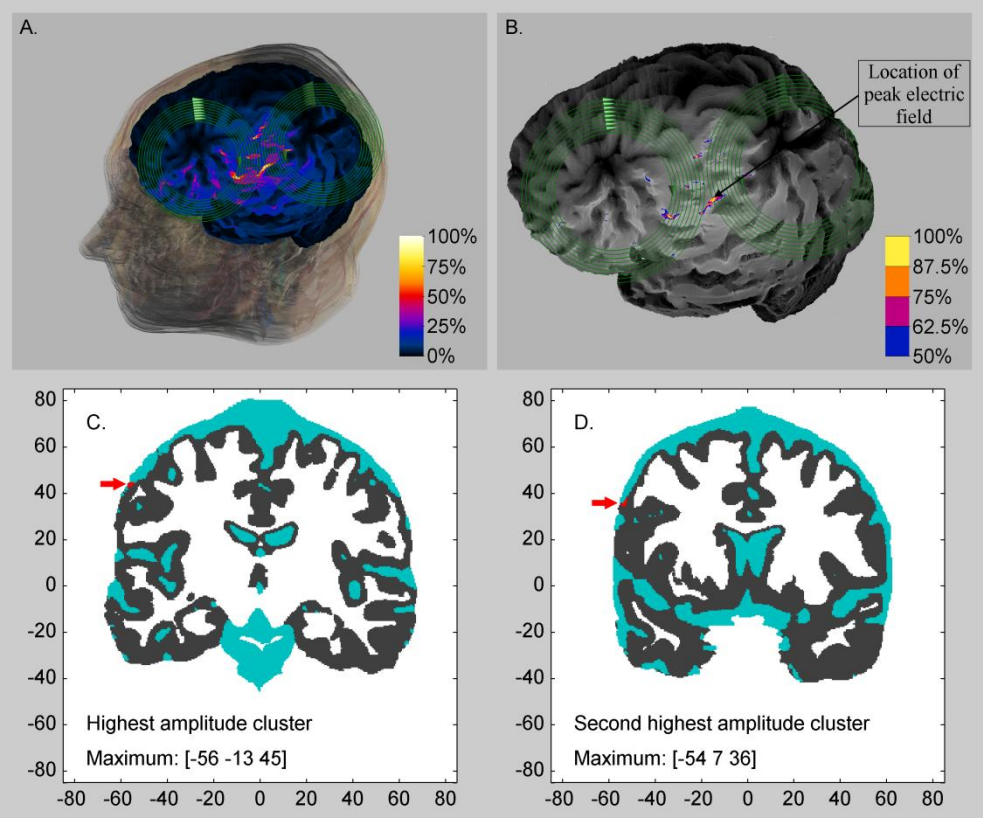

Figure 8.8: TMS-induced electric fields in the left primary motor cortex with the coil rotated 90˚ (i.e. aligned with the AC-PC line). The induced electric field strength is shown on a rendered view of the grey matter surface in the full range (Figure A: 0-100% of 1069 V/m) and in the threshold range (Figure B: 50-100% of 1069 V/m). Please see the legend to Figure 8.1 for further information.

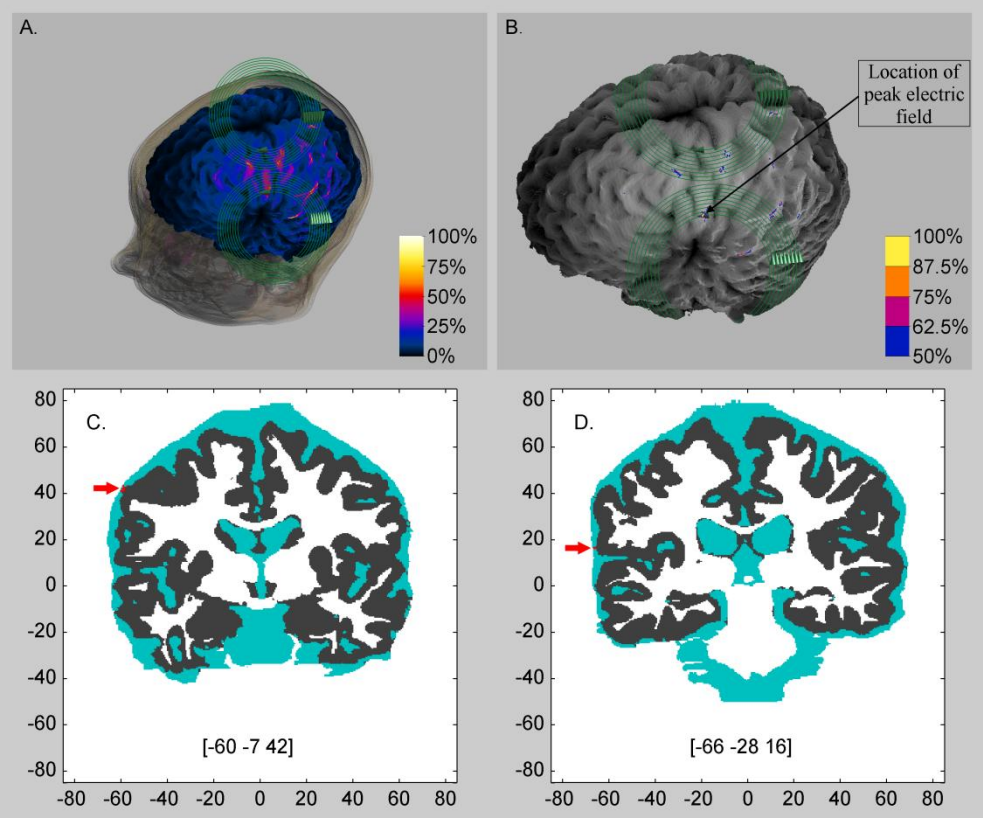

Figure 8.9: TMS-induced electric fields in the left primary motor cortex in a different (female) human head model. The induced electric field strength is shown on a rendered view of the grey matter surface in the full range (Figure A: 0-100% of 765V/m) and in the threshold range (Figure B: 50-100% of 765 V/m). Please see the legend to Figure 8.1 for further information.

8.4.2 Subarachnoid cerebrospinal fluid

The findings suggested a major effect of subarachnoid cerebrospinal fluid (CSF) distribution on the location of peak TMS-induced electric fields. The conductivity of CSF is considerably greater than the conductivity of any other brain tissue (typically by a factor of 15 to 30 (Gabriel et al., 1996)). Therefore, the TMS-induced current preferentially follows a least-resistance path through CSF rather than through adjacent, less conductive, tissues resulting in relatively high currents in the CSF. Where the CSF layer thins, for example between the peaks of gyri and the skull, these CSF currents (which by their intrinsic physics properties have to be

'continuous') 'push' through the relatively high resistance of the grey matter in gyral peaks resulting in high electric fields therein. As a result, high induced electric fields are primarily found in grey matter regions adjacent to areas of reduced or thinning CSF thickness. For all coil positions supra-threshold electric fields occurred in grey matter regions directly underneath the centre of the TMS coil. However, the peak electric fields can occur in grey matter regions some distance from the centre of the coil due to this 'amplifying effect' caused by a local reduction in the surrounding CSF thickness.

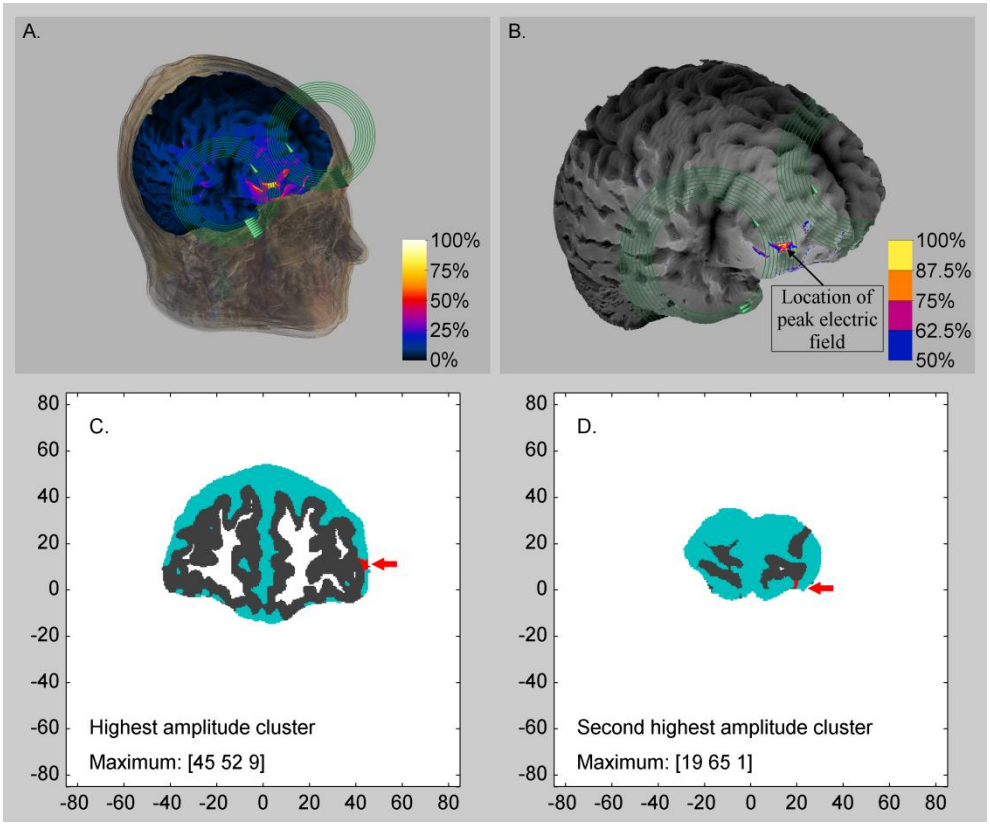

Figure 8.10: TMS-induced electric fields in the right dorsolateral prefrontal cortex. The induced electric field strength is shown on a rendered view of the grey matter surface in the full range (Figure A: 0-100% of 804 V/m) and in the threshold range (Figure B: 50-100% of 804 V/m). Please see the legend to Figure 8.1 for further information.

For example, when the coil was positioned over the right DLPFC (Figure 8.10), the peak electric field was located more inferior compared with the left DLPFC target. Accordingly, the lateral displacement in the right DLPFC was greater than that in the left DLPFC (20.2 and 4.9 mm respectively, Table 8.2). At closer inspection, this displacement of the peak electric field can be explained by the CSF distribution. The CSF thickness was relatively large directly underneath the right DLPFC coil position, whereas the peak electric field region occurred where the CSF was thinner (the red areas in Figure 8.10 C and D are superimposed on grey matter alone, which here extends through virtually the full thickness of the CSF). This example shows that TMS-induced electric fields are strongly affected by the distribution and thickness of CSF.

Table 8.2 shows that a hemispheric asymmetry in lateral displacement (greater displacement in the right than in the left hemisphere) similar to that in the DLPFC, was found for all cortical targets except for the temporo-parietal cortex. A previous study has reported a significant increase in subarachnoid CSF volume in the right hemisphere compared with the left hemisphere in a large group of healthy volunteers (Good et al., 2001). The right-lateral increase in subarachnoid CSF occurred adjacent to areas of reduced grey and white matter volume and this anatomical asymmetry was associated with a functional lateralization, for example in handedness and language function. The human head model that was used in this study displayed a comparable hemispheric asymmetry in subarachnoid CSF volume (6.7% more CSF voxels in the right than in the left hemisphere), which may explain the difference in lateral displacement of the peaks of electric field between the right and left hemisphere. Additionally, it has been reported that the resting motor threshold was significantly higher when measured over the right motor hotspot compared with the left motor hotspot, which may also be related to increased subarachnoid CSF volume (Koski et al., 2005). Taken together, these results suggest that the focal precision of TMS-induced electric fields in grey matter may be less when stimulating the right hemisphere compared with the left hemisphere.

The results showed that supra-threshold TMS-induced electric fields extent beyond the target cortical regions (Table 8.3 and 8.4, presented at the end of this Chapter). This may lead to undesirable stimulation in neighbouring areas of grey matter. For example, when the TMS coil was positioned over the cerebellum, the results showed widespread supra-threshold electric fields in the occipital lobe of the cerebral cortex (Figures 8.5, 8.6 and 8.7). These results suggest that TMS over the cerebellum may lead to stimulation of visual regions such as the primary and secondary visual cortices, as well as to cerebellar stimulation. In line with the preceding discussion, these distant regions of supra-threshold electric field in the visual cortices were caused by local thinning of the CSF because the cerebellum lies underneath a relatively thick layer of CSF compared with that over the visual cortices. Additionally, the cortical depth from the scalp to the surface of the cerebellum is greater than the cortical depth to the surface of the cerebral cortex and this will also contribute to the decrease in the cerebellar electric field intensity. Hence, future studies that apply TMS over the cerebellum should take into account that the induced stimulation may extent to the visual cortex. It may therefore be desirable to avoid the use of visual cues and other tasks that rely on visual input in such studies. These findings do not apply to the results presented in Chapter six because the experimental paradigm used auditory pacing stimuli and the task did not involve any form of visually presented input.

8.4.3 Gyral geometry

Supra-threshold electric field regions were primarily located on the surface of gyri, which is consistent with a recent study (Thielscher et al., 2011). Therefore, subject-specific gyral geometry may limit the inter-individual generalisability of electric field location and spatial distribution. This suggestion was supported by the finding that the intensity and spatial distribution of supra-threshold electric field varied between two different (male and female) human head models (Table 8.5, Figures 8.1 and 8.9). The results suggested that considerable inter-individual differences in the intensity and spatial distribution of TMS-induced electric fields are likely to occur due to individual differences in gyral folding patterns. Such inter-subject

variability in the peak amplitudes and spatial distribution of supra-threshold electric fields may help to explain inconsistencies of TMS effects over different subjects within studies and the variation in reproducibility between studies.

A further factor that influences the spatial distribution of TMS-induced electric fields is the coil orientation. To test the effect of coil orientation, the left primary motor target modelling was repeated with the coil in two different orientations (aligned with, or perpendicular to the AC-PC line). The results showed that more regions in pre-motor and somatosensory cortices were stimulated when the coil was aligned with the AC-PC line as compared to when the coil was rotated by 90˚ (Table 8.5, Figures 8.1 and 8.8). This difference in the pattern of excitation was due to the relative orientation of the gyri to the path of current flow. The 'amplification' effect referred to earlier is greatest on the peaks of gyri which run perpendicular to the path of the induced current in the CSF. Thus, because rotating the coil changes the direction of the induced current, it also tends to cause gyri having different orientations to have greater electric fields at their surface. This can be seen in Figures 8.1 A and 8.8 A where there is a trend for electric field maxima to occur along gyri approximately perpendicular to a line running between the two coil windings (which is the direction of maximum induced current in a homogeneous medium).

In summary, the results presented in this chapter provide a compendium of induced electric field patterns and amplitudes following transcranial magnetic stimulation over multiple commonly adopted cerebral and cerebellar targets. The findings suggested that electric fields induced by TMS are dependent on cortical depth, gyral folding patterns and on the thickness of the CSF layer that covers gyri and may therefore vary considerably between different subjects. These sources of inter-individual variability could have profound implications for the conventional application of TMS. Chapter nine investigates changes in the thickness of the subarachnoid CSF layer between different positions of the head with respect to gravity.

Target	Left hemisphere							Right hemisphere						
	Peak location			Label	Intensity (%)		Size	Displacement	Peak location			Label	Intensity (%)		Size	Displacement
	x	y	z	(BA)	max	M1	(mm^3)	(mm)	x	y	z	(BA)	Max	M1	(mm^3)	(mm)
Primary motor cortex	-44	-19	62	M1 (4)/S1 (3)	97	97	25.5	13.0	59	-22	42	M1 (4)/S1 (3)	100	115	7.6	15.5
	-57	-12	43	S1 (3)	83	83	14.0	12.2	51	-15	52	S1 (3)	74	85	3.1	1.3
	-53	-6	49	M1 (4)/PMC (6)	100	100	13.9	7.3								
	-35	-18	66	PMC (6)	82	82	5.6	21.0								
	-45	14	50	PMC (6)	74	74	4.2	25.7								
Pre-motor cortex	-42	16	52	PMC (6)	100	93	20.9	8.3	59	-22	42	M1 (4)/S1 (3)	100	82	6.7	33.0
	-56	-13	44	S1 (3)	67	62	5.2	27.5	51	-15	52	S1 (3)	80	66	5.1	21.3
	-44	-19	62	S1 (3)	72	66	3.6	27.9								
Dorsolateral pre-frontal cortex	-36	49	34	dLPFC (9)	93	51	38.1	7.2	45	52	9	mPFC (10/46)	100	62	104.4	20.2
	-36	54	26	mPFC (10/9)	100	55	30.3	4.9	19	65	1	sPFC (10)	97	61	13.6	36.6
	-28	62	7	mPFC (10)	91	50	15.8	24.6	53	41	9	dLPFC (46)	78	48	11.9	26.3
	-44	35	35	dLPFC (9)	100	55	13.5	22.2	37	59	17	mPFC (10/46)	76	47	7.7	14.9
	-36	56	4	mPFC (10)	97	53	9.6	26.0								
	-46	26	39	FEF (8/9)	71	39	8.7	32.4								
	-37	31	48	FEF (8)	73	40	5.5	28.9								
	-36	58	19	mPFC (10)	74	40	4.4	11.5								
	-45	14	50	PMC (6)	64	35	3.5	46.6								
	20	65	3	sPFG (10)	96	52	3.2	60.8								
	-40	53	15	mPFC (10)	62	34	3.0	15.7								
Temporo-parietal cortex	-60	-48	29	SMG (39/40)	100	61	23.9	8.5	59	-46	32	SMG (40)	100	76	16.5	6.0
	-61	-55	15	STG (22/39)	81	49	7.2	7.5	61	-39	37	iPL/SMG (40)	84	64	16.4	14.2
	-66	-47	0	MTG (21/22)	100	61	5.0	21.3	62	-42	16	STG (22)	66	50	4.1	12.0
	-65	-37	13	STG (22)	71	43	3.8	15.0	55	-54	34	SMG (40)	67	51	4.0	10.6
	-62	-58	1	MTG (21)	66	40	3.5	22.0	64	-35	17	STG (22)	73	56	4.0	15.8
	-63	-31	20	LS (42)	68	41	3.2	19.0								
Posterior parietal cortex	-22	-69	58	sPL (7)	100	46	60.0	18.4	48	-65	36	AG (39)	89	48	25.5	20.9
	-50	-55	46	iPL (40)	92	42	53.8	22.9	59	-22	42	S1 (3)	100	54	7.9	56.6
	-56	-13	44	S1 (3)	82	38	13.6	63.0	40	-75	30	AG (39)	61	33	3.0	19.8
	-46	-65	43	iPL (40)	70	33	7.5	13.3								
	-38	-68	51	sPL (7)	74	34	6.6	6.8								
	-37	-82	31	V3 (19)	74	34	6.4	18.3								
	-38	-78	36	AG (39/19)	74	34	5.3	12.1								
	-37	-70	37	AG (39/19)	79	36	4.6	9.9								
	-30	-75	47	iPL (7)	66	30	3.8	6.3								

Table 8.3: Cluster results for cerebral coil positions. Supra-threshold voxels (>50% of the overall maximum electric field) are divided into clusters by grouping those voxels that are within 5 voxels (Euclidian distance) of other supra-threshold voxels. The position (Talairach coordinates) of the peak electric field of each local maximum is shown for all clusters greater than 3 mm3. The intensity of the local maximum is shown relative to the overall maximum electric field of the particular model (max) and relative to the peak electric field in the left primary motor cortex model (M1). The lateral displacement is measured as the distance (mm) from the coil central axis intersection point on the grey matter surface to the peak electric field location in Talairach space. The size of the clusters is also shown and represents the sum of the volumes of all supra-threshold voxels within the cluster. These results were obtained in collaboration with Professor Anthony Barker (Department of Medical Physics and Clinical Engineering, University of Sheffield). BA = Brodmann's area, M1 = primary motor cortex, S1 = primary somatosensory cortex, PMC = pre-motor cortex, dLPFC = dorsolateral prefrontal cortex, mPFC = medial prefrontal gyrus, sPFC = superior prefrontal gyrus, FEF = frontal eye fields, SMG = supramarginal gyrus, STG = superior temporal gyrus, MTG = middle temporal gyrus, LS = lateral sulcus, sPL = superior parietal lobule, iPL = inferior parietal lobule, V3 = Associative visual cortex, AG = angular gyrus.

Target	Cerebellum								Cerebrum							
	Peak location			Label	Intensity (%)		Size	Displacement	Peak location			Label	Intensity (%)		Size	Displacement
	x	y	z	(52)[52]	Max	M1	(mm^3)	(mm)	x	y	z	(BA)	Max	M1	(mm^3)	(mm)
Medial cerebellum	10	-87	-25	Crus I	20	8	97.8	14.9[a]	2	-92	-11	V1 (17)	100	40	58.3	10.3
	-4	-76	-18	Lobule VI	100	39	17.7	4.4[a]	0	-98	2	V1 (17)	98	40	24.9	23.9
	6	-86	-37	Lobule VII At	80	31	3.6	20.7[a]	-2	-90	17	V2 (18)	89	36	36.2	38.2
									-12	-98	10	V1 (17)	83	33	10.1	34.5
									5	-98	-11	V1 (17)	78	31	3.3	13.0
Left cerebellum	-17	-88	-26	Crus I	100	41	41.6	6.1[a]	-28	-97	2	V1 (17)	100	49	31.3	25.5
	-5	-76	-18	Lobule VI	81	33	6.9	21.8[a]	-30	-91	-17	V2 (18)	74	37	5.0	10.4
	-33	-91	-17	Crus I	65	26	3.6	12.5[a]	-27	-96	10	V2 (18)	79	39	4.3	32.9
Right cerebellum	22	-89	-25	Crus I	100	33	148.9	3.5[a]	33	-90	1	V2 (18)	100	41	110.3	26.1
	0	-76	-18	Lobule VI	95	31	8.9	26.2[a]	5	-99	1	V1 (17)	81	33	27.0	29.7
									2	-92	-11	V1 (17)	72	30	7.7	22.3
									2	-92	17	V2 (18)	64	26	7.2	44.0
									9	-100	-8	V2 (18)	79	33	4.6	20.9

Table 8.4: Cluster results for cerebellar coil positions. Cluster results for cerebellar coil positions calculated within the cerebellar grey matter (left column) and within the cerebral grey matter (right column). Supra-threshold voxels (>50% of the overall maximum electric field) are divided into clusters by grouping those voxels that are within 5 voxels (Euclidian distance) of other supra-threshold voxels. The position (Talairach coordinates) of the peak electric field of each local maximum is shown for all clusters greater than 3 mm3. The intensity of the local maximum is shown relative to the overall maximum electric field of the particular model (max) and relative to the peak electric field in the left primary motor cortex model (M1). The lateral displacement is measured as the distance (mm) from the coil central axis intersection point on the cortical or cerebellar (a) grey matter surface to the peak electric field location in Talairach space. The size of the clusters is also shown and represents the sum of the volumes of all supra-threshold voxels within the cluster. These results were obtained in collaboration with Professor Anthony Barker (Department of Medical Physics and Clinical Engineering, University of Sheffield). BA = Brodmann's area, V1 = primary visual cortex, V2 = secondary visual cortex.

Target	Peak location			Label	Intensity (%)		Size	Displacement
	x	y	z	(BA)	Max	M1	(mm^3)	(mm)
Left primary motor cortex	-44	-19	62	M1 (4)/S1 (3)	97	97	25.5	13.3
	-57	-12	43	S1 (3)	83	83	14.0	12.2
	-53	-6	49	M1 (4)/PMC (6)	100	100	13.9	7.3
	-35	-18	66	PMC (6)	82	82	5.6	21.0
	-45	14	50	PMC (6)	74	74	4.2	25.7
Left primary motor cortex (coil 90 degrees)	-56	-13	45	S1 (3)	100	83	36.9	11.4
	-54	7	36	PMC (6)	97	80	26.2	26.5
	-40	-9	61	M1 (4)/PMC (6)	90	74	6.8	11.7
	-51	-30	54	S1 (3)	75	62	4.1	18.3
	-36	-15	65	PMC (6)	66	55	3.1	18.0
Left primary motor cortex (on female head model)	-60	-7	42	PMC (6)	100	59	12.0	16.8
	-64	-43	36	SMG (40)	76	45	8.2	39.1
	-41	1	56	M1 (4)/PMC (6)	79	47	7.8	14.6
	-46	-20	58	S1 (3)	76	45	5.5	9.6
	-66	-28	16	STG (42)	86	51	4.6	43.9
	-17	-56	64	sPL (7)	81	48	3.9	55.1
	-38	-24	64	M1 (4)	71	42	3.3	19.0

Table 8.5: Cluster results to compare results of additional models performed to assess the effects of coil orientation and individual gyral folding patterns to the original coil placement over the left primary motor cortex (results are the same as in Table 3). Supra-threshold voxels (>50% of the overall maximum electric field) are divided into clusters by grouping those voxels that are within 5 voxels (Euclidian distance) of other supra-threshold voxels. The position (Talairach coordinates) of the peak electric field of each local maximum is shown for all clusters greater than 3 mm3. The intensity of the local maximum is shown relative to the overall maximum electric field of the particular model (max) and relative to the peak electric field in the left primary motor cortex model (M1). The lateral displacement is measured as the distance (mm) from the coil central axis intersection point on the grey matter surface to the peak electric field location in Talairach space. The size of the clusters is also shown and represents the sum of the volumes of all supra-threshold voxels within the cluster. These results were obtained in collaboration with Professor Anthony Barker (Department of Medical Physics and Clinical Engineering, University of Sheffield). BA = Brodmann's area, M1 = primary motor cortex, S1 = primary somatosensory cortex, PMC = pre-motor cortex, SMG = supramarginal gyrus, STG = superior temporal gyrus, sPL = superior parietal lobule.

9 Study 7: The effect of gravity on cerebrospinal fluid distribution: implications for transcranial magnetic stimulation

9.1 Aims and rationale

The results presented in Chapter eight revealed that the local thickness of the highly conductive layer of cerebrospinal fluid (CSF) that lies between the skull and the grey matter surface of the brain significantly affected the location and intensity of the electric fields induced by transcranial magnetic stimulation (TMS). Cerebrospinal fluid encapsulates the brain and spinal cord and functions to provide nutrients, dispose of metabolites and to cushion the brain (Johanson et al., 2008). Gravitational forces may influence the distribution of intra-cranial CSF and lead to variance in subarachnoid CSF thickness. This study aimed to determine the effect of gravitational pull associated with different head positions on the distribution of subarachnoid CSF using structural magnetic resonance imaging (MRI). Based on in-vitro measurements of the specific gravity of grey matter, white matter and CSF (1.051, 1.049 and 1.0006 g/ml respectively, (Lui et al., 1998; Torack et al., 1976)), it was hypothesized that there would be a reduction of subarachnoid CSF volume on the side of the head closest to the ground due to downward brain movement with gravity.

9.2 Materials and methods

Structural MRI scans were performed at 3T (Achieva 3.0T, Philips Medical Systems, Best, The Netherlands) at the University of Sheffield. Three-dimensional volumes, covering the entire brain, were acquired using a Magnetization Prepared Rapid Acquisition Gradient Echo (MPRAGE) sequence (acquisition matrix 256×256, TR=15 ms, TE=4.4 ms). Scans were acquired on a single subject (female, age 25yrs) positioned: 1) in the normal supine position 2) in the left lateral decubitus orientation, arms down along the body and 3) prone, arms down, head supported with a cushioned block. Images of this single subject's brain in the three

positions were statistically compared with three-dimensional volumes obtained from twenty healthy subjects (10 male, mean age 22.7±3.8) in the standard, supine orientation. These comparison data were acquired on the same 3T scanner using the same MPRAGE data acquisition sequence.

All images were processed in SPM8 (www.fil.ion.ucl.ac.uk/spm/). Scans were manually aligned to the anterior-posterior commissure line as viewed in the supine position. The realigned images were segmented into probability maps for grey matter, white matter and CSF in normalized MNI space ($2mm^3$ voxel size) and modulated by Jacobian determinants. Thus, if the brain region doubled in size as a result of normalization, the tissue probability value for this region was halved (Ashburner & Friston, 2001). The resulting CSF probability maps were smoothed (Gaussian kernel 6mm full width half maximum). Each smoothed CSF-probability map was divided into three equal sections of the normalized MNI template image in the x-plane (left–middle–right) and y-plane (anterior–central–posterior). The number of voxels with a CSF-probability greater than 0.3 in each section was represented as a percentage of the subject-specific total number of CSF voxels (>0.3). For further analyses, the middle and central sections were excluded because the primary focus was on displacement of CSF in the brain margins. The 'left divided by right' and 'anterior divided by posterior' ratios of CSF were calculated. One-sample t-tests were performed in which the CSF ratios from the 20 subjects were compared against values of the single subject in the supine, left lateral and prone positions.

9.3 Results

The results show that, in the supine position there were no significant differences in the left-to-right and anterior-to-posterior CSF ratios between the comparison group and the single subject ([$t(19)$=0.94, p=.36] for the left-to-right ratio and [$t(19)$=-0.63, p=.53] for the anterior-to-posterior ratio). However, there was a significant increase in the left-to-right CSF ratio in the single subject in the left lateral position compared with the comparison data [$t(19)$=-8.17, p<.001] (Figure 9.1 A).

Furthermore, there was a significant increase in the anterior-to-posterior CSF ratio when the subject was in the left lateral position [$t(19)$=-4.597, p<.001] and in the prone position [$t(19)$=-7.52, p<.001] compared with the control group (Figure 9.1 B).

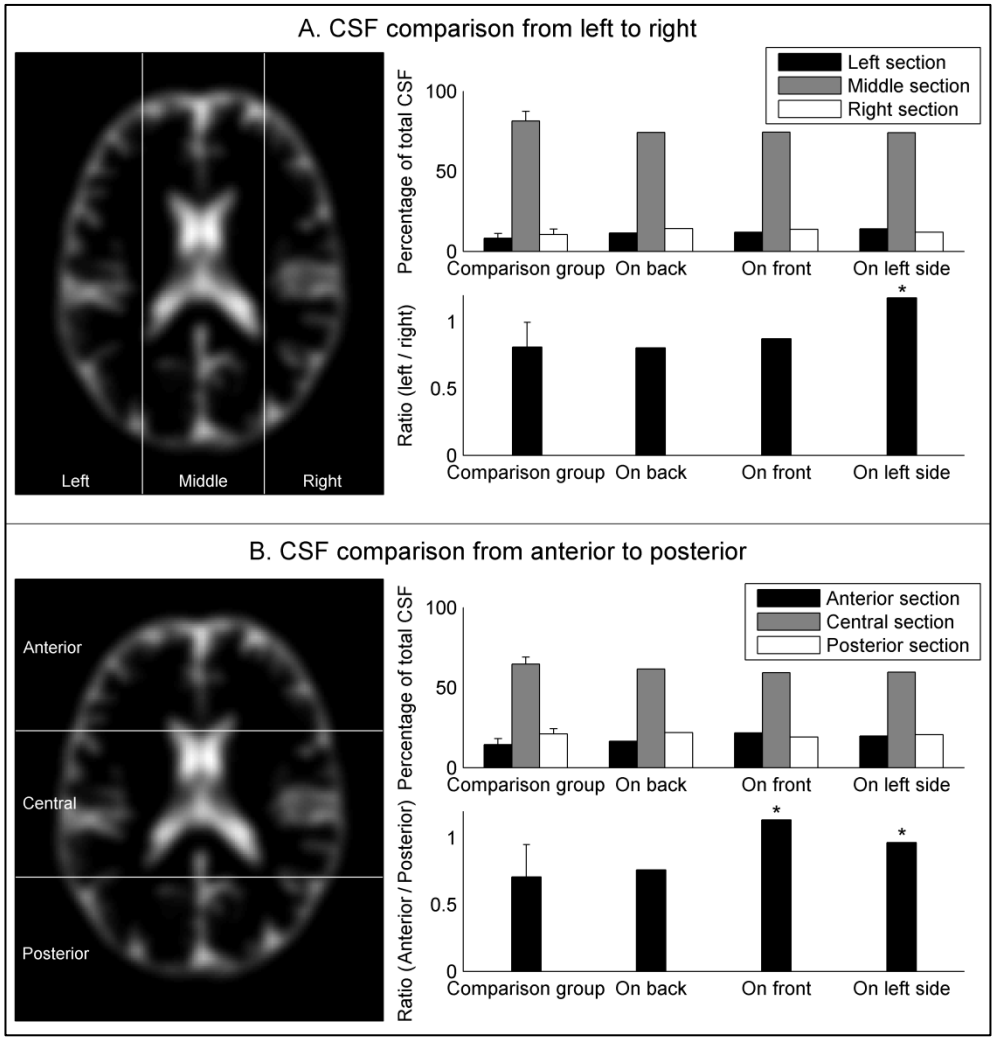

Figure 9.1: The effect of gravity on the distribution of CSF in the brain. The images on the left illustrate how the smoothed CSF probability maps were divided into equal sections for left-middle-right (A) and anterior-central-posterior (B). The top graph in figure A shows the percentage of total CSF in the left (black), middle (grey) and right (white). The bottom graph in figure A shows the left-to-right ratio (black bars of top graph divided by white bars of top graph). Figure B shows the same two graphs for the anterior-to-posterior CSF (percentage on top and ratio on

bottom). Data from the single subject in the supine, prone and left lateral positions are statistically compared with the comparison group (n=20) in the supine position (error bars indicate one standard deviation). Ratios of the single subject data that are significantly different (p<.05) from the comparison group data are marked (*). Comparison data (n=20) were provided by Dr Tom Farrow, Academic Clinical Psychiatry, University of Sheffield.

9.4 Discussion

The findings presented in this study suggested that, contrary to the hypothesis, subarachnoid CSF pooled towards the gravitational direction, as shown by a significant change in the ratio of CSF in the brain margins. Hence, there was a relative increase of CSF in the left lateral section of the brain when the subject was positioned on their left side and in the anterior section of the brain when the subject was prone. In-vivo, the position of the brain is maintained by the brain stem, cranial meninges and skull osteology, which may restrict movement. Therefore, relative changes in the subarachnoid CSF distribution with gravity may be influenced by additional factors such as intracranial pressure, pulsation and anchoring vasculature, as well as differences in specific gravity. These preliminary findings warrant future research into currently unexplored (gravitation-induced) changes in regional subarachnoid CSF thickness. The conductivity of CSF is considerably greater than the conductivity of any brain tissue (typically by a factor of 15 to 30 (Gabriel et al., 1996)). Therefore, local, (gravitation-induced) changes in subarachnoid CSF thickness may significantly affect the efficacy of TMS.

Transcranial magnetic stimulation (TMS) utilizes magnetic field pulses over the skull to temporarily alter neural excitability (Wagner et al., 2009; Walsh & Cowey, 2000). Subarachnoid CSF contributes modestly to the overall distance between the scalp surface and target grey matter and may therefore affect the magnitude of stimulation achieved with TMS (Knecht et al., 2005; Stokes et al., 2007). More importantly, the results presented in Chapter eight suggested that minor changes in local CSF thickness significantly affect the TMS-induced electric field distribution

(and thereby the stimulus intensity) due to the high electrical conductivity of CSF. Hence, the spatial distribution of the stimulation achieved with TMS may vary with the orientation of the subject's head with respect to gravity. It is possible that specific orientations of the head relative to gravity could be used to improve the comfort and tolerability of TMS, although this hypothesis remains to be tested experimentally. By decreasing local CSF thickness (for example by lying the subject on their left side during stimulation of the right hemisphere) it may be possible to reduce the stimulator output required for cortical stimulation, thus decreasing the degree of sensation and muscular contraction and hence improving tolerability.

It has been shown that the use of MRI-guided neuronavigation methods to position the coil improves the efficacy of TMS (Herwig et al., 2001; Lioumis et al., 2009; Sack et al., 2009). However, these methods are based on the assumption that the peak induced electric field occurs underneath the centre of the figure-of-eight coil. This assumption may not always be valid because regional differences in the thickness of CSF may result in distant TMS-induced electric fields in grey matter as shown in Chapter eight. Additionally, the orientation of the head relative to gravity is different during acquisition of the MRI (obtained in a supine position) and during TMS stimulation (generally performed in a seated position). In the future, neuronavigation methods may be improved by calculating the induced electric field based on the tissue geometry and CSF distribution obtained from an MRI scan of each individual. To make optimal use of this fully personalised coil positioning approach, the brain should be in the same gravitational position for both the MRI scan and during TMS stimulation to ensure optimal correspondence in CSF distribution. Given the technical challenges and resources required, future research is needed to investigate the efficacy and feasibility of fully personalised TMS coil placement.

In both the comparison group and in the single subject, the results reveal a hemispheric asymmetry in subarachnoid CSF volume in the supine position (there was on average 18% more subarachnoid CSF in the right compared with the left

lateral hemisphere). These results are consistent with previous research, which suggested that the right-lateral increase in subarachnoid CSF volume occurred adjacent to regions of reduced grey and white matter volumes (Good et al., 2001). This anatomical asymmetry is associated with a functional lateralisation, for example in handedness and language function. Patients with schizophrenia exhibit reduced anatomical and functional hemispheric asymmetry and also show regionally specific increases in subarachnoid CSF thickness compared with healthy subjects (Narr et al., 2003; Sommer et al., 2001). These differences in subarachnoid CSF thickness may be one of the factors that explain why sensitivity to TMS is reduced in patients with schizophrenia compared with healthy volunteers (Fitzgerald et al., 2004).

10 General discussion

10.1 Summary of main findings

The central aim of this thesis was to determine the behavioural and neural correlates of sensorimotor timing and error correction. This overall aim was subdivided into four objectives: 1) to characterize sensorimotor timing performance; 2) to determine the neural correlates of sensorimotor timing and error correction; 3) to investigate functional connectivity networks associated with sensorimotor timing and error correction and 4) to establish the efficacy of transcranial magnetic stimulation. These four objectives were addressed across seven studies. This chapter begins with a brief summary of the main findings of each study and subsequently integrates these findings into a theoretical framework. Lastly, this chapter discusses limitations of the work presented in this thesis and directions for future research.

Chapter one reviewed the literature on sensorimotor timing and error correction research. Sensorimotor synchronization (SMS) provides a movement-based task to measure timing performance. During SMS, subjects are required to tap their finger in synchrony with a pacing stimulus presented at regular intervals. Performance measures of an SMS task include the tap-tone asynchrony (time in milliseconds between the pacing tone and the corresponding tap), the inter-response interval (IRI, time in milliseconds between two subsequent taps) and the tapping variability (Repp, 2005). The total tapping variability can be further subdivided into variability originating from the central time-keeper mechanism and variability caused by peripheral motor implementation (Wing & Kirstofferson, 1973). Accurate performance during SMS requires ongoing error correction to account for deviations resulting from tapping variability. Error correction can be studied by introducing occasional temporal perturbations (single stimulus-onset asynchronies that are shorter or longer than the standard interval) in an otherwise regular pacing sequence. Previous studies have shown that subjects show a rapid error correction response following such local phase shifts (Repp, 2002b).

Study one (Chapter three) aimed to investigate the effects of task-related aspects and of subject-specific factors on SMS performance in a large cohort of healthy subjects (objective one). The main novel finding of this study was that bimanual SMS led to a reduction in tapping variability in both the central and the peripheral components, compared with unimanual SMS. A reduction in peripheral motor implementation variability was not previously shown, although prior studies have revealed a reduction in central and overall tapping variability (Helmuth & Ivry, 1996; Pollok et al., 2007). It was suggested that the reduction in motor implementation variability during bimanual SMS may reflect improved stability of perceptual delays as a result of the use of both hands (Semjen et al., 2000; Vorberg & Schulze, 2002). The results presented in Chapter three furthermore revealed that tapping variability was reduced during performance with the dominant hand compared with the non-dominant hand and in subjects with previous musical training in addition to those with a strong hand preference.

Study two (Chapter four) aimed to investigate the effects of suppression and facilitation theta burst stimulation (TBS) over the left and right primary and pre-motor cortices on SMS performed uni- and bi-manually (objective two). The main result of this study was that ongoing error correction performance during unimanual and bimanual SMS was differentially affected by lateralized TBS over the left or right pre-motor cortex. During unimanual performance, suppression TBS over the left pre-motor cortex increased error correction in both hands, whereas suppression TBS over the right pre-motor cortex only increased error correction during left-handed SMS performance. During bimanual SMS, error correction increased in both hands following suppression TBS over either the left or the right pre-motor cortex. These findings implied that the pre-motor cortices may play a specific role in ongoing error correction during SMS. This hypothesis was tested in study three (Chapter five).

Study three (Chapter five) aimed to determine the effect of suppression and facilitation TBS over the left pre-motor cortex on error correction responses

following induced phase shifts in order to test the hypothesis that the left pre-motor region is important for error correction (objective two). The results showed that the error correction response to induced phase shifts occurred faster after suppression TBS over the left pre-motor cortex, consistent with the findings of study two (Chapter four). Conversely, suppression TBS over the left pre-motor cortex negatively affected timing accuracy because the tap-tone asynchrony and tapping variability increased after TBS in line with previous research (Pollok et al., 2008b). It was suggested that the improvement in error correction after suppression of the left pre-motor cortex may result from accurate automatic responses following a relative reduction of conscious control. In addition, the findings of Experiment two revealed a practice effect on the error correction responses to positive phase shifts (when the tone occurred later than expected).

Study four (Chapter six) aimed to determine the neural correlates of sensorimotor timing and error correction using functional magnetic resonance imaging (objectives two and three). The main results of this study revealed a lateralized response in the cerebellum such that the right cerebellum was activated during all timing and error correction conditions relative to rest, whereas the left posterior cerebellar cortex was exclusively activated during the correction of supraliminal phase shifts. Furthermore, the left cerebellum exhibited enhanced functional connectivity with a cerebello-cortical network during supraliminal error correction compared with regular timing. Based on these findings, the aim of Experiment two was to determine the causal role of the cerebellum during sub- and supra-liminal error correction using theta burst stimulation. The results of this second experiment confirmed that suppression TBS over the left cerebellum significantly affected error correction of supraliminal phase shifts, whereas suppression of the right cerebellum did not affect error correction performance.

Study five (Chapter seven) aimed to investigate changes in interhemispheric functional connectivity between the primary motor cortices during uni- and bi-manual SMS using wavelet coherence analysis (objective three). The results showed that there was greater connectivity (both in terms of correlation and

coherence) between the left and right primary motor cortices during bimanual SMS, compared with unimanual performance. Furthermore, the phase relationship between both hemispheres was more stable over time during bimanual SMS, compared with unimanual SMS. These results suggest that the bilateral primary motor cortices were more synchronized and functionally connected when both hands performed the same task. In Experiment two of study five, the wavelet coherence approach was applied to resting state fMRI data to examine functional connectivity in resting state networks. The results of Experiment two provide proof-of-concept evidence for the applicability of wavelet coherence analysis to characterize and compare dynamic coherence and phase in different resting state networks.

Study six (Chapter eight) aimed to determine the efficacy of transcranial magnetic stimulation using computational modelling to calculate TMS-induced electric fields in an anatomically detailed model of the human head (objective four). The results confirmed that, for all TMS coil positions, supra-threshold electric fields occurred at the predicted site of stimulation directly underneath the centre of the figure-of-eight coil. However, the findings also revealed that the local distribution of subarachnoid cerebrospinal fluid, together with individual gyral geometry, can lead to the induction of supra-threshold electric fields at some distance from the TMS coil. Such unexpected distant stimulations occurred when there was a relatively thick layer of highly conductive CSF underneath the centre of the TMS coil.

Study seven (Chapter nine) aimed to investigate changes in subarachnoid CSF thickness between different head positions with respect to gravity using structural magnetic resonance imaging (objective four). The results showed that CSF pooled towards the direction of gravity such that there was a relative increase in subarachnoid CSF at the side of the head that was closest to the ground. This result may have important implications for the conventional use of TMS. For example, these findings may be used to improve and personalize the use of MRI-guided neuronavigation tools to accurately determine the optimal TMS coil position for focal stimulation.

10.2 Theoretical integration

10.2.1 Sensorimotor timing

Timing plays a crucial, but often unnoticed, role in every aspect of human life because it is essential for all movement and cognition (Dawson, 2004). However, it is currently unclear how temporal information is processed in the human brain. It has been suggested that a dedicated timing mechanism performs temporal information processing. Dedicated timing may be achieved in a localized brain region and several neural substrates have been proposed as candidates for this 'centralized clock', or dedicated timing could be a function of a distributed brain network (Buhusi & Meck, 2005; Ivry & Spencer, 2004). Alternatively, it may be that temporal processing is an intrinsic feature of neural firing patterns (Ivry & Spencer, 2004; Karmarkar & Buonomano, 2007). The findings of the first study in this thesis (Chapter three) revealed that sensorimotor timing performance changed significantly depending on specific task requirements. For example, timing performance with the dominant right hand was more stable than with the non-dominant left hand and tapping variability was reduced further during bimanual performance with both hands in synchrony. This sensitivity of behavioural performance may suggest that temporal processing is not achieved by a task-independent localized mechanism, because one would expect that a dedicated neural 'clock' would be robust against minor movement-related alterations in an otherwise identical timing task. Hence, based on the behavioural features of sensorimotor timing performance it is likely that temporal information processing occurs in distributed brain regions. This hypothesis is supported by previous research that showed that some timing functions are preserved in patients with damage to the basal ganglia or cerebellum (neural substrates that have been proposed as 'internal clocks') (Ivry & Spencer, 2004). However, the question remains whether there exist distributed brain networks that are dedicated to the explicit encoding of time or whether temporal information is intrinsically reflected in the patterns of neural firing (Ivry & Spencer, 2004; Spencer et al., 2009).

The results of studies two and three (Chapters four and five) revealed that suppression of the pre-motor cortex using theta burst transcranial magnetic stimulation significantly affected timing performance, as opposed to suppression of the primary motor cortex which did not affect performance. Additionally, the findings of study four (Chapter six) suggested that the cerebellum was significantly activated during sensorimotor synchronization compared with rest, consistent with a recent meta-analysis of the neural correlates of time-perception (Wiener et al., 2010). Lastly, study five (Chapter seven) demonstrated a significant change in interhemispheric functional connectivity between the bilateral primary motor cortices in the context of task requirements (greater connectivity during bimanual SMS, compared with unimanual SMS). The results of these studies suggest that the pre-motor cortex and the cerebellum play an important role in interval timing and may form a distributed brain network together with other areas such as the bilateral primary motor cortices. Taken together, the findings presented in this thesis suggest that this distributed network, that includes pre-motor and cerebellar regions, is dedicated to the explicit encoding of temporal information (Figure 10.1). The following paragraphs discuss the specific role of the pre-motor cortex and the cerebellum in this dedicated distributed network.

The results presented in Chapter four provide evidence for a crucial role of the left lateralized pre-motor cortex in sensorimotor timing, consistent with previous research (Pollok et al., 2008a; Pollok et al., 2006b; Pollok et al., 2009; Pollok et al., 2008b; Pollok et al., 2005). It has been suggested that the functional importance of the left pre-motor cortex during sensorimotor timing may be associated with a more general role in movement planning and preparation (Churchland & Shenoy, 2007; Pollok et al., 2008b). In particular, the left pre-motor cortex may inhibit and subsequently initiate movement based on temporal information received from the cerebellum. This hypothesis is supported by recent research that revealed the existence of both inhibitory and excitatory input directed from the pre-motor cortex to the primary motor cortices (Buch et al., 2010; Verstynen & Ivry, In press). Furthermore, previous research has consistently reported the existence of strong anatomical and functional connections between the cerebellum and the pre-motor

cortex (Bestmann et al., 2005; Hashimoto et al., 2010; Pollok et al., 2006b). Hence, the left pre-motor cortex may be involved in the temporal control of inhibition and subsequent initiation of movement during sensorimotor timing.

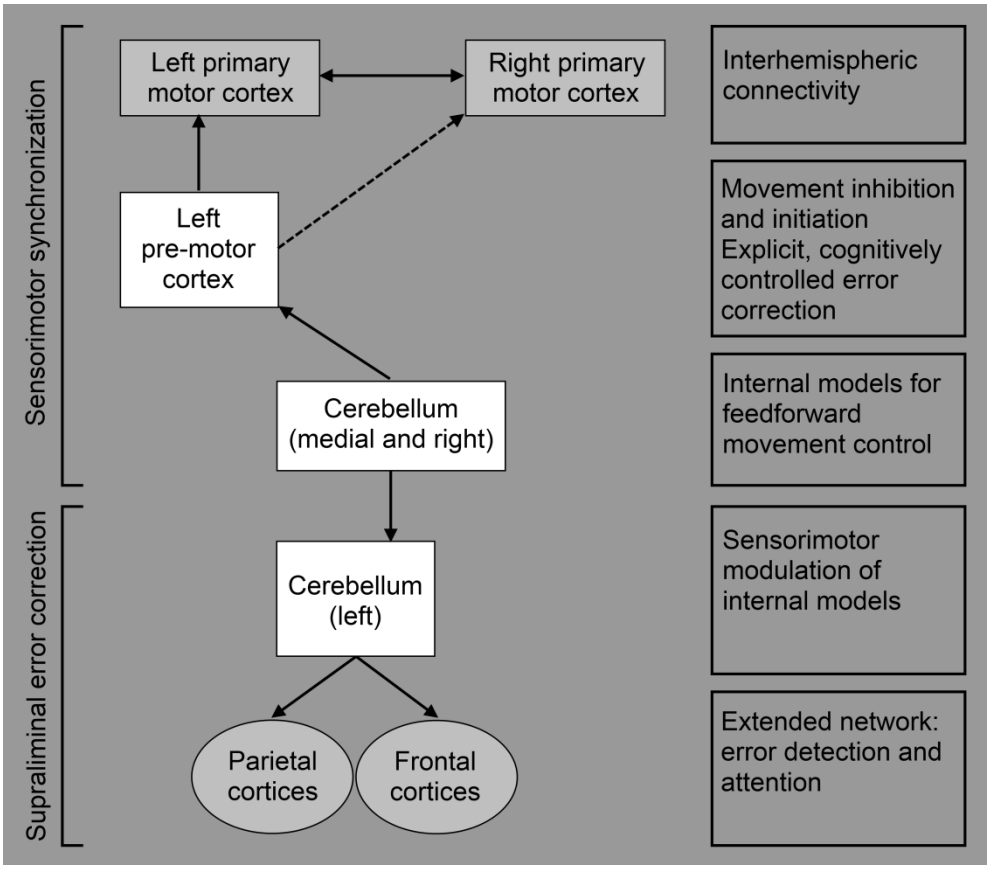

Figure 10.1: Theoretical integration. During sensorimotor synchronization with a regular pacing stimulus, a functional network comprising the left pre-motor cortex, the medial and right-lateralized cerebellum and the bilateral primary motor cortices is engaged. When an error correction response to perceivable phase shifts is required, the original network is extended to include the left cerebellum and parietal and frontal cortices. The hypothesized function of each region is summarized in the boxes on the right side of the image.

It was suggested in Chapter one that the specific function of the cerebellum in interval timing may be related to feedforward movement control or to sensorimotor modulation. A more generalized theory of cerebellar processing suggests that it is

involved in the production and modification of internal models that can be used to create predictions about future events (Ito, 2008; Stoodley, In press). In the internal model theory, cerebellar processing during a sensorimotor synchronization task initially produces an internal model for the temporal expectancy of future pacing tones. This internal model can be used to perform efficient and accurate synchronized movements based on feedforward control. During ongoing SMS performance, sensorimotor feedback can be used to optimize internal models through sensorimotor modulation. Hence, the internal model theory proposes that the cerebellum functions to compute and update internal models of predictable external events. A generalized cerebellar function for internal model production and optimization is consistent with a wide range of experimental findings that have revealed cerebellar contributions to motor learning, adaptive motor control and to a range of cognitive, executive and affective processes (Ito, 2008; Schmahmann, 2010; Stoodley, In press).

10.2.2 Sensorimotor error correction

Ongoing error correction is essential to maintain tap-tone synchrony during a paced finger tapping task (Repp, 2005). The behavioural results of study four (Chapter six) revealed that there was no difference in the behavioural error correction response following temporal shifts that fall either below (subliminal) or above (supraliminal) the perceptual threshold, consistent with previous research (Repp, 2001a). However, the results did provide evidence for the existence of different neural mechanisms for sub- and supra-liminal error correction. Error correction responses to large shifts activated a cortico-cerebellar network, whereas there was no evidence of additional activation during the responses to subliminal shifts. It was suggested that subliminal error correction may be achieved by resetting the phase relative to the previous pacing tone and does not, therefore, differ from ongoing correction in response to motor variability (Repp, 2005). Hence, ongoing error correction, which includes the correction of subliminal phase shifts, may be an intrinsic feature of sensorimotor timing performance that is achieved through

interactions between the cerebellum and the pre-motor cortex as discussed in the previous section.

Study four (Chapter six) showed that the left lateral cerebellum and parietal and frontal cortices were engaged during supraliminal error correction compared with regular sensorimotor timing performance. Additionally, disruption of both the left pre-motor cortex and of the left cerebellum significantly affected supraliminal error correction performance as shown in studies three and four (Chapters five and six). These findings suggest that supraliminal error correction differs from regular timing and may rely on the left cerebellum and pre-motor cortex. It may be that supraliminal error correction engages two different mechanisms (Repp, 2002a, 2002b). Implicit error correction, that uses internal models in the cerebellum, may continue to correct for supraliminal phase shifts. A greater degree of adaptation to the internal models is required to adjust for large shifts which may explain the recruitment of additional, left-lateralized cerebellar regions compared with subliminal or ongoing error correction. Additionally, an explicit, cognitively controlled error correction process may be engaged because the large shifts fall above the perceptual threshold. Such an explicit error correction system may include error detection mechanisms in parietal and frontal cortices. Explicit error correction may also be related to the contribution of the left pre-motor cortex (Figure 10.1). The relative contribution of explicit error correction may reduce with practice because the results presented in Chapter five showed that suppression of the left pre-motor cortex affected error correction performance on day one, but no longer had an effect after subjects gained practice. Previous research that differentially targeted implicit and explicit correction mechanisms confirmed that the cerebellum was exclusively involved in implicit error correction responses (Mazzoni & Krakauer, 2006; Taylor et al., 2010). Future research (see section 10.4) will be required to further elucidate the neural and behavioural correlates of implicit and explicit error correction mechanisms.

The behavioural results presented in studies three and four (Chapters five and six) showed a significant difference between the correction of supraliminal negative

shifts (which occur unexpectedly early) and supraliminal positive shifts (which occur unexpectedly late). It was suggested that the error correction response to negative and positive phase shifts may be controlled differently. In particular, negative error correction may be performed reactively, whereas positive error correction may be achieved with the help of feedforward movement control because there is time to adjust the predictive response. In line with the hypothesis that negative and positive error correction are behaviourally different, the findings of Experiment two in study four (Chapter six) suggested that there may be different neural mechanisms that underlie negative and positive error correction because suppression of the medial cerebellum selectively affected positive error correction. Additionally, the results of study three (Chapter five) revealed a practice effect on the correction of positive shifts, but not on the correction of negative shifts. These results confirm that error correction responses to negative and positive phase shifts are behaviourally and neuro-physiologically different. The correction of negative phase shifts appears to depend primarily on reaction time and cannot be improved with practice (Repp, 2011). The correction of positive phase shifts, on the other hand, can benefit from practice because the internal models can be optimized to correctly estimate the timing of a delayed phase shift with experience.

10.2.3 Transcranial magnetic stimulation

Theta burst transcranial magnetic stimulation was used in studies two, three and four (Chapters four, five and six) to determine the causal role of the primary and pre-motor cortices and of the cerebellum in sensorimotor timing and error correction. However, it was discussed in Chapter two that the focality of TMS stimulation depends on many geometric and (neuro-) physiological parameters and is therefore not fully understood. The fourth objective of this thesis was to determine the efficacy of TMS stimulation. The results presented in study six (Chapter eight) confirmed that TMS-induced stimulation always occurred at the predicted location directly underneath the centre of the TMS coil. However, the results also showed that TMS-induced stimulation was distributed over a wider region and occasionally occurred at gyral peaks located some distance from the

centre of the TMS coil. Such distal regions of TMS-induced stimulation occurred as a result of local thinning of the subarachnoid cerebrospinal fluid distribution. It was shown in study seven (Chapter nine) that the thickness of local CSF can vary significantly between different subjects and within a subject in different positions of the head with respect to gravity. Hence, the distribution of TMS-induced stimulation was shown to be significantly influenced by local CSF thickness and associated gyral geometry patterns. These findings suggest that stimulation achieved with TMS may vary between different subjects.

With regards to the coil positions used in this thesis, the findings presented in Chapter eight revealed that TMS over the primary motor cortex induced additional electric fields in neighbouring regions including the pre-motor and somatosensory areas. Similarly, TMS over the pre-motor cortex led to additional electric fields in primary motor and somatosensory areas. Hence, these results may suggest that there may be some overlap in the site of stimulation when TMS is applied over the primary and pre-motor cortex in the same hemisphere (as in study two, Chapter four). However, the strength of the electric fields was lower in neighbouring regions compared with the target brain region (i.e. the field strength was higher in the primary motor cortex than in the pre-motor cortex when the primary motor cortex was the target and vice versa). These findings of suprathreshold electric field in neighbouring areas may explain the variability between different subjects in the measured effects of TMS stimulation on behavioural performance that was seen in the studies presented in this thesis and in TMS research in general.

Regarding cerebellar stimulation, the results presented in Chapter eight showed that electric fields were induced in neighbouring regions in the visual cortices. Contrary to the cortical findings, the electric field strength was greater in these neighbouring visual regions than in the target region in the cerebellum. The relatively low TMS-induced electric field strength in the cerebellum occurred as a result of cortical depth combined with a relatively thick layer of CSF that encapsulates the cerebellum, compared with cortical targets. As discussed in Chapter eight, these findings suggest that it may be desirable to avoid experimental

paradigms that depend on visual input or cues in studies that wish to apply TMS over the cerebellum. The experimental paradigm adopted in study four (Chapter six) did not involve any visual input because the pacing stimulus consisted of an auditory sequence and the results presented in this study are therefore not influenced by the TMS-induced stimulation in the visual cortex. Additionally, the proximity of the lateral and medial cerebellar targets may result in some overlap of the induced supra-threshold electric fields between these targets. Hence, although it is possible to differentially stimulate the left and right cerebellum, stimulation of the medial cerebellar target may lead to additional electric fields in neighbouring regions in the left and right lateral cerebellum. This may potentially explain the similarity between the effects of medial and left-lateral cerebellar TMS on error correction shown in Experiment two of study four (Chapter six).

The findings presented in Chapters eight and nine reveal a hemispheric asymmetry in gyral structure and subarachnoid cerebrospinal fluid thickness, which leads to differences in the intensity and distribution of TMS induced electric fields between the left and right hemispheres. This hemispheric asymmetry may potentially contribute to differential effects of lateralized TMS such as the effects of left and right pre-motor TMS on error correction presented in study three (Chapter five). Further research is needed to determine the reliability and reproducibility of left compared with right lateralized TMS stimulation.

10.3 Limitations

Specific limitations of each study were highlighted in the discussion sections at the end of each Chapter. Most importantly, no stereotaxic neuronavigation methods were used to locate the TMS coil in Chapters four, five and six. The findings presented in Chapters eight and nine suggest that TMS-induced electric fields may occur some distance from the centre of the coil and can vary between different subjects. These limitations may explain the heterogeneity of TMS-induced effects on behavioural performance seen in Chapters four, five and six. Future studies may

benefit from a fully personalized approach to coil placement as discussed in the next section (10.4).

A second important limitation relates to the use of the linear phase correction model to analyse sensorimotor synchronization data in Chapters three and four. In the linear phase correction model, incorrect autocovariate estimates may lead to biased estimates for the outcome measures of motor and central variability and of error correction, as discussed in Chapter two. Additionally, negative estimates for motor variability occurred repeatedly in Chapters three and four and may influence statistical comparisons. To avoid these issues, more direct measures of sensorimotor timing performance and of error correction responses to induced phase shifts were adopted in subsequent studies (Chapters five, six and seven).

Lastly, a remaining challenge for the wavelet coherence analysis introduced in Chapter seven is to develop principled approaches to address the problem of multiple comparisons. For example, an equivalent of random field theory may be developed that can be applied to wavelet results in time-frequency space (Worsley et al., 1996). In the next section, areas for future research based on the work presented in this thesis are discussed.

10.4 Suggestions for future research

The findings presented in this thesis provide evidence for a significant role of the left pre-motor cortex and of the cerebellum in timing and error correction. Furthermore, the findings revealed the importance of task-dependent functional connectivity networks for timing and error correction. Future research should aim to investigate functional connectivity networks during timing and error correction further, whilst focusing specifically on the role of the left pre-motor cortex and the cerebellum. For instance, a future study could be designed in which fMRI data is obtained whilst subjects perform a sensorimotor synchronization task both before and after suppression TBS applied over the cerebellum or over the left pre-motor cortex. Connectivity approaches such as psychophysiological interaction analysis

and wavelet coherence analysis could be used to compare functional brain connectivity before and after TBS suppression of these brain structures. The resulting changes in connectivity may be used to gain a greater insight into the information flow within these networks and to learn more about the specific functional role of the pre-motor and cerebellar regions.

Future research is also needed to explore the feasibility and efficiency of subject-specific positioning of the TMS coil. A high-resolution structural MRI of subject-specific gyral folding patterns and subarachnoid CSF distribution could be loaded into a TMS modelling program and used to calculate the TMS-induced electric field for different coil positions. This approach requires computational resources and the availability of a finite element method solver such as the commercially available package SEMCAD that was used in Chapter eight. If these resources are available, a subject-specific localization approach is feasible and could be used to determine the optimal coil position in order to avoid unwanted stimulation of particular neighbouring areas or in order to optimize the tolerability of TMS. An additional benefit of subject-specific coil positioning is that the variability of TMS-induced effects on behavioural measurements may be reduced, which would result in greater statistical power and potentially greater consistency within and between different studies.

Lastly, Experiment two of study five (Chapter seven) provided proof-of-concept evidence for the applicability of wavelet coherence analysis to investigate dynamic fluctuations in coherence and phase in resting state networks. The use of this frequency-based analysis to investigate changes in functional connectivity over time provides a great opportunity to study and compare both task-related and resting state functional networks. Future studies should aim to determine the consistency and reliability of wavelet coherence findings in resting state and task-related data. Additionally, wavelet coherence analysis may, for example, be used to study dynamic resting state fluctuations in psychiatric and neurological disorders in order to better understand brain dysfunction. Resting state fMRI networks are increasingly studied in order to investigate abnormalities in intrinsic brain

organization in patients with complex psychiatric disorders such as schizophrenia and autism and in patients with affective disorders such as depression. However, resting state fMRI studies in patient groups do not always reveal consistent results (Fornito & Bullmore, 2010). This lack of consistency may be due to non-stationary dynamic fluctuations in resting state networks. Wavelet coherence analysis is able to detect such non-stationary signal fluctuations and may therefore help to improve our understanding of abnormal resting state functional connectivity in many psychiatric disorders. An important consideration for the use of resting state fMRI measures to compare patient groups with healthy controls is the potential for systematic biases due to differences in emotional states and resulting differences in physiological arousal (Fornito & Bullmore, 2010; Gray et al., 2009; Harrison & Critchley, 2007). Future research is required to differentiate between dynamic differences in emotional and physiological arousal and in resting state networks in patient groups compared with healthy controls. The wavelet coherence analysis described in this thesis is well-placed to contribute to future research in these areas.

10.5 Conclusion

In conclusion, the work presented in this thesis provides evidence that sensorimotor timing and error correction critically depend on the pre-motor cortex and the cerebellum. Specifically, it was shown that the left-lateralized pre-motor cortex subserves timing and error correction for both hands. In the cerebellum, medial and right-lateralized regions are associated with sensorimotor timing and additional left-lateralized cerebellar regions are required for the correction of perceivable timing shifts. These results can be interpreted within feedforward motor control theory. Internal models are stored in the cerebellum and used by the left pre-motor cortex to initiate timed movements. Additionally, proof-of-concept evidence is provided in this thesis for the applicability of wavelet coherence analysis to investigate dynamic coherence and phase in resting state networks at a group level. The final main finding presented in this thesis relates to the intensity and distribution of electric fields induced by transcranial magnetic stimulation (TMS). It was shown that TMS-induced electric fields occur primarily on the tops of those

gyri that are covered by a relatively thin layer of cerebrospinal fluid compared with surrounding gyri. These results suggest that TMS effects may vary between different subjects and can be optimized in the future by using a personalised method for coil placement.

11 References

Amassian, V. E., Maccabee, P. J., Cracco, R. Q., Cracco, J. B., Somasundaram, M., Rothwell, J. C., Eberle, L., Henry, K., & Rudell, A. P. (1994). The polarity of the induced electric field influences magnetic coil inhibition of human visual cortex: implications for the site of excitation. *Electroencephalogr Clin Neurophysiol, 93*(1), 21-26.

Amunts, K., Jäncke, L., Mohlberg, H., Steinmetz, H., & Zilles, K. (2000). Interhemispheric asymmetry of the human motor cortex related to handedness and gender. *Neuropsychologia, 38*(3), 304-312.

Amunts, K., Schlaug, G., Schleicher, A., Steinmetz, H., Dabringhaus, A., Roland, P. E., & Zilles, K. (1996). Asymmetry in the Human Motor Cortex and Handedness. *NeuroImage, 4*(3), 216-222.

Aramaki, Y., Honda, M., & Sadato, N. (2006). Suppression of the non-dominant motor cortex during bimanual symmetric finger movement: a functional magnetic resonance imaging study. *Neuroscience, 141*(4), 2147-2153.

Aramaki, Y., Osu, R., & Sadato, N. (2010). Resource-demanding versus cost-effective bimanual interaction in the brain. *Exp Brain Res, 203*(2), 407-418.

Aschersleben, G. (2002). Temporal control of movements in sensorimotor synchronization. *Brain Cogn, 48*(1), 66-79.

Ashburner, J., & Friston, K. J. (2001). Why Voxel-Based Morphometry Should Be Used. *NeuroImage, 14*(6), 1238-1243.

Bares, M., Lungu, O., Liu, T., Waechter, T., Gomez, C. M., & Ashe, J. (2007). Impaired predictive motor timing in patients with cerebellar disorders. *Exp Brain Res, 180*(2), 355-365.

Barker, A. T., Garnham, C. W., & Freeston, I. L. (1991). Magnetic nerve stimulation: the effect of waveform on efficiency, determination of neural membrane time constants and the measurement of stimulator output. *Electroencephalogr Clin Neurophysiol Suppl, 43*, 227-237.

Barker, A. T., Jalinous, R., & Freeston, I. L. (1985). Non-invasive magnetic stimulation of human motor cortex. *Lancet, 1*(8437), 1106-1107.

Bastian, A. J. (2006). Learning to predict the future: the cerebellum adapts feedforward movement control. *Curr Opin Neurobiol, 16*(6), 645-649.

Berens, P. (2009). CircStat: A MATLAB Toolbox for Circular Statistics. *Journal of Statistical Software, 31*(10), 1-21.

Bestmann, S., Baudewig, J., Siebner, H. R., Rothwell, J. C., & Frahm, J. (2003). Subthreshold high-frequency TMS of human primary motor cortex modulates interconnected frontal motor areas as detected by interleaved fMRI-TMS. *Neuroimage, 20*(3), 1685-1696.

Bestmann, S., Baudewig, J., Siebner, H. R., Rothwell, J. C., & Frahm, J. (2004). Functional MRI of the immediate impact of transcranial magnetic stimulation on cortical and subcortical motor circuits. *Eur J Neurosci, 19*(7), 1950-1962.

Bestmann, S., Baudewig, J., Siebner, H. R., Rothwell, J. C., & Frahm, J. (2005). BOLD MRI responses to repetitive TMS over human dorsal premotor cortex. *Neuroimage, 28*(1), 22-29.

Bijsterbosch, J. D., Lee, K.-H., Hunter, M. D., Tsoi, D. T., Lankappa, S., Wilkinson, I. D., Barker, A. T., & Woodruff, P. W. R. (2011). The Role of the Cerebellum in Sub- and Supraliminal Error Correction during Sensorimotor Synchronization: Evidence from fMRI and TMS. *Journal of Cognitive Neuroscience, 23*(5), 1100-1112.

Birn, R. M., Diamond, J. B., Smith, M. A., & Bandettini, P. A. (2006). Separating respiratory-variation-related fluctuations from neuronal-activity-related fluctuations in fMRI. *Neuroimage, 31*(4), 1536-1548.

Biswal, B., Yetkin, F. Z., Haughton, V. M., & Hyde, J. S. (1995). Functional connectivity in the motor cortex of resting human brain using echo-planar MRI. *Magn Reson Med, 34*(4), 537-541.

Biswal, B. B., Mennes, M., Zuo, X. N., Gohel, S., Kelly, C., Smith, S. M., Beckmann, C. F., Adelstein, J. S., Buckner, R. L., Colcombe, S., Dogonowski, A. M., Ernst, M., Fair, D., Hampson, M., Hoptman, M. J., Hyde, J. S., Kiviniemi, V. J., Kotter, R., Li, S. J., Lin, C. P., Lowe, M. J., Mackay, C., Madden, D. J., Madsen, K. H., Margulies, D. S., Mayberg, H. S., McMahon, K., Monk, C. S., Mostofsky, S. H., Nagel, B. J., Pekar, J. J.,

Peltier, S. J., Petersen, S. E., Riedl, V., Rombouts, S. A., Rypma, B., Schlaggar, B. L., Schmidt, S., Seidler, R. D., Siegle, G. J., Sorg, C., Teng, G. J., Veijola, J., Villringer, A., Walter, M., Wang, L., Weng, X. C., Whitfield-Gabrieli, S., Williamson, P., Windischberger, C., Zang, Y. F., Zhang, H. Y., Castellanos, F. X., & Milham, M. P. (2010). Toward discovery science of human brain function. *Proc Natl Acad Sci U S A, 107*(10), 4734-4739.

Blakemore, S. J., & Sirigu, A. (2003). Action prediction in the cerebellum and in the parietal lobe. *Exp Brain Res, 153*(2), 239-245.

Bohning, D. E., Shastri, A., Nahas, Z., Lorberbaum, J. P., Andersen, S. W., Dannels, W. R., Haxthausen, E. U., Vincent, D. J., & George, M. S. (1998). Echoplanar BOLD fMRI of brain activation induced by concurrent transcranial magnetic stimulation. *Invest Radiol, 33*(6), 336-340.

Brammer, M. J. (1998). Multidimensional wavelet analysis of functional magnetic resonance images. *Hum Brain Mapp, 6*(5-6), 378-382.

Buch, E. R., Mars, R. B., Boorman, E. D., & Rushworth, M. F. (2010). A network centered on ventral premotor cortex exerts both facilitatory and inhibitory control over primary motor cortex during action reprogramming. *J Neurosci, 30*(4), 1395-1401.

Bueti, D., Bahrami, B., & Walsh, V. (2008). Sensory and association cortex in time perception. *J Cogn Neurosci, 20*(6), 1054-1062.

Buhusi, C. V., & Meck, W. H. (2005). What makes us tick? Functional and neural mechanisms of interval timing. *Nat Rev Neurosci, 6*(10), 755-765.

Bullmore, E., Fadili, J., Maxim, V., Sendur, L., Whitcher, B., Suckling, J., Brammer, M., & Breakspear, M. (2004). Wavelets and functional magnetic resonance imaging of the human brain. *NeuroImage, 23*(Supplement 1), S234-S249.

Bullmore, E., Long, C., Suckling, J., Fadili, J., Calvert, G., Zelaya, F., Carpenter, T. A., & Brammer, M. (2001). Colored noise and computational inference in neurophysiological (fMRI) time series analysis: resampling methods in time and wavelet domains. *Hum Brain Mapp, 12*(2), 61-78.

Buzsáki, G., Buhl, D. L., Harris, K. D., Csicsvari, J., Czéh, B., & Morozov, A. (2003). Hippocampal network patterns of activity in the mouse. *Neuroscience, 116*(1), 201-211.

Chang, C., & Glover, G. H. (2009). Effects of model-based physiological noise correction on default mode network anti-correlations and correlations. *NeuroImage, 47*(4), 1448-1459.

Chang, C., & Glover, G. H. (2010). Time-frequency dynamics of resting-state brain connectivity measured with fMRI. *Neuroimage, 50*(1), 81-98.

Chen, R., Gerloff, C., Classen, J., Wassermann, E. M., Hallett, M., & G. Cohen, L. (1997). Safety of different inter-train intervals for repetitive transcranial magnetic stimulation and recommendations for safe ranges of stimulation parameters. *Electroencephalography and Clinical Neurophysiology/Electromyography and Motor Control, 105*(6), 415-421.

Christ, A., Kainz, W., Hahn, E. G., Honegger, K., Zefferer, M., Neufeld, E., Rascher, W., Janka, R., Bautz, W., Chen, J., Kiefer, B., Schmitt, P., Hollenbach, H. P., Shen, J., Oberle, M., Szczerba, D., Kam, A., Guag, J. W., & Kuster, N. (2010). The Virtual Family--development of surface-based anatomical models of two adults and two children for dosimetric simulations. *Phys Med Biol, 55*(2), N23-38.

Churchland, M. M., & Shenoy, K. V. (2007). Delay of movement caused by disruption of cortical preparatory activity. *J Neurophysiol, 97*(1), 348-359.

Cohen, D., & Cuffin, B. N. (1991). Developing a more focal magnetic stimulator. Part I: Some basic principles. *J Clin Neurophysiol, 8*(1), 102-111.

Cohen, L. G., Roth, B. J., Nilsson, J., Dang, N., Panizza, M., Bandinelli, S., Friauf, W., & Hallett, M. (1990). Effects of coil design on delivery of focal magnetic stimulation. Technical considerations. *Electroencephalography and Clinical Neurophysiology, 75*(4), 350-357.

Cohen, M. R., & Newsome, W. T. (2004). What electrical microstimulation has revealed about the neural basis of cognition. *Curr Opin Neurobiol, 14*(2), 169-177.

Cordes, D., Haughton, V. M., Arfanakis, K., Carew, J. D., Turski, P. A., Moritz, C. H., Quigley, M. A., & Meyerand, M. E. (2001). Frequencies contributing

to functional connectivity in the cerebral cortex in "resting-state" data. *AJNR Am J Neuroradiol, 22*(7), 1326-1333.

Cordes, D., Haughton, V. M., Arfanakis, K., Wendt, G. J., Turski, P. A., Moritz, C. H., Quigley, M. A., & Meyerand, M. E. (2000). Mapping functionally related regions of brain with functional connectivity MR imaging. *AJNR Am J Neuroradiol, 21*(9), 1636-1644.

Coull, J. T., Cheng, R.-K., & Meck, W. H. (2011). Neuroanatomical and Neurochemical Substrates of Timing. *Neuropsychopharmacology, 36*(1), 3-25.

Coull, J. T., & Nobre, A. C. (1998). Where and When to Pay Attention: The Neural Systems for Directing Attention to Spatial Locations and to Time Intervals as Revealed by Both PET and fMRI. *J. Neurosci., 18*(18), 7426-7435.

Coull, J. T., & Nobre, A. C. (2008). Dissociating explicit timing from temporal expectation with fMRI. *Current Opinion in Neurobiology, 18*(2), 137-144.

Coull, J. T., Vidal, F., Nazarian, B., & Macar, F. (2004). Functional anatomy of the attentional modulation of time estimation. *Science, 303*(5663), 1506-1508.

Damoiseaux, J. S., Rombouts, S. A. R. B., Barkhof, F., Scheltens, P., Stam, C. J., Smith, S. M., & Beckmann, C. F. (2006). Consistent resting-state networks across healthy subjects. *Proceedings of the National Academy of Sciences, 103*(37), 13848-13853.

Danckert, J., Ferber, S., Pun, C., Broderick, C., Striemer, C., Rock, S., & Stewart, D. (2007). Neglected time: impaired temporal perception of multisecond intervals in unilateral neglect. *J Cogn Neurosci, 19*(10), 1706-1720.

Dassonville, P., Zhu, X.-H., Ugurbil, K. m., Kim, S.-G., & Ashe, J. (1997). Functional activation in motor cortex reflects the direction and the degree of handedness. *Proceedings of the National Academy of Sciences of the United States of America, 94*(25), 14015-14018.

Dawson, K. A. (2004). Temporal organization of the brain: Neurocognitive mechanisms and clinical implications. *Brain and Cognition, 54*(1), 75-94.

De Lucia, M., Parker, G. J., Embleton, K., Newton, J. M., & Walsh, V. (2007). Diffusion tensor MRI-based estimation of the influence of brain tissue

anisotropy on the effects of transcranial magnetic stimulation. *NeuroImage, 36*(4), 1159-1170.

Del Olmo, M. F., Cheeran, B., Koch, G., & Rothwell, J. C. (2007). Role of the cerebellum in externally paced rhythmic finger movements. *J Neurophysiol, 98*(1), 145-152.

Diedrichsen, J. (2006). A spatially unbiased atlas template of the human cerebellum. *Neuroimage, 33*(1), 127-138.

Doumas, M., Praamstra, P., & Wing, A. M. (2005). Low frequency rTMS effects on sensorimotor synchronization. *Exp Brain Res, 167*(2), 238-245.

Drewing, K., & Aschersleben, G. (2003). Reduced timing variability during bimanual coupling: a role for sensory information. *Q J Exp Psychol A, 56*(2), 329-350.

Dubach, P., Guggisberg, A. G., Rösler, K. M., Hess, C. W., & Mathis, J. (2004). Significance of coil orientation for motor evoked potentials from nasalis muscle elicited by transcranial magnetic stimulation. *Clinical Neurophysiology, 115*(4), 862-870.

Duque, J., Mazzocchio, R., Dambrosia, J., Murase, N., Olivier, E., & Cohen, L. G. (2005). Kinematically Specific Interhemispheric Inhibition Operating in the Process of Generation of a Voluntary Movement. *Cereb. Cortex, 15*(5), 588-593.

Eliassen, J. C., Baynes, K., & Gazzaniga, M. S. (2000). Anterior and posterior callosal contributions to simultaneous bimanual movements of the hands and fingers. *Brain, 123*(12), 2501-2511.

Fadili, M. J., & Bullmore, E. T. (2002). Wavelet-Generalized Least Squares: A New BLU Estimator of Linear Regression Models with 1/f Errors. *NeuroImage, 15*(1), 217-232.

Fadili, M. J., & Bullmore, E. T. (2004). A comparative evaluation of wavelet-based methods for hypothesis testing of brain activation maps. *NeuroImage, 23*(3), 1112-1128.

Fierro, B., Palermo, A., Puma, A., Francolini, M., Panetta, M. L., Daniele, O., & Brighina, F. (2007). Role of the cerebellum in time perception: a TMS study in normal subjects. *J Neurol Sci, 263*(1-2), 107-112.

Fischer, S., Nitschke, M. F., Melchert, U. H., Erdmann, C., & Born, J. (2005). Motor Memory Consolidation in Sleep Shapes More Effective Neuronal Representations. *J. Neurosci., 25*(49), 11248-11255.

Fitzgerald, P. B., Brown, T. L., Marston, N. A. U., Oxley, T., de Castella, A., Daskalakis, Z. J., & Kulkarni, J. (2004). Reduced plastic brain responses in schizophrenia: a transcranial magnetic stimulation study. *Schizophrenia Research, 71*(1), 17-26.

Fitzpatrick, S. M., & Rothman, D. L. (2000). Meeting report: transcranial magnetic stimulation and studies of human cognition. *J Cogn Neurosci, 12*(4), 704-709.

Fornito, A., & Bullmore, E. T. (2010). What can spontaneous fluctuations of the blood oxygenation-level-dependent signal tell us about psychiatric disorders? *Current Opinion in Psychiatry, 23*(3), 239-249 210.1097/YCO.1090b1013e328337d328378d.

Fox, M. D., & Greicius, M. (2010). Clinical applications of resting state functional connectivity. *Front Syst Neurosci, 4*, 19.

Fox, M. D., Snyder, A. Z., Vincent, J. L., Corbetta, M., Van Essen, D. C., & Raichle, M. E. (2005). The human brain is intrinsically organized into dynamic, anticorrelated functional networks. *Proc Natl Acad Sci U S A, 102*(27), 9673-9678.

Fox, M. D., Zhang, D., Snyder, A. Z., & Raichle, M. E. (2009). The Global Signal and Observed Anticorrelated Resting State Brain Networks. *J Neurophysiol, 101*(6), 3270-3283.

Fransson, P. (2005). Spontaneous low-frequency BOLD signal fluctuations: an fMRI investigation of the resting-state default mode of brain function hypothesis. *Hum Brain Mapp, 26*(1), 15-29.

Friston, K. J. (1994). Functional and effective connectivity in neuroimaging: A synthesis. *Human Brain Mapping, 2*(1-2), 56-78.

Friston, K. J. (1998). The disconnection hypothesis. *Schizophr Res, 30*(2), 115-125.

Friston, K. J., Buechel, C., Fink, G. R., Morris, J., Rolls, E., & Dolan, R. J. (1997). Psychophysiological and modulatory interactions in neuroimaging. *Neuroimage, 6*(3), 218-229.

Friston, K. J., Frith, C. D., Liddle, P. F., & Frackowiak, R. S. (1993). Functional connectivity: the principal-component analysis of large (PET) data sets. *J Cereb Blood Flow Metab, 13*(1), 5-14.

Funnell, M. G., Corballis, P. M., & Gazzaniga, M. S. (2003). Temporal discrimination in the split brain. *Brain and Cognition, 53*(2), 218-222.

Gabriel, S., Lau, R. W., & Gabriel, C. (1996). The dielectric properties of biological tissues: III. Parametric models for the dielectric spectrum of tissues. *Phys Med Biol, 41*(11), 2271-2293.

Gaser, C., & Schlaug, G. (2003). Brain Structures Differ between Musicians and Non-Musicians. *J. Neurosci., 23*(27), 9240-9245.

George, M. S., Padberg, F., Schlaepfer, T. E., O'Reardon, J. P., Fitzgerald, P. B., Nahas, Z. H., & Marcolin, M. A. (2009). Controversy: Repetitive transcranial magnetic stimulation or transcranial direct current stimulation shows efficacy in treating psychiatric diseases (depression, mania, schizophrenia, obsessive-complusive disorder, panic, posttraumatic stress disorder). *Brain Stimulation, 2*(1), 14-21.

Gibbon, J., Malapani, C., Dale, C. L., & Gallistel, C. (1997). Toward a neurobiology of temporal cognition: advances and challenges. *Curr Opin Neurobiol, 7*(2), 170-184.

Glover, G. H., Li, T. Q., & Ress, D. (2000). Image-based method for retrospective correction of physiological motion effects in fMRI: RETROICOR. *Magn Reson Med, 44*(1), 162-167.

Good, C. D., Johnsrude, I., Ashburner, J., Henson, R. N. A., Friston, K. J., & Frackowiak, R. S. J. (2001). Cerebral Asymmetry and the Effects of Sex and Handedness on Brain Structure: A Voxel-Based Morphometric Analysis of 465 Normal Adult Human Brains. *NeuroImage, 14*(3), 685-700.

Gooddy, W. (1969). *Disorders of the time sense* (Vol. 3). Amsterdam: North-Holland publishing.

Gray, M. A., Minati, L., Harrison, N. A., Gianaros, P. J., Napadow, V., & Critchley, H. D. (2009). Physiological recordings: Basic concepts and

implementation during functional magnetic resonance imaging. *NeuroImage, 47*(3), 1105-1115.

Greicius, M. D., Krasnow, B., Reiss, A. L., & Menon, V. (2003). Functional connectivity in the resting brain: A network analysis of the default mode hypothesis. *Proceedings of the National Academy of Sciences of the United States of America, 100*(1), 253-258.

Grinsted, A., Moore, J. C., & Jevrejeva, S. (2004). Application of the cross wavelet transform and wavelet coherence to geophysical time series: HAL - CCSD.

Grondin, S., & Rousseau, R. (1991). Judging the relative duration of multimodal short empty time intervals. *Percept Psychophys, 49*(3), 245-256.

Grubbs, F. E. (1969). Procedures for Detecting Outlying Observations in Samples. *Technometrics, 11*(1), 1-21.

Grube, M., Cooper, F. E., Chinnery, P. F., & Griffiths, T. D. (2010a). Dissociation of duration-based and beat-based auditory timing in cerebellar degeneration. *Proc Natl Acad Sci U S A, 107*(25), 11597-11601.

Grube, M., Lee, K.-H., Griffiths, T. D., Barker, A. T., & Woodruff, P. W. R. (2010b). Transcranial magnetic theta-burst stimulation of the human cerebellum distinguishes absolute, duration-based from relative, beat-based perception of subsecond time intervals. *Frontiers in Psychology, 1*.

Hagura, N., Oouchida, Y., Aramaki, Y., Okada, T., Matsumura, M., Sadato, N., & Naito, E. (2008). Visuokinesthetic Perception of Hand Movement Is Mediated by Cerebro-Cerebellar Interaction between the Left Cerebellum and Right Parietal Cortex. *Cereb Cortex*.

Hallett, M. (2007). Transcranial magnetic stimulation: a primer. *Neuron, 55*(2), 187-199.

Hammond, G. (2002). Correlates of human handedness in primary motor cortex: a review and hypothesis. *Neuroscience & Biobehavioral Reviews, 26*(3), 285-292.

Harrington, D. L., Lee, R. R., Boyd, L. A., Rapcsak, S. Z., & Knight, R. T. (2004). Does the representation of time depend on the cerebellum? Effect of cerebellar stroke. *Brain, 127*(Pt 3), 561-574.

Harrison, N. A., & Critchley, H. D. (2007). Affective neuroscience and psychiatry. *Br J Psychiatry, 191*, 192-194.

Harrison, P. J. (2005). Neuropathology of schizophrenia. *Psychiatry, 4*(10), 18-21.

Hary, D., & Moore, G. P. (1985). Temporal tracking and synchronization strategies. *Hum Neurobiol, 4*(2), 73-79.

Hary, D., & Moore, G. P. (1987a). On the performance and stability of human metronome-synchronization strategies. *Br J Math Stat Psychol, 40 (Pt 2)*, 109-124.

Hary, D., & Moore, G. P. (1987b). Synchronizing human movement with an external clock source. *Biol Cybern, 56*(5-6), 305-311.

Hashimoto, M., Takahara, D., Hirata, Y., Inoue, K.-i., Miyachi, S., Nambu, A., Tanji, J., Takada, M., & Hoshi, E. (2010). Motor and non-motor projections from the cerebellum to rostrocaudally distinct sectors of the dorsal premotor cortex in macaques. *European Journal of Neuroscience, 31*(8), 1402-1413.

Helmuth, L. L., & Ivry, R. B. (1996). When two hands are better than one: reduced timing variability during bimanual movements. *J Exp Psychol Hum Percept Perform, 22*(2), 278-293.

Herwig, U., Schonfeldt-Lecuona, C., Wunderlich, A. P., von Tiesenhausen, C., Thielscher, A., Walter, H., & Spitzer, M. (2001). The navigation of transcranial magnetic stimulation. *Psychiatry Res, 108*(2), 123-131.

Hester, R., Foxe, J. J., Molholm, S., Shpaner, M., & Garavan, H. (2005). Neural mechanisms involved in error processing: a comparison of errors made with and without awareness. *Neuroimage, 27*(3), 602-608.

Hodge, V., & Austin, J. (2004). A Survey of Outlier Detection Methodologies. *Artificial Intelligence Review, 22*(2), 85-126.

Hoffman, R. E., Hawkins, K. A., Gueorguieva, R., Boutros, N. N., Rachid, F., Carroll, K., & Krystal, J. H. (2003). Transcranial Magnetic Stimulation of Left Temporoparietal Cortex and Medication-Resistant Auditory Hallucinations. *Arch Gen Psychiatry, 60*(1), 49-56.

Hoogendam, J. M., Ramakers, G. M. J., & Di Lazzaro, V. (2010). Physiology of repetitive transcranial magnetic stimulation of the human brain. *Brain Stimulation, 3*(2), 95-118.

Horwitz, B. (2003). The elusive concept of brain connectivity. *NeuroImage, 19*(2), 466-470.

Huang, Y.-Z., Chen, R.-S., Rothwell, J. C., & Wen, H.-Y. (2007). The after-effect of human theta burst stimulation is NMDA receptor dependent. *Clinical Neurophysiology, 118*(5), 1028-1032.

Huang, Y.-Z., Rothwell, J. C., Chen, R.-S., Lu, C.-S., & Chuang, W.-L. (2011). The theoretical model of theta burst form of repetitive transcranial magnetic stimulation. *Clinical Neurophysiology, 122*(5), 1011-1018.

Huang, Y.-Z., Sommer, M., Thickbroom, G., Hamada, M., Pascual-Leonne, A., Paulus, W., Classen, J., Peterchev, A. V., Zangen, A., & Ugawa, Y. (2009). Consensus: New methodologies for brain stimulation. *Brain Stimulation, 2*(1), 2-13.

Huang, Y. Z., Edwards, M. J., Rounis, E., Bhatia, K. P., & Rothwell, J. C. (2005). Theta burst stimulation of the human motor cortex. *Neuron, 45*(2), 201-206.

Huerta, P. T., & Volpe, B. T. (2009). Transcranial magnetic stimulation, synaptic plasticity and network oscillations. *J Neuroeng Rehabil, 6*, 7.

Ito, M. (2008). Control of mental activities by internal models in the cerebellum. *Nat Rev Neurosci, 9*(4), 304-313.

Ivry, R. B., & Schlerf, J. E. (2008). Dedicated and intrinsic models of time perception. *Trends Cogn Sci, 12*(7), 273-280.

Ivry, R. B., & Spencer, R. M. (2004). The neural representation of time. *Curr Opin Neurobiol, 14*(2), 225-232.

Jalinous, R. (1991). Technical and practical aspects of magnetic nerve stimulation. *J Clin Neurophysiol, 8*(1), 10-25.

Jäncke, L., Loose, R., Lutz, K., Specht, K., & Shah, N. J. (2000). Cortical activations during paced finger-tapping applying visual and auditory pacing stimuli. *Brain Res Cogn Brain Res, 10*(1-2), 51-66.

Johanson, C. E., Duncan, J. A., Klinge, P. M., Brinker, T., Stopa, E. G., & Silverberg, G. D. (2008). Multiplicity of cerebrospinal fluid functions: New challenges in health and disease. *Cerebrospinal Fluid Research, 5*, 10.

Jones, C. R., Rosenkranz, K., Rothwell, J. C., & Jahanshahi, M. (2004). The right dorsolateral prefrontal cortex is essential in time reproduction: an investigation with repetitive transcranial magnetic stimulation. *Exp Brain Res, 158*(3), 366-372.

Jones, T. B., Bandettini, P. A., & Birn, R. M. (2008). Integration of motion correction and physiological noise regression in fMRI. *Neuroimage, 42*(2), 582-590.

Jueptner, M., Ottinger, S., Fellows, S. J., Adamschewski, J., Flerich, L., Muller, S. P., Diener, H. C., Thilmann, A. F., & Weiller, C. (1997). The relevance of sensory input for the cerebellar control of movements. *Neuroimage, 5*(1), 41-48.

Kagerer, F. A., Wittmann, M., Szelag, E., & Steinbüchel, N. v. (2002). Cortical involvement in temporal reproduction: evidence for differential roles of the hemispheres. *Neuropsychologia, 40*(3), 357-366.

Kammer, T., Beck, S., Thielscher, A., Laubis-Herrmann, U., & Topka, H. (2001). Motor thresholds in humans: a transcranial magnetic stimulation study comparing different pulse waveforms, current directions and stimulator types. *Clinical neurophysiology : official journal of the International Federation of Clinical Neurophysiology, 112*(2), 250-258.

Kantak, S. S., Sullivan, K. J., Fisher, B. E., Knowlton, B. J., & Winstein, C. J. (2010). Neural substrates of motor memory consolidation depend on practice structure. *Nat Neurosci, 13*(8), 923-925.

Karmarkar, U. R., & Buonomano, D. V. (2007). Timing in the absence of clocks: encoding time in neural network states. *Neuron, 53*(3), 427-438.

Kay, K. N., David, S. V., Prenger, R. J., Hansen, K. A., & Gallant, J. L. (2008). Modeling low-frequency fluctuation and hemodynamic response timecourse in event-related fMRI. *Hum Brain Mapp, 29*(2), 142-156.

Klein, A., Sauer, T., Jedynak, A., & Skrandies, W. (2006). Conventional and wavelet coherence applied to sensory-evoked electrical brain activity. *IEEE Trans Biomed Eng, 53*(2), 266-272.

Knecht, S., Sommer, J., Deppe, M., & Steinstrater, O. (2005). Scalp position and efficacy of transcranial magnetic stimulation. *Clinical Neurophysiology, 116*(8), 1988-1993.

Koch, G., Oliveri, M., Torriero, S., Salerno, S., Lo Gerfo, E., & Caltagirone, C. (2007). Repetitive TMS of cerebellum interferes with millisecond time processing. *Exp Brain Res, 179*(2), 291-299.

Koski, L., Schrader, L. M., Wu, A. D., & Stern, J. M. (2005). Normative data on changes in transcranial magnetic stimulation measures over a ten hour period. *Clinical Neurophysiology, 116*(9), 2099-2109.

Lee, D. J., Chen, Y., & Schlaug, G. (2003). Corpus callosum: musician and gender effects. *NeuroReport, 14*(2), 205-209.

Lee, K. H., Bhaker, R. S., Mysore, A., Parks, R. W., Birkett, P. B., & Woodruff, P. W. (2009). Time perception and its neuropsychological correlates in patients with schizophrenia and in healthy volunteers. *Psychiatry Res, 166*(2-3), 174-183.

Lee, K. H., Egleston, P. N., Brown, W. H., Gregory, A. N., Barker, A. T., & Woodruff, P. W. (2007). The role of the cerebellum in subsecond time perception: evidence from repetitive transcranial magnetic stimulation. *J Cogn Neurosci, 19*(1), 147-157.

Lejeune, H. (1998). Switching or gating? The attentional challenge in cognitive models of psychological time. *Behavioural Processes, 44*(2), 127-145.

Lewis, P. A., & Miall, R. C. (2003). Distinct systems for automatic and cognitively controlled time measurement: evidence from neuroimaging. *Curr Opin Neurobiol, 13*(2), 250-255.

Lewis, P. A., Wing, A. M., Pope, P. A., Praamstra, P., & Miall, R. C. (2004). Brain activity correlates differentially with increasing temporal complexity of rhythms during initialisation, synchronisation, and continuation phases of paced finger tapping. *Neuropsychologia, 42*(10), 1301-1312.

Li, K., Guo, L., Nie, J., Li, G., & Liu, T. (2009). Review of methods for functional brain connectivity detection using fMRI. *Comput Med Imaging Graph, 33*(2), 131-139.

Li, X., Yao, X., Fox, J., & Jefferys, J. G. (2007). Interaction dynamics of neuronal oscillations analysed using wavelet transforms. *J Neurosci Methods, 160*(1), 178-185.

Lioumis, P., Kičić, D., Savolainen, P., Mäkelä, J. P., & Kähkönen, S. (2009). Reproducibility of TMS—Evoked EEG responses. *Human Brain Mapping, 30*(4), 1387-1396.

Lisanby, S. H., Gutman, D., Luber, B., Schroeder, C., & Sackeim, H. A. (2001). Sham TMS: intracerebral measurement of the induced electrical field and the induction of motor-evoked potentials. *Biological Psychiatry, 49*(5), 460-463.

Liu, J., & Newsome, W. T. (2005). Correlation between speed perception and neural activity in the middle temporal visual area. *J Neurosci, 25*(3), 711-722.

Lontis, E. R., Voigt, M., & Struijk, J. J. (2006). Focality Assessment in Transcranial Magnetic Stimulation With Double and Cone Coils. *Journal of Clinical Neurophysiology, 23*(5), 463-472 410.1097/1001.wnp.0000229944.0000263011.a0000229941.

Lui, A., Polis, T., & Cicutti, N. (1998). Densities of cerebrospinal fluid and spinal anaesthetic solutions in surgical patients at body temperature. *Canadian Journal of Anesthesia / Journal canadien d'anesthésie, 45*(4), 297-303.

Lutz, K., Specht, K., Shah, N. J., & Jäncke, L. (2000). Tapping movements according to regular and irregular visual timing signals investigated with fMRI. *Neuroreport, 11*(6), 1301-1306.

Macar, F., Anton, J. L., Bonnet, M., & Vidal, F. (2004). Timing functions of the supplementary motor area: an event-related fMRI study. *Brain Res Cogn Brain Res, 21*(2), 206-215.

Macar, F., Coull, J., & Vidal, F. (2006). The supplementary motor area in motor and perceptual time processing: fMRI studies. *Cogn Process, 7*(2), 89-94.

Macar, F., Lejeune, H., Bonnet, M., Ferrara, A., Pouthas, V., Vidal, F., & Maquet, P. (2002). Activation of the supplementary motor area and of attentional networks during temporal processing. *Exp Brain Res, 142*(4), 475-485.

Maccabee, P. J., Amassian, V. E., Eberle, L. P., & Cracco, R. Q. (1993). Magnetic coil stimulation of straight and bent amphibian and mammalian peripheral nerve in vitro: Locus of excitation. *Journal of Physiology, 460*, 201-219.

Malcolm, M. P., Lavine, A., Kenyon, G., Massie, C., & Thaut, M. (2008). Repetitive transcranial magnetic stimulation interrupts phase synchronization during rhythmic motor entrainment. *Neurosci Lett, 435*(3), 240-245.

Matell, M. S., & Meck, W. H. (2000). Neuropsychological mechanisms of interval timing behavior. *Bioessays, 22*(1), 94-103.

Matell, M. S., & Meck, W. H. (2004). Cortico-striatal circuits and interval timing: coincidence detection of oscillatory processes. *Brain Res Cogn Brain Res, 21*(2), 139-170.

Matthews, P. M., Honey, G. D., & Bullmore, E. T. (2006). Applications of fMRI in translational medicine and clinical practice. *Nat Rev Neurosci, 7*(9), 732-744.

Mauk, M. D., & Buonomano, D. V. (2004). The neural basis of temporal processing. *Annu Rev Neurosci, 27*, 307-340.

Mayville, J. M., Jantzen, K. J., Fuchs, A., Steinberg, F. L., & Kelso, J. A. (2002). Cortical and subcortical networks underlying syncopated and synchronized coordination revealed using fMRI. Functional magnetic resonance imaging. *Hum Brain Mapp, 17*(4), 214-229.

Mazzoni, P., & Krakauer, J. W. (2006). An implicit plan overrides an explicit strategy during visuomotor adaptation. *J Neurosci, 26*(14), 3642-3645.

Meck, W. H. (2003). *Functional and neural mechanisms of interval timing*. Boca Raton, Fla. ; London: CRC.

Meegan, D. V., Aslin, R. N., & Jacobs, R. A. (2000). Motor timing learned without motor training. *Nat Neurosci, 3*(9), 860-862.

Meyer-Lindenberg, A., Ziemann, U., Hajak, G. r., Cohen, L., & Berman, K. F. (2002). Transitions between dynamical states of differing stability in the

human brain. *Proceedings of the National Academy of Sciences of the United States of America, 99*(17), 10948-10953.

Miranda, P. C., Hallett, M., & Basser, P. J. (2003). The electric field induced in the brain by magnetic stimulation: a 3-D finite-element analysis of the effect of tissue heterogeneity and anisotropy. *IEEE Trans Biomed Eng, 50*(9), 1074-1085.

Molholm, S., Martinez, A., Ritter, W., Javitt, D. C., & Foxe, J. J. (2005). The neural circuitry of pre-attentive auditory change-detection: an fMRI study of pitch and duration mismatch negativity generators. *Cereb Cortex, 15*(5), 545-551.

Molinari, M., Leggio, M. G., & Thaut, M. H. (2007). The cerebellum and neural networks for rhythmic sensorimotor synchronization in the human brain. *Cerebellum, 6*(1), 18-23.

Müller, K., Lohmann, G., Neumann, J., Grigutsch, M., Mildner, T., & von Cramon, D. Y. (2004). Investigating the wavelet coherence phase of the BOLD signal. *Journal of Magnetic Resonance Imaging, 20*(1), 145-152.

Murphy, K., Birn, R. M., Handwerker, D. A., Jones, T. B., & Bandettini, P. A. (2009). The impact of global signal regression on resting state correlations: Are anti-correlated networks introduced? *NeuroImage, 44*(3), 893-905.

Narr, K. L., Sharma, T., Woods, R. P., Thompson, P. M., Sowell, E. R., Rex, D., Kim, S., Asuncion, D., Jang, S., Mazziotta, J., & Toga, A. W. (2003). Increases in Regional Subarachnoid CSF Without Apparent Cortical Gray Matter Deficits in Schizophrenia: Modulating Effects of Sex and Age. *Am J Psychiatry, 160*(12), 2169-2180.

O'Shea, J., & Walsh, V. (2007). Transcranial magnetic stimulation. *Current Biology, 17*(6), R196-R199.

Oberman, L., Edwards, D., Eldaief, M., & Pascual-Leone, A. (2011). Safety of Theta Burst Transcranial Magnetic Stimulation: A Systematic Review of the Literature. *Journal of Clinical Neurophysiology, 28*(1), 67-74 10.1097/WNP.1090b1013e318205135f.

Ohyama, T., Nores, W. L., Murphy, M., & Mauk, M. D. (2003). What the cerebellum computes. *Trends Neurosci, 26*(4), 222-227.

Okamoto, M., Dan, H., Sakamoto, K., Takeo, K., Shimizu, K., Kohno, S., Oda, I., Isobe, S., Suzuki, T., Kohyama, K., & Dan, I. (2004). Three-dimensional probabilistic anatomical cranio-cerebral correlation via the international 10-20 system oriented for transcranial functional brain mapping. *NeuroImage, 21*(1), 99-111.

Oldfield, R. C. (1971). The assessment and analysis of handedness: the Edinburgh inventory. *Neuropsychologia, 9*(1), 97-113.

Pascual-Leone, A., Valls-Sole, J., Wassermann, E. M., & Hallett, M. (1994). Responses to rapid-rate transcranial magnetic stimulation of the human motor cortex. *Brain, 117*(4), 847-858.

Paus, T., Jech, R., Thompson, C. J., Comeau, R., Peters, T., & Evans, A. C. (1997). Transcranial magnetic stimulation during positron emission tomography: a new method for studying connectivity of the human cerebral cortex. *J Neurosci, 17*(9), 3178-3184.

Paus, T., Sipila, P. K., & Strafella, A. P. (2001). Synchronization of neuronal activity in the human primary motor cortex by transcranial magnetic stimulation: an EEG study. *J Neurophysiol, 86*(4), 1983-1990.

Perez, M. A., & Cohen, L. G. (2009). Interhemispheric inhibition between primary motor cortices: what have we learned? *J Physiol, 587*(Pt 4), 725-726.

Peters, M. (1980). Why the preferred hand taps more quickly than the non-preferred hand: Three experiments on handedness. *Canadian Journal of Psychology/Revue canadienne de psychologie, 34*(1), 62-71.

Pikovsky, A., Rosenblum, M., & Kurths, J. (2001). *Synchronization: a universal concept in nonlinear sciences*. Cambridge: Cambridge University Press.

Pollok, B., Butz, M., Gross, J., & Schnitzler, A. (2007). Intercerebellar coupling contributes to bimanual coordination. *J Cogn Neurosci, 19*(4), 704-719.

Pollok, B., Gross, J., Kamp, D., & Schnitzler, A. (2008a). Evidence for anticipatory motor control within a cerebello-diencephalic-parietal network. *J Cogn Neurosci, 20*(5), 828-840.

Pollok, B., Gross, J., & Schnitzler, A. (2006a). Asymmetry of interhemispheric interaction in left-handed subjects. *Exp Brain Res, 175*(2), 268-275.

Pollok, B., Gross, J., & Schnitzler, A. (2006b). How the brain controls repetitive finger movements. *J Physiol Paris, 99*(1), 8-13.

Pollok, B., Krause, V., Butz, M., & Schnitzler, A. (2009). Modality specific functional interaction in sensorimotor synchronization. *Human Brain Mapping, 30*(6), 1783-1790.

Pollok, B., Rothkegel, H., Schnitzler, A., Paulus, W., & Lang, N. (2008b). The effect of rTMS over left and right dorsolateral premotor cortex on movement timing of either hand. *Eur J Neurosci, 27*(3), 757-764.

Pollok, B., Sudmeyer, M., Gross, J., & Schnitzler, A. (2005). The oscillatory network of simple repetitive bimanual movements. *Brain Res Cogn Brain Res, 25*(1), 300-311.

Posner, M. I., & Raichle, M. E. (1994). *Images of mind*. New York: Scientific American Library.

Praamstra, P., Kourtis, D., Kwok, H. F., & Oostenveld, R. (2006). Neurophysiology of implicit timing in serial choice reaction-time performance. *J Neurosci, 26*(20), 5448-5455.

Praamstra, P., Turgeon, M., Hesse, C. W., Wing, A. M., & Perryer, L. (2003). Neurophysiological correlates of error correction in sensorimotor-synchronization. *Neuroimage, 20*(2), 1283-1297.

Pridmore, S., Fernandes Filho, J. A., Nahas, Z., Liberatos, C., & George, M. S. (1998). Motor threshold in transcranial magnetic stimulation: a comparison of a neurophysiological method and a visualization of movement method. *J Ect, 14*(1), 25-27.

Raichle, M. E., MacLeod, A. M., Snyder, A. Z., Powers, W. J., Gusnard, D. A., & Shulman, G. L. (2001). A default mode of brain function. *Proc Natl Acad Sci U S A, 98*(2), 676-682.

Ramnani, N. (2006). The primate cortico-cerebellar system: anatomy and function. *Nat Rev Neurosci, 7*(7), 511-522.

Rao, S. M., Harrington, D. L., Haaland, K. Y., Bobholz, J. A., Cox, R. W., & Binder, J. R. (1997). Distributed neural systems underlying the timing of movements. *J Neurosci, 17*(14), 5528-5535.

Ravazzani, P., Ruohonen, J., Grandori, F., & Tognola, G. (1996). Magnetic stimulation of the nervous system: induced electric field in unbounded, semi-infinite, spherical, and cylindrical media. *Ann Biomed Eng, 24*(5), 606-616.

Repp, B. H. (1999). Control of Expressive and Metronomic Timing in Pianists. *J Mot Behav, 31*(2), 145-164.

Repp, B. H. (2000). Compensation for subliminal timing perturbations in perceptual-motor synchronization. *Psychol Res, 63*(2), 106-128.

Repp, B. H. (2001a). Phase correction, phase resetting, and phase shifts after subliminal timing perturbations in sensorimotor synchronization. *J Exp Psychol Hum Percept Perform, 27*(3), 600-621.

Repp, B. H. (2001b). Processes underlying adaptation to tempo changes in sensorimotor synchronization. *Human Movement Science, 20*(3), 277-312.

Repp, B. H. (2002a). Automaticity and voluntary control of phase correction following event onset shifts in sensorimotor synchronization. *J Exp Psychol Hum Percept Perform, 28*(2), 410-430.

Repp, B. H. (2002b). Phase correction in sensorimotor synchronization: nonlinearities in voluntary and involuntary responses to perturbations. *Hum Mov Sci, 21*(1), 1-37.

Repp, B. H. (2005). Sensorimotor synchronization: a review of the tapping literature. *Psychon Bull Rev, 12*(6), 969-992.

Repp, B. H. (2010). Sensorimotor synchronization and perception of timing: Effects of music training and task experience. *Human Movement Science, 29*(2), 200-213.

Repp, B. H. (2011). Tapping in synchrony with a perturbed metronome: the phase correction response to small and large phase shifts as a function of tempo. *J Mot Behav, 43*(3), 213-227.

Repp, B. H., & Keller, P. E. (2004). Adaptation to tempo changes in sensorimotor synchronization: effects of intention, attention, and awareness. *Q J Exp Psychol A, 57*(3), 499-521.

Roberts, S. (1982). Cross-modal use of an internal clock. *J Exp Psychol Anim Behav Process, 8*(1), 2-22.

Roth, B. J., Cohen, L. G., & Hallett, M. (1991a). The electric field induced during magnetic stimulation. *Electroencephalogr Clin Neurophysiol Suppl, 43*, 268-278.

Roth, B. J., Saypol, J. M., Hallett, M., & Cohen, L. G. (1991b). A theoretical calculation of the electric field induced in the cortex during magnetic stimulation. *Electroencephalogr Clin Neurophysiol, 81*(1), 47-56.

Ruohonen, J., & Ilmoniemi, R. J. (1998). Focusing and targeting of magnetic brain stimulation using multiple coils. *Med Biol Eng Comput, 36*(3), 297-301.

Sack, A. T., Cohen Kadosh, R., Schuhmann, T., Moerel, M., Walsh, V., & Goebel, R. (2009). Optimizing Functional Accuracy of TMS in Cognitive Studies: A Comparison of Methods. *Journal of Cognitive Neuroscience, 21*(2), 207-221.

Sack, A. T., & Linden, D. E. (2003). Combining transcranial magnetic stimulation and functional imaging in cognitive brain research: possibilities and limitations. *Brain Res Brain Res Rev, 43*(1), 41-56.

Sadato, N., Yonekura, Y., Waki, A., Yamada, H., & Ishii, Y. (1997). Role of the Supplementary Motor Area and the Right Premotor Cortex in the Coordination of Bimanual Finger Movements. *J. Neurosci., 17*(24), 9667-9674.

Salinas, F. S., Lancaster, J. L., & Fox, P. T. (2009). 3D modeling of the total electric field induced by transcranial magnetic stimulation using the boundary element method. *Physics in Medicine and Biology, 54*(12), 3631-3647.

Schaal, S., Sternad, D., Osu, R., & Kawato, M. (2004). Rhythmic arm movement is not discrete. *Nat Neurosci, 7*(10), 1136-1143.

Schindler, K., Nyffeler, T., Wiest, R., Hauf, M., Mathis, J., Hess, C. W., & Müri, R. (2008). Theta burst transcranial magnetic stimulation is associated with increased EEG synchronization in the stimulated relative to unstimulated cerebral hemisphere. *Neuroscience Letters, 436*(1), 31-34.

Schmahmann, J. (2010). The Role of the Cerebellum in Cognition and Emotion: Personal Reflections Since 1982 on the Dysmetria of Thought Hypothesis,

and Its Historical Evolution from Theory to Therapy. *Neuropsychology Review, 20*(3), 236-260.

Seidler, R. D., Noll, D. C., & Thiers, G. (2004). Feedforward and feedback processes in motor control. *NeuroImage, 22*(4), 1775-1783.

Semjen, A., Schulze, H. H., & Vorberg, D. (2000). Timing precision in continuation and synchronization tapping. *Psychol Res, 63*(2), 137-147.

Serrien, D. J. (2008). Coordination constraints during bimanual versus unimanual performance conditions. *Neuropsychologia, 46*(2), 419-425.

Serrien, D. J., & Brown, P. (2002). The functional role of interhemispheric synchronization in the control of bimanual timing tasks. *Exp Brain Res, 147*(2), 268-272.

Serrien, D. J., Cassidy, M. J., & Brown, P. (2003). The importance of the dominant hemisphere in the organization of bimanual movements. *Hum Brain Mapp, 18*(4), 296-305.

Serrien, D. J., Ivry, R. B., & Swinnen, S. P. (2006). Dynamics of hemispheric specialization and integration in the context of motor control. *Nat Rev Neurosci, 7*(2), 160-166.

Shehzad, Z., Kelly, A. M., Reiss, P. T., Gee, D. G., Gotimer, K., Uddin, L. Q., Lee, S. H., Margulies, D. S., Roy, A. K., Biswal, B. B., Petkova, E., Castellanos, F. X., & Milham, M. P. (2009). The resting brain: unconstrained yet reliable. *Cereb Cortex, 19*(10), 2209-2229.

Shmueli, K., van Gelderen, P., de Zwart, J. A., Horovitz, S. G., Fukunaga, M., Jansma, J. M., & Duyn, J. H. (2007). Low-frequency fluctuations in the cardiac rate as a source of variance in the resting-state fMRI BOLD signal. *Neuroimage, 38*(2), 306-320.

Smith, S. M., Miller, K. L., Salimi-Khorshidi, G., Webster, M., Beckmann, C. F., Nichols, T. E., Ramsey, J. D., & Woolrich, M. W. (2011). Network modelling methods for FMRI. *NeuroImage, 54*(2), 875-891.

Sommer, I., Ramsey, N., Kahn, R., Aleman, A., & Bouma, A. (2001). Handedness, language lateralisation and anatomical asymmetry in schizophrenia: Meta-analysis. *The British Journal of Psychiatry, 178*(4), 344-351.

Spencer, R. M., Karmarkar, U., & Ivry, R. B. (2009). Evaluating dedicated and intrinsic models of temporal encoding by varying context. *Philos Trans R Soc Lond B Biol Sci, 364*(1525), 1853-1863.

Spencer, R. M. C., Zelaznik, H. N., Diedrichsen, J., & Ivry, R. B. (2003). Disrupted timing of discontinuous but not continuous movements by cerebellar lesions. *Science, 300*(5624), 1437-1439.

Stephan, K. M., Thaut, M. H., Wunderlich, G., Schicks, W., Tian, B., Tellmann, L., Schmitz, T., Herzog, H., McIntosh, G. C., Seitz, R. J., & Homberg, V. (2002). Conscious and subconscious sensorimotor synchronization--prefrontal cortex and the influence of awareness. *Neuroimage, 15*(2), 345-352.

Stokes, M. G., Chambers, C. D., Gould, I. C., English, T., McNaught, E., McDonald, O., & Mattingley, J. B. (2007). Distance-adjusted motor threshold for transcranial magnetic stimulation. *Clinical Neurophysiology, 118*(7), 1617-1625.

Stokes, M. G., Chambers, C. D., Gould, I. C., Henderson, T. R., Janko, N. E., Allen, N. B., & Mattingley, J. B. (2005). Simple metric for scaling motor threshold based on scalp-cortex distance: application to studies using transcranial magnetic stimulation. *J Neurophysiol, 94*(6), 4520-4527.

Stoodley, C. (In press). The Cerebellum and Cognition: Evidence from Functional Imaging Studies. *The Cerebellum, DOI: 10.1007/s12311-011-0260-7*, 1-14.

Synofzik, M., Lindner, A., & Thier, P. (2008). The cerebellum updates predictions about the visual consequences of one's behavior. *Curr Biol, 18*(11), 814-818.

Tagamets, M. A., & Horwitz, B. (2001). Interpreting PET and fMRI measures of functional neural activity: the effects of synaptic inhibition on cortical activation in human imaging studies. *Brain Research Bulletin, 54*(3), 267-273.

Talairach, J., & Tournoux, P. (1988). *Co-planar stereotaxic atlas of the human brain: 3-dimensional proportional system - an approach to cerebral imaging*. New York: Thieme Medical Publishers.

Taylor, J. A., Klemfuss, N. M., & Ivry, R. B. (2010). An explicit strategy prevails when the cerebellum fails to compute movement errors. *Cerebellum, 9*(4), 580-586.

Teki, S., Grube, M., Kumar, S., & Griffiths, T. D. (2011). Distinct neural substrates of duration-based and beat-based auditory timing. *J Neurosci, 31*(10), 3805-3812.

Theoret, H., Haque, J., & Pascual-Leone, A. (2001). Increased variability of paced finger tapping accuracy following repetitive magnetic stimulation of the cerebellum in humans. *Neurosci Lett, 306*(1-2), 29-32.

Thickbroom, G. W. (2007). Transcranial magnetic stimulation and synaptic plasticity: experimental framework and human models. *Exp Brain Res, 180*(4), 583-593.

Thickbroom, G. W., Byrnes, M. L., & Mastaglia, F. L. (2003). Dual representation of the hand in the cerebellum: activation with voluntary and passive finger movement. *Neuroimage, 18*(3), 670-674.

Thielscher, A., Opitz, A., & Windhoff, M. (2011). Impact of the gyral geometry on the electric field induced by transcranial magnetic stimulation. *NeuroImage, 54*(1), 234-243.

Tofts, P. S. (1990). The distribution of induced currents in magnetic stimulation of the nervous system. *Phys Med Biol, 35*(8), 1119-1128.

Tominaga, T., Tominaga, Y., & Ichikawa, M. (2002). Optical Imaging of Long-Lasting Depolarization on Burst Stimulation in Area CA1 of Rat Hippocampal Slices. *J Neurophysiol, 88*(3), 1523-1532.

Torack, R. M., Alcala, H., Gado, M., & Burton, R. (1976). Correlative assay of computerized cranial tomography CCT, water content and specific gravity in normal and pathological postmortem brain. *Journal of Neuropathology and Experimental Neurology, 35*(4), 385-392.

Toro, R., Fox, P. T., & Paus, T. (2008). Functional coactivation map of the human brain. *Cereb Cortex, 18*(11), 2553-2559.

Torrence, C., & Compo, G. P. (1998). A Practical Guide to Wavelet Analysis. *Bulletin of the American Meteorological Society, 79*(1), 61-78.

Torriero, S., Oliveri, M., Koch, G., Lo Gerfo, E., Salerno, S., Petrosini, L., & Caltagirone, C. (2007). Cortical networks of procedural learning: evidence from cerebellar damage. *Neuropsychologia, 45*(6), 1208-1214.

Toschi, N., Welt, T., Guerrisi, M., & Keck, M. E. (2008). A reconstruction of the conductive phenomena elicited by transcranial magnetic stimulation in heterogeneous brain tissue. *Phys Med, 24*(2), 80-86.

Ueno, S., Tashiro, T., & Harada, K. (1988). Localized stimulation of neural tissue in the brain by means of a paired configuration of time-varying electric fields. *Journal of Applied Physics, 64*(10), 5862-5864.

Ullen, F., Forssberg, H., & Ehrsson, H. H. (2003). Neural networks for the coordination of the hands in time. *J Neurophysiol, 89*(2), 1126-1135.

Ulrich, R., Nitschke, J., & Rammsayer, T. (2006). Crossmodal temporal discrimination: assessing the predictions of a general pacemaker-counter model. *Percept Psychophys, 68*(7), 1140-1152.

van den Berg, F. E., Swinnen, S. P., & Wenderoth, N. (2010). Hemispheric Asymmetries of the Premotor Cortex are Task Specific as Revealed by Disruptive TMS During Bimanual Versus Unimanual Movements. *Cereb. Cortex*, bhq034.

Van Dijk, K. R. A., Hedden, T., Venkataraman, A., Evans, K. C., Lazar, S. W., & Buckner, R. L. (2010). Intrinsic Functional Connectivity As a Tool For Human Connectomics: Theory, Properties, and Optimization. *J Neurophysiol, 103*(1), 297-321.

Verstynen, T., & Ivry, R. B. (In press). Network Dynamics Mediating Ipsilateral Motor Cortex Activity during Unimanual Actions. *Journal of Cognitive Neuroscience, DOI: 10.1162/jocn.2011.21612*, 1-13.

Verstynen, T., Konkle, T., & Ivry, R. B. (2006). Two types of TMS-induced movement variability after stimulation of the primary motor cortex. *J Neurophysiol, 96*(3), 1018-1029.

Vidalaki, V. N., Ho, M. Y., Bradshaw, C. M., & Szabadi, E. (1999). Interval timing performance in temporal lobe epilepsy: differences between patients with left and right hemisphere foci. *Neuropsychologia, 37*(9), 1061-1070.

Vorberg, D., & Schulze, H.-H. (2002). Linear Phase-Correction in Synchronization: Predictions, Parameter Estimation, and Simulations. *Journal of Mathematical Psychology, 46*(1), 56-87.

Vorberg, D., & Wing, A. M. (1996). Modeling variability and dependence in timing. In H. Heuer & S. W. Keele (Eds.), *Handbook of perception and action* (Vol. 2, pp. 181-262). London: Academic Press.

Wagner, T., Gangitano, M., Romero, R., Théoret, H., Kobayashi, M., Anschel, D., Ives, J., Cuffin, N., Schomer, D., & Pascual-Leone, A. (2004a). Intracranial measurement of current densities induced by transcranial magnetic stimulation in the human brain. *Neuroscience Letters, 354*(2), 91-94.

Wagner, T., Rushmore, J., Eden, U., & Valero-Cabre, A. (2009). Biophysical foundations underlying TMS: Setting the stage for an effective use of neurostimulation in the cognitive neurosciences. *Cortex, 45*(9), 1025-1034.

Wagner, T., Zahn, M., Grodzinsky, A. J., & Pascual-Leone, A. (2004b). Three-dimensional head model simulation of transcranial magnetic stimulation. *IEEE Trans Biomed Eng, 51*(9), 1586-1598.

Walsh, R. R., Small, S. L., Chen, E. E., & Solodkin, A. (2008). Network activation during bimanual movements in humans. *Neuroimage, 43*(3), 540-553.

Walsh, V., & Cowey, A. (2000). Transcranial magnetic stimulation and cognitive neuroscience. *Nature Reviews Neuroscience, 1*(1), 73-80.

Warm, J., Stutz, R., & Vassolo, P. (1975). Intermodal transfer in temporal discrimination. *Attention, Perception, & Psychophysics, 18*(4), 281-286.

Wassermann, E. M. (1998). Risk and safety of repetitive transcranial magnetic stimulation: report and suggested guidelines from the International Workshop on the Safety of Repetitive Transcranial Magnetic Stimulation, June 5-7, 1996. *Electroencephalogr Clin Neurophysiol, 108*(1), 1-16.

Wassermann, E. M., Wang, B., Zeffiro, T. A., Sadato, N., Pascual-Leone, A., Toro, C., & Hallett, M. (1996). Locating the Motor Cortex on the MRI with Transcranial Magnetic Stimulation and PET. *NeuroImage, 3*(1), 1-9.

Wiener, M., Turkeltaub, P., & Coslett, H. B. (2010). The image of time: A voxel-wise meta-analysis. *NeuroImage, 49*(2), 1728-1740.

Wimpory, D., Nicholas, B., & Nash, S. (2002). Social timing, clock genes and autism: a new hypothesis. *Journal of Intellectual Disability Research, 46*(4), 352-358.

Wing, A. M., & Kirstofferson, A. B. (1973). Response delays and the timing of discrete motor responses. *Perception and psychophysics, 14*, 5-12.

Wolf, S. L., Butler, A. J., Campana, G. I., Parris, T. A., Struys, D. M., Weinstein, S. R., & Weiss, P. (2004). Intra-subject reliability of parameters contributing to maps generated by transcranial magnetic stimulation in able-bodied adults. *Clinical neurophysiology : official journal of the International Federation of Clinical Neurophysiology, 115*(8), 1740-1747.

Worsley, K. J., Marrett, S., Neelin, P., Vandal, A. C., Friston, K. J., & Evans, A. C. (1996). A unified statistical approach for determining significant signals in images of cerebral activation. *Human Brain Mapping, 4*(1), 58-73.

Zafar, N., Paulus, W., & Sommer, M. (2008). Comparative assessment of best conventional with best theta burst repetitive transcranial magnetic stimulation protocols on human motor cortex excitability. *Clinical Neurophysiology, 119*(6), 1393-1399.

Zhan, Y., Halliday, D., Jiang, P., Liu, X., & Feng, J. (2006). Detecting time-dependent coherence between non-stationary electrophysiological signals--a combined statistical and time-frequency approach. *J Neurosci Methods, 156*(1-2), 322-332.

12 Appendices

12.1 Copyright permission

MIT Press Journals
55 Hayward Street
Cambridge, MA 02142-1315

Permissions Invoice

Date: 4/19/2011 JRNL- 24871

Sold to: Janine Bijsterbosch
University of Sheffield
Academic Clinical Psychiatry, The Longley Centre, Norwood Grange Drive
S5 7JT

FAX: 44 114 226 1522

Your Ref.
The following article to be reprinted in a PhD thesis "Behavioural and Neural Correlates of Sensorimotor Timing and Error Correction", published by the University of Sheffield in July 2011, authored by Janine D. Bijsterbosch. Permission granted for republication of article in print and electronic formats, standard fees waived for author's use of own article.

Thank you for your request for permission to reprint the following material:

Janine D. Bijsterbosch, Kwang-Hyuk Lee, Michael D. Hunter, Daniel T. Tsoi, Sudheer Lankappa, Iain D. Wilkinson, Anthony T. Barker and Peter W. R. Woodruff, 'The Role of the Cerebellum in Sub- and Supraliminal Error Correction during Sensorimotor Synchronization: Evidence from fMRI and TMS', Journal of Cognitive Neuroscience, 23:5 (May, 2011), pp. 1100-1112. © 2011 by the Massachusetts	$0.00

Prices are USD on date of invoice. In Canada, please add 6% GST

Total amount due: $0.00

Make check payable to ***MIT Press Journals***. Checks can only be drawn on a **U.S Bank in U.S. funds**. Credit card payments by **MC**, **VISA** or **AMEX** are also accepted (please refer to secure fax number below.) For all payments, enclose invoice copy or clear reference to JRNL-Number (found in upper right corner) with your payment. Failure to do so may result in payment being returned. More information at: http://www.mitpressjournals.org/page/howtopay/journal/invoices.

Reprinting/Republication Fees: **$30 per article page / $75 per figure/illustration**

Permission is granted to use the material described above, subject to the conditions stated below:

1. Acknowledgment is required to author, journal and publisher. Correct copyright information must be displayed on all copies made.
2. All rights granted herein are non-exclusive world rights for one edition in the format(s) specified above and specifically does not cover: digest or abridgment of the material, any reproduction/distribution in any format other than what is indicated above, nor any subsidiary rights.
3. This permission does not allow translation of the quoted material into languages other than English, unless stated above.
4. This permission does not cover any material which is credited to another source or third party material otherwise copyrighted. If an original source is credited anywhere in the material, this permission is contingent upon obtaining permission from that source. It is the customer's responsibility to check and confirm copyright ownership.
5. This permission is extended to cover publication or transcription in Braille, large-type editions or recordings for the blind (and other special editions for use by visually and/or learning impaired persons) by approved nonprofit organizations
6. Payment of the fee is due upon publication of your work or six months from the date of this invoice, whichever is earlier. Failure to remit within this time period will automatically void this permission.

Signed: Christina Ellas

Christina Ellas
Permissions & Subsidiary Rights Manager
MIT Press Journals

MIT Federal ID # 04-2103594
Phone Number: 617-258-0591
FAX Number: 617-253-1709
Secure Fax for CC payment: 617-258-5028

12.2 Publication: Journal of Cognitive Neuroscience (2011), 23 (5), 1100-12

The Role of the Cerebellum in Sub- and Supraliminal Error Correction during Sensorimotor Synchronization: Evidence from fMRI and TMS

Janine D. Bijsterbosch[1], Kwang-Hyuk Lee[1], Michael D. Hunter[1], Daniel T. Tsoi[1], Sudheer Lankappa[1], Iain D. Wilkinson[1], Anthony T. Barker[2], and Peter W. R. Woodruff[1]

Abstract

■ Our ability to interact physically with objects in the external world critically depends on temporal coupling between perception and movement (sensorimotor timing) and swift behavioral adjustment to changes in the environment (error correction). In this study, we investigated the neural correlates of the correction of subliminal and supraliminal phase shifts during a sensorimotor synchronization task. In particular, we focused on the role of the cerebellum because this structure has been shown to play a role in both motor timing and error correction. Experiment 1 used fMRI to show that the right cerebellar dentate nucleus and primary motor and sensory cortices were activated during regular timing and during the correction of subliminal errors. The correction of supraliminal phase shifts led to additional activations in the left cerebellum and right inferior parietal and frontal areas. Furthermore, a psychophysiological interaction analysis revealed that supraliminal error correction was associated with enhanced connectivity of the left cerebellum with frontal, auditory, and sensory cortices and with the right cerebellum. Experiment 2 showed that suppression of the left but not the right cerebellum with theta burst TMS significantly affected supraliminal error correction. These findings provide evidence that the left lateral cerebellum is essential for supraliminal error correction during sensorimotor synchronization. ■

INTRODUCTION

Accurate sensorimotor timing and rapid error correction in response to a sensorimotor mismatch are essential in many everyday tasks. Sensorimotor timing requires the temporal coupling of motor output to sensory stimuli, whereas error correction refers to adaptive movement adjustments in response to changes in the sensory stimulus. Sensorimotor synchronization (SMS) is a simple task that can be used to study both timing and error correction. In SMS, subjects tap their finger in synchrony with a repetitive isochronous auditory or visual stimulus sequence. Previous research has shown that subjects have a tendency to tap on average 20 to 80 msec before the onset of the predicted stimulus when auditory pacing is used, demonstrating an anticipatory negative mean asynchrony (Aschersleben, 2002). The size of the negative asynchrony is influenced by the modality of the pacing stimulus and is smaller when visual pacing stimuli are used (Kolers & Brewster, 1985). Error correction is required to sustain a consistent tap–tone relationship even when the pacing stimulus is regular because of inherent variability in the motor response (Repp, 2005). Such error correction mechanisms can be explicitly studied using a pacing sequence containing occasional local timing perturbations such as phase shifts. After such perturbations, subjects show a rapid behavioral adjustment and return to their baseline negative mean asynchrony within several taps (Repp, 2002b).

At present, it is not fully understood how the processing of errors is influenced by conscious perception of the phase shifts. Two different error correction processes have been suggested. Phase correction appears to be a largely automatic response to minor local perturbations, whereas period correction involves resetting the period of a hypothetical internal timekeeper mechanism and may be subject to conscious control (Repp & Keller, 2004; Repp, 2001b). The correction of phase shifts may rely mainly on automatic phase correction and may not be aided by conscious perception of the perturbation (Repp, 2005). However, when subjects intend not to react to perturbations, phase correction can be partially suppressed and period correction can be suppressed completely (Repp, 2002a, 2002b). This may suggest that conscious perception of the phase shift allows modulation of the error correction response.

Activation in the left sensory-motor cortex and right cerebellum is consistently reported during regular right-handed synchronization tapping in neuroimaging studies (Jäncke, Loose, Lutz, Specht, & Shah, 2000; Lutz, Specht, Shah, &

[1]University of Sheffield, United Kingdom, [2]Royal Hallamshire Hospital, Sheffield, United Kingdom

Jäncke, 2000; Rao et al., 1997). Activation of the premotor region and inferior parietal cortices was reported in one study (Jäncke et al., 2000), but not in others. The neural correlate of error correction was investigated in two previous studies in the context of an SMS task. Lutz et al. (2000) found activations in the sensory motor cortex, SMA, and right cerebellum when comparing visually paced irregular to regular SMS performed with the right hand. Another study used positron emission tomography to demonstrate activations in frontal, parietal, BG, and cerebellar regions during the correction of predictable supraliminal shifts in a unimanual right-handed SMS task (Stephan et al., 2002). Although previous research on both regular SMS and error correction has consistently implicated involvement of the cerebellum, the exact role of the cerebellum during the correction of sub- and supraliminal perturbations in an SMS task is largely unknown.

This study adopts two complementary techniques to investigate the neural correlates of error correction of perceivable and unperceivable perturbations in the context of SMS. Of particular interest is the role of the cerebellum, as this structure is consistently activated during regular SMS (Jäncke et al., 2000; Lutz et al., 2000; Rao et al., 1997) and was also implicated in error correction (Pollok, Gross, Kamp, & Schnitzler, 2008; Stephan et al., 2002; Lutz et al., 2000). In Experiment 1, fMRI is used to investigate the neural correlates of regular SMS and error correction of sub- and supraliminal phase shifts. Effective connectivity of the cerebellum during timing and error correction is explored using a psychophysiological interaction (PPI) analysis. In Experiment 2, the causal role of the cerebellum during sub- and supraliminal error correction is examined using theta burst transcranial magnetic stimulation (TBS) (Huang, Edwards, Rounis, Bhatia, & Rothwell, 2005).

EXPERIMENT 1—fMRI

The aim of Experiment 1 was to examine the neural correlates of SMS and of the correction of unexpected subliminal and supraliminal phase shifts during SMS using fMRI. The involvement of the cerebellum was of particular interest because this structure has been associated with both timing and error correction. To investigate the contribution of the cerebellum further, we used a PPI analysis to examine changes in effective connectivity within a cerebello-cortical network during regular timing and error correction. We hypothesized that (a) the cerebellum is active during regular timing and during error correction and (b) parietal and frontal cortices are involved in the correction of supraliminal errors.

Methods

Subjects

Sixteen healthy subjects (8 men, mean age ± *SD* = 25 ± 5 years) took part in the study. All subjects were right-handed (mean Edinburgh Handedness Inventory score of 59, range = 30–90). The subjects were naive to the experimental task, and none of them was a professional musician. The subjects had no history of psychiatric or neurological disorders.

Stimuli and Task Conditions

Subjects performed an auditory-paced SMS task inside the fMRI scanner. The pacing stimulus was a simple auditory sequence consisting of metronome tones at a frequency of 500 Hz and duration of 50 msec presented through MRI-compatible headphones. Subjects were asked to press a button using their right index finger in synchrony with the auditory stimulus, aiming for their button presses to coincide with each tone. The task consisted of three conditions: a regular condition and two irregular conditions containing perturbations of 3% (subliminal) and 15% (supraliminal) of the sequence interonset interval (IOI). In the regular condition, the pacing stimulus was isochronous with an IOI of 600 msec. In the two irregular conditions, perturbation events were introduced that shifted a single stimulus interval by 3% or 15% (18 or 90 msec, respectively) in either direction with respect to the expected time of occurrence, constituting negative and positive phase shifts. In a box-car design, a resting block (15 sec) and a tapping block (45 sec) were alternated nine times, and a further 15-sec resting block was added at the end of the final tapping block, resulting in 9 min and 15 sec total scanning time. Each tapping condition (regular, subliminal, and supraliminal) lasted for 45 sec (75 stimuli) and was repeated three times. In each of the irregular blocks, a total number of eight perturbations (four negative and four positive) of equal magnitude were introduced. Because each condition was repeated three times (in separate blocks), this resulted in 12 events for all four possible perturbations (positive and negative for subliminal and supraliminal shifts). At least seven regular stimuli occurred between two subsequent perturbations to allow subjects to reestablish synchronization before each shift. To achieve the sequences, we repeated a fixed epoch ($T - 3$ to $T + 3$ in which the shift occurs at time T) eight times, and 0, 1, or 2 tones at the standard IOI were introduced between two subsequent epochs. The order of positive and negative shifts was randomized. As such, the position of the perturbations in the sequence was semirandom, and subjects were not able to anticipate the occurrence of the next shift. To allow the subjects to focus on the synchronization task, they were not asked to report whether they were aware of perturbations. However, a previous study showed that detection of perturbations of 4% of the IOI (of 500 msec) was approximately equal to chance, whereas 90 msec shifts (18% of IOI) were detected more than 90% of the time (Repp, 2002a). Stimuli were controlled using Presentation software (version 12.8, www.neurobs.com), and behavioral responses were measured with an MRI compatible button box.

Functional Magnetic Resonance Imaging

Functional imaging data sets were acquired using a 3-T scanner (Achieva 3.0T; Philips Medical Systems, Best, The Netherlands) at the University of Sheffield. A single-shot, gradient-recalled, echo-planar technique was used to acquire 23 × 6 mm contiguous transverse slices at 370 time points (repetition time = 1500 msec, echo time = 35 msec, in-plane resolution = 1.8 × 1.8 mm, sense factor = 1.5). A standard receive-only six-channel head coil was used, and subject-specific, localized shimming was performed. Subjects viewed a projected black screen with a white fixation cross in the center through a mirror in the head coil throughout the experiment. Subjects were told that the sounds would start and asked to start tapping in synchrony with the tones as soon as it started.

Behavioral Data Analysis

From each of the nine experimental blocks, the first 10 taps were discarded to allow the subject to establish tapping synchrony. In the regular SMS condition, measures of timing performance include the mean and standard deviation of tap–tone asynchrony and of interresponse interval (IRI). These were calculated over the three regular blocks and represent the timing performance for all subjects. Subsequently, error correction data from the irregular blocks were analyzed in an event-related approach including four taps before and four taps after ($T - 4$ to $T + 4$) each shifted stimulus (T). Within each subject, outlier responses (tap–tone asynchronies more than two standard deviations away from the average asynchrony) were identified separately for each position ($T - 4$ to $T + 4$) and were removed prior to averaging. To allow a direct comparison of the error correction response in all conditions, we normalized the asynchrony during T to $T + 4$ to range from baseline asynchrony to the maximum initial shift at time T, and the sign was removed (Figure 1). Baseline performance was defined as the average tap–tone asynchrony over trials $T - 4$ to $T - 1$ (Praamstra, Turgeon, Hesse, Wing, & Perryer, 2003; Repp, 2000). The resulting normalized error correction data were averaged over all trials. If the averaged normalized error correction scores represented extreme values (more than three times the interquartile range away from the group median) at three or four positions (in $T + 1$ to $T + 4$) for a single subject, these data were replaced by the group average of the value. This led to the replacement of data from two subjects in the negative subliminal condition and data from one subject from the positive subliminal condition.

To investigate the natural occurrence of error correction (i.e., after spontaneous motor variability in the absence of perturbations in the sequence), we performed a

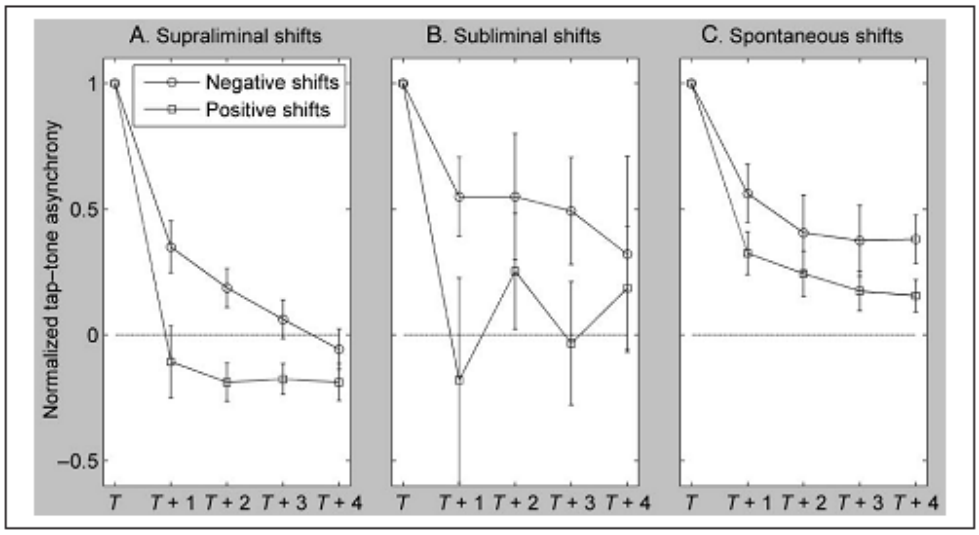

Figure 1. Normalized error correction response as a function of stimulus position after induced subliminal (A) and supraliminal (B) perturbations and spontaneous motor variability (C) in Experiment 1. Error correction of positive shifts is faster compared with negative error correction. Error correction after spontaneous large deviation from the average tap–tone asynchrony does occur, but baseline asynchrony is not achieved within four taps. Tap–tone asynchronies are shown for the time of the perturbation (T) and four subsequent taps ($T + 1 - T + 4$). The data are normalized to range from baseline asynchrony (0, dashed line) to the magnitude of the initial shift at time (T), and the sign is removed. Baseline performance is defined as the subject mean tap–tone asynchrony during $T - 4$ to $T - 1$. Spontaneous shifts are defined as deviations from the subject mean asynchrony greater than 50 msec during the standard blocks. In negative shifts (circles), the tone occurs earlier than expected, and in positive shifts (squares), the tone occurs later than expected. Error bars express a standard error.

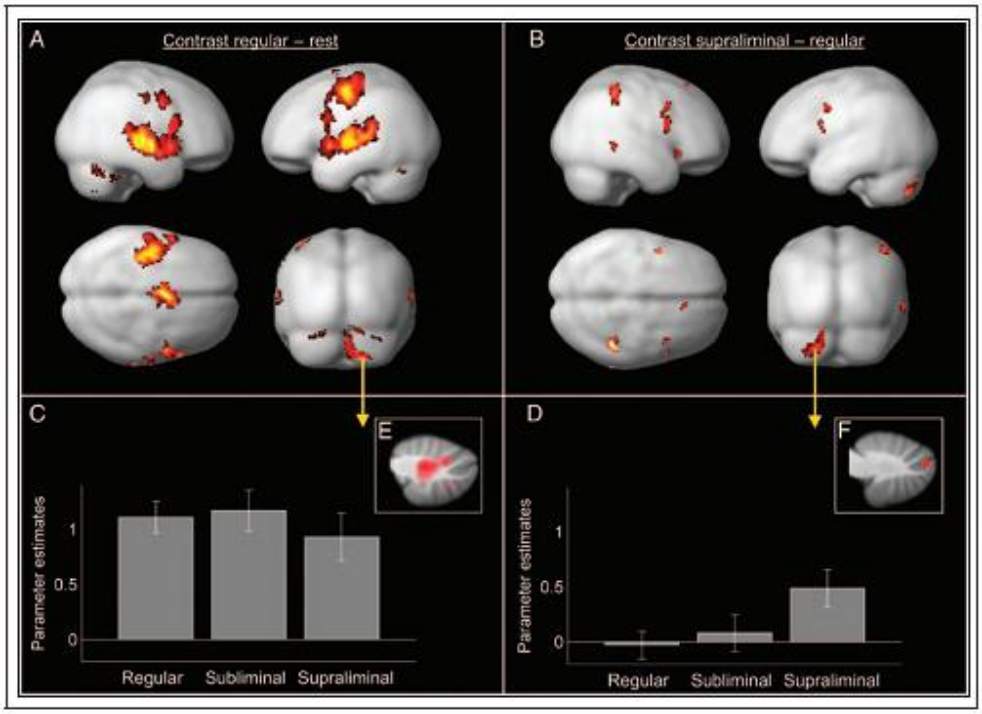

Figure 2. Functional imaging contrasts between regular tapping and rest (A) and between the supraliminal and the regular conditions (B) and associated parameter estimates (C and D) in peak cerebellar foci (E and F). fMRI activations are rendered on a normalized smooth brain surface showing (clockwise starting at the upper left corner): a sagittal view from the right and left, an axial view from the top, and a coronal view from the back. Findings are significant at $p < .001$ uncorrected and exceed a cluster-extent threshold of 20 voxels. Plots C and D show parameter estimates for the three active conditions compared with rest in two regions of peak activation in the right dentate nucleus [20 −52 −28] and left posterior cerebellar cortex [−20 −80 −44]. Error bars indicate the 90% confidence interval. In-plot figures E and F show the same fMRI activations on a sagittal slice through the cerebellum to illustrate the differential position of activation foci in the deep nuclei (right dentate nucleus) and in the cortex (left posterior cerebellar cortex). Figures E and F were created with the SUIT toolbox in SPM5 (Diedrichsen, 2006).

data-driven analysis using only data from regular blocks. For each subject, the data were searched for instances (minimally five taps apart), where the asynchrony deviated from the subject's mean asynchrony by more than 50 msec. All subjects showed such spontaneous deviations; on average, 13 shifts ($SD = 5$, range = 7–21) occurred during the three regular blocks (5 in the positive direction and 8 negative). These data were analyzed in the same way as for externally induced error correction events (see above) to show the correction response to spontaneous errors (Figure 1C).

Imaging Data: Cognitive Subtraction

The imaging data were analyzed using SPM5 (http://www.fil.ion.ucl.ac.uk/spm). Motion correction was performed by realigning the images to the central image with a six-parameter (rigid body) spatial transformation. Further preprocessing stages involved normalization into standard space and smoothing using Gaussian kernels of 5-mm FWHM. On an individual level, statistical analysis was based on the general linear model using the boxcar design convolved with a canonical hemodynamic response function, creating contrast images for all conditions. Thereafter, a one-sample t test was performed to obtain second-level group results (Figure 2A and B). Subsequently, parameter estimates were derived from single-voxel locations to allow closer investigation of activation patterns in several ROIs. These locations were experimentally informed Montreal Neurological Institute coordinates resulting from local maxima in second-level functional contrasts (regular–rest for right cerebellar ROI and supraliminal–regular for left cerebellar ROI). Figure 2C and D shows parameter estimates for the contrasts between all active conditions (regular, subliminal, and supraliminal) and rest.

To further investigate the lateralization of cerebellar activation, we performed a laterality analysis. Parameter estimates were extracted for a 5-mm sphere centered on the left cerebellar ROI [−20 −80 −44] and on the mirrored right cerebellar region [20 −80 −44]. A paired *t* test was performed to analyze whether there was a statistically significant difference between the parameter estimates indicating a lateralization of activation.

Imaging Data: Normalization to Cerebellar Template

Individual subject contrast images resulting from first-level general linear model analysis were normalized to a spatially unbiased template of the human cerebellum with the use of the SUIT toolbox in SPM5 (Diedrichsen, 2006). In each subject, the cerebellum and the brainstem were isolated on the basis of a segmentation algorithm, and functional images were normalized to the SUIT template using nonlinear deformation. The subsequent cerebellar contrast images were smoothed and entered into a second-level one-sample *t* test producing group results to create Figure 2E and F.

Imaging Data: PPI Analysis

To further investigate the role of the cerebellum during supraliminal error correction, we performed a PPI analysis (Friston et al., 1997) using SPM5. For each subject, a left cerebellar seed ROI was identified by locating the suprathreshold voxel nearest to the group ROI (left cerebellar local maxima in supraliminal–regular contrast [−20 −80 −44]). A suitable ROI in the left posterior cerebellar cortex was located from the first-level contrast (supraliminal–regular) for all subjects. The zero-mean corrected first principle component was extracted from all voxels in a radius (5 mm) centered on the subject-specific ROI to form the physiological time course. The PPI term was produced by convolving the physiological time series with a psychological vector that described the paradigm (1 for the supraliminal condition, −1 for regular tapping). The interaction term was entered at the first level as the effect of interest, and the psychological and the physiological time series were entered as effects of no interest. Subject-specific interaction contrasts were entered into a second-level one-sample *t* test to achieve group results (Figure 3). The identical PPI analysis was also performed with a seed ROI in the right cerebellum. Here, subject-specific physiological time series were extracted from a radius centered on the nearest suprathreshold voxel to the group ROI [4 −68 −16] in the regular–rest contrast.

Results and Discussion

During regular blocks, taps preceded the tones by an average of 53 msec, demonstrating an anticipatory negative mean asynchrony. The standard deviation was 45 msec as calculated by averaging the within-block *SD* over three regular blocks and over all subjects. The average IRI was 600 msec (group-averaged within-block *SD* = 45 msec). In the subliminal condition, the average tap–tone asynchrony was 65 msec (group-averaged within-block *SD* = 43 msec), and the IRI was 600 msec (group-averaged within-block *SD* = 37 msec). During supraliminal blocks, the average tap–tone asynchrony was 53 msec (group-averaged within-block *SD* = 56 msec) and the average IRI was 599 msec (group-averaged within-block *SD* = 50 msec).

PPI left cerebellum [−20 −80 −44]	Left	Right
Cerebellum		24 −70 −50 (3.76; 21)
Temporal cortex (BA 21, 22)	−50 −46 8 (3.75; 60) −52 4 10 (3.65; 39)	
Somatosensory cortex (BA 1,2,3)	−54 −16 28 (3.99; 40)	
Inferior frontal cortex (BA 45)		46 20 20 (4.34; 26)

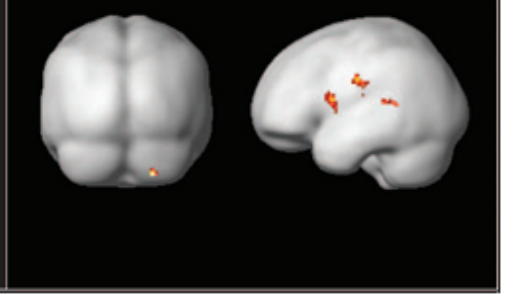

Figure 3. PPI analysis results with a seed ROI in the left cerebellum [−20 −80 −44]. In the table, Montreal Neurological Institute coordinates of local maxima are provided (*x y z*, in millimeters), and values in parentheses provide corresponding *Z* scores and cluster sizes (voxels). Areas that display enhanced effective connectivity with the left cerebellum during the supraliminal condition compared with regular SMS are shown on a normalized smooth brain surface showing a coronal view from the back (left) and a sagittal view from the left (right). Findings are significant at $p < .001$ uncorrected and exceed a cluster-extent threshold of 20 voxels.

Event-related error correction analysis revealed a behavioral error correction response in all four possible phase shifts (Figure 1). The average number of outlier responses removed was 3.4 (SD = 2) of 108 responses. There was no difference in the number of outlier responses removed from the analysis between the conditions ($p > .2$). A three-way repeated measures ANOVA on the normalized relative asynchrony with factors direction (positive or negative), size (subliminal or supraliminal), and position ($T + 1$ to $T + 4$) indicated a significant main effect of direction, $F(1, 15) = 5.59$, $p = .032$, such that the correction of negative shifts was less efficient than of positive shifts. Furthermore, there was a main effect of size, $F(1, 15) = 8.20$, $p = .012$, in which baseline performance was achieved faster after the correction of supraliminal errors compared with subliminal error correction. The main effect of position did not reach significance ($p > .5$), and none of the interactions were significant ($p > .1$).

Subliminal phase shifts (18 msec) fall within the range of tapping variability (SD = 46 msec) as opposed to supraliminal shifts (90 msec). In view of this, we analyzed the behavioral response after extreme cases of motor variability (deviations from the mean asynchrony greater than 50 msec) and compared this with the error correction response to phase shifts introduced in the pacing stimulus (Figure 1C). Error correction after spontaneous motor variability is apparent, but baseline asynchrony is not achieved within the four taps after the deviation. Hence, it may well be that this form of "error correction" after spontaneous motor variability is better interpreted as a general regression to the mean asynchrony.

Functional imaging data from all three experimental conditions were contrasted with baseline rest, and the subliminal and supraliminal error correction conditions were contrasted with regular SMS. Compared with baseline rest, the regular condition showed activations in the right premotor cortex, left primary motor cortex, bilateral primary auditory cortices, and right cerebellum extending to vermis (Figure 2A, Table 1). The subliminal condition compared with regular SMS did not produce any significant activations. The contrast between the supraliminal and the regular conditions revealed that bilateral frontal cortices, right inferior parietal cortex, and left cerebellum were significantly activated during the supraliminal condition (Figure 2B, Table 1). To investigate whether subliminal error correction may lead to less activity in the same circuitry, we lowered the significance threshold of the comparison between subliminal correction and regular tapping ($p < .01$ uncorrected). Lowering the threshold resulted in scattered activity that was not consistent with the contrast between supraliminal and regular tapping. In summary, the right cerebellum is active in all three conditions compared with rest, whereas the left cerebellum is only engaged in the condition including perceivable shifts.

A laterality analysis was performed to compare activation in the left cerebellar local maximum with the mirrored right cerebellar region in the contrast between the supraliminal and the regular conditions. Results of the laterality analysis confirm that the cerebellar activation during the supraliminal conditions was significantly left lateralized, $t(1, 15) = 4.47$, $p < .001$. The lateralization of cerebellar activation is also confirmed by the parameter estimates for the two local maxima in the left and right cerebellar hemispheres (Figure 2C and D). Furthermore, when the subtraction results are normalized to a template confined to the cerebellum, a dissociation in activation foci is highlighted: Activation in the right cerebellum is mainly located in the dentate nucleus, whereas activity on the left-hand side is confined to the cortex (crus I, Figure 2E and F).

Functional imaging data were further analyzed in a PPI analysis using a seed ROI in the left cerebellum. Group results are summarized in Figure 3. The PPI analysis identifies brain areas that exhibit enhanced connectivity with the left cerebellum during the condition that included supraliminal perturbations compared with regular tapping. Significantly enhanced connectivity with the left cerebellum was observed in the frontal, auditory, and sensory cortices and in the right cerebellum. The same PPI analysis was also performed using a seed ROI in the right cerebellum. Results show no change in effective connectivity of the right cerebellum during supraliminal tapping compared with regular SMS.

In summary, we found involvement of the cerebellar vermis and right cerebellar dentate in all active conditions compared with rest. The left lateral cerebellar cortex was activated only during the condition that required supraliminal error correction. Furthermore, the left cerebellum exhibited enhanced functional connectivity with a cerebello-cortical network during supraliminal error correction compared with regular timing. These findings suggest that the left cerebellum may play an essential role during supraliminal error correction.

EXPERIMENT 2—TBS

Results from Experiment 1 indicated that the left cerebellum is involved only during the correction of supraliminal phase shifts. In Experiment 2, we investigated the effect of TBS over the medial, left lateral, and right lateral cerebellum on error correction performance. On the basis of Experiment 1, we hypothesized that suppression of the left cerebellum would impair supraliminal error correction, whereas suppression of the medial or right cerebellum would not affect error correction performance.

Methods

Subjects

Forty right-handed healthy subjects (mean age ± SD = 23 ± 5 years) took part in the study. They were students from the University of Sheffield. All were randomly assigned to one of four experimental groups: (1) medial

Table 1. Statistical Contrasts between Regular, Subliminal, and Supraliminal Conditions and Rest and between the Supraliminal and the Regular Conditions

	Regular–Rest (Figure 2A)		*Subliminal–Rest*		*Supraliminal–Rest*		*Supraliminal–Regular (Figure 2B)*	
	Left	*Right*	*Left*	*Right*	*Left*	*Right*	*Left*	*Right*
Cerebellum	−24 −66 −26 (5.23; 292)	4 −68 −16* (6.07; 2157)	−24 −62 −26 (4.23; 61)	4 −66 −22 (4.86; 1424)	−18 −72 −32 (5.29; 798)	12 −52 −22 (5.42; 1946)	−20 −80 −44* (4.46; 161)	
				36 −58 −36 (4.58; 25)		0 −56 −2 (4.16; 21)		
				12 −66 −50 (4.10; 118)				
Temporal cortex	−54 −20 0 (5.63; 4871)	60 −18 −2 (5.94; 2381)	−48 −22 2 (5.55; 1576)	62 −18 −4 (5.65; 522)	−52 −20 0 (5.58; 6229)	64 −16 −2 (6.03; 3440)		34 18 −10 (4.21; 25)
			−34 −64 8 (3.69; 22)	46 0 −4 (3.95; 59)				66 −42 0 (3.53; 23)
			−58 8 4 (3.51; 25)	42 −16 −20 (4.30; 29)				
Motor cortex	−48 −8 54 (5.41;[a])		−44 −14 52 (5.04; 1057)		−42 −6 54 (4.71;[a])			
Parietal cortex					−44 −40 46 (4.80; 392)	42 −38 38 (4.60; 282)		50 −40 54 (4.34; 247)
Frontal cortex				54 4 44 (4.17; 121)		34 20 −6 (5.29; 1766)	−48 4 40 (4.54; 34)	42 8 34 (4.23; 45)
							−48 10 22 (3.43; 26)	6 30 58 (3.86; 22)
								52 10 16 (3.63; 68)
Premotor cortex/ SMA (BA 6)	−4 −4 54 (5.16; 837)	54 0 40 (4.32; 169)	−4 −6 56 (4.01; 90)			12 4 64 (4.39; 798)		
		62 −14 44 (4.58; 35)						
Thalamus	−16 −22 −2 (4.23; 104)	22 8 −16 (4.35; 390)	−14 −24 −2 (4.12; 43)					
BG		32 18 6 (3.57; 42)	−26 2 −8 (5.09; 385)	20 4 8 (3.89; 121)				

Montreal Neurological Institute coordinates of local maxima are provided (*x y z*, in millimeters) for all clusters that were significant at $p < .001$ uncorrected and exceed a cluster-extent threshold of 20 voxels. Values in parentheses provide corresponding *Z* scores and cluster sizes (voxels). Voxel locations marked with an asterisk (*) are used as seed ROIs in the PPI analysis. BA = Brodmann's area.

[a]Motor cortex local maxima included in left temporal cortex clusters.

cerebellar TBS, (2) left cerebellar TBS, (3) right cerebellar TBS, and (4) sham TBS. The groups were matched for age (mean age ± *SD*: Group 1 = 22 ± 6 years, Group 2 = 22 ± 2 years, Group 3 = 24 ± 6 years, and Group 4 = 24 ± 6 years) and sex (six men and four women in each group).

Stimuli and Task Conditions

All subjects performed an identical auditory-paced SMS task before and after TBS. As in Experiment 1, four different perturbations (subliminal: 3%, 18 msec and supraliminal: 15%, 90 msec in both positive and negative direction) were introduced into an otherwise regular auditory pacing sequence consisting of metronome tones presented at an IOI of 600 msec (frequency of 500 Hz and duration of 50 msec). The occurrence of sub- and supraliminal perturbations was intermixed within blocks to further avoid anticipation effects. After an initial 30-sec practice block, subjects performed a total of three 5-min SMS blocks with period of rest in between. At the beginning of each 5-min block, 10 regular tones were presented to allow subjects to synchronize their tapping to the regular pacing stimulus, and these data are excluded from all further analysis. After the initial 10 tones, a fixed epoch ($T - 4$ to $T + 4$ in which the shift occurs at time T) was repeated eight times for each of four different shifts in pseudorandomized order. Between two subsequent epochs, two to six stimuli at the standard IOI were introduced to avoid predictability of the next perturbation. Hence, over the three 5-min blocks, a total of 24 event-related error correction responses were obtained for each of the four shift conditions. Data analysis was identical to that of Experiment 1 and was based on an event-related approach including four taps before and four taps after ($T - 4$ to $T + 4$) each shifted stimulus (T). As with Experiment 1, if average normalized error correction scores represented extreme values (more than three times the interquartile range away from the group median) at three or four positions (in $T + 1$ to $T + 4$) for a single subject, these data were replaced by the group average of the value calculated within the relevant cerebellar TBS group. This led to the replacement of data from two subjects in the pre-TBS positive subliminal condition.

TBS Protocol

After completion of the full SMS task, the TBS procedure was explained to the subjects in detail, and any questions were answered. Subsequently, the resting motor threshold of each subject was determined using the thumb movement visualization method (Pridmore, Fernandes Filho, Nahas, Liberatos, & George, 1998). Each subject then received 40 sec of continuous TBS (Huang et al., 2005). A total of 600 pulses were applied at 80% of the resting motor threshold using a 70-mm figure-of-eight coil and a Magstim Super Rapid stimulator (Magstim Company, Whitland, UK). The target TBS locations were (1) the medial cerebellum (1 cm below inion), (2) the left lateral cerebellum (1 cm below inion and 3 cm left of midline), (3) the right lateral cerebellum (1 cm below inion and 3 cm right of midline), or (4) the sham TBS (1 cm below inion) (Lee et al., 2007; Theoret, Haque, & Pascual-Leone, 2001). The coil was positioned vertically with the handle pointing upward (Lee et al., 2007). For sham TBS, the coil was held at 90° angle to the scalp over the medial cerebellum. During and after TBS, none of our subjects reported any adverse effects.

Results and Discussion

To assess whether there were any differences in error correction performance between the four different TBS groups before stimulation, we performed a multivariate general linear model with a fixed factor for the TBS group and within-subject factors for direction (positive and negative), size (subliminal and supraliminal), and position ($T + 1$ to $T + 4$). The results indicate a trend-level effect of TBS group on pre-TBS performance ($p = .073$, Figure 4). Closer investigation of individual subject performance showed that the difference in pre-TBS performance was explained by two outlier subjects (one subject from the left and one from the medial cerebellar TBS groups). There was no significant difference in pre-TBS performance when data from these two subjects were removed ($p > .1$). Because the removal of these subjects did not affect the significance of the TBS findings, data from all subjects were included in the results presented below.

To compare error correction performance before and after TBS of the cerebellum, we performed a repeated measures ANOVA with within subject factors for TBS (before and after stimulation), direction (positive and negative), and position ($T + 1$ tot $T + 4$) separately for the subliminal and supraliminal conditions on normalized error correction values for each group. In the left cerebellar TBS group, results indicate a trend-level main effect of TBS, $F(1, 9) = 4.84$, $p = .055$, and a significant TBS by position interaction, $F(3, 27) = 3.31$, $p = .035$. Post hoc analysis indicated that there was a significant effect of left cerebellar TBS at $T + 1$ ($p = .013$) but not at $T + 2$ to $T + 4$ ($p > .09$). At $T + 1$, the average normalized error correction value increased from −0.13 to 0.09 (Figure 4B). Left cerebellar TBS did not affect subliminal error correction performance ($p > .2$). By contrast, suppression of the right cerebellum did not change error correction of sub- or supraliminal phase shifts (Figure 4C). In the medial cerebellar TBS group, there was a trend-level TBS by direction interaction, $F(1, 9) = 3.75$, $p = .085$. Post hoc analysis showed a trend-level difference between performance before and after TBS during positive supraliminal error correction ($p = .09$) but not during negative supraliminal error correction ($p > .3$, Figure 4A). Further investigation showed a significant effect

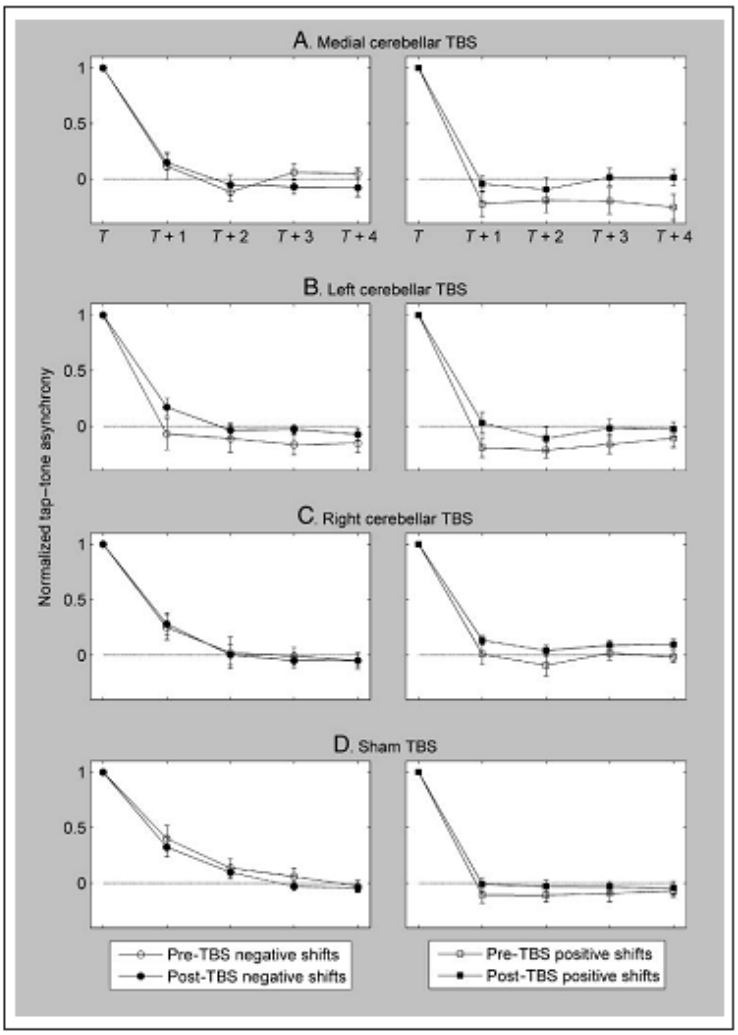

Figure 4. Normalized error correction response as a function of stimulus position before and after suppression of the medial (A), left (B), and right (C) cerebellum with theta burst TMS and after sham TBS (D). Suppression of the medial cerebellum (A) only affected the correction of positive (right) supraliminal phase shifts. Suppression of the left cerebellum (B) affected supraliminal error correction of positive and negative shifts. TBS over the right lateral cerebellum (C) had no effect on error correction performance. Tap–tone asynchronies are shown for the time of the perturbation (T) and four subsequent taps (T + 1 to T + 4). The data are normalized to range from baseline asynchrony (0, dashed line) to the magnitude of the initial shift at time (T), and the sign is removed. Baseline performance is defined as the subject mean tap–tone asynchrony during $T - 4$ to $T - 1$. Performance before TBS (open circles and squares) is compared with post-TBS performance (filled circles and squares). In negative shifts (left side, circles), the tone occurs earlier than expected, and in positive shifts (right side, squares), the tone occurs later than expected. Error bars express a standard error.

of medial cerebellar TBS at time $T + 1$ on positive supraliminal error correction ($p = .045$) but not at the other time points ($p > .1$) and no effect on negative supraliminal error correction at any time point ($p > .1$). Medial cerebellar TBS did not affect subliminal error correction. There were no significant changes in error correction performance after sham TBS (Figure 4D). In the data set, the number of outlier error correction responses removed from the analysis was not statistically different between the conditions ($p > .4$) and was not affected by TBS ($p > .7$). The average number of outlier error correction responses removed across subjects was 10.4 ($SD = 2.4$) of 216 total responses.

In summary, suppression of the left cerebellum significantly affected supraliminal error correction at the tap immediately after the phase shift. Suppression of the right cerebellum did not affect error correction performance. As such, the findings of Experiment 2 support results of Experiment 1 and provide further evidence that the left cerebellar cortex is necessary for the correction of supraliminal phase shifts during SMS.

GENERAL DISCUSSION

This study investigated the role of the cerebellum during sub- and supraliminal error correction in the context of an SMS task. Imaging results from Experiment 1 indicate a functionally lateralized response such that the right cerebellar dentate and vermis are activated in all SMS conditions compared with rest, whereas the left posterior cerebellar cortex is only engaged during the correction of large, supraliminal phase shifts. Furthermore, the left cerebellum exhibited enhanced connectivity with a cerebello-cortical network including the right lateral frontal cortex and the right cerebellum during the condition that included supraliminal error correction compared with regular SMS. In Experiment 2, TBS applied to the left cerebellum significantly affected the correction of positive and negative supraliminal errors, which confirms the causal contribution of the left cerebellum to the supraliminal error correction process.

The imaging results of Experiment 1 show that the right cerebellum is activated in all experimental conditions compared with rest (Figure 2C). The activation is mainly localized in the right dentate nucleus extending to the vermis (Figure 2E). The finding of persistent right cerebellar dentate activation closely replicates an earlier fMRI study investigating right-handed SMS and continuation (Rao et al., 1997). It is possible that cerebellar activation ipsilateral to the moving limb is related to movement control, in line with a traditional view of the cerebellum (Ramnani, 2006). However, activation of the right cerebellum during SMS may play a critical role in the timing of movement. There is neuroimaging evidence to suggest that the right cerebellum is essential for perceptual timing even when little or no movement is required (Lewis & Miall, 2003). Furthermore, it was shown in two independent rTMS studies that suppression of the right, but not the left, cerebellum affects perceptual timing abilities (Fierro et al., 2007; Lee et al., 2007). Nonetheless, future research will be needed to differentiate conclusively between the control of timing and movement within the cerebellum. For example, the present study may be replicated using the left hand to examine whether the right cerebellum is consistently activated during movement timing.

The left cerebellum was only involved during the condition that included error correction of perceivable changes in the pacing stimulus (Figure 2D). In contrast to the right dentate activation, activity in the left cerebellar hemisphere was located exclusively in the cortex (Figure 2F). The finding of involvement of the left lateral cerebellum during the correction of supraliminal errors closely replicates earlier findings (Stephan et al., 2002). Furthermore, our PPI results showed that during supraliminal error correction the left cerebellum displayed enhanced effective connectivity with a cerebello-cortical network that included the frontal and sensory cortices and the right cerebellum (Figure 3). The pattern of task-dependent effective connectivity between the left cerebellum and the auditory, sensory, and frontal cortices has, to our knowledge, not been shown in previous studies. Although the functional significance of this cerebello-cortical network is currently unclear, it may be that sensory input from the auditory and somatosensory domains are rapidly integrated in the frontal region and passed to the left cerebellum to facilitate prompt behavioral error correction. Further research will be needed to fully understand the function of the emerging cerebello-cortical network during supraliminal error correction. Lastly, the findings of Experiment 2 show that suppression of the left lateral cerebellum significantly affected the correction of supraliminal errors at the tap immediately after the perturbation (Figure 4), whereas suppression of the right cerebellum did not affect error correction performance. Hence, Experiment 2 provides evidence that the left cerebellum causally contributes to supraliminal error correction.

In both experiments, behavioral error correction occurred after subliminal perturbations. Yet no left cerebellar activation was found during subliminal error correction compared with regular SMS in Experiment 1. Furthermore, in Experiment 2, the correction of subliminal phase shifts was not affected by any of the TBS protocols. These findings suggest that the mechanism of subliminal error correction differs from that of supraliminal error correction. Repp (2005) previously proposed that synchronization during regular SMS is achieved through a continuous phase resetting mechanism. In the phase resetting hypothesis, the timing of each response is calculated on the basis of the previous pacing tone rather than the tap–tone asynchrony. Phase resetting after a perturbation that falls below the perceptual threshold is not different from phase resetting after a tone at the regular interval. Hence, the use of the same neural mechanism to achieve both regular SMS and subliminal error correction may explain why there was no additional brain activation during subliminal error correction in Experiment 1 and why cerebellar TBS did not affect subliminal error correction in Experiment 2. The phase resetting hypothesis is also consistent with the finding that spontaneous error correction was less efficient than induced error correction (because baseline asynchrony was not achieved within four taps; Figure 1C). This less efficient response to spontaneous shifts is expected if response timing is relative to the previous pacing tone rather than to the tap–tone asynchrony. Overall, these findings provide evidence that the correction of subliminal shifts may be achieved by a continuous phase resetting process that also controls accurate timing during regular SMS.

In addition to involvement of the left cerebellum, inferior parietal and frontal areas were activated during the condition that involved perceivable phase perturbations in Experiment 1. These results replicate findings by Stephan et al. (2002). However, the PPI analysis did not show increased connectivity between the left cerebellum and the parietal-frontal network. The lack of effective connectivity between the left cerebellum and the parietal-frontal cortices may suggest that the parietal-frontal network is engaged in more cognitive processes associated with the perception of errors rather than behavioral error correction. Consistent

with our interpretation, a number of studies have indicated the role of the parietal-frontal network in error perception. One study investigated the perception of supraliminal irregularities in pitch and duration of an auditory sequence (Molholm, Martinez, Ritter, Javitt, & Foxe, 2005), and another study looked at awareness of behavioral errors in a go/no-go task (Hester, Foxe, Molholm, Shpaner, & Garavan, 2005). Both studies showed activation in a parietal-frontal network similar to our findings, but without involvement of the cerebellum. Activation of a parietal-frontal network during the perception of irregularities and during awareness of behavioral errors may suggest that these regions are involved in conscious error detection. The right-hemispheric lateralization of parietal-frontal activation in Experiment 1 of our study provides further evidence that these areas are associated with conscious error detection. The right parietal and frontal areas are thought to play a role in directing attention (Posner & Raichle, 1994) and processing sensory feedback (Coull & Nobre, 2008), whereas the left cerebral hemisphere may be specialized in movement control (Serrien, Ivry, & Swinnen, 2006) and temporal attention (Coull & Nobre, 1998). In summary, activation of a parietal-frontal network during the condition that included supraliminal phase shifts may be related to conscious detection of supraliminal irregularities and of behavioral errors. Furthermore, the lack of cerebellar activation (despite cerebellar coverage) during the detection of irregularities and of behavioral errors (Hester et al., 2005; Molholm et al., 2005) supports the hypothesis that the left posterior cerebellum plays a crucial role in error correction rather than in the detection of perceptual mismatch or of sensorimotor error.

Behavioral data from both experiments show that the correction of positive shifts is faster than that of negative shifts (Figure 1). A similar dichotomy in error correction response was previously suggested (Praamstra et al., 2003) but was not seen in other similar studies (Repp, 2000, 2001a). Using electroencephalography, it has been shown that error-related negativity (associated with committing a behavioral error) is only present for positive supraliminal shifts and not for negative supraliminal shifts or subliminal shifts of either direction (Praamstra et al., 2003). The difference in error-related negativity for positive and negative supraliminal shifts suggests that the correction of these may be achieved by fundamentally different neural mechanisms. Although the experimental paradigm used in Experiment 1 did not allow a direct comparison between positive and negative shifts, the findings in Experiment 2 provide evidence that different neural mechanisms are involved in the correction of supraliminal positive and negative phase shifts. Experiment 2 shows that suppression of the medial cerebellum affects the correction of only positive phase perturbations, whereas left cerebellar suppression affects both positive and negative error correction. A previous study showed differential effects of unexpectedly early and late tone onsets in a temporal discrimination task (McAuley & Jones, 2003). Here, the discrimination threshold (i.e., the minimum time difference required to differentiate between two durations) was significantly larger when a comparison interval was presented unexpectedly early with respect to a context rhythm. The different behavioral effects of early and late stimulus presentation may be due to the temporal expectancy created by the entrainment of an internal oscillator with an external rhythm (Large & Jones, 1999). In line with the above studies, we suggest that after positive shifts during SMS an expectancy mechanism may be used to prepare the correction response. In response to negative shifts, the expectancy mechanism may not be utilized as the errors should be corrected reactively (similar to a simple RT task). The results of Experiment 2 suggest that the medial cerebellum may play a role in the expectancy mechanism because suppression of the medial cerebellum affected only positive error correction. Future studies are needed to specifically test this hypothesis.

There are some methodological issues to consider in interpreting our results. The experimental design of Experiment 1 did not allow a direct comparison between positive and negative error correction. However, the TBS results of Experiment 2 provide evidence that the neural mechanisms for positive and negative error correction may differ. Future research may wish to investigate the difference between the correction of positive and negative supraliminal phase shifts using fMRI. Furthermore, the criterion used to find extreme cases of motor variability (deviations from mean asynchrony greater than 50 msec) may be considered arbitrary. However, it was chosen because it is similar to the group-averaged standard deviation of the asynchrony during regular taps (45 msec) and because it falls above the threshold for conscious perception (Repp, 2002a). The data were also analyzed adopting the criteria of 50-msec deviation from the target IRI (<550 or >650 intertap interval), which yielded similar results. Lastly, it is possible that the lack of right cerebellar activation during supraliminal error correction in Experiment 1 is associated with sensitivity issues because the right cerebellum is already significantly activated during all conditions compared with rest. Future research may wish to replicate our findings during left-handed SMS to exclude this possibility. Such research should also aim to extend scanning time to increase statistical power whilst maintaining sufficient levels of task performance. In addition, future research on the role of cortical regions in the emerging cerebello-cortical network is needed to gain a complete understanding of supraliminal error correction.

Conclusions

The current study aimed to investigate the neural networks for error correction of sub- and supraliminal phase shifts during SMS. The functional imaging results of Experiment 1 indicate two neural networks: (1) the primary motor and sensory cortices and the right cerebellar dentate

nucleus are involved in regular motor timing and correction of subliminal errors, and (2) the inferior parietal and frontal cortices and the left posterior cerebellar cortex are engaged during the detection and correction of perceivable errors. A PPI analysis furthermore shows that the left cerebellum exhibited enhanced connections with frontal, auditory, and sensory cortices and with the right cerebellum during supraliminal error correction compared with regular SMS. Experiment 2 shows that suppression of the left, but not the right, lateral cerebellum significantly affects supraliminal error correction. Taken together, the results of Experiments 1 and 2 provide evidence for a crucial role of the left cerebellum in conscious error correction but not in the correction of subliminal errors. Furthermore, findings of both experiments highlight differences between the response to positive and the negative shifts. We suggest that temporal expectancy may be used to correct positive shifts, and the medial cerebellum may play a role in temporal expectancy mechanisms. Negative shifts, on the other hand, may be corrected reactively.

Acknowledgments

J. Bijsterbosch was supported by a Medical Research Council PhD studentship.

Reprint requests should be sent to Janine D. Bijsterbosch or Kwang-Hyuk Lee, Academic Clinical Psychiatry, The Longley Centre, Norwood Grange Drive, Sheffield, S5 7JT, United Kingdom, or via e-mail: J.Bijsterbosch@sheffield.ac.uk; K.H.Lee@sheffield.ac.uk.

REFERENCES

Aschersleben, G. (2002). Temporal control of movements in sensorimotor synchronization. *Brain and Cognition, 48,* 66–79.

Coull, J. T., & Nobre, A. C. (1998). Where and when to pay attention: The neural systems for directing attention to spatial locations and to time intervals as revealed by both PET and fMRI. *Journal of Neuroscience, 18,* 7426–7435.

Coull, J. T., & Nobre, A. C. (2008). Dissociating explicit timing from temporal expectation with fMRI. *Current Opinion in Neurobiology, 18,* 137–144.

Diedrichsen, J. (2006). A spatially unbiased atlas template of the human cerebellum. *Neuroimage, 33,* 127–138.

Fierro, B., Palermo, A., Puma, A., Francolini, M., Panetta, M. L., Daniele, O., et al. (2007). Role of the cerebellum in time perception: A TMS study in normal subjects. *Journal of the Neurological Sciences, 263,* 107–112.

Friston, K. J., Buechel, C., Fink, G. R., Morris, J., Rolls, E., & Dolan, R. J. (1997). Psychophysiological and modulatory interactions in neuroimaging. *Neuroimage, 6,* 218–229.

Hester, R., Foxe, J. J., Molholm, S., Shpaner, M., & Garavan, H. (2005). Neural mechanisms involved in error processing: A comparison of errors made with and without awareness. *Neuroimage, 27,* 602–608.

Huang, Y. Z., Edwards, M. J., Rounis, E., Bhatia, K. P., & Rothwell, J. C. (2005). Theta burst stimulation of the human motor cortex. *Neuron, 45,* 201–206.

Jäncke, L., Loose, R., Lutz, K., Specht, K., & Shah, N. J. (2000). Cortical activations during paced finger-tapping applying visual and auditory pacing stimuli. *Brain Research, Cognitive Brain Research, 10,* 51–66.

Kolers, P. A., & Brewster, J. M. (1985). Rhythms and responses. *Journal of Experimental Psychology: Human Perception and Performance, 11,* 150–167.

Large, E. W., & Jones, M. R. (1999). The dynamics of attending: How people track time-varying events. *Psychological Review, 106,* 119–159.

Lee, K. H., Egleston, P. N., Brown, W. H., Gregory, A. N., Barker, A. T., & Woodruff, P. W. (2007). The role of the cerebellum in subsecond time perception: Evidence from repetitive transcranial magnetic stimulation. *Journal of Cognitive Neuroscience, 19,* 147–157.

Lewis, P. A., & Miall, R. C. (2003). Distinct systems for automatic and cognitively controlled time measurement: Evidence from neuroimaging. *Current Opinion in Neurobiology, 13,* 250–255.

Lutz, K., Specht, K., Shah, N. J., & Jäncke, L. (2000). Tapping movements according to regular and irregular visual timing signals investigated with fMRI. *NeuroReport, 11,* 1301–1306.

McAuley, J. D., & Jones, M. R. (2003). Modeling effects of rhythmic context on perceived duration: A comparison of interval and entrainment approaches to short-interval timing. *Journal of Experimental Psychology: Human Perception and Performance, 29,* 1102–1125.

Molholm, S., Martinez, A., Ritter, W., Javitt, D. C., & Foxe, J. J. (2005). The neural circuitry of pre-attentive auditory change-detection: An fMRI study of pitch and duration mismatch negativity generators. *Cerebral Cortex, 15,* 545–551.

Pollok, B., Gross, J., Kamp, D., & Schnitzler, A. (2008). Evidence for anticipatory motor control within a cerebello-diencephalic-parietal network. *Journal of Cognitive Neuroscience, 20,* 828–840.

Posner, M. I., & Raichle, M. E. (1994). *Images of mind*. New York: Scientific American Library.

Praamstra, P., Turgeon, M., Hesse, C. W., Wing, A. M., & Perryer, L. (2003). Neurophysiological correlates of error correction in sensorimotor-synchronization. *Neuroimage, 20,* 1283–1297.

Pridmore, S., Fernandes Filho, J. A., Nahas, Z., Liberatos, C., & George, M. S. (1998). Motor threshold in transcranial magnetic stimulation: A comparison of a neurophysiological method and a visualization of movement method. *Journal of ECT, 14,* 25–27.

Ramnani, N. (2006). The primate cortico-cerebellar system: Anatomy and function. *Nature Reviews Neuroscience, 7,* 511–522.

Rao, S. M., Harrington, D. L., Haaland, K. Y., Bobholz, J. A., Cox, R. W., & Binder, J. R. (1997). Distributed neural systems underlying the timing of movements. *Journal of Neuroscience, 17,* 5528–5535.

Repp, B. H. (2000). Compensation for subliminal timing perturbations in perceptual-motor synchronization. *Psychological Research, 63,* 106–128.

Repp, B. H. (2001a). Phase correction, phase resetting, and phase shifts after subliminal timing perturbations in sensorimotor synchronization. *Journal of Experimental Psychology: Human Perception and Performance, 27,* 600–621.

Repp, B. H. (2001b). Processes underlying adaptation to tempo changes in sensorimotor synchronization. *Human Movement Science, 20,* 277–312.

Repp, B. H. (2002a). Automaticity and voluntary control of phase correction following event onset shifts in sensorimotor synchronization. *Journal of Experimental Psychology: Human Perception and Performance, 28,* 410–430.

Repp, B. H. (2002b). Phase correction in sensorimotor synchronization: Nonlinearities in voluntary and involuntary responses to perturbations. *Human Movement Science, 21,* 1–37.

Repp, B. H. (2005). Sensorimotor synchronization: A review of the tapping literature. *Psychonomic Bulletin & Review, 12,* 969–992.

Repp, B. H., & Keller, P. E. (2004). Adaptation to tempo changes in sensorimotor synchronization: Effects of intention, attention, and awareness. *Quarterly Journal of Experimental Psychology: A, 57,* 499–521.

Serrien, D. J., Ivry, R. B., & Swinnen, S. P. (2006). Dynamics of hemispheric specialization and integration in the context of motor control. *Nature Reviews Neuroscience, 7,* 160–166.

Stephan, K. M., Thaut, M. H., Wunderlich, G., Schicks, W., Tian, B., Tellmann, L., et al. (2002). Conscious and subconscious sensorimotor synchronization-prefrontal cortex and the influence of awareness. *Neuroimage, 15,* 345–352.

Theoret, H., Haque, J., & Pascual-Leone, A. (2001). Increased variability of paced finger tapping accuracy following repetitive magnetic stimulation of the cerebellum in humans. *Neuroscience Letters, 306,* 29–32.